UNIVERSITY OF ALMERÍA

Department of Chemical Engineering

Solar Energy Research Center (CIESOL)

KINETIC MODELING OF SOLAR PHOTO-FENTON PROCESS FOR MICROPOLLUTANT REMOVAL FROM MUNICIPAL WWTP EFFLUENTS IN LOW-COST REACTORS

Paula Soriano Molina

Ph.D. Thesis

Almería 2019

Departamento de Ingeniería Química

Doctorado en Biotecnología y Bioprocesos Industriales Aplicados a la Agroalimentación y Medioambiente

Modelado cinético del proceso foto-Fenton solar para la eliminación de microcontaminantes presentes en efluentes de depuradora con reactores de bajo coste

Memoria presentada para aspirar al grado de Doctor por la Universidad de Almería

Paula Soriano Molina

Fdo. Paula Soriano Molina

DIRECTORES DE TESIS

Dr. José Antonio Sánchez Pérez
Catedrático de Universidad
Departamento de Ingeniería Química

Dr. Sixto Malato Rodríguez
Profesor de Investigación de OPI-CIEMAT
Plataforma Solar de Almería
CIEMAT

``La ilusión, la fe y las ganas son el motor de la voluntad´´

Mar Molina

``La ciencia será siempre una búsqueda,
jamás un descubrimiento real. Es un viaje, nunca una llegada´´

Karl Popper

Quiero expresar mi agradecimiento al Ministerio de Educación Cultura y Deporte por concederme la beca FPU (AP2014/01030) y la financiación (EST16/00602) para los tres meses de estancia.

A José Antonio y Sixto, por ofrecerme la oportunidad de iniciarme en el mundo científico avalada por la mejor de las direcciones. Por estar al pie del cañón las 24 h los 365 días del año y, sobre todo, por confiar en mí más que yo misma y hacer que mi afán investigador haya ido in crescendo a lo largo de estos años, claro ejemplo de una buena dirección.

A José Luis García, por enseñarme desde cero todo lo que hoy sé sobre modelado, por contagiarme su visión crítica y ayudarme a lograr lo que para mí ha sido, sin duda, uno de los mayores retos en esta tesis.

A las doctoras, Patricia, Sara, Belén y Gracia, por estar disponible siempre que lo he necesitado.

A mis niñas de arriba: Irene, Ana, Sandra, Marina, Ahlam, Alba e Inma, por celebrar cada logro, por encontrar siempre una excusa para reírnos de todo y por el apoyo en los malos momentos; porque después de tantas horas diarias juntas y tantas emociones compartidas os considero una segunda familia. De cada una me llevo una lección, tanto personal como profesional.

Además, quiero agradecer a Ahlam, Alba, Inma y Ana por ayudarme en la última etapa a llevar a cabo el trabajo experimental, dando siempre lo mejor y más de sí mismas, y a Ana Ruiz, por su apoyo incondicional desde la PSA (y desde CIESOL estos últimos meses). Mis agradecimientos también a Octavio, Juan y Gregorio, por su paciencia infinita para ayudarnos a resolver cualquier problema técnico, siempre con una sonrisa.

Sin olvidar a los técnicos de transporte, Antonio y Andrés, por hacer posible el trabajo a escala piloto.

A los estudiantes de estancia, en especial a Chiara y Amal.

Al grupo de Alfano, en el que no pude ser mejor acogida durante mi estancia en el INTEC. No todos los que trabajan en mi campo han tenido la oportunidad de recibir lecciones de un referente como Orlando (con papel y lápiz), y además de una forma humilde y cercana. Mención especial a Antonio Negro, por tratarme como un miembro más de su familia, por su gran sentido del humor y por su paciencia para esperar a que mis iteraciones terminaran para cerrar el laboratorio. A Joana y a todas las chicas por ofrecerme su amistad desde el principio y por hacer que el tiempo libre de la estancia fuera aventura y diversión.

A Gema, Lorena, Carolina y Fani, por el calor de tantos años de amistad, aunque no terminen de comprender a qué me dedico.

A Álex, por cuidarme y hacerme la vida más sencilla, por ayudarme siempre a ver las cosas como realmente son, y, en definitiva, por haber sido el pilar más importante en los momentos más difíciles.

A mi padre, Javier, por preocuparse por mi futuro, por inculcarme desde pequeña el valor del esfuerzo y la constancia, y por sus siempre valiosas palabras ``para adelante´´.

Y a mi madre, Mar, la principal artífice de lo que hoy soy, quien me inculcó los valores culturales, el amor por las artes y de quien llevo por bandera el ejemplo de coraje y entrega a los demás.

TABLE OF CONTENTS

THESIS FRAMEWORK

The work presented in this Ph.D. thesis has been developed in the framework of three projects funded by the European Regional Development Fund (ERDF) and the Ministry for Economy and Competitiveness (Spanish Government):

- Cost reduction of the solar photo-Fenton process through open extensive reactors for water reclamation (REAQUA, CTQ2013-46398-R).
- New photocatalytic materials and reactors for removal of micropollutants and pathogens (FOTOCAT, CTM2015-71054-REDT).
- Disinfection of WWTP secondary effluents by solar photo-Fenton process in raceway pond reactors. Effect on antibiotic resistance transfer (SOLFENDIS, CTQ2016-78255-R).

These projects are aimed to evaluate the technical and economical feasibility of raceway pond reactors for micropollutant removal, disinfection and wastewater reclamation on a large scale.

The research has been carried out at the Solar Energy Research Center (CIESOL), joint center between the CIEMAT and the University of Almería. Paula Soriano Molina was granted an FPU scholarship (AP2014/01030) for the formation of teaching staff at universities from September 16th, 2015 to September 16th, 2019 by the Spanish Ministry of Education, Culture and Sport. The Ministry also funded a research stay abroad (EST16/00602) at the Institute of Technological Development for the Chemical Industry (INTEC) from September 15th, 2017 to December 15th, 2017.

ABSTRACT

The reuse of effluents from wastewater treatment plants (WWTPs) is becoming an increasingly widespread and necessary alternative to conventional water sources in regions of the world with water scarcity. Conventional treatment plants are not designed to remove certain organic compounds, which are usually at low concentration and also biorecalcitrant. Despite being found at very low concentrations of the order of μg L^{-1} to ng L^{-1} (and therefore named as micropollutants), their accumulation in ecosystems can cause negative effects on crops (when using water for irrigation), in water and aquatic organisms and, consequently, on human health as well. Although there is still no legislation shared by European countries, some countries have started regulating their treatment and discharge. As such, there is a growing interest in the development of tertiary treatments for micropollutant removal. In this regard, the solar photo-Fenton process stands out as being one of the most efficient and environmentally sustainable advanced oxidation processes (AOPs). However, further research is needed to reduce operating costs as well as to scale up the process.

This Ph.D. thesis is aimed at the development of mechanistic models which allow the operation of the low-cost raceway pond reactors (RPRs) as tertiary treatment in municipal WWTPs (MWWTPs) to be designed and optimized.

Section 4.1 focuses on the development of a model at the optimum pH of the photo-Fenton reaction (pH 2.8) for micropollutant removal from secondary effluents. For this, the effect of temperature and photon absorption on the kinetics of the process was studied. The assays were carried out at lab-scale in synthetic secondary effluent with 0.1 mM Fe^{2+} and 1.47 mM H_2O_2 varying the temperature (10 - 40 ºC), the ultraviolet A (UVA) irradiance (10 - 40 W m^{-2}) and the liquid depth in the reactor (5 and 15 cm). The pesticide acetamiprid (ACTM) was used as a model pollutant at an initial concentration of 100 μg L^{-1}, similar to that of the total load of micropollutants detected in MWWTP effluents. This compound was selected as it is a highly recalcitrant neonicotinoid included on the EU watch list of priority hazardous substances. The results showed a double contribution by temperature to the process, namely, the Fenton reaction being accelerated, and the Fe^{3+} light absorption coefficient being increased. Concerning the effect of photon absorption, the ACTM degradation rate increased with the volumetric rate of photon absorption (VRPA) up to VRPA values of 866 μE m^{-3} s^{-1}. Nonetheless, at higher VRPA values the process became photosaturated. To explain this phenomenon, the formation of an

activated state of iron was proposed. Once Fe^{3+} is photoactivated, it is reduced to Fe^{2+}, with a fraction of the absorbed radiation being converted into heat. Consequently, a fraction of iron remains in its initial state as Fe^{3+}. From these observations, a mechanistic model consisting of a set of 8 reactions was proposed, and the parameters were estimated from the results obtained at lab-scale. The model was successfully validated outdoors in RPRs of 5 and 15 cm of liquid depth (120 and 360 L capacity). Moreover, its relevance in terms of variations in the catalyst concentration was demonstrated. In terms of mass of pollutant removed per reactor surface area unit and unit of time, high treatment capacities (135 mg m^{-2} h^{-1}) were achieved with 0.18 mM Fe^{2+} and 15 cm liquid depth.

Certain economic and environmental drawbacks related to the operation at acidic pH hinder the scaling of the process. The wastewater acidification to reduce pH to 2.8 implies an increase in its salinity as well as the operating costs. To avoid this, other alternatives such as the operation at neutral pH with iron complexes are being investigated. Among iron chelating agents, the biodegradable [S,S]-ethylenediamine-N,N'-disuccinic acid ([S,S]-EDDS) is gaining a growing interest due to the high photochemical efficiency of Fe^{3+}-EDDS.

With this aim in mind, Section 4.2 focuses on the phenomenological study of the process at neutral pH with the Fe^{3+}-EDDS complex. The assays were conducted at lab-scale with 0.1 mM Fe^{3+} at Fe^{3+}:EDDS molar ratio of 1:1. Firstly, the reactions involved in the photolysis of Fe^{3+}-EDDS as well as the effect of H_2O_2 concentration (0.74, 1.47 and 2.94 mM) were studied. No effect by the initial H_2O_2 concentration on Fe^{3+}-EDDS decomposition was observed, meaning the use of an H_2O_2 concentration of 0.88 mM H_2O_2, lower than that used previously (1.47 mM), was proposed. Once Fe^{3+}-EDDS had decomposed, a small fraction of the total amount of iron remained in solution, which could be explained by the presence of oxidized Fe^{3+}-EDDS species.

Afterwards, the effect of photon absorption on the kinetics of the photo-Fenton process was investigated. The experiments were carried out at 25 ºC (the annual average temperature of the wastewater in the MWWTP located in Almería city) in synthetic effluent doped with 100 µg L^{-1} ACTM. The effect of photon absorption was evaluated by varying both the liquid depth (5 and 15 cm) and the UVA irradiance on the reactor surface (10 W m^{-2} – 50 W m^{-2}).

Reaction rates of micropollutant removal and reactant consumption linearly increased with the initial VRPA up to VRPA values of 1547 μE m^{-3} s^{-1} (first order reaction with regard to VRPA), in other words, the process was photolimited. At higher VRPA values, the reaction rates remained constant (zero order reaction with regard to VRPA), pointing out that the process was photosaturated. The fact that photosaturation takes place at higher VRPA values than at acidic pH is due to the higher absorptivity of Fe^{3+}-EDDS in comparison with Fe^{3+}. Finally, the effect of light path length on treatment capacity was studied. It was found that, even under photolimiting conditions, treatment capacity can be increased by increasing liquid depth.

To scale up the process, it is necessary to evaluate its efficiency when applying the optimum operating conditions found with synthetic effluents to real effluents of very different composition. As such, Section 4.3 addresses the micropollutant removal in real effluents from 5 different MWWTPs located along the Mediterranean cost of Spain. The assays were developed outdoors in an RPR of 5 cm liquid depth (19 L capacity). Liquid chromatography-triple quadrupole-linear ion trap-mass spectrometry (LC-QqLiT-MS/MS) was used to detect and quantify the micropollutants, in collaboration with the Environmental Analysis and Water Treatment research group at the Solar Energy Research Center (CIESOL). The results showed that the mild oxidation conditions previously studied are suitable for treatment in real conditions. Regardless of the origin and composition of the effluents, more than 80% of the total load of micropollutants was removed in less than 15 min reaction time. Regarding salinity, in spite of the large number of works that pointed out a negative effect on the degradation of micropollutants by photo-Fenton of chlorides and sulfates, it was not observed when treating real effluents. Indeed, the results showed faster removal rates in the effluent with the highest concentration of anions.

In Section 4.4, the modeling of the process at neutral pH with the Fe^{3+}-EDDS complex is addressed for the first time. During a three-month research stay with Professor Orlando Alfano´s research group in Santa Fe (Argentina), an in-depth study on the coupling of the modeling of photochemical kinetics with the radiation field in RPRs was carried out. The two components of solar radiation were considered: direct radiation, which comes directly from the sun, and diffuse component, which is the scattered radiation. The effect of diffuse radiation, not previously considered, could be significant especially in winter, when the solar zenith angle may be greater than 50º at noon. The VRPA corresponding

to this component of radiation was estimated assuming the hypothesis of azimuthal symmetry, that is, propagation of rays in one spatial coordinate (the liquid depth) and one angular coordinate. From the previous kinetic studies as well as the hypotheses deduced from the experimental results, a complex mechanistic model of 16 reactions was proposed. The experimental data of ACTM removal in synthetic effluent, discussed in Section 4.2, were used to estimate the kinetic parameters. The model was successfully validated outdoors in an RPR of 5 cm liquid depth both in winter and summer.

Once the efficiency of the process to treat real effluents was demonstrated and a mechanistic model was developed, Section 4.5 deals with the application of the model to design and optimize the operation of the RPRs. To this end, the reactions corresponding to the removal of the three most abundant compounds detected in the five effluents studied in Section 4.3 (gabapentin, *O*-desmethyltramadol and *O*-desmethylvenlafaxine) were included in the model. The kinetic parameters were estimated from the experimental data of the removal of each compound, being of the same order of magnitude in all the effluents. Afterwards, the performance of the model for being applied to the operation of RPRs in continuous flow mode was validated, and the effect of liquid depth and hydraulic residence time on treatment capacity was simulated. The simulation results are of relevance for RPR design, since the reactor area could be estimated as a function of the hydraulic residence time and liquid depth. This maximizes the treatment capacity as a function of solar irradiation conditions.

In short, the work presented in this Ph.D. thesis is of relevance in terms of extending the use of the low-cost and highly efficient RPRs to a large scale. From the phenomenological study of the photo-Fenton process at lab-scale, mechanistic models of the process both at acidic pH with Fe^{3+} and neutral pH with Fe^{3+}-EDDS have been proposed. These models can be fine-tuned as a function of the operating conditions (radiation power, wastewater composition, reactor geometry, etc.) for the design and optimization of the operation of RPRs when treating real effluents from MWWTPs.

RESUMEN

La reutilización de los efluentes de estaciones depuradoras de aguas residuales (EDAR) es una alternativa a las fuentes convencionales de agua cada vez más extendida y necesaria en las zonas del mundo con escasez de agua. Las EDAR convencionales no están diseñadas para eliminar ciertos compuestos biorecalcitrantes. Aunque estos compuestos se encuentran en concentraciones muy bajas, del orden de $\mu g\ L^{-1}$ – $ng\ L^{-1}$ (y, por lo tanto, son llamados microcontaminantes) su acumulación en los ecosistemas puede causar efectos negativos en los cultivos (cuando el agua se usa para riego), en el agua y en los organismos acuáticos y, por consiguiente, en la salud humana. Aunque aún no hay una legislación establecida a nivel europeo, algunos países están empezando a regular su tratamiento y descarga, y por lo tanto, el interés por la investigación y desarrollo de tratamientos terciarios para eliminar estos contaminantes es cada vez mayor. En este sentido, el proceso foto-Fenton solar destaca por ser uno de los procesos de oxidación avanzados más eficientes y ambientalmente sostenibles. Sin embargo, aún se necesita más investigación para reducir los costes de operación, así como escalar el proceso.

Este trabajo de tesis doctoral se enfoca en el desarrollo de modelos mecanísticos que permitan el diseño y la optimización de la operación de los reactores tipo ``raceway´´, de bajo coste, como tratamiento terciario en las EDAR urbanas.

El Apartado 4.1 se centra en el desarrollo de un modelo al pH óptimo de la reacción photo-Fenton (pH 2.8) para la eliminación de microcontaminantes en efluentes secundarios. Para ello se estudió el efecto de la temperatura, así como de la absorción de fotones en la cinética del proceso. Los ensayos se realizaron a escala de laboratorio en un efluente secundario sintético con 0.1 mM Fe^{2+} y 1.47 mM H_2O_2 variando la temperatura entre 10 y 40 ºC, la irradiancia ultravioleta A (UVA) en la superficie del reactor entre 10 y 40 $W\ m^{-2}$ y la profundidad de líquido en el reactor, 5 y 15 cm. Se utilizó el plaguicida acetamiprid como contaminante modelo a una concentración inicial de 100 $\mu g\ L^{-1}$, concentración similar a la carga total de microcontaminantes detectados en los efluentes de EDAR. Se seleccionó este compuesto por ser un neonicotinoide altamente recalcitrante incluido en la lista de observación de sustancias a efectos de seguimiento a nivel de la Unión Europea. Los resultados mostraron una doble contribución del incremento de temperatura al proceso, acelerando la reacción de Fenton, y aumentando el coeficiente de absorción de fotones del Fe^{3+}. Respecto al efecto de la absorción de fotones, la velocidad de degradación del acetamiprid aumentó con la velocidad volumétrica de absorción de

fotones a valores inferiores a 866 μE m^{-3} s^{-1}. Sin embargo, a valores superiores el proceso se fotosaturó. Para explicar este fenómeno se propuso la formación de un estado activado del hierro. Una vez el hierro es fotoactivado, se reduce a Fe^{2+}, mientras que una fracción de la radiación absorbida se convierte en calor. En consecuencia, una fracción del hierro permanece en su estado inicial como Fe^{3+}. A partir de estas observaciones, se propuso un modelo mecanístico de 8 reacciones y se estimaron sus parámetros a partir de los datos obtenidos a escala de laboratorio. El modelo fue exitosamente validado en externo en reactores de bajo coste tipo ``raceway´´ de 5 y 15 cm de profundidad de líquido (120 y 306 L de capacidad). Además, se demostró su relevancia ante variaciones en la concentración de catalizador. En términos de masa de contaminante eliminada por unidad de superficie de reactor y unidad de tiempo, se alcanzaron altas capacidades de tratamiento (135 mg m^{-2} h^{-1}) con 0.18 mM Fe^{2+} y 15 cm de profundidad de líquido.

La operación del proceso foto-Fenton a pH ácido presenta ciertas desventajas económicas y ambientales que dificultan su viabilidad para ser implantado en las plantas de tratamiento de aguas residuales. La necesidad de acidificar el efluente para reducir el pH a 2.8 implica el incremento de la salinidad del efluente y de los costes de operación. Para evitar esto, se están investigando otras alternativas tales como la operación a pH neutro mediante el uso de complejos de hierro. Entre los agentes quelantes del hierro, el ácido (S,S)-Etilendiamino-N,N'-disuccínico ([S,S]-EDDS), biodegradable, está ganando creciente interés debido a la alta eficiencia fotoquímica del Fe^{3+}-EDDS.

Con este objetivo, el Apartado 4.2 se centra en el estudio fenomenológico del proceso a pH neutro con el complejo Fe^{3+}-EDDS. Los ensayos se realizaron a escala de laboratorio con 0.1 mM Fe^{3+} a relación molar Fe^{3+}:EDDS 1:1. En primer lugar, se estudiaron las reacciones implicadas en la fotólisis del complejo así como el efecto de la concentración de H_2O_2 (0.74, 1.47 y 2.94 mM). No se observó efecto de la concentración inicial de H_2O_2 en la descomposición del complejo, por lo tanto, se propuso el uso de 0.88 mM de concentración de H_2O_2, inferior a la usada previamente (1.47 mM). Tras la descomposición del Fe^{3+}-EDDS, quedó un remanente de hierro en disolución, lo que podría deberse a la presencia de especies oxidadas de Fe^{3+}-EDDS.

Una vez concluido este estudio, se investigó el efecto de la absorción de fotones en la cinética del proceso foto-Fenton. Los ensayos se llevaron a cabo a 25 ºC (la temperatura promedia anual del agua en la EDAR de la ciudad de Almería) en un efluente sintético dopado con 100 μg L^{-1} de acetamiprid. El efecto de la absorción de fotones se evaluó

variando la profundidad de líquido (5 y 15 cm) y la irradiancia UVA en la superficie del reactor (10 W m^{-2} – 50 W m^{-2}). Las velocidades de eliminación de microcontaminante y de consumo de reactivos aumentaron linealmente con la velocidad volumétrica inicial de absorción de fotones hasta valores de 1547 μE m^{-3} s^{-1} (reacción de primer orden con respecto a la velocidad volumétrica de absorción de fotones), es decir, el proceso estaba fotolimitado. A valores superiores de velocidad de absorción de fotones, las velocidades de reacción se mantuvieron constantes (reacción de orden cero con respecto a la velocidad volumétrica de absorción de fotones), indicando que el proceso estaba fotosaturado. El hecho de que a pH neutro la fotosatuación tenga lugar a valores de velocidad volumétrica de absorción de fotones más altos que a pH ácido se debe a la mayor absortividad del Fe^{3+}-EDDS en comparación con el Fe^{3+}. Finalmente, se evaluó el efecto de la longitud de paso óptico en la capacidad de tratamiento, y se observó que, incluso en condiciones de fotolimitación, la capacidad de tratamiento aumenta al incrementar la profundidad de líquido.

Como paso previo al escalado del proceso, es necesario evaluar su eficiencia cuando las condiciones óptimas de operación, obtenidas a partir de los ensayos en efluentes sintéticos, se aplican a efluentes reales de composición muy variable. Con este fin, el Apartado 4.3 aborda la eliminación de microcontaminantes en efluentes procedentes de 5 EDAR localizadas en la costa mediterránea de España. Los ensayos se realizaron en externo en un reactor tipo ``raceway´´ de 5 cm de profundidad (19 L de capacidad). La detección y cuantificación de los microcontaminantes se llevó a cabo en colaboración con el grupo de investigación de Análisis Ambiental y Tratamiento de Agua del Centro de Investigación en Energía Solar (CIESOL), mediante el uso de la técnica analítica LC-QqLIT-MS/MS, cuyas siglas en inglés refieren a ``Liquid chromatography-triple quadrupole-linear ion trap-mass spectrometry´´. Los resultados mostraron que las condiciones leves de oxidación previamente estudiadas son adecuadas para el tratamiento en condiciones reales. Independientemente del origen y la composición de los efluentes, se eliminó más del 80% de la carga total de microcontaminantes en menos de 15 min de reacción. Respecto a la salinidad, a pesar de los numerosos estudios que indicaban un efecto negativo de los cloruros y sulfatos en la degradación de microcontaminantes mediante foto-Fenton, no se observó ese efecto en el tratamiento de efluentes reales. De hecho, los resultados mostraron velocidades de eliminación de microcontaminantes más rápidas en el efluente con mayor concentración de estos aniones.

En el Apartado 4.4 se aborda por primera vez la modelización del proceso a pH neutro con el complejo Fe^{3+}-EDDS. Durante una estancia de investigación de tres meses con el grupo de investigación del Profesor Orlando Alfano en Santa Fe (Argentina), se llevó a cabo un estudio detallado del acoplamiento de la modelización de la cinética fotoquímica con el campo de radiación en los reactores tipo ``raceway´´. Para ello, se tuvieron en cuenta las dos componentes de la radiación solar: la directa que proviene directamente del sol, y la difusa, que proviene de la atmósfera por dispersión de parte de la radiación solar en ella. El efecto de la radiación difusa, no considerada previamente, podría ser significativo especialmente en invierno, cuando el ángulo cenital solar al mediodía puede ser superior a 50º. Para estimar la velocidad volumétrica de absorción de fotones correspondiente a esta componente de la radiación, se aplicó la hipótesis de simetría acimutal, es decir, propagación de los rayos en una coordenada espacial (la profundidad de líquido) y en una coordenada angular. A partir de los estudios cinéticos previos y las hipótesis deducidas de los resultados experimentales, se propuso un modelo mecanístico complejo de 16 reacciones. Los datos experimentales de eliminación de acetamiprid en efluente sintético, discutidos en el Apartado 4.2, se usaron para la estimación de los parámetros cinéticos. El modelo propuesto se validó con éxito en externo en un reactor tipo ``raceway´´ de 5 cm de profundidad en invierno y en verano.

Tras demostrar la eficiencia del proceso para tratar efluentes reales y desarrollar un modelo mecanístico, el Apartado 4.5 aborda la aplicación del modelo para diseñar y optimizar la operación de los reactores tipo ``raceway´´. Para ello, se incluyeron en el modelo las reacciones correspondientes a la eliminación de los tres contaminantes más abundantes detectados en todos los efluentes reales estudiados en el Apartado 4.3 (gabapentina, *O*-desmetiltramadol y *O*-desmetilvenlafaxina), y se estimaron los parámetros cinéticos a partir de los datos de eliminación de dichos microcontaminantes en cada efluente, resultando del mismo orden de magnitud en todos los efluentes. Posteriormente, se validó la aplicación del modelo para la operación de los reactores tipo ``raceway´´ en modo flujo continuo, y se simuló el efecto de la profundidad de líquido y el tiempo de residencia hidráulico en la capacidad de tratamiento. Los resultados de la simulación son de relevancia para el diseño de reactores tipo ``raceway´´, puesto que el área del reactor podría ser estimada en función del tiempo de residencia hidráulico y la profundidad de líquido que maximicen la capacidad de tratamiento en función de las condiciones de irradiación solar.

En resumen, el trabajo presentado en esta tesis doctoral es de relevancia para extender a gran escala el uso de los reactores tipo ``raceway´´, de bajo coste y alta eficiencia. A partir del estudio fenomenológico del proceso a escala de laboratorio, se han propuesto y validado modelos mecanísticos para del proceso tanto a pH ácido con Fe^{3+} como a pH neutro con Fe^{3+}-EDDS. Estos modelos, pueden ser adaptados a las condiciones de operación (radiación, composición del efluente, geometría del reactor etc.), para diseñar y optimizar la operación de los reactores tipo ``raceway´´ empleados para el tratamiento de efluentes reales de EDAR urbanas.

INTRODUCTION

1. INTRODUCTION

According to statistics mentioned in the World Water Development Report 2018 (UN Water, 2018), global water demand has been estimated to be around 4,600 km^3 y^{-1} and is expected to increase between 20% and 30% (from 5,500 to 6,000 km^3 y^{-1}) by 2050 (Burek et al., 2016). This report also ilustrates that the global use of water has increased by six times in the last 100 years, and continues to grow at a rate of approximately 1% per year. Furthermore, water pollution creates risks to human health and ecosystems, while reducing the availability of freshwater resources for human needs and the capacity of water-related ecosystems to provide goods and services, including the natural purification of water. Agricultural runoff is the principal source of pollutant loading such as pesticides. Inadequate management of municipal and industrial wastewater is another sizeable source of water pollution, especially in low-income countries, where only 8% of this type of wastewater is treated (Sato et al., 2013). Consequently, the development of policies and measures to promote sustainable water use is a global need. In Europe, the Water Framework Directive (WFD), which was approved in December 2000, arose from the need to establish a uniform legal framework throughout the EU territory to ensure the sustainable use of water resources (Directive 2000/60/EC). As a first consideration, it stated that "Water is not a commercial good, but a heritage that must be protected, defended and treated as such." In summary, the WFD includes the following points:

- The protection of all forms of water (superficial, subterranean, continental and transition).
- The regeneration of the ecosystems within these bodies of water and their surroundings.
- The reduction of pollution in water bodies.
- The commitment to sustainable water use by individuals and companies.

To mitigate the problem of water scarcity, wastewater regeneration is a challenge that needs to be deal with. Contaminants such as pesticides, pharmaceuticals, hormones and industrial chemicals, are resistant to treatment in conventional wastewater treatment plants (WWTPs). Consequently, they are continuously discharged into water bodies. The development of advanced analytical techniques allows these contaminants to be detected and quantified. Although their concentration is not high (ng L^{-1} - µg L^{-1}) they can result in toxic and adverse effects on aquatic organisms, crops and consequently on humans (Tousova et al., 2017). Despite the discharge of these compounds, named as

micropollutants or contaminants of emerging concern (CECs), from WWTPs into the environment not yet being regulated, there is increasing environmental concern about their removal (Barbosa et al.,2016). In the European Union, the first Watch List of substances for European Union-wide monitoring was reported in Decision 2015/495/EU of 20 March 2015 and updated in Decision 2018/840/EU of 5 June 2018. The updated list highlights 15 compounds to be monitored: three estrogens, (estrone, 17-alpha-ethinylestradiol and 17-beta-estradiol), five antibiotics (azithromycin, clarithromycin, erythromycin, amoxicillin and ciprofloxacin) and seven pesticides (methiocarb, imidacloprid, thiacloprid, thiamethoxam, clothianidin, acetamiprid (ACTM) and metaflumizone). To date, Switzerland is the only country which regulates micropollutant removal. The new Swiss water protection act came into force on January 2016 and requires that WWTPs be upgraded over the next twenty years to achieve 80% micropollutant removal with respect to raw wastewater (Eggen et al., 2014; Bourgin et al., 2018). However, a regulation shared by all European Countries is still under debate. In this regard, the monitoring of micropollutants in WWTP effluents for agricultural reuse is still one of the main issues to be addressed (Rizzo et al., 2018; European Parliament, 2019).

1.1- Advanced Oxidation Processes (AOPs)

Micropollutants are not successfully removed during the activated sludge process conventionally used as secondary treatment in WWTPs (Krzeminski et al., 2019). Consequently, research now focuses on the development of economic and environmentally sustainable tertiary treatments (Rizzo et al., 2019). In line with this, AOPs have been proposed as suitable techniques for micropollutant removal (Ribeiro et al., 2015). AOPs generate hydroxyl radicals, $HO^{\bullet}$, but also other free radical species such as hydroperoxyl radicals, $HO_2^{\bullet}$ and superoxide anion radicals, $O_2^{\bullet -}$, which contain at least one unpaired electron and are strongly oxidant. As a result, they degrade micropollutants to other simpler organic molecules until their complete mineralization. Among these radicals, $HO^{\bullet}$ stands out as the most oxidant (E^0 = +2.80 V) (Jain et al., 2018). Due to its non-selective nature, it reacts fast with a wide range of organic and inorganic contaminants, the rate constant of organic contaminant oxidation being in the order of 10^6 - 10^9 M^{-1} s^{-1} (Andreozzi et al., 1999). AOPs involve widely different methods of activation and oxidant generation, based on the combination of oxidants (H_2O_2, ozone), ultraviolet-

visible (UV-Vis) radiation and catalysts (Fe^{2+}/Fe^{3+}, TiO_2). Although the mechanisms of each micropollutant degradation are very different, they all occur in two steps, i) the in-situ generation of oxidative species and ii) their reaction with target contaminants, giving rise to oxidized intermediates or CO_2, H_2O and inorganic acids, in the case of complete mineralization. These mechanisms depend on process parameters and are affected by system design and wastewater components. A classification of the different AOPs, from processes established at full-scale to processes only studied at lab-scale is shown in Figure 1.

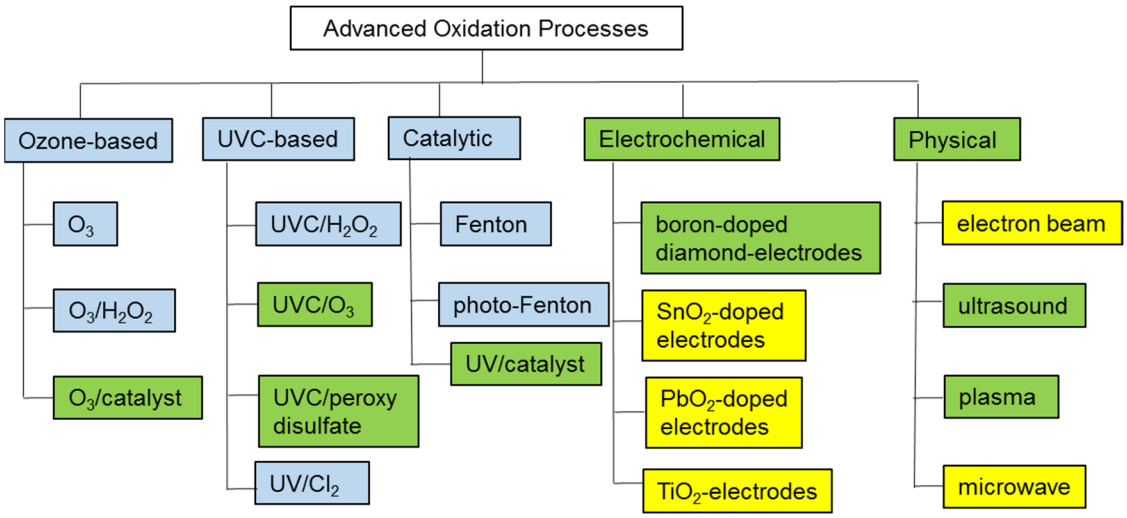

Fig. 1. Classification of AOPs (blue: processes at full-scale, green: processes at lab- and pilot-scale, and yellow: processes at lab-scale) (modified from Miklos et al., 2018).

The main drawbacks of ozone-based and UVC-based processes (processes established at full-scale) for micropollutant abatement are the operating costs related to equipment and energy consumption (Salimi et al., 2017; Krishnan et al., 2017). In this regard, photo-Fenton and UV/catalyst, such as UV/TiO_2, could be competitive, since they can be powered by sunlight. However, electrochemical, ultrasound and microwave processes are not currently considered as being energy efficient for micropollutants abatement.

In short, AOPs can be aimed at removing micropollutants from secondary WWTP effluents, disinfecting these effluents, or natural water. They can also be aimed at increasing the industrial wastewater biodegradability before conventional biological processes.

1.2- The photo-Fenton process

Among AOPs, the Fenton and photo-Fenton processes stands out as two of the most effective, energetically efficient and simple processes for micropollutant removal in wastewater. The Fenton reaction was described for the first time by Henry John Horstman Fenton, who discovered that H_2O_2 could be activated in the presence of ferrous ions to oxidize tartaric acid (Fenton, 1894). To put it briefly, it relies on the reaction between ferrous iron (as catalyst) and H_2O_2 (as oxidant) generating $HO^{\bullet}$ through the following sequence of reactions (Malato et al., 2009):

$$Fe^{2+} + H_2O_2 \rightarrow Fe^{3+} + HO^{\bullet} + HO^{-} \quad \text{Eq. (1)}$$

$$Fe^{3+} + H_2O_2 \rightarrow Fe^{2+} + H^{+} + HO_2^{\bullet} \quad \text{Eq. (2)}$$

$$Fe^{2+} + HO^{\bullet} \rightarrow Fe^{3+} + HO^{-} \quad \text{Eq. (3)}$$

$$H_2O_2 + HO^{\bullet} \rightarrow H_2O + HO_2^{\bullet} \quad \text{Eq. (4)}$$

$$Fe^{3+} + HO_2^{\bullet} \rightarrow Fe^{2+} + O_2 + H^{+} \quad \text{Eq. (5)}$$

$$Fe^{2+} + HO_2^{\bullet} + H^{+} \rightarrow Fe^{3+} + H_2O_2 \quad \text{Eq. (6)}$$

$$2HO^{\bullet} \rightarrow H_2O_2 \quad \text{Eq. (7)}$$

$$2HO_2^{\bullet} \rightarrow H_2O_2 + O_2 \quad \text{Eq. (8)}$$

$$HO_2^{\bullet} + HO^{\bullet} \rightarrow H_2O + O_2 \quad \text{Eq. (9)}$$

In the presence of proper illumination ferric iron is photoreduced to ferrous iron, Eq. (10), which is oxidized by H_2O_2 again, in a redox cycle (photo-Fenton). This process can be conducted under solar radiation or artificial lamps ($\lambda > 300$ nm) (Clarizia et al., 2017), being active until near visible ($\lambda < 560$ nm), depending on the iron complexes formed with water and other iron ligands dissolved in water. The use of solar radiation could make the process both economical and environmentally sustainable.

$$Fe^{3+} + H_2O + h\upsilon \rightarrow Fe^{2+} + HO^{\bullet} + H^{+} \quad \text{Eq. (10)}$$

The photo-reduction of the ferric ion is a reaction of ligand-metal charge transfer (LMCT). The ligand is any Lewis base capable of forming a complex with Fe^{3+}, such as aqua-complexes, Eq. (12) and carboxylate complexes, Eq. (13) - (Pignatello et al., 2006).

$$[Fe^{3+}L] + h\upsilon \rightarrow Fe^{2+} + L^{\bullet} \quad \text{Eq. (11)}$$

$$[Fe(H_2O)]^{3+} + h\upsilon \rightarrow Fe^{2+} + HO^{\bullet} + H^{+} \quad \text{Eq. (12)}$$

$$[Fe(OOC\text{-}R)]^{2+} + h\upsilon \rightarrow Fe^{2+} + CO_2 + R^{\bullet} \quad \text{Eq. (13)}$$

The maximum catalytic activity of iron has been reported to be at pH 2.8 (Pignatello et al., 1992), $Fe(OH)^{2+}$ being the predominant specie. At pH above 3, the concentration of photoactive $Fe(OH)^{2+}$ and dissolved iron decrease, and at pH higher than 4 the iron precipitates as ferric hydroxide, $Fe(OH)_3$ (Clarizia et al., 2017). Despite the high process efficiency at acidic pH, the need for acidification pretreatment as well as neutralization before discharge or reuse increases effluent salinity, environmental impact and treatment costs (Gallego-Schmid et al., 2019). Moreover, in the presence of sulfides or cyanides, the acidification can give rise to the discharge of gases into the atmosphere (Lipczynska-Kochany & Kochany, 2008). To deal with these drawbacks, research is currently beig focused on the study of the process at neutral pH.

Polycarboxylates and aminocarboxylates such as oxalate, citrate, nitrilotriacetic acid (NTA), ethylenediaminetetraacetic acid (EDTA), and ethylenediamine-N,N'-disuccinic acid (EDDS) form stable complexes with iron, allowing the homogeneous photo-Fenton to be run at neutral pH. These complexes absorb light in the UV-Vis range and also undergo photocatalytic decomposition, meaning, the ligand gives one electron to iron allowing it to be reduced. The quantum yields of these complexes are higher than that of $Fe(OH)^{2+}$, which is another advantage with respect to the photo-Fenton process at acidic pH. Several works show the high efficiency of the homogeneous process (De la Cruz et al.,2012; De Luca et al., 2014, De Luca et al., 2015; Santos-Juanes et al., 2017). However, further study regarding operating costs and process efficiency in real wastewater is needed.

Another way of carrying out the process at neutral pH is the application of heterogeneous photo-Fenton using mineral sources (such as goethite and hematite), suspended oxides (such as hydrolytic Fe^{3+} species), or iron fixed on a support structure (such us clays, zeolite, alumina and silica) (Scaratti et al., 2018; Redouane-Salah et al., 2018; Mahamallik & Pal, 2017). The main advantage of this strategy is the easy separation of the catalyst. Nonetheless, reaction rates are lower in comparison with the homogeneous

photo-Fenton process, due to the mass transfer limitations as well as the decrease in light penetration in the presence of solids (Malato et al., 2009).

1.3- The photo-Fenton process with Fe^{3+}-EDDS

EDDS is a structural isomer of EDTA with similar metal-complexing properties and two chiral centers in its structures. With six coordinating sites, EDDS forms both five- and six-membered chelate rings with metal ions, the molar ratio being of 1:1. Figure 2 shows the three stereoisomers, each of a different degree of biodegradability: [S,S]-EDDS (highly biodegradable), [R,R]-EDDS (resistant) and [R,S]-EDDS (relatively biodegradable). EDDS relies on forming a highly photon absorbent complex with Fe^{3+}, the redox potential being of 0.19 V. Fe^{3+}-EDDS is stable over a wide pH range of 3 – 9, the optimal pH for photo-Fenton being around 7.5 (Zhang et al., 2019).

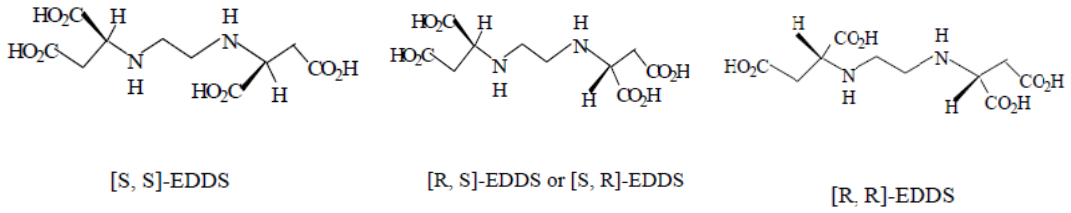

Fig. 2. Stereoisomers of EDDS (modified from Zhang et al., 2009).

In the presence of UV-Vis radiation, the Fe^{3+}-EDDS degradation is very fast, the 90% being degraded after 10 min of irradiation, and consequently the process is almost finished after 10 min (Wu et al, 2014). Zhang (2009) proposed a mechanism for photogeneration of $HO^{\bullet}$ by the photolysis of Fe^{3+}–EDDS, Eq. (14) – Eq. (18), the quantum yield being increased with the increase in the pH (Stasicka et al., 2011).

$$Fe^{3+} - EDDS + h\upsilon \rightarrow [Fe^{3+} - EDDS]^{*} \rightarrow Fe^{2+} + \text{organic radical} \quad \text{Eq. (14)}$$

$$\text{organic radical} + O_2 \rightarrow O_2^{\bullet -} + \text{oxidized organic radical} \quad \text{Eq. (15)}$$

$$Fe^{3+} + O_2^{\bullet -} \rightarrow Fe^{2+} + O_2 \quad \text{Eq. (16)}$$

$$2H^{+} + 2O_2^{\bullet -} \rightarrow H_2O_2 + O_2 \quad \text{Eq. (17)}$$

$$H_2O_2 + Fe^{2+} \rightarrow Fe^{3+} + HO^{\bullet} + HO^{-} \quad \text{Eq. (18)}$$

Huang et al. (2013) studied the degradation of bisphenol-A by the Fenton process with different concentrations of Fe^{3+}-EDDS, from 0.1 mM to 1 mM, and 5 mM H_2O_2, finding that high Fe^{3+}-EDDS concentrations promote the formation of $HO_2^{\bullet}/O_2^{\bullet-}$ and $HO^{\bullet}$, Eq. (19) and Eq. (20), and consequently micropollutant removal. Around 80% bisphenol-A was removed after 100 min of the reaction with 1 mM Fe^{3+}-EDDS. However, less than 20% bisphenol-A was removed after just over 200 min with 0.1 mM and 0.25 mM Fe^{3+}-EDDS. The effect of Fe^{3+}-EDDS concentration for degradation of bisphenol-A by photo-Fenton was also studied, using lower concentrations of Fe^{3+}-EDDS (in the range of 0.01 – 0.4 mM) and H_2O_2 (0.1 mM H_2O_2) (Huang et al., 2012). More than 80% bisphenol-A was removed after 5 min of the reaction, except with Fe^{3+}-EDDS concentrations lower than 0.05 mM. The results revealed that the higher the complex concentration the faster the rate of micropollutant removal. However, Fe^{3+}-EDDS acts as a scavenger of hydroxyl radicals at concentrations above 0.2 mM, and consequently, micropollutant removal is inhibited. The short reaction time as well as low Fe^{3+}-EDDS concentration required for the photo-Fenton process in comparison with the Fenton process point out the relevance of Fe^{3+}-EDDS photoreduction, Eq. (14), on the kinetics of the process.

$$Fe^{3+} - EDDS + H_2O_2 \rightarrow Fe^{2+} - EDDS + HO_2^{\bullet}/O_2^{\bullet-} + H^+ \quad \text{Eq. (19)}$$

$$Fe^{2+} - EDDS + H_2O_2 \rightarrow Fe^{3+} - EDDS + HO^{\bullet} + HO^- \quad \text{Eq. (20)}$$

Klamerth (2013) compared the efficiency of the photo-Fenton process both at neutral pH with Fe^{3+}-EDDS and at acidic pH to treat real municipal WWTP (MWWTP) effluents. With both treatments, around 95% micropollutant removal was achieved in tens of minutes with low reactant concentration, 0.09 mM iron and additions of H_2O_2 to maintain the concentration at 50 mg L^{-1}.

In addition, the efficiency of Fe^{3+}-EDDS for photo-Fenton has been compared with other complexes. Huang (2012) studied the effect of Fe^{3+}-EDDS, Fe^{3+}-EDTA, Fe^{3+}-citrate and Fe^{3+}-oxalate on bisphenol-A removal, the results showing much higher degradation rates with Fe^{3+}-EDDS than with the other complexes. Miralles-Cuevas (2014) compared the efficiencies of Fe^{3+}-EDDS and Fe^{3+}-citrate for solar photo-Fenton in real MWWTP effluents. Although high micropollutant efficiencies were achieved with both complexes, the Fe^{3+}:EDDS and Fe^{3+}:citrate molar ratios needed to achieve the same micropollutant abatement were 1:2 and 1:4, respectively.

Concerning the toxicity of the treatment with Fe^{3+}-EDDS, Rivas Ibáñez (2017) applied a battery of in vivo and in vitro bioassays to evaluate toxicity of the effluents before and after the treatment. The results revealed that estrogenicity and androgenic/glucorticoid activity are removed and the potential phytotoxicity and cytotoxicity are attenuated after the process. Cuervo Lumbaque (2019) investigated the toxicity of the transformation products (TPs) generated during the treatment. 16 TPs were classified as highly toxic, carcinogenic and mutagenic substances, among which 14 TPs were successfully removed at the end of the treatment.

A summary of the studies related to the application of Fe^{3+}-EDDS in both the Fenton and photo-Fenton processes is shown in Table 1. The efficiency of the processes in tubular reactors with compound parabolic collectors (CPCs) has been widely demonstrated with Fe^{3+} concentrations of around 0.1 mM at an Fe^{3+}:EDDS molar ratio of 1:2 (Klamerth et al., 2012). Recently, De la Obra (2017) has demonstrated the practicality of the low-cost raceway pond reactors (RPRs) under these conditions for the first time. However, working at this molar ratio could be a drawback for the treatment of real MWWTP effluents, since EDDS adds organic carbon to the water (0.2 mM EDDS add 24 mg L^{-1} dissolved organic carbon (DOC)), and consequently the limits for DOC established by legislation could be exceeded. In Andalusia (southern Spain), the daily emission limit for DOC to surface waters is 45.9 mg L^{-1}, Decree 109/2015. Consequently, the study of the effect of using lower Fe^{3+}:EDDS ratios could be of interest. Indeed, further studies on the operation of low-cost reactors such as RPRs are required.

Table 1. Studies on the Fenton and photo-Fenton processes with Fe^{3+}-EDDS.

Process	Water matrix	Scale of study	Target compound	$[H_2O_2]_0$	$[Fe^{3+}]_0$ (mM)	Fe^{3+}:EDDS	Micropollutant abatement (%)	Reaction time (min)	Reference
Fenton	Aqueous solution	Lab-scale	20 µM Bisphenol-A	5 mM	1	1:1	>80	100	Huang et al., 2013
Fenton	Aqueous solution	Lab-scale	0.15 mM trichloroethylene	$[CaO_2]_0$=2.25 mM	$[Fe^{2+}]_0$=0.75	1:1	98	180	Zhang et al., 2016
Photo-Fenton	Aqueous solution	Lab-scale	20 µM Bisphenol-A	0.1 mM	0.1	1:1	>80	5	Huang et al., 2012
Solar photo-Fenton	MWWTP effluent	CPC pilot plant	34.5 µg L^{-1} CECs	50* mg L^{-1}	0.09	1:2	88	8	Klamerth et al., 2012
Solar photo-Fenton	MWWTP effluent	CPC pilot plant	40.8 µg L^{-1} CECs	50* mg L^{-1}	0.09	1:2	95	63	Klamerth et al., 2013
Solar photo-Fenton	MWWTP effluent	CPC pilot plant	75 µg L^{-1} CECs	50* mg L^{-1}	0.1	1:2	90	4	Miralles-Cuevas et al., 2014
Solar photo-Fenton	MWWTP effluent	CPC pilot plant	500 µg L^{-1} CECs	65* mg L^{-1}	0.1375	1:2	90	10	Papoutsakis et al., 2015
Solar photo-Fenton	MWWTP effluent	RPR pilot plant	500 µg L^{-1} CECs	50 mg L^{-1}	0.1	1:2	90	30 – 90	De la Obra et al., 2017

*Concentration maintained during the experiment.

1.4- Solar photoreactors

Solar photocatalytic technology may be defined as that which efficiently collects solar photons and transfers them to a suitable reactor to promote specific catalytic reactions. The equipment that does this is called a solar collector. Traditionally, solar collector systems have been classified into three broad groups depending on the degree of concentration reached in them, which is directly related to the temperature attainable by the system (Rabl et al., 1979). The concentration factor (C) of a solar collector is defined as the relationship between collector aperture area and absorber area. The aperture area is the area that intercepts the radiation and the absorber area is the area of the component that receives the solar radiation. These three groups are: (i) non-concentrating, low concentration systems (up to 150ºC); (ii) medium-concentrating, systems (from 150ºC to 400ºC); (iii) high-concentrating systems (over 400ºC).

In contrast with thermal applications, photochemical processes normally use only high-energy photons (short wavelengths) to promote specific chemical reactions. However, in spite of the above, the technology needed to carry out solar liquid-phase photochemical applications has much in common with the technology used in thermal applications. This is the reason that the design of photochemical systems was initially based on conventional solar thermal collector designs like the parabolic-trough collector (PTC) (Anderson et al., 1991; Kelly & De Laquil (1992). Furthermore, the reactor must be transparent to photons and the reflective elements must reflect the appropriate wavelength for the process. Apart from that, thermal insulation is not necessary since the temperature plays no significant role in photocatalytic processes. Due precisely to this last point, the technology has been based on medium, low or non-concentrating solar devices (Alfano et al., 2000; Minero et al., 1993; Wyness et al., 1994).

Once these initial technological systems had been developed, the issue of whether to use concentrating (movable devices with solar tracking) or non-concentrating (static without solar tracking) collectors arose (Bockelmann et al., 1995; Malato et al., 1997). The main advantages and disadvantages of each of the different technologies for solar photocatalytic applications were summarized a long time ago, as follows (Malato et al., 2002). Advantages of non-concentrating systems: (i) they can make use of both direct and diffuse solar radiation; (ii) they are simpler systems; (iii) Water may not heat up significantly; (iv) they have both high optical efficiency, especially when there are no reflective devices, and quantum efficiency since there is a lower recombination of e^-/h^+

(semiconductor photocatalysis applications), given that the photonic density is lower than in a concentrating system. Disadvantages of non-concentrating systems: (i) they usually work with laminar flow, which can cause mass transfer problems. Advantages of concentrating systems: (i) they have a noticeably smaller reactor tube area in which to confine, control and handle the water; (ii) turbulent flow (favors mass transfer and avoids catalyst sedimentation); (iii) there is no evaporation of volatile compounds. Disadvantages of concentrating systems: (i) they only use direct solar radiation; (ii) usually expensive (iii) lower efficiency, both optical and quantum, the second arising from a high recombination of e^-/h^+ (semiconductor photocatalysis applications); (iv) water overheating.

The CPCs are a promising option, somewhere between parabolic concentrators and static flat systems, since they combine characteristics of both: they concentrate radiation, but they are static and collect diffuse radiation. They are also static collectors with a reflective surface designed for any given reactor shape and were invented in the 60s to achieve solar concentration with static devices (Collares-Pereira et al., 1991). They do so by illuminating the complete perimeter of the receiver, rather than just the "front" of it, as in conventional flat plates. These concentrating devices can be designed for a concentration factor of 1 (C=1), thus maintaining both the advantages of the PTC and static systems. If the CPC is designed for an acceptance angle of +90º to -90º, all incident solar diffuse radiation can be collected (Malato et al., 2009).

The light reflected by the CPC is distributed all over the tubular receiver meaning almost the entire circumference of the receiver tube is illuminated (Figure 3). The advantages of CPCs can be summarized as follows. The photoreactor is tubular, which mean the water can be pumped easily. CPCs are generally manufactured with an aluminum reflector and the structure is made of a simple frame that also provides the support for connecting the tubes, normally glass (Blanco et al., 1999). There is no evaporation of possible volatile compounds and water does not heat up. They have high optical efficiency, since they make use of almost all the available radiation, along with quantum efficiency, as they do not receive a high flow of photons. Flow is turbulent inside the tube reactor. The CPCs have the advantages of both technologies and none of the disadvantages, thus being defined as the best option for photocatalytic processes based on the use of solar radiation (Ajona & Vidal, 2000; Malato, et al., 2002). They can make highly efficient use of both direct and diffuse solar radiation, without the need for solar tracking (Blanco et al., 1999).

Fig. 3. CPC basic design and pilot plant.

Currently, the tubular photoreactors with compound parabolic collectors (CPCs), are the most commonly used in photocatalytic processes for very different applications (Spasiano et al., 2015) but recently RPRs have been introduced for the specific application and mild treatment at neutral pH of micropollutants in effluents from WWTPs.

RPRs were initially developed by Oswald, in the late 1950s, for the treatment of wastewater by a biological process based on the interaction between bacteria and microalgae. They consist of extensive reactors with channels in a closed loop, provided with a paddle wheel connected to an engine to recirculate the water (Figure 4). They are also equipped with baffles to ensure homogeneous flow avoiding dead zones. The efficiency and feasibility of using RPRs for the photo-Fenton process was demonstrated for the first time by Carra (2014b). In terms of the yearly season, treatment capacities from 40 to 133 mg m^{-2} h^{-1} have been reported for the process at acidic pH (Rivas et al., 2015). In contrast with CPCs, the cost associated with the treatment in RPRs is low, since the power requirements for mixing are only just over 4 W m^{-3} and the construction costs are around 10 € m^{-2}. Additionally, the liquid depth in the reactor as well as the iron concentration can be varied according to the availability of solar radiation for a better use of photons that reach the reactor surface. This is an advantage in comparison with CPCs, in which the use of photons under high solar radiation conditions can be inefficient due the short light path lengths, limited by the tube diameter. In terms of mass of micropollutant removed per kJ of UV energy, removal efficiencies of 1.07 mg kJ^{-1} and

0.26 mg kJ^{-1} have been reported for the photo-Fenton process at neutral pH in RPRs and CPCs, respectively (De la Obra et al., 2017). Consequently, the use of RPRs for the photo-Fenton process is currently being widened. Pinheiro da Costa (2019) has studied the removal of the fungicide carbendazim at acidic pH in a 5-cm RPR, with more than 96% micropollutant removal being achieved in 15 min with low reactant concentration. The high efficiency of RPRs when treating textile industry effluents has also been demonstrated, with treatment capacities two or three times higher than those achieved in CPCs and with lower CO_2 emissions (Belalcázar-Saldarriaga et al., 2018; Cabrera-Reina et al., 2019). In addition, the operation of RPRs in continuous flow mode for the photo-Fenton process at acidic pH has recently been proposed for the first time (Arzate et al., 2017). This has opened up a new line of research based on optimizing the operation of these photoreactors. In this regard, more research on the feasibility of RPRs to carry out the process at neutral pH is required.

Due to RPRs being open channels, their use is not recommended when the treatment requires long reaction times or for the treatment of highly toxic effluents. As such rapid treatments (tens of minutes) at neutral pH of micropollutants in effluents from WWTPs is a highly promising application of RPRs.

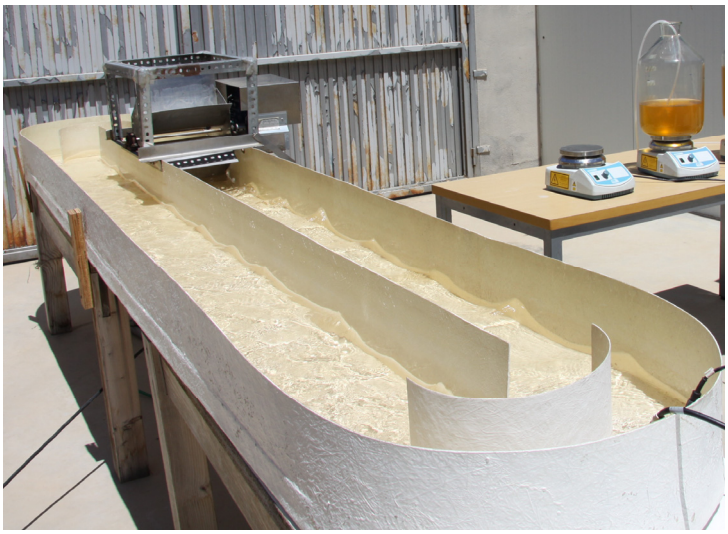

Fig. 4. 360-L RPR.

1.5- Photon absorption in the reactor

The knowledge of the radiation field in photoreactors is fundamental for maximizing the efficient use of photons as well as determining intrinsic kinetic parameters of photochemical reactions. To determine the radiation field, the Radiative Transfer

Equation (RTE) must be solved. It describes the radiation intensity at any position along a ray pathway through a medium. In homogeneous systems (without scattering) in which the photon emission by absorbing species can be neglected, the RTE is defined by Eq. (21) (Cassano et al.,1995):

$$\frac{dI_{\lambda,}(s,\Omega,t)}{ds} = -\kappa_{\lambda}(s,t)\, I_{\lambda,}(s,\Omega,t) \qquad \text{Eq. (21)}$$

where I_{λ} is the spectral specific intensity, Ω and s denote the direction and the distance of photon transport, respectively and κ_{λ} is the volumetric absorption coefficient.

When the medium is transparent and there is no absorption of radiation, the specific intensity does not change with distance. However, when there is photon absorption, the intensity changes according to the Bouguer-Lambert law for homogeneous media. However, if other phenomena, such as scattering, occur, this law is not sufficient to describe the involved phenomena, since the Bouguer-Lambert law is only valid only for photon absorption along the direction of propagation.

In a homogeneous medium, the change in the radiation intensity along the ray trajectory is only caused by the absorption process in the reaction medium. This variation can be expressed by an equation that involves the volumetric absorption coefficient, which is a function of wavelength and variables such as temperature and composition. The absorption coefficient can be determined accurately by studying the photon absorption by molecules or atoms exposed to a radiation field. Macroscopically, the volumetric absorption coefficient is linearly dependent on the concentration of absorbing species, Eq. (22) (Cassano et al.,1995).

$$\kappa_{\lambda,i} = \alpha_{\lambda,i} C_i \qquad \text{Eq. (22)}$$

where i denotes each absorbing species, $\kappa_{T,\lambda}$ is the volumetric absorption coeffcient, $\alpha_{\lambda,i}$ is the molar absorptivity and C_i stands for the molar concentration of the absorbing species.

The local volumetric rate of photon absorption (LVRPA) is defined as the amount of photons that are absorbed per unit time and unit reaction volume. It depends on the photon source, the concentration of absorbing species, the optical properties of the system and the reactor geometry. Despite being defined for monochromatic radiation, it can be extended to polychromatic fields by integrating over the wavelength. When working under solar radiation, the LVRPA values corresponding to the direct and diffuse radiation are calculated in a different way. In homogeneous systems in which radiation can be modeled with one spatial coordinate, the monochromatic LVRPA corresponding to the absorption of direct radiation can be calculated by Eq. (23), (Conte et al., 2016).

$$e_{\lambda}^{a}(x,t) = q_{w,\lambda}\kappa_{\lambda}(t)exp\left[-\kappa_{T,\lambda}(t)x\right] \quad \text{Eq. (23)}$$

where $q_{w,\lambda}$ is the discretized incident radiation, κ_{λ} is the volumetric absorption coefficient of the absorbing species, and $\kappa_{T,\lambda}$ is the volumetric absorption coefficient of the medium.

The absorption of diffuse radiation is a more complex concept. Brandi (2003) applied the hypothesis of azimuthal symmetry (rays propagating in one spatial coordinate (x) and one angular coordinate (θ)) to model the absorption of diffuse radiation in a simple lab-scale photoreactor. In this case, the RTE for homogeneous systems can be defined by Eq. (24).

$$cos\theta\,\frac{dI_{\lambda,\Omega}(x,t)}{dx} - \kappa_{\lambda}(s,t)I_{\lambda,\Omega}(x,t) = 0 \quad \text{Eq. (24)}$$

Integrating Eq. (24) with the boundary conditions corresponding to photons moving both forward and backwards, the diffuse LVRPA can be calculated as follows:

$$e_{\lambda}^{a}(x,t) = 2\Pi I_{\lambda}^{0}\kappa_{\lambda}(t)\int_{-\frac{\Pi}{2}}^{\frac{\Pi}{2}}\exp\left[-\frac{\kappa_{\lambda}(t)}{cos\theta}x\right]sen\theta\,d\theta \quad \text{Eq. (25)}$$

As mentioned above, the LVRPA is defined for monochromatic radiation. For solar radiation (polychromatic radiation), the LVRPA can be computed by Eq. (26). Furthermore, in perfectly-mixed reactors with constant cross-sectional are under

photolimitation conditions (the reaction rate depends linearly on the photon absorption), the LVRPA can be averaged across the reactor volume, Eq. (27) (Brandi et al., 2003):

$$e^a(x,t) = \int_{\lambda min}^{\lambda max} e_\lambda^a(x,t)\, d\lambda \qquad \text{Eq. (26)}$$

$$\langle e^a(x,t)\rangle_{V_R} = \frac{1}{L_R}\int_0^{L_R} e^a(x,t)\, dx \qquad \text{Eq. (27)}$$

where L_R and V_R stand for reactor length and reactor volume, respectively.

1.6- Factors affecting the photo-Fenton process

UV-Vis radiation

Sunlight has been demonstrated to be a useful radiation source for the photo-Fenton process, with a wide wavelength range (polychromatic radiation) in comparison with UV lamps. This is due to longer wavelengths overcome the effects of photon absorption by other absorbing species different to iron by photolysing Fe^{3+} complexes (Malato et al., 2009). In the not photosaturated photo-Fenton process, the reaction rate depends linearly on the intensity of radiation. Therefore, when the generation of $HO^{\bullet}$ depends on radiation availability, it becomes the limiting variable (Carra et al., 2014a). Rivas (2015) studied the effect of radiation intensity in the process carried out in RPRs, and found that shallow liquid depths of around 5 cm and low iron concentration of 5 mg L^{-1} are enough to take advantage of photons reaching the reactor surface under low UVA irradiation conditions (≈10 W m^{-2}). However, at high UVA irradiances of around 30 W m^{-2}, higher iron concentrations and liquid depths should be used to avoid photosaturation. Consequently, the limitation range of radiation is very important for the design and operation of reactors, with a more in-deepth study on the effect on photolimitation and photosaturation on the photo-Fenton process being needed.

Temperature

The temperature is also an important factor which affects the kinetics of the process. Farias (2009) found that the effect of temperature is more prominent in the absence of light (thermal Fenton), with the kinetics of micropollutant removal being strongly

accelerated. Zapata (2009) reported that photo-Fenton efficiency rises gradually with temperature, the optimum temperature range being 35 – 45 ˚C. At higher temperatures, process efficiency decreases due to iron precipitation. Furthermore, the decomposition of H_2O_2 is favored at high temperatures, and consequently high temperatures can lead to a higher H_2O_2 consumption being required to achieve the same level of decontamination (Malato et al., 2009).

Reactant concentration

The increase in iron concentration favors the reaction rate, this increase not being directly proportional as the Fenton reaction and formation of different iron-complexes are also involved. Light penetration in the reaction medium is attenuated by the extinction coefficient, which mainly depends on iron concentration. Therefore, too high a concentration (>1 mM) must be avoided in usual photoreactors designs of several cm pathlength (Malato Rodríguez et al., 2004). As for H_2O_2, too low a concentration gives rise to a lower reaction rate. In contrast, when the concentration is too high, H_2O_2 can act as an $HO^{\bullet}$ scavenger. The optimal H_2O_2 concentration depends on iron concentration, photoreactor design, type of contaminant and also its concentration. It ranges from the stoichiometric concentration (enough H_2O_2 to completely oxidize organic contaminants) to several times the stoichiometric value. Stoichiometric concentration is easy to calculate from the chemical oxygen demand (COD) of wastewater to be treated (Malato et al., 2009).

When micropollutant removal is the target of the treatment mild oxidation conditions are enough to achieve high removal efficiencies, the H_2O_2:Fe molar ratio commonly used being 2 – 150 (Clarizia et al., 2017). Concentrations of around 20 mg L^{-1} and 50 mg L^{-1} for iron and H_2O_2, respectively, have been reported as being optimal to carry out the process in CPCs of around 5 cm optical pathlength (Klamerth et al., 2009). In RPRs, the optimal iron concentration is reduced to 5.5 mg L^{-1} (Carra et al., 2014b).

Salinity

The presence of inorganic anions such as chloride, sulfate, carbonate or phosphate may significantly affect the efficiency of the Fenton process (Lado Ribeiro et al., 2019). To

put it briefly, both chlorides and sulfates form strong complexes with iron, Eq. (28) – Eq. (32) (Bacardit et al., 2007), which affects the distribution and reactivity of iron species. These complexes can absorb light yielding chlorine radicals and sulfate radicals, respectively, Eq. (33) – Eq. (35) (Kiwi et al., 2000, Machulek Jr. et al., 2009), which are less oxidant than $HO^{\bullet}$. Both ions can also scavenge hydroxyl radicals giving rise to the generation of radical anions less oxidant than hydroxyl radicals, Eq. (36) – Eq. (37).

$$Fe^{2+} + Cl^{-} \leftrightarrow FeCl^{+} \quad \text{Eq. (28)}$$

$$FeCl^{+} + Cl^{-} \leftrightarrow FeCl_2^{0} \quad \text{Eq. (29)}$$

$$Fe^{3+} + Cl^{-} \leftrightarrow FeCl^{2+} \quad \text{Eq. (30)}$$

$$Fe^{3+} + 2Cl^{-} \leftrightarrow FeCl_2^{+} \quad \text{Eq. (31)}$$

$$Fe^{3+} + {SO_4}^{2-} \leftrightarrow FeSO_4^{+} \quad \text{Eq. (32)}$$

$$FeCl^{2+} + h\upsilon \rightarrow Cl^{\bullet} + Fe^{2+} \quad \text{Eq. (33)}$$

$$FeCl_2^{+} + h\upsilon \rightarrow Cl^{\bullet} + FeCl^{+} \quad \text{Eq. (34)}$$

$$FeSO_4^{+} + h\upsilon \rightarrow Fe^{2+} + SO_4^{\bullet -} \quad \text{Eq. (35)}$$

$$Cl^{-} + HO^{\bullet} \rightarrow [ClHO]^{-} \quad \text{Eq. (36)}$$

$$SO_4^{2-} + HO^{\bullet} \rightarrow SO_4^{\bullet -} + HO^{-} \quad \text{Eq. (37)}$$

Bicarbonates are also strong scavengers of hydroxyl radicals, Eq. (38), and consequently inhibit micropollutant removal (Buxton et al.,1988). Concerning phosphates, they complex both ferrous and ferric iron, Eq. (39) – Eq. (40). This is a drawback for the photo-Fenton process, since once ferric iron is complexed by phosphates, it precipitates.

$${HCO_3}^{-} + HO^{\bullet} \rightarrow {CO_3}^{\bullet -} + H_2O \quad \text{Eq. (38)}$$

$$Fe^{2+} + {H_2PO_4}^{-} \rightarrow FeH_2PO_4^{+} \quad \text{Eq. (39)}$$

$$Fe^{3+} + {H_2PO_4}^{-} \rightarrow FeH_2PO_4^{2+} \quad \text{Eq. (40)}$$

Contaminant concentration

In general, the higher the contaminant concentration, the longer the treatment time. This affects reactor design and scaling of the process, since the correlation of treatment time and contaminant concentration must be determined experimentally (Malato et al., 2009).

For highly contaminated effluents, as in the case of industrial effluents, the application of a pre-treatment or a biological process such as a membrane bioreactor is recommended (Cabrera Reina et al., 2015a). This pre-treatment reduces organic load as well as toxicity (Ballesteros Martin et al., 2010). Another drawback of highly contaminated effluents is that certain compounds complex iron and avoid its photoactivation (Malato et al., 2009). In the case of high organic load but low concentration of hazardous organic substances (of the order of ng L^{-1}- μg L^{-1}), a biological treatment before the photo-Fenton process is recommended. Otherwise, when organic load is low and contaminant concentration represents a high fraction of it, a pre-concentration step can be used before photo-Fenton treatment (Miralles-Cuevas et al., 2014).

Accordingly, water composition can strongly affect the kinetics of the process. In order to scale-up the process, more research on the variation in salinity as well as organic matter (within the concentration ranges in real WWTP effluents) is required.

1.7- Photo-Fenton modeling

The photoreactor design plays a fundamental role when scaling up the process. Variables such as reactor geometry, environmental conditions (temperature and irradiance) and reactant concentration affect the kinetics of the process, and consequently reactor design. In this regard, the development and validation of models (empirical or mechanistic) to control and optimize the treatment in WWTPs is essential.

Empirical kinetic models such as response surface and neural networks models provide valuable information on micropollutant removal as a function of key parameters. Once the experimental setup is defined, the micropollutant removal by photo-Fenton can be investigated systematically within a selected experimental framework (Alvarez-Gallegos et al., 2018). In short, the steps to carry out these types of studies are:

- Experimental design set up according to the factors and responses to study.

- Execution of the corresponding tests.

- Selection of the model to be used.

- Estimation of model parameters based on an error criterion that must be minimized.

- Determination of the optimal operating conditions through the analysis of results.

Schenone (2015) applied a three-level factorial experimental design to model the photo-Fenton degradation of the herbicide 2,4-dichlorophenoxyacetic acid at circumneutral pH with the ferrioxalate complex. The experimental design included the effect of temperature and H_2O_2:2,4-dichlorophenoxyacetic acid initial concentration ratio. Shokry (2015) applied ordinary kriging, artificial neural networks and support vector regression to model and predict the total organic carbon (TOC) removal in a photo–Fenton pilot plant. The three methods successfully fitted experimental data even when few training points were available, which allowed the time and cost of experimental work to be saved. Rivas (2015) used a Langmuir–Hinshelwood type model to predict apparent first order rate constant of H_2O_2 consumption by photo-Fenton at acidic pH in RPR, the effects of photon absorption and irradiance saturation being included. As for the model micropollutant, ACTM, degradation rate was determined in two steps: in the first minutes of the reaction its apparent first order rate constant was determined as a linear function of iron concentration. After that, it was estimated as a linear function of H_2O_2 concentration. Recently, Giannakis (2017) has developed second degree models for removal of the antidepressant venlafaxine by photo-Fenton by using the response surface methodology (3 pH-specific central composite designs). The models were used as input for the desirability functions to obtain the optimal regions for operating the photo-Fenton process.

These empirical models provide simple kinetic expressions very useful for design, but do not provide information about the reaction mechanism. To this end, mechanistic kinetics models are developed. They consist of a set of differential equations which describe the changes in the concentration of the main chemical species involved in the process as a function of time. These models have the great advantage of being applicable to any compound or mixtures. Furthermore, different configurations of the model can be proposed by studying which of them allows a better fit. The steps to develop a mechanistic model of photo-Fenton process can be summarized as follows (Alfano et al., 2015):

- Firstly, a kinetic model to represent micropollutant removal by photo-Fenton in a lab-scale reactor must be proposed. Mass balances are applied to determine the theoretical evolution of the species involved in the process. To describe the effect of radiation absorption on the degradation rates, the evaluation of the radiation field inside the photoreactor is fundamental. In order to obtain rate equations regardless of the

experimental radiation conditions, the local volumetric rate of photon absorption (LVRPA) should be introduced into the model.

- To estimate the kinetic parameters, the differences between experimental data and model predictions are minimized by applying a nonlinear optimization algorithm.

- Finally, the model obtained at lab-scale must be validated under real conditions in a pilot-scale reactor. When working under solar radiation, the model must include direct and diffuse radiation fluxes reaching the reactor surface, since they represent the boundary conditions for the resolution of the radiation transfer equation inside the reactor.

Along these lines, Andreozzi (2000) modeled the oxidation of benzothiazole (0.01 mM) by the photo-Fenton in the pH range 2.0 - 3.2 with a set of 21 reactions. The model successfully predicted the influence of H_2O_2, Fe^{3+} and sulfate concentration on system reactivity. However, when varying the pH of the reaction medium, the model was not able to fit the results. Conte (2012) proposed a kinetic model of 15 reactions for the photo-Fenton degradation of the herbicide 2,4-dichlorophenoxyacetic acid (2,4-D) at acidic pH. The kinetic study was performed in a lab-scale reactor. The effects of iron concentration, H_2O_2:2,4-D initial concentration ratios, radiation level and temperature were all studied. Afterwards, the model was used to predict reactant concentrations over the reaction time in a pilot-plant solar reactor designed to make use of UV-Vis and infrared solar radiation. Cabrera Reina (2015b) proposed a simplified kinetic model of 9 reactions for photo-Fenton mineralization of paracetamol (1 mM) at acidic pH in RPRs, the effect of the average volumetric rate of photon absorption (VRPA) and the liquid depth being included.

The development of kinetic models at neutral pH is an even more complex task. As a previous step, it is necessary to develop more knowledge related to reaction mechanisms. In this regard, to study the effects of the variation in the rate of photon absorption due to iron precipitation as well as the generation of different iron species over reaction time is fundamental.

OBJECTIVES

AND WORK PLAN

2. OBJECTIVES AND WORK PLAN

The main goal of this Ph.D. thesis is to investigate the kinetics of micropollutant removal from MWWTP secondary effluents by the solar photo-Fenton process and to develop kinetic models that allow the operation of photoreactors to be controlled and optimized. The removal of micropollutants by the photo-Fenton process has been widely studied at acidic pH. Apart from that, there is growing interest in the development of operating strategies to deal with the drawbacks related to operating at acidic pH. In this regard, the operation of the process at neutral pH with Fe^{3+}-EDDS has been demonstrated to be an efficient alternative. However, more research on operating conditions, kinetic mechanisms as well as the assessment of low-cost reactors is needed. Furthermore, to demonstrate the efficiency of the process when applied to real MWWTP effluents of very different composition is a challenge. This is fundamental for the further development of models which allow to be adapted to perturbations in MWWTPs. To this end, the following specific objectives were addressed:

2.1- To develop a mechanistic kinetic model to predict micropollutant removal by solar photo-Fenton at acidic pH as a function of environmental variables (solar irradiance and temperature), geometrical variables (light path length) and operating variables (iron concentration). This objective is addressed in Section 4.1.

Both empirical and mechanistic kinetic models have previously been developed for the operation of the process at acidic pH. However, a model which combines the effects of all the factors affecting the process in low-cost reactors such as RPRs has not yet been proposed.

With this aim in mind, the effect of temperature and photon absorption on the kinetics of micropollutant removal in synthetic secondary MWWTP effluent was studied. The effluent was doped with 100 μg L^{-1} acetamiprid as a model micropollutant, which is a highly recalcitrant pesticide included on the EU watch list of priority hazardous substances. The assays were carried out in stirred tank reactors of 5 cm (0.35 L) and 15 cm (1.05 L) liquid depth placed inside a solar simulator. Reactant concentrations were 0.1 mM (5.5 mg L^{-1}) Fe^{2+} and 1.47 mM (50 mg L^{-1}) H_2O_2. The temperature was varied in the range 10 – 40 ˚C, and the UVA irradiance on the reactor surface was ranged from 10 to 40 W m^{-2}. The model obtained at lab-scale was validated outdoors in RPRs of 5 cm

(120 L) and 15 cm (360 L) liquid depth under UVA irradiances of around 30 W m^{-2} and temperature around 25 ˚C.

2.2- To study the effect of VRPA on the kinetics of micropollutant removal with the Fe^{3+}-EDDS complex by solar photo-Fenton at neutral pH. This objective is addressed in Section 4.2.

To reduce operating costs and to avoid an increase in water salinity related to the operation of the process at acidic pH, the operation at neutral pH with Fe^{3+}-EDDS has been proposed. However, an in-depth study of the effect of photon absorption of this complex is required to optimize the process.

Firstly, the effect of the reactions involved in the photolysis of Fe^{3+}-EDDS as well as the effect of H_2O_2 concentration (0.74, 1.47 and 2.94 mM) on Fe^{3+}-EDDS decomposition by Fenton and photo-Fenton were studied. Then, the effect of photon absorption on micropollutant removal from synthetic secondary effluent doped with 100 μg L^{-1} acetamiprid by photo-Fenton was tested. To this end, experiments were conducted with 0.1 mM Fe^{3+} at Fe^{3+}:EDDS molar ratio of 1:1 and 0.88 mM H_2O_2 in stirred tank reactors of 5 cm (0.85 L) and 15 cm (2.85 L) liquid depth. The UVA irradiance on the reactor surface was varied from 10 to 50 W m^{-2}, which corresponds to 383 and 1933 μE m^{-3} s^{-1} VRPA. Finally, the effect of VRPA on treatment capacity was evaluated.

2.3- To study the effect of the composition of MWWTP effluents on the kinetics of micropollutant removal and process efficiency by solar photo-Fenton at neutral pH. This objective is addressed in Section 4.3.

To scale-up the process, the study of the efficiency when applied to real effluents is fundamental. However, no studies comparing the efficiency in different MWWTP effluents have previously been reported.

To this end, secondary effluents of very different composition and source (0.9 – 2.2 mS cm^{-1} conductivity, 10 – 20 mg L^{-1} organic matter) were collected from MWWTPs located in different areas of Spain (Girona, Alicante and Almería). The effect of effluent composition on the kinetics of total load of micropollutant removal evaluated by LC-MS/MS was investigated. Photo-Fenton assays were developed outdoors in an RPR of 5

cm liquid depth (19 L) under UVA irradiances of around 30 W m^{-2}. The optimal oxidation conditions, previously used in the studies conducted with synthetic effluents, were tested in order to determine if they are suitable for the treatment of different real MWWTP effluents.

2.4- To develop a mechanistic kinetic model to predict micropollutant removal by solar photo-Fenton at neutral pH with the Fe^{3+}-EDDS complex as a function of UVA radiation and reactor geometry. This objective is addressed in Section 4.4.

Despite the large number of works related to the photo-Fenton process with Fe^{3+}-EDDS, a model able to predict micropollutant removal as a function of VRPA has not yet been developed.

As such, once the process phenomenology had been studied, a kinetic mechanism of solar photo-Fenton with Fe^{3+}-EDDS was proposed. The experimental data obtained from the study of the effect of photon absorption on acetamiprid removal (Objective 2.2.) were used to estimate the model parameters. The model was validated outdoors in an RPR of 5 cm liquid depth (19 L) both in winter and summer.

2.5- To design a solar photo-Fenton plant for micropollutant removal from MWWTP effluents at neutral pH. This objective is addressed in Section 4.5.

The study of the phenomenology of the process under controlled conditions with demineralized water or synthetic effluents is necessary to understand the reaction mechanisms and propose kinetic models. Afterwards, the model performance must be evaluated under real conditions, the parameters being tuned (if required) according to effluent composition. This is a difficult task but essential for extending the model application to the design of treatment plants. However, it has not been developed before.

To deal with this objective, the mechanistic kinetic model proposed for acetamiprid removal in synthetic effluent (Objective 2.4) was applied to the three most abundant compounds detected in all the real MWWTP effluents studied in Objective 2.3. The search for model parameters was done by type of effluent and the next step was the model validation for RPR operation in continuous flow mode.

MATERIALS AND METHODS

3. MATERIALS AND METHODS

3.1- Chemicals

[S,S]-EDDS (35%, w/v), sulfuric acid (95%, w/v), formic acid (95%, w/v), ascorbic acid (99%, w/w), titanium (IV) oxysulfate (1.9%, w/v), tetrabutylammonium hydrogen sulfate (97%, w/w), $MgSO_4$, (98%, w/w), $(NH_4)_2SO_4$ (99%, w/w), humic salt (99%, w/w), sodium lauryl sulfate (98.5%, w/w), sodium lignin sulfonate, arabic acid, acacia gum powder (99%, w/w), $CaSO_4 \cdot 2H_2O$ (98%, w/w) and high purity analytical standards (>97%) were obtained from Sigma-Aldrich (Steinheim, Germany). EPIK® (ACTM, $C_{10}H_{11}ClN_4$, 20% w/w) was supplied by Tecnidex S.A. (Valencia, Spain). Sodium formate (99%, w/w) was acquired from Merck Millipore (Darmstadt, Germany). Sodium bicarbonate (99.7%, w/w) was provided by Riedel-de Haën (Seelze, Germany). Ferric sulfate hydrate (75%, w/w), ferrous sulfate heptahydrate (99%, w/w), hydrogen peroxide (33%, w/v), acetic acid (99.7%, w/v), o-phenantroline (99%, w/w), KCl (99%, w/w) and hydrochloric acid (37%, w/v) were obtained from Panreac (Barcelona, Spain). Beef extract powder and peptone were purchased from Biolife (Milan, Italy) and BD Bacto (Le Pont de Claix, France), respectively. Acetonitrile and methanol were high pressure liquid chromatography (HPLC) grade and supplied by Sigma-Aldrich. Ultrapure water was produced with a Millipore Direct-Q® Ultrapure Water System (Bedford, MA, USA).

3.2- Chemical analysis

H_2O_2 and total dissolved iron were spectrophotometrically determined by colorimetric methods. H_2O_2 was measured at 410 nm using titanium (IV) oxysulfate solution (DIN 38 402H15). The concentration of iron was determined at 510 nm according to the o-phenanthroline standardized procedure (ISO 6332). The limit of quantification (LOQ) was $2.9 \cdot 10^{-2}$ and $4.5 \cdot 10^{-3}$ mM, for H_2O_2 and iron, respectively.

ACTM concentration was determined by a 1200 Series system consisting of an ultra-high pressure liquid chromatography with diode array detector (UHPLC-DAD) from Agilent Technologies (Waldbronn, Germany). The mobile phase consisted of a gradient mixture of acetonitrile and dilute formic acid (0.1%, *v*/*v*). The gradient used was initially set at 15% acetonitrile, progressively increasing the concentration to 50%, the flow being 1 mL

min^{-1} (Rivas et al., 2015). The retention time and the LOQ were 3.59 min and 5 μg L^{-1}, respectively.

The method for quantification of Fe^{3+}-EDDS was set up in collaboration with the Solar Water Treatment Department in the Plataforma Solar de Almería (PSA) according to the protocol previously described in (Hu et al., 2014). The complex was measured by (UHPLC-DAD) from Agilent Technologies (Waldbronn, Germany), using Isocratic elution. The mobile phase consisted of a mixture of methanol and an aqueous solution of sodium formate (15 mM) and tetrabutylammonium hydrogen sulfate (2 mM) at pH 4, at a percentage of 5% and 95%, respectively, the flow being 0.5 mL min^{-1}. The LOQ was 3.5 10^{-3} mM.

Fig. 5. UHPLC-DAD (Agilent Technologies 1200 series).

DOC and inorganic carbon (IC) were quantified with a Shimadzu-V CPH TOC analyzer (Shimadzu Corporation, Kyoto, Japan), the LOQ being 1 mg L^{-1}.

Fig. 6. Shimadzu analyser used for DOC and IC measurement.

The concentration of anions was measured by ion chromatography Metrohm 881 Compact IC pro (Herisau, Switzerland), the eluent being a solution of Na_2CO_3 at a flow of 0.8 mL min^{-1}. The LOQ was 0.5 mg L^{-1}.

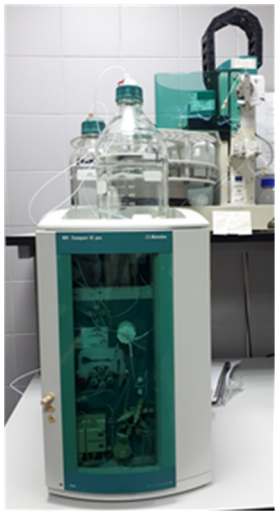

Fig. 7. Metrohm 881 Compact IC pro system.

The quantification of micropollutants in the real MWWTP effluents was carried out in collaboration with the Environmental Analysis and Water Treatment research group at the CIESOL, according to the protocol developed by Campos-Mañas (2017). The micropollutants were determined by LC coupled to a hybrid quadrupole lineal ion trap trap-mass spectrometry analyzer (LC-QqLIT-MS/MS), the instrumentation consisting of an Agilent 1200 LC system (Agilent Technologies, Foster City, CA, USA) and a 5500 QTRAP analyzer (AB Sciex Instruments, Wilmington, DE, USA).

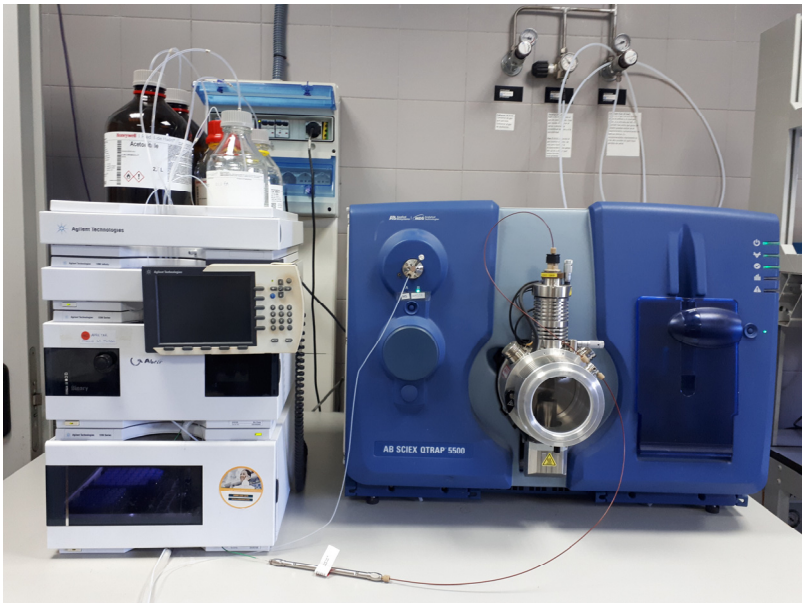

Fig. 8. Agilent 1200 LC system and a 5500 QTRAP analyzer.

3.3- Water matrices

The experiments were carried out with demineralized water, synthetic and real secondary MWWTP effluents. The recipe for synthetic effluent is shown in Table 2 (Rivas et al., 2014).

Table 2. Synthetic secondary effluent composition.

Compound	Concentration (mg L^{-1})
Beef extract powder	1.8
Peptone	2.7
Acacia gum powder	4.7
Arabic acid	5.0
Sodium lauryl sulfate	0.9
Sodium lignin sulfonate	2.4
Humic salt	4.2
$CaSO_4 \cdot 2H_2O$	60.0
$MgSO_4$	60.0
KCl	4.0
$(NH_4)_2SO_4$	23.6
K_2HPO_4	7.0
$NaHCO_3$	96.0

For the experiments conducted with real wastewaters, secondary effluents were collected from five MWWTPs located in the Mediterranean area of Spain: Alcoy (Alicante province, east of Spain), El Bobar (Almeria city, southeastern of Spain), El Ejido (Almeria province), El Toyo (Almeria province) and Girona (Catalonia, northeastern of Spain). The plants treat the wastewater for a population equivalent to 120,679; 315,000; 108,000; 52,000 and 206,250; respectively. The organic and inorganic content varied in the range 10 – 20 mg L^{-1} (DOC), 133 – 538 mg L^{-1} (chloride) and 161 – 641 mg L^{-1} (sulfate).

3.4- Experimental set-up

Lab-scale experiments

Lab-scale assays were performed in cylindrical stirred tank reactors (3-L maximum capacity) placed inside a SunTest CPS+ solar box from Atlas with an emission range of

250 – 765 W m^{-2}. The reactors were connected to a thermostatic bath (Thermo Scientific NESLAB RTE7) for temperature control. To study the effect of photon absorption, the liquid depth and the UVA irradiance on the reactor surface were varied in the range 5 – 15 cm and 10 – 50 W m^{-2}, respectively. The UV radiation was measured with a spectroradiometer (Avantes AvaSpec Dual-Cannel Fiber Optic Spectrometer) for a wavelength range from 327 to 384 nm.

Fig. 9. SunTest CPS+ solar box with stirred tank reactor.

Outdoor experiments

The kinetic models proposed from the data obtained at lab-scale were further validated outdoors in three different RPRs:

- 360-L fiberglass-RPR of 15 cm liquid depth, 3.85 m channel length and 0.64 channel width, Figure 4.
- 19-L PVC-RPR of 5 cm liquid depth, 0.97 m channel length and 0.22 m channel width, Figure 10.
- 78-L PVC-RPR of 15 cm liquid depth, 1.39 m channel length and 0.20 channel width, Figure 10.

In these reactors, the flow is turbulent with a low mixing time (of around 2.5 min) in comparison with the reaction time (tens of minutes), meaning the hypothesis of perfect mixing could be assumed. pH and temperature were measured online with probes connected to a LabJack USB/Ethernet data acquisition device. For model validation in

continuous flow operation, the hydraulic residence times assayed were 10 and 15 min in 19-L RPR (1.90 and 1.27 L min^{-1}) and 20 and 30 min in 78-L RPR (3.90 and 2.60 L min^{-1}).

The spectral radiation model SMARTS2 was used to estimate the spectral distribution of incident radiation from spectral transmittance functions for the main extinction processes in the atmosphere (Gueymard, 1995). The results were corroborated by measuring solar radiation, averaged over the wavelength range 327 – 384 nm, with a global UV radiometer (Delta Ohm, LPUVA02AV).

Fig. 10. 19-L and 78-L RPRs.

The methodology used to carry out the work presented in this Ph.D. thesis is described in detail in Section 4.

RESULTS AND DISCUSSION

4. RESULTS AND DISCUSSION

According to the objectives and work plan described in Section 2, the results obtained in this Ph.D. thesis are grouped into the following sections:

Objective 2.1:

4.1- Effect of temperature and photon absorption on the kinetics of micropollutant removal by solar photo-Fenton in raceway pond reactors.

Objective 2.2:

4.2- Effect of volumetric rate of photon absorption on the kinetics of micropollutant removal by solar photo-Fenton with Fe^{3+}-EDDS at neutral pH.

Objective 2.3:

4.3- Assessment of solar raceway pond reactors for removal of contaminants of emerging concern by photo-Fenton at circumneutral pH from very different municipal wastewater effluents.

Objective 2.4:

4.4- Mechanistic modeling of solar photo-Fenton process with Fe^{3+}-EDDS at neutral pH.

Objective 2.5:

4.5- On the design and operation of solar photo-Fenton open reactors for the removal of contaminants of emerging concern from WWTP effluents at neutral pH.

4.1- Effect of temperature and photon absorption on the kinetics of micropollutant removal by solar photo-Fenton in raceway pond reactors

Published:

Sánchez Pérez, J.A., Soriano-Molina, P., Rivas, G., García Sánchez, J.L. Casas López, J.L. & Fernández Sevilla, J.M. (2017). Effect of temperature and photon absorption on the kinetics of micropollutant removal by solar photo-Fenton in raceway pond reactors. Chemical Engineering Journal, 310, 464 – 472. DOI:10.1016/j.cej.2016.06.055.

Chemical Engineering Journal 310 (2017) 464–472

Contents lists available at ScienceDirect

Chemical Engineering Journal

journal homepage: www.elsevier.com/locate/cej

Effect of temperature and photon absorption on the kinetics of micropollutant removal by solar photo-Fenton in raceway pond reactors

J.A. Sánchez Pérez *, P. Soriano-Molina, G. Rivas, J.L. García Sánchez, J.L. Casas López, J.M. Fernández Sevilla

Department of Chemical Engineering, University of Almería, 04120 Almería, Spain
CIESOL, Joint Centre of the University of Almería-CIEMAT, 04120 Almería, Spain

HIGHLIGHTS

- The activated iron Fe^{3+*} is proposed to explain irradiance saturation of photo-Fenton.
- The photo-Fenton model fits irradiance and temperature effects on reaction rate.
- Model parameters were obtained at lab scale and validated at pilot plant scale.
- Light absorption coefficient of ferric iron increases with temperature.
- High treatment capacity of 135 mg/m^2 h was achieved for 90% acetamiprid removal.

GRAPHICAL ABSTRACT

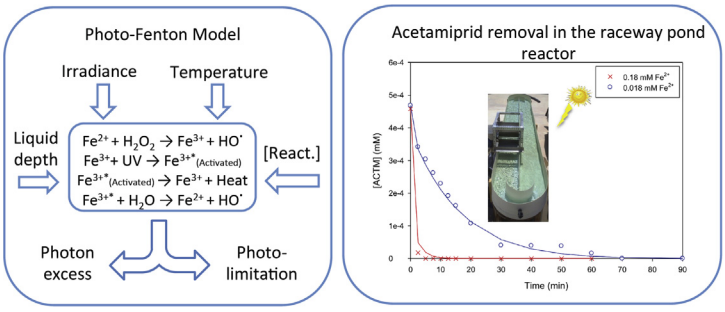

ARTICLE INFO

Article history:
Available online 10 June 2016

Keywords:
Irradiance
Temperature
Kinetic model
Acetamiprid
Treatment capacity

ABSTRACT

Solar driven photocatalysis is considered as an environmental friendly treatment for micropollutant removal from secondary wastewater treatment plant effluents. The photo-Fenton process is efficient in persistent organic pollutant degradation and the use of low cost reactors with variable light path length such as raceway pond reactors (RPR) has been recently proposed. The aim of the study was to develop a simplified kinetic model predicting micropollutant removal rate as a function of environmental variables (irradiance and temperature), geometrical variables (light path length) and operating variables (reactant concentration). The parameters were obtained by fitting the model to 36 experimental conditions in 1.25-L cylindrical reactors at lab scale and then validated in a 360-L RPR at pilot plant scale. In the studied range, 10–40 °C, temperature enhances the photo-Fenton reaction rate by: i) accelerating the oxidation of ferrous iron with hydrogen peroxide (thermal Fenton); and ii) making the light absorption coefficient of ferric iron higher, that is the VRPA. The proposed photo-Fenton model takes into account both effects and properly fit experimental data. Considering 90% removal of the pesticide acetamiprid at an initial concentration of 100 μg/L, a treatment capacity of 135 mg/m^2 h was achieved with low reactant concentrations, 10 mg/L Fe^{2+} and 50 mg/L H_2O_2. The presented results encourage the application of this modeling strategy for process optimization, design and operation of raceway pond reactors for micropollutant removal by solar photo-Fenton.

* Corresponding author at: Department of Chemical Engineering, University of Almería, 04120 Almería, Spain.
E-mail address: jsanchez@ual.es (J.A. Sánchez Pérez).

http://dx.doi.org/10.1016/j.cej.2016.06.055
1385-8947/

1. Introduction

There is an increasing environmental concern on the removal of persistent organic pollutants in treated wastewaters, which remain in the WWTP effluents discharged to natural water bodies at very low concentrations (ng/L–μg/L) [1,2] but with accumulative effects on the flora and fauna in aquatic ecosystems [3–6]. Some countries have started to limit the emission of such pollutants, called micropollutants [1,7]. For instance, in Switzerland new rules regarding measures to eliminate organic trace substances in WWTP will demand to remove at least 80% of a selected list of pollutants [8]. Therefore, the modification of existing water treatment technologies to match this goal is becoming a new demand to scientists and environmental engineers.

The photo-Fenton process has been widely studied for organic pollutant removal in aqueous solutions covering different operating conditions with industrial and municipal wastewaters [5,9–11]. The photo-Fenton process involves the generation of hydroxyl radicals ($HO^{\cdot}$) by the reaction between hydrogen peroxide and iron in acidic medium, under natural or artificial UV irradiation. Particularly, the generation of hydroxyl radicals relies on the cyclically oxidation and photoreduction of iron (catalyst) in aqueous solution with hydrogen peroxide (H_2O_2) consumption. Moreover, the reduction of Fe^{3+} can take place with H_2O_2 in the dark, the Fenton process, although this reaction is much slower than when illuminated. The rate of hydroxyl radicals generation in the photo-Fenton process depends on several variables, but reagent concentrations (H_2O_2 and Fe) and irradiance have demonstrated to be of particular significance [12].

The range of reactant concentrations changes with the contaminant level of the water to treat [13]. Regarding micropollutant removal in secondary WWTP effluents, it is frequently proposed to use low iron and hydrogen peroxide concentrations around 5 mg/L for Fe and some tens of mg/L for H_2O_2 [14,15]. As for the solar photoreactor, the most common geometry is tubular reactors provided with compound parabolic collectors (CPC), the most popular tube diameter being 5 cm [16]. The fact of using short light path lengths and low concentration of light-absorbing species gave rise to small optical densities and consequently, an inefficient use of the photons reaching the reactor surface [17]. Additionally, and related to this effect, a reaction rate saturation at increasing irradiances was observed, UV-light excess taking place for a few cm light path. Increasing path length is recommended in this situation to make better use of the irradiance reaching the system and to increase the treated volume [18].

To take advantage of most of the photons and reduce costs, photo-Fenton in raceway pond reactors (RPRs) has been reported recently [14]. RPRs consist of extensive reactors with channels through which the water is recirculated by a paddlewheel. They are made of low cost materials, mainly plastic liners, giving rise to low construction costs of about 100,000 €/ha, that is 10 €/m^2 and it would significantly reduce investment costs compared with CPCs for the use of the photo-Fenton process as tertiary treatment. Additionally, the power requirements for mixing are also small – over 4 W/m^3. In previous works, high treatment capacity per surface area was reported (40–133 mg/h m^2 with 5.5 mg Fe/L (0.095 mM) and 15 cm liquid depth), proving the feasibility of using RPRs for micropollutant removal [19].

Nonetheless, little attention has been paid to the temperature effect on the photo-Fenton process in spite of being a main variable in reaction kinetics. Only a few works take into account this effect on reactor design and process performance [20,21]. Alfano and coworkers estimated the Arrhenius parameters between 20 °C and 55 °C, and proposed a kinetic model of the Fenton and photo-Fenton degradation of formic acid in aqueous solution, for relatively low iron concentrations (1–9 mg/L). The proposed kinetic model was able to reproduce the combined effects of changing the ferric iron concentration, reaction temperature and formic acid to hydrogen peroxide molar ratio on the pollutant degradation rate [22,23]. This paper is focused on the development of a photo-Fenton kinetic model to predict micropollutant removal rate as a function of environmental variables (irradiance and temperature), geometrical variables (light path length) and operating variables (catalyst concentration). The model tracks the effects of irradiance saturation and takes into account the influence of temperature on photon absorption. To this end, the pesticide acetamiprid (ACTM) was chosen as model pollutant due to its low degradation rate and easy tracking by UPLC to allow kinetics determination. To favour reproducibility, a synthetic secondary WWTP effluent was used along the experimentation.

2. Materials and methods

2.1. Chemicals

Sulphuric acid (95–97%) and hydrogen peroxide (35%) were obtained from J.T. Baker and ferrous sulphate (99%) from Fluka. $CaSO_4{\cdot}2H_2O$, $MgSO_4$, KCl, $(NH_4)_2SO_4$, $NaHCO_3$, beef extract, peptone, humic salts, sodium lignin sulfonate, sodium lauryle sulphate, acacia gum powder, formic acid and Arabic acid were acquired from Sigma-Aldrich. Commercial formulation of acetamiprid ($C_{10}H_{11}ClN_4$) was used: EPIK® (20% w/w ACTM). HPLC grade acetonitrile from BDH PROLABO CHEMICALS and Milli-Q grade water were used in the chromatographic analysis.

2.2. Experimental set-up

Experimentation was carried out with synthetic secondary effluent at two scales: within a solar box device at lab scale and a 360L-raceway pond reactor for outdoor conditions. The constituents of the synthetic secondary effluent were: $CaSO_4{\cdot}2H_2O$ (60 mg/L), $MgSO_4$ (60 mg/L), KCl (4 mg/L), $(NH_4)_2SO_4$ (23.6 mg/L), K_2HPO_4 (7.0 mg/L), $NaHCO_3$ (96 mg/L), beef extract (1.8 mg/L), peptone (2.7 mg/L), humic salts (4.2 mg/L), sodium lignin sulfonate (2.4 mg/L), sodium lauryle sulphate (0.9 mg/L), acacia gum powder (4.7 mg/L), and Arabic acid (5.0 mg/L) [24]. The dissolved organic carbon concentration, DOC, was 16 mg/L.

pH was adjusted with sulphuric acid. A value of 2.8 was chosen because it is the optimum for the photo-Fenton process [25] and iron species are in solution allowing a correct determination of the light absorption properties of the liquid [22]. Initial hydrogen peroxide concentration was 50 mg/L (1.47 mM) to work in mild excess of oxidant.

ACTM a pesticide commonly used for citrus crops protection in the Mediterranean area [26,27] was selected as model pollutant with a concentration of 100 μg/L (4.49×10^{-4} mM).

2.2.1. Lab scale experiments

Fenton and photo-Fenton experiments were carried out in 1.25-L stirred tank reactors. The reactor was placed inside a SunTest CPS+ solar box from Atlas with an emission range of 250–765 W/m^2 (complete emission spectrum). The cylindrical vessels were laterally covered to prevent the diffuse component of incoming radiation. In this way only direct radiation perpendicular to the vessel surface is considered as incident light. UV irradiance inside the solar box was measured with a PMA2100 radiometer from Solar Light Company in the 327–384 nm range. Plank's equation was used to convert irradiance data from W/m^2 to Einstein/m^2 s.

The jacketed reactors were connected to a thermostatic bath (Thermo Scientific NESLAB RTE7) for temperature regulation. At each temperature assayed (10, 20 30 and 40 °C) a series of experimental runs were carried out at two liquid depths (5 and 15 cm) with irradiances on water surface ranging from 5 to 40 W/m^2, four irradiance values at each depth. This procedure was used to simulate reaction conditions found in pilot plant scale raceway pond reactors with eight values of the volumetric rate of photon absorption (VRPA) at each temperature. The chosen experimental conditions comprise the temperature and solar irradiation attainable outdoors at the location of the experimentation, 5 cm liquid depth was taken as the common diameter used in CPCs tubular reactors and 15 cm as the maximum depth for the RPR reactor used in this study.

Iron concentration was kept at 5.5 mg/L (0.095 mM) through all the experimentation.

Preliminary blank assays were conducted with simulated secondary effluent in the dark at the 4 levels of temperature selected. No remarkable ACTM degradation was observed. Likewise, direct photolysis and hydrolysis were negligible for the studied pollutant, coinciding with the information given by the Environmental Protection Agency [28–30]. Moreover, further assays in the dark were conducted to study the effect of the temperature on the hydrogen peroxide decomposition. Similarly, no decomposition was observed.

2.2.2. Experiments carried out in the raceway pond reactor

The experiments were carried out in a fiberglass-RPR pilot plant at the Solar Energy Research Centre (CIESOL) in Almería, Spain. The fiberglass-RPR has a maximum capacity of 360 L, a length of 3.85 m and width of 0.64 m. The RPR includes a paddlewheel connected to an engine to obtain a mixed and homogeneous flow during the process. More details were previously reported by Carra et al. [14]. In this case, three values of iron concentration were used, 0.018, 0.095 and 0.18 mM Fe^{2+}. UV radiation was measured using a global UV radiometer (Delta Ohm, LPUVA02AV) with a spectral response range from 327 to 384 nm, mounted on a horizontal platform, providing data in terms of incident UV radiation (W/m^2). In concordance with Section 2.2.1, irradiance data in W/m^2 were converted to Einstein/m^2 s using the Planck's equation.

2.3. Radiation field and VRPA estimation

According to Rivas et al. [19], the volumetric rate of photon absorption (VRPA) in the photochemical reactors was calculated using a simplified model of radiation field, that is assuming spatial dependence in one direction (depth) and taking the beam irradiance as the active light. To account for the solar UV fractions, direct and diffuse, an approximation was made considering that all irradiance reaching the reactor surface was direct in clear day condition [19]. In this way, the local volumetric rate of photon absorption, expressed in Einstein/s m^3, at a specific depth was defined by Eq. (1):

$$LVRPA(z) = k_A \cdot C_{Fe} \cdot UV_o \cdot 10^{-k_A \cdot C_{Fe} \cdot z/\cos\theta} \quad (1)$$

where k_A, C_{Fe}, UV_o and θ stand for absorption coefficient, ferric species concentration, total UV irradiance at reactor surface and incident angle, respectively. By integrating over reactor depth, D, multiplying by the reactor surface (S_R) for incoming photons and dividing by the whole reactor volume (V_R), the VRPA per unit of volume was expressed in Einstein/s m^3 by:

$$VRPA = \frac{S_R}{V_R} \int_0^D k_A \cdot C_{Fe} \cdot UV_o \cdot 10^{-k_A \cdot C_{Fe} \cdot z/\cos\theta} dz \quad (2)$$

The application of Eq. (2) in outdoor conditions was realized averaging the values of global UV irradiance, UV_o, and angle of incidence θ over the experimental time of each run carried out at near noon [19]. Regarding the absorption of the incident radiation, the ferric iron species in solution are dominant for UV-light absorption as hydrogen peroxide and ferrous iron do not absorb any radiation over 300 nm [23,31]. Absorption of acetamiprid, and generated intermediates was checked and found negligible over 300 nm at the concentration used in the experiments.

For the computation of the specific absorption coefficient k_A (mM^{-1} m^{-1}) of solution species, Eq. (3), a series of UV absorption spectra of Fe^{3+} solutions in simulated secondary effluent were conducted at each of the temperature studied. So the computation of Eq. (3) was applied with its corresponding temperature data. Some authors have pointed out a temperature dependence effect in the absorption properties of Fe^{3+} complexes [22]

$$k_A = \frac{\int_{\lambda min}^{\lambda max} \varepsilon_\lambda I_\lambda d\lambda}{\int_{\lambda min}^{\lambda max} I_\lambda d\lambda} \quad (3)$$

Wavelength range in Eq. (3) was 327–384 nm, which is the response range of the UV sensors used in this study. Regarding the spectral distribution of incident radiation, I_λ, the reference data supplied by the solar box manufacturer were used and compared with measured data obtained by a double channel spectrometer AvaSpec ULS2048-2 with 200–1100 nm range, once the lamp regime was settled. As can be seen in Fig. 1, similar results were obtained with both procedures and a linear relationship was observed with temperature.

For indoor simulations the actual value found in the computations of k_A with the referenced spectral properties was used. In the case of the outdoor experiments, the airmass 1.5 spectra (ASTM) reference standard, sampled at the wavelength interval defined above for indoor experiments was taken as I_λ, for computations. As previously found, a linear relationship with temperature was assumed, the regressed line for the absorption coefficient expressed in mM^{-1} m^{-1} under solar light and 10–40 °C temperature range is shown in Eq. (4):

$$K_A = 36.84 + 0.51 * T \ (r^2 = 0.998) \quad (4)$$

where T is the water bulk temperature in °C.

2.4. Chemical analysis

All the samples, each one being 3 mL, were taken from the reactor and immediately filtered (nylon filters from Millipore® with pores of 0.20 μm-diameter). The filter was then washed with acetonitrile in an acetonitrile: sample relationship of 1:10 and mixed with the filtered sample. This was done because acetonitrile acts as an HO· scavenger, stopping the reaction [32], and also sweeps out any trace of pollutant that may have been retained by the filter and avoid any possible adsorption.

Hydrogen peroxide was measured by a colorimetric method using ammonium metavanadate, measuring the absorbance at 450 nm [33]. The concentration of iron was determined according to the o-phenanthroline standardized procedure (ISO 6332) and the red complex formed was determined spectrophotometrically at 510 nm. DOC determinations were carried out in a Shimadzu-V CPH TOC analyser.

ACTM concentrations were determined by means of liquid chromatography (UPLC Agilent 1200 Series equipped with a column oven, degasser, autosampler and diode array detector) with a reversed-phase column (Agilent XDB-C18). The mobile phase consisted of a gradient mixture of acetonitrile and 1% v/v formic acid in water. ACTM retention time was 3.59 min and the detection wavelength was 248 nm. The gradient used was initially set at 15% acetonitrile, progressively increasing the concentration to 50% in a 5-min method. The ACTM limit of detection (LOD) was 2 μg/L.

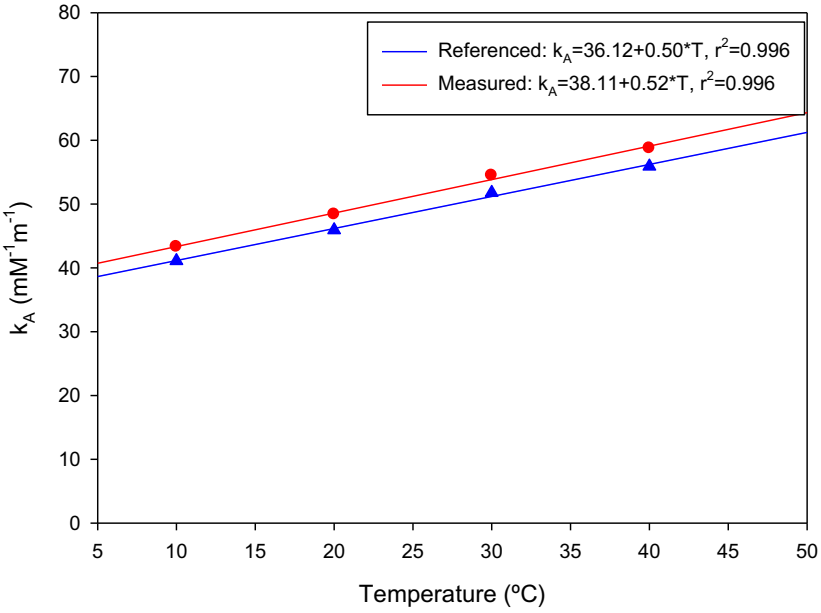

Fig. 1. Variation of the specific absorption coefficient, k_A, with temperature based on the referenced and the measured lamp spectral distribution in the solar box.

3. Results and discussion

The time-courses of ACTM and hydrogen peroxide concentrations are shown in Fig. 2. as an illustrative synthesis of the lab-scale experiments carried out in the solar box for the identification of model parameters. It comprises the experimental ranges for the process variables studied: temperature, irradiance and liquid depth. Summarizing the 36 conditions assayed, the positive effect of temperature on the Fenton process is shown at 10 and 40 °C. Indeed, Fenton process performance at 40 °C is close to that obtained with 20 W/m^2 of UV irradiation at 20 °C, as previously reported by Alfano and coworkers [22,34], whose results showed that, although solar radiation improves the effectiveness of the Fenton process, this effect is less important at high temperatures. Besides of the occurrence of thermal reactions, temperature affects the iron speciation. The most photoactive iron species ($FeOH^{2+}$) increases its molar fraction from 14% to 40% for temperature variation from 10 to 40 °C [35]. On the other hand, $Fe(OH)_3$ precipitation is favored by the temperature [36], becoming significant above 55 °C [20]. In this case, no precipitation of iron was observed and this phenomenon was not considered in the kinetic modeling.

At 20 °C and 15 cm liquid depth, the photolimitation of reaction rate is clearly observed by increasing irradiance from 5 to 20 W/m^2. And conversely, at 30 °C the photosaturation effect becomes relevant when irradiance rises from 30 to 40 W/m^2 and liquid depth is set at 5 cm. These observations corroborate previous works [18,19], where an increase in irradiance does not mean an improvement of reaction rate. Additionally, there exists parallelism between contaminant degradation and oxidant consumption profiles.

In all the cases, an initial drop of ≈55% and ≈12% for ACTM and for H_2O_2 was observed, respectively. This is due to the very fast reaction between ferrous iron and hydrogen peroxide (R. (1) in Table 1) because the experiments were started with the addition of hydrogen peroxide to the system, which already had the pesticide and ferrous salt. This reaction yields hydroxyl radicals, responsible for the initial ACTM oxidation and H_2O_2 consumption. This effect is the same for Fenton and photo-Fenton processes. Then, in the Fenton process, ferric iron is reduced through reaction (5) closing the redox cycle and giving rise to a progressive H_2O_2 consumption, radical generation and consequently ACTM oxidation. As for the photo-Fenton process, ferric iron absorbs light, again yielding hydroxyl radicals and reducing ferric iron to ferrous iron and so on. UV driven reduction of ferric iron is faster than in the dark although the later is strongly enhanced at higher temperatures. One could expect that increasing radiation absorption would increase reaction rate, as was the case for 5–20 W/m^2 in Fig. 2. Nonetheless, at a higher irradiance level, rising irradiance from 30 to 40 W/m^2 did not improve process rate, neither for ACTM nor for H_2O_2. Therefore, the shift between photolimitation and photon excess has to be included in process kinetics.

3.1. Kinetic modeling

A model of the photo-Fenton process with main focus on the photocatalytic cycle has been proposed. The model was developed for a synthetic WWTP secondary effluent (see Section 2.2) to avoid real effluent variations during experimentation although the effect of dissolved organic matter on reaction kinetics was included by defining the model state OM corresponding to a generic organic matter.

As for the photo-reduction of the aqua-hydroxo complexes of ferric iron, the formation of an activated electronic state (Fe^{3+*}) was considered when using the elementary rate laws [37]. The excited Fe^{3+} can transfer an electron to the hydroxo ligand yielding a hydroxyl radical and Fe^{2+}, although a fraction of absorbed radiation can be converted into heat and ferric iron remains in its initial state. This step in the set of reactions allows explaining the saturation of the ferric iron photoreduction, as the excess of photon absorbed is split towards heat release. Therefore, the model states are: the iron species, Fe^{2+}, Fe^{3+} and Fe^{3+*} (activated), including the aqua-complexes that they may form, the hydrogen peroxide, the target micropollutant denoted as A (could be calibrated for any contaminant, ACTM in this case), the organic matter, OM, and the generated radicals, R, (hydroxyl radicals, mainly) responsible for pollutant oxidation.

MX stands for a generic oxidized organic matter, including micropollutant transformation products and Q denotes heat released due to Fe^{3+*} deactivation back to its initial state (R. (3)).

The representative reactions and the corresponding elementary rate law expressions are shown in Table 1.

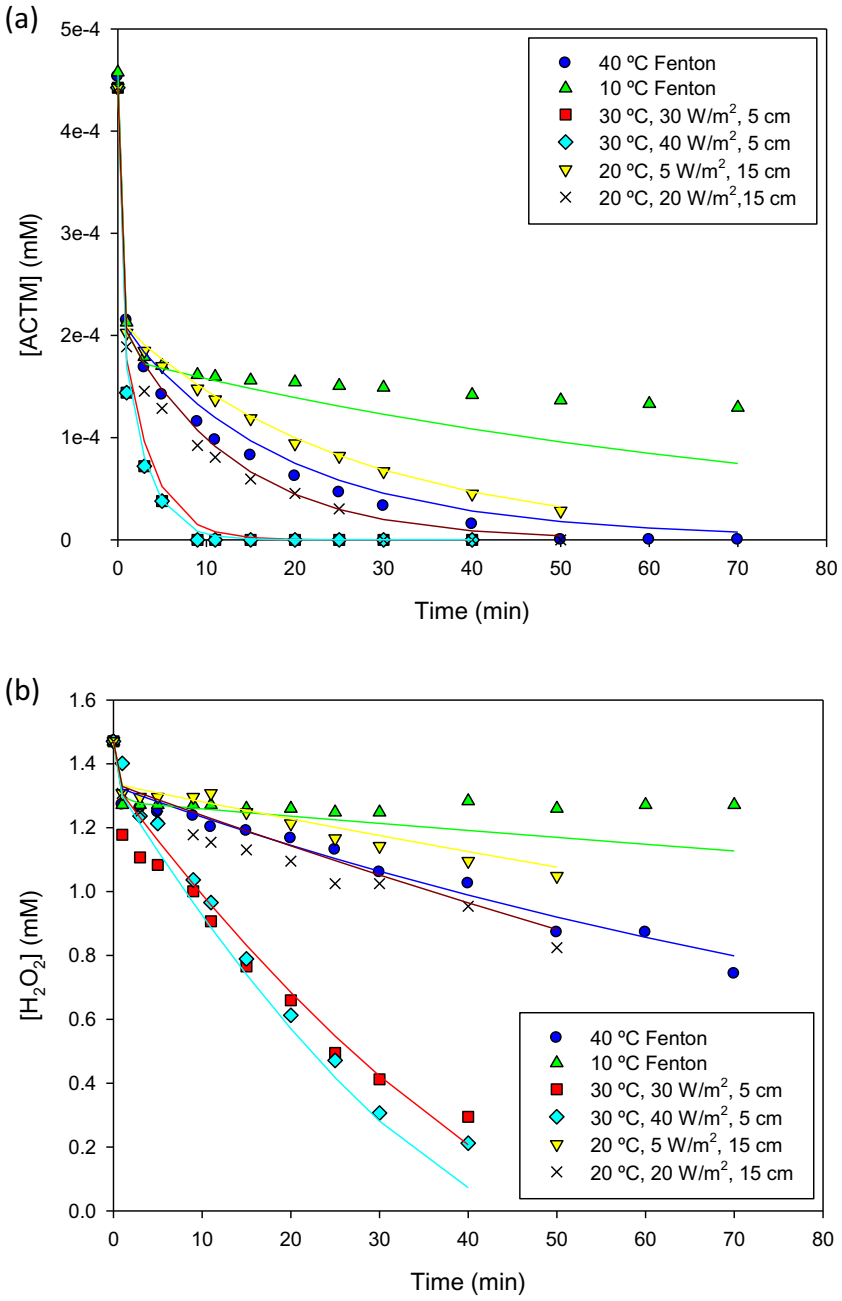

Fig. 2. ACTM degradation profiles (a) and H_2O_2 consumption (b) at several experimental conditions (temperature, irradiance, liquid depth). Lines represent model estimations.

Table 1
Model reactions and rate law equations.

Reaction	Rate equation	Reaction number
$Fe^{2+} + H_2O_2 \rightarrow Fe^{3+} + R$	$r_1 = k_1 [H_2O_2] [Fe^{2+}]$	R. (1)
$Fe^{3+} + UV \rightarrow Fe^{3+*}$	$r_2 = VRPA$	R. (2)
$Fe^{3+*} \rightarrow Fe^{3+} + Q$	$r_3 = k_3 [Fe^{3+*}]$	R. (3)
$Fe^{3+*} + H_2O \rightarrow Fe^{2+} + R$	$r_4 = k_4 [Fe^{3+*}]$	R. (4)
$Fe^{3+} + H_2O_2 \rightarrow Fe^{2+} + R$	$r_5 = k_5 [H_2O_2] [Fe^{3+}]$	R. (5)
$OM + R \rightarrow MX$	$r_6 = k_6 [OM] [R]$	R. (6)
$H_2O_2 + R \rightarrow H_2O + O_2$	$r_7 = k_7 [H_2O_2] [R]$	R. (7)
$A + R \rightarrow MX$	$r_8 = k_8 [A] [R]$	R. (8)

As stated and for the sake of simplicity, no distinction was applied for the type of radical formed (all radicals were considered as a single type although hydroxyl radical can be considered the predominant) [38]. Reactions (1) and (5) constituted the thermal Fenton process, which is the normal closure of Fenton cycle. Photo-Fenton process comprised Reactions (2)–(4), where the unstable intermediate Fe^{3+*} generated by the absorption of a UV photon turns back to its normal state by an ineffective step realising heat (R. (3)) or is efficiently reduced to Fe^{2+} giving more hydroxyl radicals, photo-Fenton cycle closure (R. (4)).

The remaining reactions in the proposed model are related with the use of the radical formed in the catalytic cycle, that is: some radicals are employed in pollutant degradation (oxidation of the parent compound, R. (8)) and a great proportion are consumed in reactions with the organic matter which acts as a sink for radicals, Reaction (6). There is also some radical-driven decomposition of hydrogen peroxide, Reaction (7), releasing molecular oxygen, which is barely detected by DO2 sensors because of the low hydrogen peroxide dosage level assayed.

Table 2
Dynamic model equations.

Mass balance model states	Equation number
$\frac{d[Fe^{2+}]}{dt} = -r_1 + r_4 + r_5$	Eq. (5)
$\frac{d[Fe^{3+}]}{dt} = -r_2 + r_1 + r_3 - r_5$	Eq. (6)
$\frac{d[Fe^{3++}]}{dt} = r_2 - r_4 - r_3$	Eq. (7)
$\frac{d[H_2O_2]}{dt} = -r_1 - r_5 - r_7$	Eq. (8)
$\frac{d[R]}{dt} = r_1 + r_4 + r_5 - r_6 - r_7 - r_8$	Eq. (9)
$\frac{d[A]}{dt} = -r_8$	Eq. (10)
$\frac{d[OM]}{dt} = -0.0005$	Eq. (11)

Table 4
Kinetic constants used for modeling outdoor experiments.

Kinetic constant	Unit constant
$k_1 = 5.9310^6 e^{-\left(\frac{34200}{RT}\right)}$, $r^2 = 0.94$	(mM^{-1} min^{-1})
$k_3 = 16.8$	(min^{-1})
$k_4 = 4.98$	(min^{-1})
$k_5 = 3.28\ 10^5 e^{-\left(\frac{42000}{RT}\right)}$, $r^2 = 0.98$	(mM^{-1} min^{-1})
$k_6 = 1.83$	(mM^{-1} min^{-1})
$k_7 = 1.67$	(mM^{-1} min^{-1})
$k_8 = 35.8$	(mM^{-1} min^{-1})

The dynamic model was obtained by imposing mass balances for each of the model states, assuming the hypothesis of batch operation and perfect mixing as can be seen in Table 2. In the case of mild oxidising conditions used for micropollutant removal, mineralization is almost negligible, and the organic content in terms of DOC remains approximately constant [39]. From our own experience and for model fitting purposes, mineralization rate was set at −0.0005 mM min^{-1}, sufficient to simulate the stable content of DOC during the experiments. A sensitivity analysis was also run to test the selected value.

The kinetic parameters were obtained by the built-in functions of the MATLAB® optimization toolbox in which the objective was the minimization of the function of the squared errors between experimental results and model prediction for the set of monitored variables:

$$J = \sum_{j=1}^{8}\left[\sum_{i=1}^{n}\left(\frac{Hm(i,j) - Hx(i,j)}{Hx(1,j)}\right)^2 + \left(\frac{Am(i,j) - Ax(i,j)}{Ax(1,j)}\right)^2\right] \quad (12)$$

where H and A stand for hydrogen peroxide and acetamiprid, respectively. Subscript m is for model and x for experimental data, with n being the number of data points in each experiment. The procedure was conducted at each temperature. The parameter values obtained by fitting the model to experimental results are shown in Table 3.

Two kinetic constants, k_1 and k_5, corresponding with the thermal Fenton reactions, increase with temperature and properly fit with the Arrhenius expression. Indeed the value of k1 at 20 °C is consistent with the value found in literature (76 M^{-1} s^{-1} which corresponds to 4.56 mM^{-1} min^{-1} [40,41]). No other clear dependence with temperature is inferred in Table 3. The constants for deactivation of excited ferric iron (k_3 and k_4) were expected not to depend on temperature, due to their photochemical nature. As for their relative values, k_4 is significantly lower than k_3 pointing out that most of the energy absorbed is released to the medium as heat. The constant for Fenton reduction of ferric iron, k_5, is much smaller than k4 in correspondence with the slower reaction rate for Fenton compared with photo-Fenton. Considering the radical consuming reactions, k_6, k_7 and k_8, their dependence with temperature is negligible in the studied interval because of their high values proper of radical reactivity. Indeed, Reaction (8) is a very fast reaction in concordance with the frequent observation that parent compound degradation is much faster than organic matter mineralization and that this reaction is also faster in distilled water (R. (6) does not take place) than in complex water matrices.

Fig. 2 shows the comparison between experimental results and model estimation for the time profiles of hydrogen peroxide consumption and ACTM removal obtained in the solar simulator for some significant experimental conditions. In general, the model adequately fits the experimental data and properly takes into account the variation in temperature and VRPA. In this case, VRPA also depends on temperature due to the linear increase of the absorption coefficient with T (Fig. 1). This means that for a given value of irradiance, liquid depth and iron concentration, the higher the temperature, the higher the VRPA. It is worth highlighting that the model includes the changes in the concentration of the absorbing species (ferric iron) and temperature during a run and consequently the change in VRPA. Additionally, the model also tracks the observed phenomena of photolimitation of the reaction rate as shown at 20 °C when irradiance rose from 17 μE/m^2 s up to 54 μE/m^2 s, that is VRPA from 88.35 μE/m^3 s to 282.83 μE/m^3 s and photosaturation at 30 °C increasing irradiance from 100 μE/m^2 s to 127 μE/m^2 s, VRPA from 866 to 1080 μE/m^3 s.

3.2. Model validation in the raceway reactor

The kinetic parameters obtained from lab-scale indoor experiments were averaged over the temperature range studied, except k_1 and k_5 that were fitted to the Arrheniuśs expression. These averaged values (Table 4) were used for further model validation and scaling up with data from outdoor experiments carried out in a 360-L raceway pond reactor, using mean values of incident angle of solar radiation, temperature and UV radiation at an horizontal plane parallel to the surface of the raceway. Eq. (4) is used now in VRPA calculations (see Section 2.3) to include the change of the absorption coefficient with the temperature. Experiments for testing the model were run with 0.095 mM of Fe^{2+} at the beginning of the assay. To check the applicability of the model at different iron concentrations, two additional values 0.018 and 0.18 mM of Fe^{2+} were also tested, which are shown in Figs. 3 and 4.

Fig. 3 shows the effect of iron concentration on process performance for 5 cm liquid depth with an acceptable model fit to the experimental results. The addition of different amounts of iron is taken into account in five main reactions. First, the fresh ferrous iron reacting through Reaction (1) yields a stoichiometric amount

Table 3
Kinetics model parameters.

Temp (°C)	k_1 (mM^{-1} min^{-1})	k_3 (min^{-1})	k_4 (min^{-1})	k_5 (mM^{-1} min^{-1})	k_6 (mM^{-1} min^{-1})	k_7 (mM^{-1} min^{-1})	k_8 (mM^{-1} min^{-1})
10	2.45	30.56	2.98	0.0049	0.21	2.41	33.99
20	5.61	15.87	4.62	0.0101	2.55	1.32	36.88
30	7.38	15.84	7.81	0.0184	2.54	1.53	38.82
40	10.47	5.06	4.49	0.0270	2.02	1.41	33.66

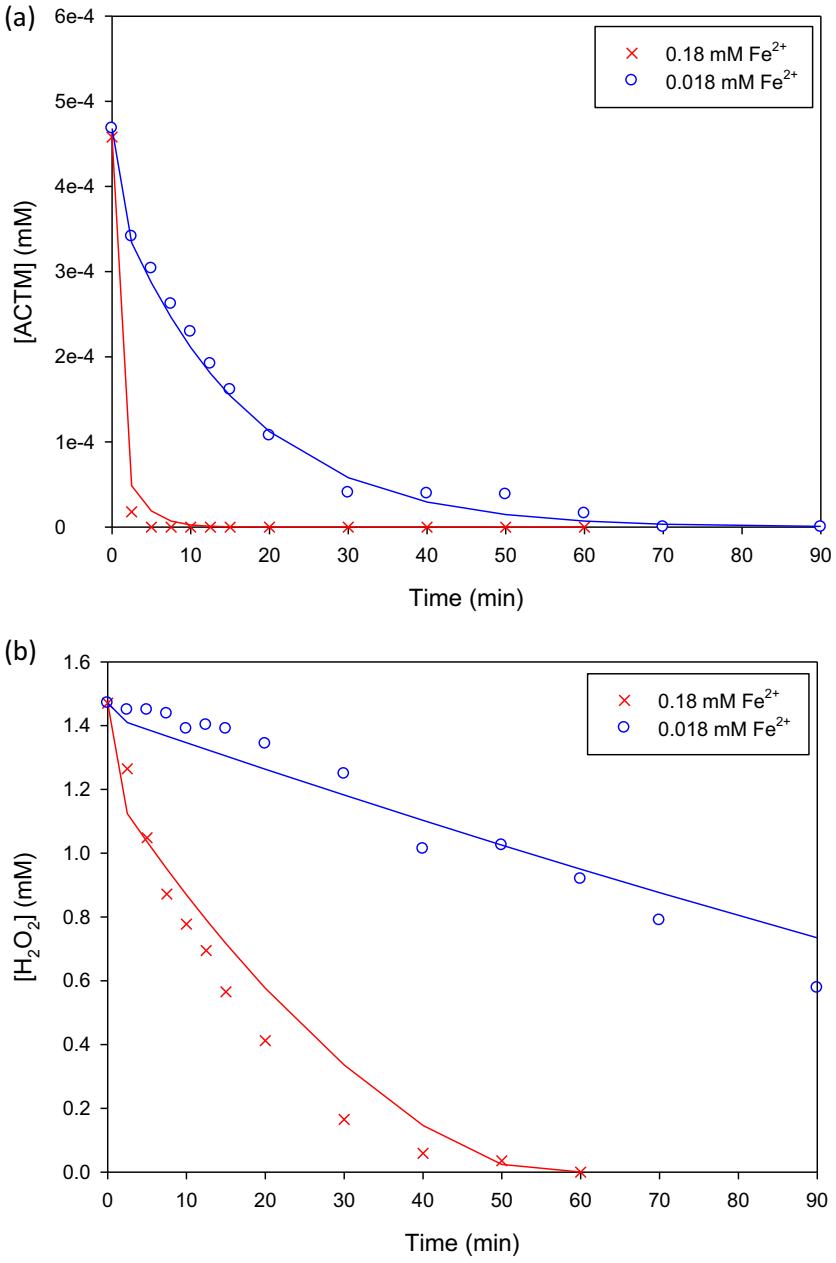

Fig. 3. Effect of iron concentration on ACTM removal (a) and H_2O_2 consumption (b) rates in a raceway pond reactor set at 5 cm liquid depth and operated with 0.018 mM Fe^{2+} (22.7 °C, 29.2 W/m^2 of irradiance and 22,7° incident angle) or 0.18 mM Fe^{2+} (27.5 °C, 28.2 W/m^2 of irradiance and 21° incident angle). Lines represent model estimations.

of HO· giving rise to a proportional drop in H_2O_2 and ACTM concentrations, the higher the iron concentration added, the deeper the drop. Next, the progressive reaction takes place with increasing rate at higher iron concentration due to the higher VRPA that determines Reaction (2) and consequently, Reactions (3) and (4). Simultaneously, Reaction (5) (Fenton) is also enhanced at higher iron concentration. This effect is clearly observed in Figs. 3 and 4. As for the effect of liquid depth, results obtained with 15 cm are shown in Fig. 4. The same analysis presented for data obtained with 5 cm liquid depth is valid in this case, and the model adequately reproduces the variation in ACTM and H_2O_2 concentrations with time.

Reaction rate on a volume basis was slightly slower when liquid depth was set at 15 cm compared with 5 cm. Indeed, to achieve 90% ACTM removal expressed in concentration, from 4.49 10^{-4} mM to 4.49 10^{-5} mM, reaction time increased from 3 min to 6 min working with 0.18 mM Fe when liquid depth increased three times, from 5 cm to 15 cm. Nonetheless, when the amount of ACTM removed is considered in terms of treatment capacity per surface area [14], increasing the liquid depth enhances the treatment efficiency from 90 mg/h m^2 for 5 cm to 135 mg/h m^2 for 15 cm liquid depth. These results demonstrate the convenience of increasing liquid depth to make better use of the photons entering the liquid surface.

Finally, the applicability of the model under variable environmental conditions makes it useful for process optimization, monitoring, design and operation of raceway pond reactors for micropollutant removal by solar photo-Fenton.

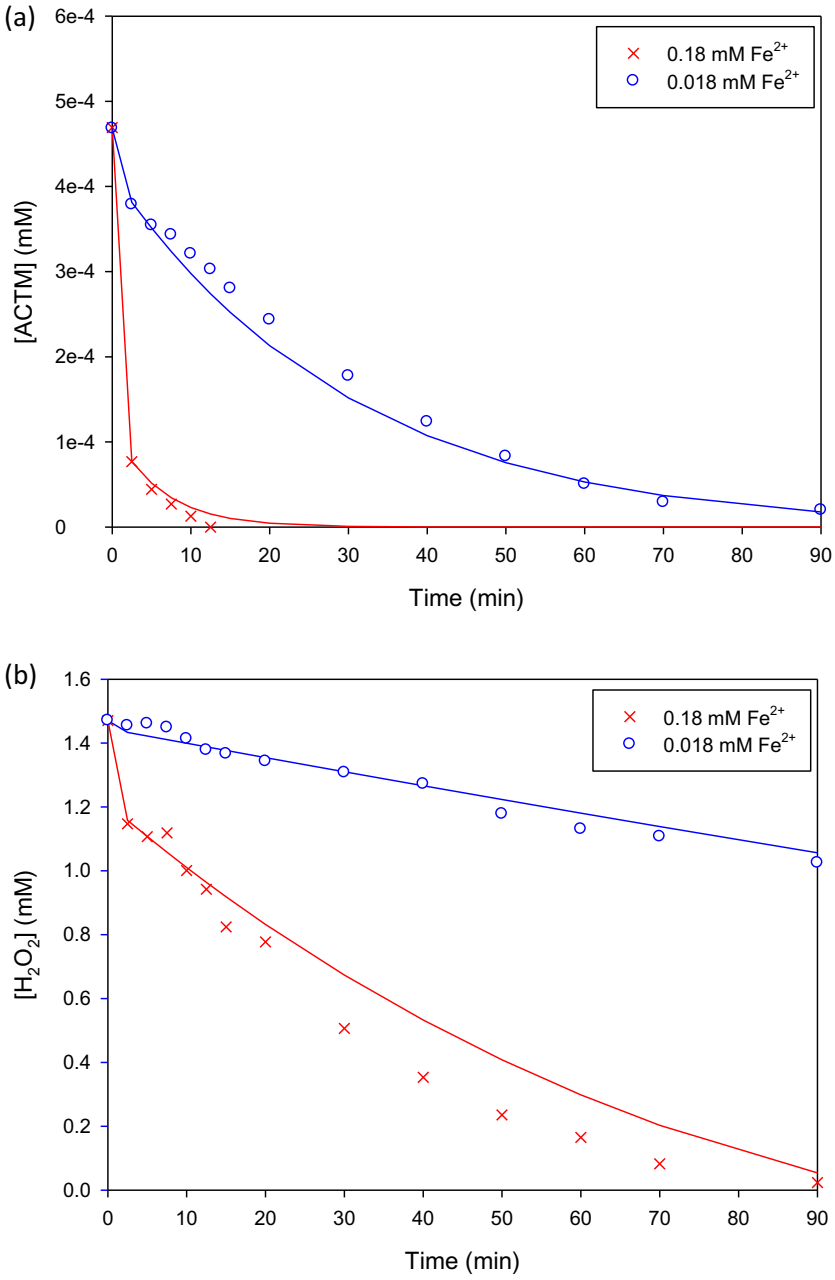

Fig. 4. Effect of iron concentration on ACTM removal (a) and H_2O_2 consumption (b) rates in a raceway pond reactor set at 15 cm liquid depth and operated with 0.018 mM Fe^{2+} (21 °C, 27 W/m^2 of irradiance and 22,7° incident angle) or 0.18 mM Fe^{2+} (26 °C, 27 W/m^2 of irradiance and 21° incident angle). Lines represent model estimations.

4. Conclusions

A two-way contribution of temperature on the enhancement of the photo-Fenton reaction rate was noted. Temperature increases the thermal Fenton process, especially k_1, which is the common reaction for the dark and irradiated processes. Additionally, the ferric iron absorption coefficient rises with temperature, making the VRPA higher for a given irradiance and light path length. Both effects were taken into account in the proposed photo-Fenton model, including the case of photon excess. The model can be tuned for several kinds of pollutant maintaining the structure of rate law expressions. The presented results encourage the application of this modeling strategy for different conditions as neutral pH and real effluents.

Acknowledgements

This research was supported by the Ministry for Economy and Competitiveness (Spanish Government) CTQ2013-46398-R, by the Junta de Andalucía (Andalusian Regional Government) P10-RNM-05951 and the European Regional Development Fund (ERDF). Gracia Rivas would like to acknowledge the Junta de Andalucía for

her FPI scholarship. Paula Soriano-Molina would like to acknowledge the Ministerio de Educación, Cultura y Deporte for her FPU scholarship (AP14/01030).

References

[1] Y. Luo, W. Guo, H.H. Ngo, L.D. Nghiem, F.I. Hai, J. Zhang, et al., A review on the occurrence of micropollutants in the aquatic environment and their fate and removal during wastewater treatment, Sci. Total Environ. 473–474 (2014).

[2] D.W. Bahnemann, P.K.J. Robertson, Persistent organic pollutants in the great lakes: an overview, in: P.K.J.R. Detlef, W. Bahnemann (Eds.), Handb. Environ. Chem., Springer-Verlag, 2015, pp. 1–21.

[3] B. Ferrari, N. Paxéus, R. Lo Giudice, A. Pollio, J. Garric, Ecotoxicological impact of pharmaceuticals found in treated wastewaters: study of carbamazepine, clofibric acid and diclofenac, Ecotoxicol. Environ. Saf. 55 (2003) 359–370.

[4] M. Cleuvers, Aquatic ecotoxicity of pharmaceuticals including the assessment of combination effects, Toxicol. Lett. 142 (2003) 185–194.

[5] Y. Segura, F. Martínez, J.A. Melero, J.L. García Fierro, Zero valent iron (ZVI) mediated Fenton degradation of industrial wastewater: treatment performance and characterization of final composites, Chem. Eng. J. 269 (2015) 298–305.

[6] E. Cho, J. Khim, S. Chung, D. Seo, Y. Son, Occurrence of micropollutants in four major rivers in Korea, Sci. Total Environ. 491–492 (2014) 138–147.

[7] J. Siemens, G. Huschek, C. Siebe, M. Kaupenjohann, Concentrations and mobility of human pharmaceuticals in the world's largest wastewater irrigation system, Mexico City-Mezquital Valley, Water Res. 42 (2008) 2124–2134.

[8] FOEN, Swiss Federal Office for the Environment, Wastewater treatment measures to reduce micropollutants, Furth. Action Newsl. 9 (2011) 2.

[9] S. Papoutsakis, S. Miralles-Cuevas, I. Oller, J.L. Garcia Sanchez, C. Pulgarin, S. Malato, Microcontaminant degradation in municipal wastewater treatment plant secondary effluent by EDDS assisted photo-Fenton at near-neutral pH: an experimental design approach, Catal. Today 252 (2015) 61–69.

[10] H. Zhuang, H. Han, S. Jia, B. Hou, Q. Zhao, Advanced treatment of biologically pretreated coal gasification wastewater by a novel integration of heterogeneous catalytic ozonation and biological process, Bioresour. Technol. 166 (2014) 592–595.

[11] A. Durán, J.M. Monteagudo, J. Gil, A.J. Expósito, I. San Martín, Solar-photo-Fenton treatment of wastewater from the beverage industry: intensification with ferrioxalate, Chem. Eng. J. 270 (2015) 612–620.

[12] J.J. Pignatello, E. Oliveros, A. MacKay, Advanced oxidation processes for organic contaminant destruction based on the Fenton reaction and related chemistry, Crit. Rev. Environ. Sci. Technol. 36 (2006) 1–84.

[13] Y. Samet, I. Wali, R. Abdelhédi, Kinetic degradation of the pollutant guaiacol by dark Fenton and solar photo-Fenton processes, Environ. Sci. Pollut. Res. 18 (2011) 1497–1507.

[14] I. Carra, L. Santos-Juanes, F.G. Acién Fernández, S. Malato, J.A. Sánchez Pérez, J. Hazard. Mater. 279 (2014) 322–329.

[15] L. Prieto-Rodríguez, D. Spasiano, I. Oller, I. Fernández-Calderero, A. Agüera, S. Malato, Solar photo-Fenton optimization for the treatment of MWTP effluents containing emerging contaminants, Catal. Today 209 (2013) 188–194.

[16] D. Bahnemann, Photocatalytic water treatment: solar energy applications, Sol. Energy 77 (2004) 445–459.

[17] J. Colina-Márquez, F. MacHuca-Martínez, G.L. Puma, Radiation absorption and optimization of solar photocatalytic reactors for environmental applications, Environ. Sci. Technol. 44 (2010) 5112–5120.

[18] I. Carra, J.L. García Sánchez, J.L. Casas López, S. Malato, et al., Phenomenological study and application of the combined influence of iron concentration and irradiance on the photo-Fenton process to remove micropollutants, Sci. Total Environ. 478 (2014) 123–132.

[19] G. Rivas, I. Carra, J.L. García Sánchez, J.L. Casas López, S. Malato, J.A. Sánchez Pérez, Modelling of the operation of raceway pond reactors for micropollutant removal by solar photo-Fenton as a function of photon absorption, Appl. Catal. B Environ. 178 (2015) 210–217.

[20] A. Zapata, I. Oller, L. Rizzo, S. Hilgert, M.I. Maldonado, J.A. Sánchez Pérez, et al., Evaluation of operating parameters involved in solar photo-Fenton treatment of wastewater: interdependence of initial pollutant concentration, temperature and iron concentration, Appl. Catal. B Environ. 97 (2010) 292–298.

[21] A. Cabrera Reina, J.L. Casas López, M.I. Maldonado, L. Santos-Juanes, J.L. Garcia Sánchez, J.A. Sánchez Pérez, Effects of environmental variables on the photo-Fenton plant design, Chem. Eng. J. (Amsterdam, Netherlands) 237 (2014) 469–477.

[22] J. Farias, E.D. Albizzati, O.M. Alfano, Solar degradation of formic acid: temperature effects on the photo-Fenton reaction, Chem. Eng. J. 46 (2007) 7580–7586.

[23] J. Farias, E.D. Albizzati, O.M. Alfano, Kinetic study of the photo-Fenton degradation of formic acid. Combined effects of temperature and iron concentration, Catal. Today 144 (2009) 117–123.

[24] R. Zhang, S. Vigneswaran, H. Ngo, H. Nguyen, A submerged membrane hybrid system coupled with magnetic ion exchange (MIEX®) and flocculation in wastewater treatment, Desalination 216 (2007) 325–333.

[25] E. Neyens, J. Baeyens, A review of classic Fenton's peroxidation as an advanced oxidation technique, J. Hazard. Mater. 98 (2003) 33–50.

[26] C.J.J. Fitzgerald, Crop protection, Anal. Chem. 30 (2011) 1178–1183.

[27] J.F. García Reyes, B. Gilbert-López, A. Molina-Díaz, Determination of pesticide residues in fruit-based soft drinks, Anal. Chem. 80 (2008) 8966–8974.

[28] EPA, Office of Prevention, Pesticides and Toxic Substances, Conditional Registration, 2002a7501C, 2002.

[29] EPA, Office of Prevention, Pesticides and Toxic Substances, EPA-738-F-02-002, 2002b7508W, 2002.

[30] EPA, Office of Prevention, Pesticides and Toxic Substances, OPP-2002-0333, 2002.

[31] E. Oliveros, M. Maurette, G. Orellana, J. Cadet, T. Douki, J. Ravanat, et al., The local and observed photochemical reaction rates revisited, Photochem. Photobiol. Sci. 8 (2009) 1047–1058.

[32] S. Mitroka, S. Zimmeck, D. Troya, J.M. Tanko, How solvent modulates hydroxyl radical reactivity in hydrogen atom abstractions, J. Am Chem. Soc. 132 (2010) 2907–2913.

[33] R.F. Nogueira, M.C. Oliveira, W.C. Paterlini, Simple and fast spectrophotometric determination of H_2O_2 in photo-Fenton reactions using metavanadate, Talanta 66 (2005) 86–91.

[34] O.M. Alfano, E.D. Albizzati, L.O. Conte, Modelling of photo-Fenton solar reactors for environmental applications, Environ. Photochem. (2015).

[35] F.C. Moreira, R.A.R. Boaventura, E. Brillas, V.J.P. Vilar, Degradation of trimethoprim antibiotic by UVA photoelectro-Fenton process mediated by Fe (III)-carboxylate complexes, Appl. Catal. B Environ. 162 (2015) 34–44.

[36] E. Ortega-Gómez, P. Fernández-Ibáñez, M.M. Ballesteros Martín, M.I. Polo-López, B. Esteban García, J.A. Sánchez Pérez, Water disinfection using photo-Fenton: effect of temperature on *Enterococcus faecalis* survival, Water Res. 46 (2012) 6154–6162.

[37] P. Cieśla, P. Kocot, P. Mytych, Z. Stasicka, Homogeneous photocatalysis by transition metal complexes in the environment, J. Mol. Catal. A Chem. 224 (2004) 17–33.

[38] A. Cabrera Reina, L. Santos-Juanes, J.L. García Sánchez, J.L. Casas López, M.I.M. Rubio, G.L. Puma, et al., Modelling the photo-Fenton oxidation of the pharmaceutical paracetamol in water including the effect of photon absorption (VRPA), Appl. Catal. B Environ. 166–167 (2015) 295–301.

[39] L. Santos-Juanes, J.L. Garcia Sánchez, J.L. Casas López, I. Oller, S. Malato, J.A. Sánchez Pérez, Dissolved oxygen concentration: a key parameter in monitoring the photo-Fenton process, Appl. Catal. B Environ. 104 (2011) 316–323.

[40] J.J. Pignatello, Role of quinone intermediates as electron shuttles in Fenton and photoassisted Fenton oxidations of aromatic compounds, Environ. Photochem. 31 (1997) 2399–2406.

[41] H. Gallard, J. De Laat, Kinetic modelling of Fe (III)/H_2O_2 oxidation reactions in dilute aqueous solution using atrazine as a model organic compound, Water Res. 34 (2000) 3107–3116.

4.2- Effect of volumetric rate of photon absorption on the kinetics of micropollutant removal by solar photo-Fenton with Fe^{3+}-EDDS at neutral pH

Published:

Soriano-Molina, P., García Sánchez, J.L., Malato, S., Pérez-Estrada, L.A. & Sánchez Pérez, J.A. (2018). Effect of volumetric rate of photon absorption on the kinetics of micropollutant removal by solar photo-Fenton with Fe^{3+}-EDDS at neutral pH. Chemical Engineering Journal, 331, 84 – 92. DOI:10.1016/j.cej.2017.08.096.

Chemical Engineering Journal 331 (2018) 84–92

Contents lists available at ScienceDirect

Chemical Engineering Journal

journal homepage: www.elsevier.com/locate/cej

Effect of volumetric rate of photon absorption on the kinetics of micropollutant removal by solar photo-Fenton with Fe^{3+}-EDDS at neutral pH

P. Soriano-Molina[a,b], J.L. García Sánchez[a,b], S. Malato[a,c], L.A. Pérez-Estrada[c], J.A. Sánchez Pérez[a,b,*]

[a] Solar Energy Research Centre (CIESOL), Ctra de Sacramento s/n, ES04120 Almería, Spain
[b] Chemical Engineering Department, University of Almería, Ctra de Sacramento s/n, ES04120 Almería, Spain
[c] Plataforma Solar de Almería, CIEMAT, Carretera Senés Km. 4, 04200 Tabernas, Spain

GRAPHICAL ABSTRACT

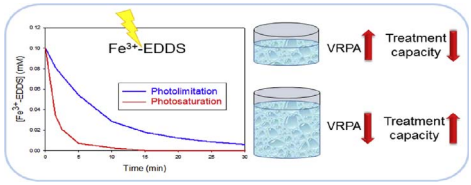

ARTICLE INFO

Keywords:
VRPA
Iron complex
Acetamiprid
Irradiance
Treatment capacity

ABSTRACT

To run the photo-Fenton process at circumneutral pH as a tertiary wastewater treatment, the use of chelating agents, such as ethylenediamine disuccinic acid (EDDS), has been proposed. For the design and optimization of photocatalytic reactors, the concept of volumetric rate of photon absorption (VRPA) is very useful, since it combines the effects of light absorption and reactor geometry. This research is focused on the study of the effect of VRPA of the Fe^{3+}-EDDS complex on the kinetics of micropollutant removal by solar photo-Fenton at neutral pH. To this end, experiments were carried out at different values of VRPA, from 383 to 1933 $\mu E\ m^{-3}\ s^{-1}$, using the pesticide acetamiprid (ACTM) as a model pollutant at an initial concentration of 100 $\mu g\ L^{-1}$. Despite instability of the complex with light, high removal percentages were achieved for short reaction times with 0.1 mM Fe^{3+}-EDDS. Due to the higher absorptivity of the complexed iron, the process became photosaturated at higher values of VRPA than those reported at pH 2.8 for Fe^{3+} allowing to work under photolimitation conditions at shorter optical path lengths than at acidic pH. The higher absorptivity of the complexed iron at neutral pH than Fe^{3+} at pH 2.8 allowed to work under photolimitation conditions at shorter optical path lengths because the process became photosaturated at higher values of VRPA. Nonetheless, a 50% increase in the treatment capacity was achieved by increasing the liquid depth by three times. As far as the authors know, this is the first work that quantitatively describes the effect of the radiation and the optical path length on micropollutant removal with Fe^{3+}-EDDS.

1. Introduction

In most countries the majority of wastewater is currently treated in conventional wastewater treatment plants (WWTPs), although secondary treatments are not efficient enough to completely remove certain organic pollutants such as drugs, pesticides, pharmaceuticals,

* Corresponding author at: Department of Chemical Engineering, University of Almería, 04120 Almería, Spain.
E-mail address: jsanchez@ual.es (J.A. Sánchez Pérez).

http://dx.doi.org/10.1016/j.cej.2017.08.096
Received 27 May 2017; Received in revised form 17 August 2017; Accepted 18 August 2017
Available online 23 August 2017
1385-8947/

hormones and personal care products [1,2]. These compounds, called micropollutants, are found in secondary WWTP effluents at concentrations levels of μg L^{-1} and ng L^{-1} and cause ecological harm as well as adverse health effects [3,4]. There are still no legal discharge limits for these pollutants in the WWTP effluents, but some regulations have been published in the last few years. In Switzerland, the rules demand the removal of 80% of a list of micropollutants [5] as part of the overall processes applied to municipal WWTP. In addition, the Commission Implementing Decision (EU) 2015/495 has recently established the first watch list of substances for EU-wide monitoring, and recommending further research and various treatments to remove them [6]. This list includes the pesticide acetamiprid (ACTM). In previous works, this neonicotinoid insecticide was used as a model pollutant because it is highly recalcitrant and can be easily determined by high performance liquid chromatography (HPLC) [7].

New technologies are undergoing research and development to remove micropollutants from secondary effluents, among which advanced oxidation processes (AOPs) are being intensively investigated [8,9]. The photo-Fenton process stands out for its efficiency in the removal of micropollutants [10]. It relies on the reaction between ferrous iron and hydrogen peroxide to produce the highly oxidative hydroxyl radicals. The ferric iron generated in this reaction is photoreduced by UV–Visible radiation to ferrous iron, giving rise to a redox cycle driven by the photon availability and consuming hydrogen peroxide. The optimum pH to carry out the process is 2.8 [11], albeit with the disadvantage that the treatment at acidic pH requires a previous acidification of the water as well as further neutralization before disposal into the environment or reuse. The fact that iron precipitates at neutral pH, requiring a final decantation stage, increases the overall operating costs. As such, the economic viability of the whole process is yet to be demonstrated. In this regard, two operating strategies at neutral pH have been reported: sequential additions of ferrous iron salt [12,13] or using iron chelating agents, such as oxalic acid, citric acid and Ethylenediamine-N,N′-disuccinic acid (EDDS) which form a complex with ferric iron, maintaining it in solution over a wide pH range [14–16]. Among the assayed chelating agents, EDDS is gaining a growing interest due to its biodegradability and high efficiency for micropollutant removal. Regarding toxicity, a recent study indicates that the treatment of secondary effluents using the Fe^{3+}-EDDS complex removes androgenic/glucocorticoid activity and estrogenicity, and attenuates the potential phytotoxicity and cytotoxicity of the treated water [17].

As for the photoreactors used for the application of the photo-Fenton process, tubular reactors with compound parabolic collectors (CPC) have been extensively studied to take advantage of solar UV radiation. The optical path length is short, the common tube diameter being 5 cm, giving rise to low optical thickness when using low iron concentrations (0.1 mM being the most common concentration in the literature for micropollutant removal [18,19]). Consequently, an inefficient use of photons reaching the reactor surface has been reported, pointing out the need for longer light path lengths [20]. More recently, the efficiency of micropollutant removal by solar photo-Fenton in raceway pond reactors (RPRs) compared with CPC reactors has been reported [21]. RPRs are extensive, low cost reactors in which the light path length can be varied by changing the liquid depth [22].

To achieve an efficient photonic use, the knowledge about the radiation field in the reactor is fundamental. The absorption of solar radiation is represented by the spatial distribution of the local volumetric rate of photon absorption (LVRPA). This variable combines the effects of light absorption and reactor geometry resulting in a very useful concept for the design and optimization of photocatalytic reactors [23]. In perfect mixing systems, under photolimitation conditions (reaction rate linearly depends on the photon absorption) an approximation can be made by averaging the LVRPA across the reactor volume and the average VRPA can be used [24,25]. For solar conditions at noon, the radiation field incident to the liquid surface can be assumed as parallel rays normal to the reactor surface [23], and the radiation field in the reactor can be simplified in only one-dimension in space. Therefore, the irradiance in the liquid could only change with liquid depth. This approach has been applied in previous works [26,27], and results obtained at lab scale under artificial light have been validated outdoors under solar light [28].

Until now, the effect of VRPA has been widely studied for the modelling of the photo-Fenton process at pH 2.8 [26–29]. However, Conte et al. recently proposed a kinetic model at pH 5 considering the effect of the VRPA of Fe^{3+} as ferrioxalate complex [30]. To optimize the photo-Fenton process at neutral pH, an in depth study of the VRPA of iron complexes is needed.

This research is focused on the study of the effect of the average VRPA on the kinetics of micropollutant removal with the Fe^{3+}-EDDS complex by solar photo-Fenton at neutral pH. For this purpose the pesticide ACTM was selected as a model pollutant at an initial concentration of 100 μg L^{-1}, within the concentration range of the whole concentration of micropollutants in secondary WWTP effluents. The average VRPA was varied from 383 to 1933 μE m^{-3} s^{-1}, corresponding to UV irradiances on the reactor surface from 10 to 50 W m^{-2} and 5 and 15 cm liquid depth with 0.1 mM Fe^{3+}-EDDS.

2. Materials and methods

2.1. Chemicals

Sulphuric acid (98%) and sodium hydroxide were supplied by J.T Baker®. HPLC grade Acetonitrile and sodium formate were obtained from BDH Prolabo Chemicals and Merck Millipore, respectively. Ferric sulphate (75%), ammonium nitrate, hydrogen peroxide (33%), acetic acid, hydrochloric acid (37%) and $CaSO_4{\cdot}H_2O$ were acquired from Panreac. $MgSO_4$, KCl, $(NH_4)_2SO_4$, Peptone, humic salt, sodium lauryle sulfonate, sodium lignin sulfonate, acacia gum powder, arabic acid, ortho-phenanthroline, titanium (IV) oxysulfate, ethylenediamine disuccinic acid (35%) and ascorbic acid, tetrabutylammonium bisulfate, formic acid (98%) and methanol were obtained from Sigma-Aldrich. Beef extract and peptone were purchased from Biolife and BD Bacto, respectively. Acetamiprid ($C_{10}H_{11}ClN_4$, 20% w/w) was acquired from EPIK®.

2.2. Experimental set-up

Experimentation was carried out at the Solar Energy Research Center (CIESOL), located at the University of Almería. For the purpose of this study, it was necessary to work at lab scale, under controlled experimental conditions; controlling the irradiance and the temperature, and using synthetic secondary effluent which composition is close to real secondary effluents and the same in each experimental run.

Experiments were conducted in 0.85-L (5 cm liquid depth) and 2.85-L (15 cm liquid depth) cylindrical stirred tank reactors placed inside a SunTest CPS+ solar box from Atlas, the emission range being 250–765 W m^{-2}. The walls of the reactors were opaque (walls of PVC), to avoid any incoming radiation through the walls, taking into account only radiation entering through the liquid surface. A scheme of the reactor layout inside the solar simulator is shown in Fig. S1.

UV irradiance at the reactor surface was measured with a spectroradiometer (Avantes AvaSpec Dual-Cannel Fiber Optic Spectrometer) in the wavelength range from 327 to 384 nm. A cooling coil connected to a thermostatic bath was used for temperature control.

The assays were performed at a temperature of 25 °C, the mean value of water temperature in the WWTP of the city of Almería, in the south-eastern Spain. Experiments at UV irradiances ranging from 10 to 50 W m^{-2} were carried out under these conditions by changing the distance from the water surface to the lamp and setting the power of the lamp in the SunTest CPS+ solar box. All the experiments were replicated and results show mean value ± standard deviation.

Regarding the concentration of reagents, that of hydrogen peroxide

was 30 mg L^{-1} (0.88 mM). This concentration value was selected because it was efficiently used in the treatment of secondary effluents by solar photo-Fenton performed at pH 2.8 [7]. For the experiments in which the effect of H_2O_2 concentration was studied, three values were tested, from 25 to 100 mg L^{-1} (from 0.74 to 2.94 mM), including the concentration set for experimentation within range.

2.3. Preparation of Fe^{3+}-EDDS complex

The complex stock solution was prepared by dissolving ferric iron salt in Milli-Q grade water previously acidified at pH 3 with HCl 1N. Once the iron had dissolved, the EDDS was added and the mixture was stirred for 5 min to ensure the formation of the complex at a Fe^{3+}:EDDS ratio of 1:1. Due to the instability of the complex with light, it was prepared in the dark. The concentration of iron in this stock solution was 85 mM and was diluted down to 0.1 mM for experiments. The EDDS increased the dissolved organic carbon concentration (DOC) of the water matrix by 12 mg L^{-1}. After adding the complex to the reactor, the surface was uncovered at the same time as the hydrogen peroxide was added and the reaction started.

2.4. Water matrix

The experiments were carried out in demineralised water and synthetic secondary effluent with a DOC content of around 12 mg L^{-1} [27]. The pH ranged from 7 to 7.5.

As for the $HO^{\cdot}$ scavenger effect of CO_3^{2-}/HCO_3^- ions in wastewater, three different concentrations expressed as total inorganic carbon (TIC) were preliminarily assayed to assess its impact on the proposed study. The TIC levels were 10, 50 and 100 mg L^{-1}, corresponding to 51, 254 and 510 mg L^{-1} of HCO_3^-, respectively.

Fig. 1 shows that the higher the TIC concentration, the lower the ACTM degradation. Therefore, bicarbonates inhibit micropollutant degradation and consequently high TIC concentrations should be avoided. For the rest of the experiment, 96 mg L^{-1} of $NaHCO_3$ were added to the synthetic effluent (14 mg L^{-1} TIC), according to [31]

2.5. Determination of the volumetric rate of photon absorption (VRPA) and optical thickness

The average VRPA over the liquid volume in the photoreactor, expressed in μE m^{-3} s^{-1}, was calculated by Eq. (1) [27]. Taking into account that Fe^{3+}-EDDS concentration changes over time, the photon absorption also changes, so the average VRPA was calculated at the start of the reaction ($VRPA_0$). This equation, defined for monochromatic light, can be used with polychromatic light by averaging the values of k_A and UV_0 in the wavelength range of the measurement given by the radiometer.

$$VRPA_0 = \frac{S_R}{V_R}\int_0^D k_A \cdot C_{Fe} \cdot UV_o \cdot 10^{-k_A \cdot C_{Fe} \cdot z} dz \quad (1)$$

where UV_0 is total UV photon irradiance at the reactor surface, C_{Fe} is Fe^{3+}-EDDS concentration, k_A is the decadic specific spectral averaged absorption coefficient of Fe^{3+}-EDDS complex, D is reactor depth, S_R is reactor surface and V_R reactor volume. Irradiance data were converted from W m^{-2} to μE m^{-2} s^{-1} by Planck's equation.

k_A was calculated by Eq. (2) [26]. The UV absorption spectra in the synthetic secondary effluent was measured at several Fe^{3+}-EDDS concentrations, from 1 to 15 mg L^{-1} (from 0.018 to 0.269 mM), and a temperature of 25 °C (Fig. S2). The value of k_A was 89.38 mM^{-1} m^{-1}.

$$k_A = \frac{\int_{\lambda min}^{\lambda max} \varepsilon_\lambda I_\lambda d\lambda}{\int_{\lambda min}^{\lambda max} I_\lambda d\lambda} \quad (2)$$

where ε_λ is the specific absorption coefficient (mM^{-1} m^{-1}) and I_λ is the spectral distribution of incident radiation (lamp power), measured with a spectroradiometer (Avantes AvaSpec Dual-Cannel Fiber Optic Spectrometer). For both parameters λ ranged from 327 to 384 nm.

The optical thickness, τ, was calculated by Eq. (3):

$$\tau = k_A C_{Fe} D \quad (3)$$

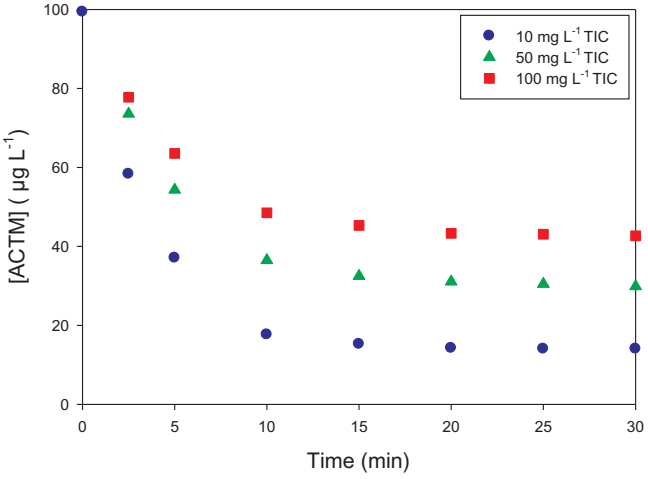

Fig. 1. Effect of TIC concentration on ACTM degradation.

2.6. Chemicals analysis

Once taken from the reactor, the samples were filtered through nylon filters from Millipore® (0.20 μm diameter pore). After that, the filter was washed with acetonitrile at a sample: acetonitrile ratio of 10:1. Acetonitrile was used as an $HO^{\cdot}$ scavenger to stop the reaction and draw out any trace of contaminant that had been trapped in the filter [32].

Total dissolved iron and ferrous iron concentrations were spectrophotometrically determined at 510 nm according to the 1, 10-phenanthroline method (ISO 6332), while hydrogen peroxide was determined at 410 nm using titanium (IV) oxysulfate solution (DIN 38 402 H15). The iron and hydrogen peroxide limits of detection (LOD) were 1.8 10^{-3} mM and 7.9 10^{-3} mM, respectively.

Dissolved Organic Carbon (DOC) and Total inorganic Carbon (TIC) were quantified by a Shimadzu-V CPH TOC analyser with a LOD of 1 mg L^{-1} and the pH was measured with a pH METER GLP 21.

Fe^{3+}-EDDS concentration was measured by liquid chromatography (HPLC Agilent 1100 Series) using an Ion-Pair method with a reversed-phase column (Luna C18, 150 × 3 mm, 5 μm particle size) [33]. The LOD was 1.8 10^{-3} mM.

Model micropollutant concentration was determined by liquid chromatography (HPLC Agilent 1200 Series). Equipment characteristics and method were previously reported by Sánchez Pérez et al. [28]. The LOD was 5 μg L^{-1}

3. Results and discussion

3.1. Photolysis of Fe^{3+}-EDDS complex

The main product generated by the Fe^{3+}-EDDS photolysis is Fe^{2+}, R. (1), which in the presence of H_2O_2 yields hydroxyl radicals by the Fenton's reaction, R. (2). Micropollutants are further oxidised by the attack of $HO^{\cdot}$ radicals. As previously reported by Li et al. [34], the photolysis of the Fe^{3+}-EDDS complex also promotes the generation of H_2O_2 through reactions R. (4)–(7),

$$[Fe^{3+}\text{-EDDS}]^- + h\nu \rightarrow Fe^{2+} + EDDS^{\cdot 3-} \quad (R.1)$$

$$Fe^{2+} + H_2O_2 \rightarrow Fe^{3+} + HO^{\cdot} + OH^- \quad (R.2)$$

$$EDDS^{\cdot 3-} + O_2 \rightarrow O_2^{\cdot -} + EDDS' \quad (R.3)$$

$$Fe^{2+} + O_2^{\cdot -} + 2H_2O \rightarrow Fe^{3+} + H_2O_2 + 2OH^- \quad (R.4)$$

$$Fe^{2+} + HO_2^{\cdot} + H_2O \rightarrow Fe^{3+} + H_2O_2 + OH^- \quad (R.5)$$

$$O_2^{\cdot -} + HO_2^{\cdot} + H_2O \rightarrow H_2O_2 + O_2 + OH^- \quad (R.6)$$

$$HO_2^{\cdot} + HO_2^{\cdot} \rightarrow H_2O_2 + O_2 \quad (R.7)$$

Therefore, for operating purposes of the photo-Fenton process conducted with Fe^{3+}-EDDS, it would be interesting to clarify whether the generated H_2O_2 can contribute to Fe^{3+}-EDDS complex decomposition through R. (2) and R. (8) without any initial addition of hydrogen peroxide:

$$[Fe^{3+}\text{-EDDS}]^- + HO^{\cdot} \rightarrow Fe^{\cdot}\text{-EDDS}_{ox} \quad (R.8)$$

To assess the relevance of R. (8) due to the generated H_2O_2, two experiments in demineralised water exposing Fe^{3+}-EDDS to 30 W m^{-2} of UV irradiance with and without 2-propanol (0.5 mM) were carried out in the reactor with 5 cm liquid depth, the initial VRPA being 1160 μE m^{-3} s^{-1}. 2-propanol was used to trap all $HO^{\cdot}$ radicals ($k_{2Pr,HO^{\cdot}}$ = 1.9 10^9 M^{-1} s^{-1}) [35] in solution after irradiation. As can be seen in Fig. 2, the profiles overlapped, thus it could be concluded that R. (8) has no effect on the decomposition of the complex when no hydrogen peroxide is added. In both cases, the total dissolved iron concentration remained constant after the complex decomposition.

Although Fe^{3+}-EDDS photolysis can generate H_2O_2, in photo-Fenton treatments the concentration of added H_2O_2 is much higher than that generated by R. (4)–(7), making these reactions irrelevant for the decomposition mechanism of the complex.

The next step was to check the effect of H_2O_2 on Fe^{3+}-EDDS under irradiation. To this end, experiments were performed at three H_2O_2 concentrations (0.74, 1.47 and 2.94 mM), in demineralised water (with 14 mg L^{-1} of TIC) at an initial VRPA value of 1160 μE m^{-3} s^{-1}. As can be seen in Fig. 3, there was no effect of the different H_2O_2 concentration on total dissolved iron and ferrous iron profiles. However, with a higher H_2O_2 concentration, the complex decomposition was slightly faster, the pseudo-first order rate constant being 0.59 ± 0.02 min^{-1}, 0.61 ± 0.01 min^{-1} and 0.81 ± 0.03 min^{-1} at H_2O_2 concentrations of 0.74 mM, 1.47 mM and 2.94 mM, respectively.

Both the total dissolved iron concentration and complex concentration decreased in the first few minutes of reaction. Ferrous iron concentration was very low, below 0.02 mM, due to R. (2). In all cases, part of the iron species remained in solution after the complete disappearance of the complex [36]. Comparing Figs. 2 and 3(b) it can be seen that the complex concentration decreased faster in the presence of H_2O_2 and UV radiation (photo-Fenton process) than by photolysis. Comparing Figs. 2 and 3(b) it can be seen that the complex concentration decreased four times faster in the presence of H_2O_2 and UV radiation (photo-Fenton process) than by photolysis, with pseudo-first order rate constant of 0.61 ± 0.01 min^{-1} for photo-Fenton and 0.15 ± 0.02 min^{-1} for photolysis. It may be due to the fact that once the complex is degraded by light, R. (1), Fe^{2+} is oxidized by H_2O_2, R. (1), generating a significant concentration of $HO^{\cdot}$ to oxidize the complex. Thus, R. (8) could be relevant when H_2O_2 is added. The oxidized form of the complex would not be detected by the HPLC method, which could explain that once the complex is degraded part of the iron species remains in solution.

Another way of Fe^{3+}-EDDS decomposition would be by the direct attack of H_2O_2, R. (9):

$$[Fe^{3+}-EDDS]^- + H_2O_2 \rightarrow Fe_{2+}-EDDS + HO_2^{\cdot} / O_2^{\cdot -} + H^+ \quad (R.9)$$

Thus, the described above experiments were repeated in the dark. No change in the concentration of the present species was observed, pointing out that R. (9) does not have a significant effect on the kinetics of the process in the conditions selected for the experimentation.

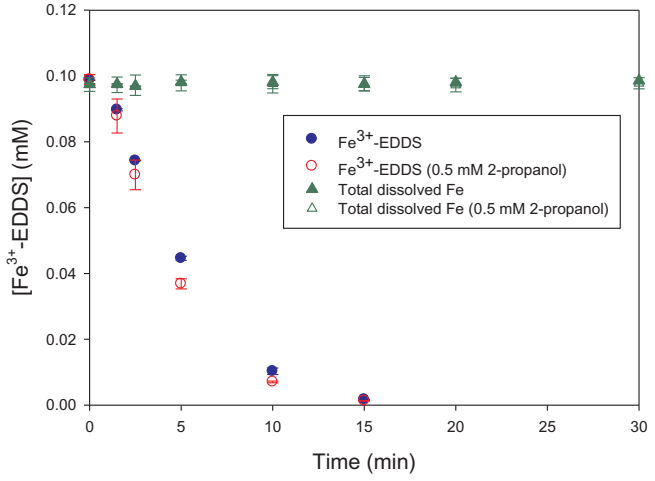

Fig. 2. Complex and total dissolved iron profiles at $VRPA_0$ of 1160 μE m^{-3} s^{-1} with and without 2-propanol.

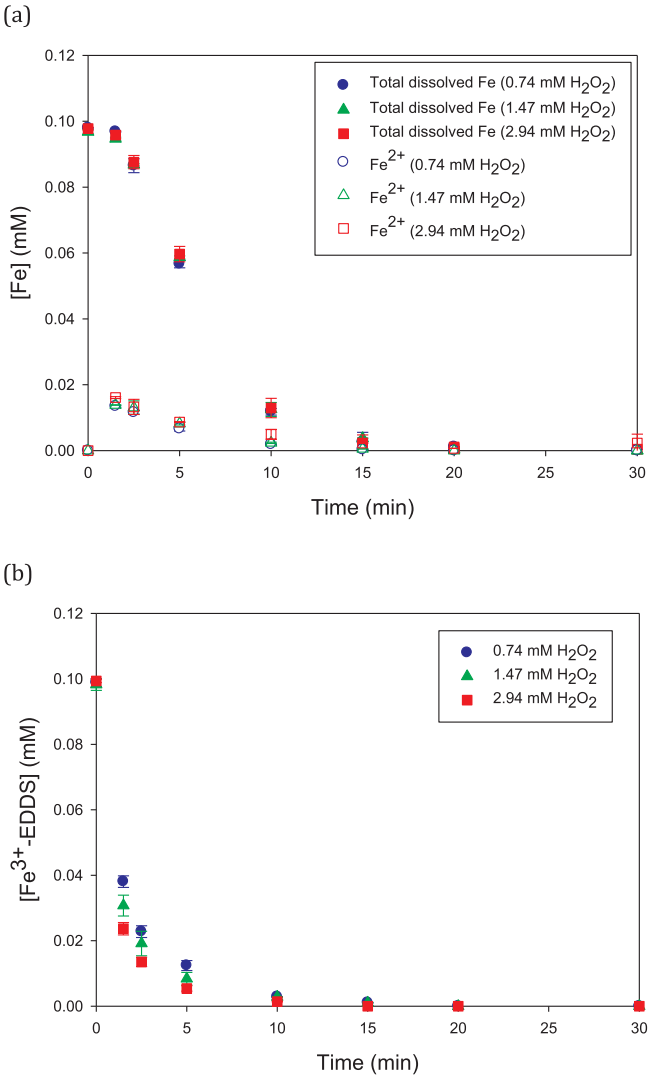

Fig. 3. Total dissolved iron (closed symbols), ferrous iron (open symbols) (a) and Fe^{3+}-EDDS complex (b) profiles at different H_2O_2 concentrations at $VRPA_0$ of 1160 μE m^{-3} s^{-1}.

3.2. Effect of photon absorption on the photo-Fenton process operated with Fe^{3+}-EDDS

The photoreduction of ferric iron at pH 2.8 has been previously studied, in doing so showing that the linear increase of reaction rate with the volumetric rate of photon absorption, i.e. first order reaction with regard to VRPA, turns into zero order at high VRPA values, in particular, above 866 μE m^{-3} s^{-1} [28]. However, this effect with the Fe^{3+}-EDDS complex at neutral pH has not been reported. To fill this gap, photo-Fenton degradation of the pesticide ACTM in synthetic secondary effluent at neutral pH was conducted at 5 cm liquid depth and 5 levels of UV irradiance: 10, 20, 30, 40 and 50 W m^{-2}, corresponding to $VRPA_0$ values of 387, 773, 1160, 1547 and 1933 μE m^{-3} s^{-1}, respectively. The concentration profiles with reaction time are shown in Figs. 4 and 5.

As for iron species behaviour, Fig. 4 shows that increasing irradiance from 10 to 40 W m^{-2} gives rise to a faster photolysis of the complex, decreasing its concentration 5 times faster and releasing Fe^{2+} which is oxidised to Fe^{3+} by H_2O_2 and then Fe^{3+} precipitates as ferric hydroxides, causing a drop in total dissolved iron concentration. Nonetheless, no significant differences were observed when increasing irradiance from 40 W m^{-2} to 50 W m^{-2}.

Concerning the hydrogen peroxide consumption and ACTM removal, as seen in Fig. 5, a similar effect was found. The higher the irradiance, the higher the H_2O_2 consumption and ACTM degradation up to 40 W m^{-2} (the photolimitation phenomenon), decreasing the H_2O_2 and ACTM concentrations 4 times faster, while the profiles overlapped when irradiance was increased from 40 W m^{-2} to 50 W m^{-2}, due to the photosaturation phenomenon.

Regarding the evolution of DOC, no mineralization was observed under these mild oxidation conditions. The DOC concentration of the final treated water was the same as the initial value, around 24 mg L^{-1} (12 mg L^{-1} DOC due to the water composition and 12 mg L^{-1} provided by the EDDS). This increase in DOC can be considered a drawback although the mineralization of DOC is not a matter in the treatment of municipal wastewater secondary effluents whenever accomplishing the legislation limits. In this case, the daily emission limit for DOC to surface waters established by the Andalusian Regional Government is 45.9 ppm [37] and in general emission limit of municipal wastewater treatment plants are in the range of < 125 mg L^{-1} of chemical oxygen demand in whole developed countries [38]. As for water toxicity, it has been previously reported that the treatment of secondary effluents by solar photo-Fenton with Fe^{3+}-EDDS efficiently removes toxicity and micropollutants [17], which is the final objective of this study.

These photolimitation (increasing irradiance causing a higher reaction rate) and photosaturation (increasing irradiance not causing any effect) phenomena could be explained with the same rationale reported for ferric iron photoreduction at acidic pH [28]. Once Fe^{3+}-EDDS absorbs light, it reaches an activated electronic state, R. (10). In this state, the iron transfers an electron to the organic ligand yielding an EDDS radical and ferrous iron, R. (11), but a fraction of absorbed radiation can be converted into heat (Q) meaning the activated complex turns back into Fe^{3+}-EDDS, R. (12).

$$[Fe^{3+}\text{–}EDDS]^{-} + h\nu \rightarrow [Fe^{3+}\text{–}EDDS]^{-*} \quad \text{(R.10)}$$

$$[Fe^{3+}-EDDS]^{-*} \rightarrow Fe^{2+} + EDDS^{\cdot 3-} \quad \text{(R.11)}$$

$$[Fe^{3+}-EDDS]^{-*} \rightarrow [Fe^{3+}-EDDS]^{-} + Q \quad \text{(R.12)}$$

It was also observed (Fig. 5) that after 20 min of the reaction, there was practically no effect by irradiance on hydrogen peroxide consumption and micropollutant degradation except for the lowest irradiance value tested, 10 Wm^{-2}. This is due to the fact that the complex decomposed after a short time under higher irradiation. In all the cases more than 80% of ACTM removal was achieved after 10 min of the reaction, except at the lowest $VRPA_0$ (387 μE m^{-3} s^{-1}).

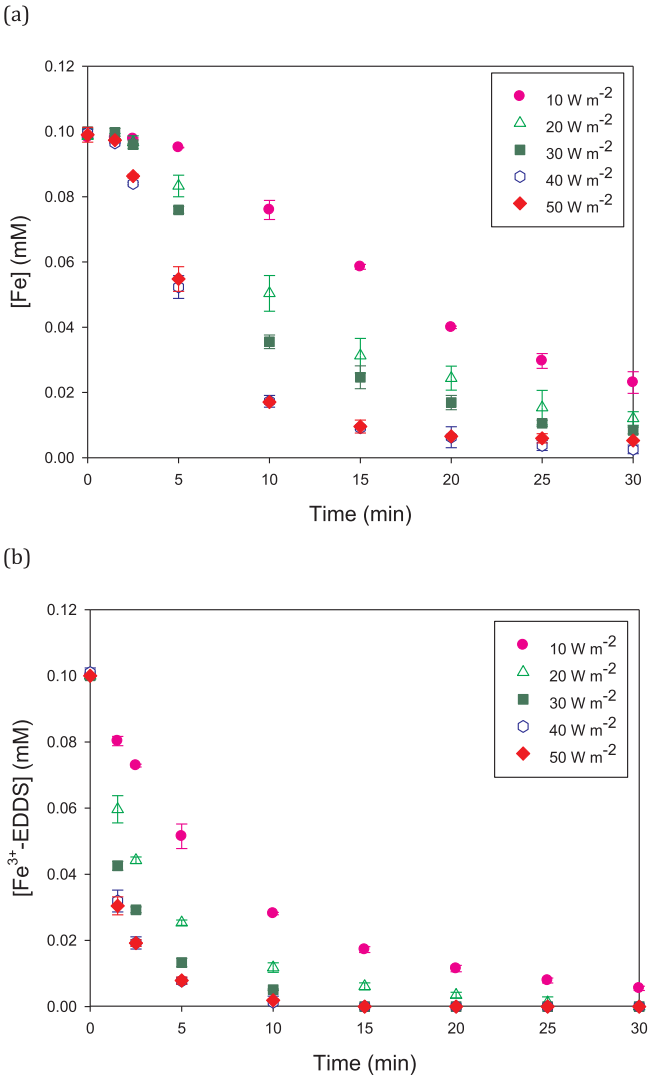

Fig. 4. Effect of the UV irradiance on total dissolved iron, ferrous iron (a) and Fe^{3+}-EDDS complex (b) concentrations at 5 cm liquid depth.

Fig. 6. shows the variation of the pseudo-first order rate constants of H_2O_2 consumption, ACTM degradation and Fe^{3+}-EDDS decomposition as a function of $VRPA_0$. In each of the three cases, a linear dependence was observed until reaching photosaturation for $VRPA_0$ values above 1547 μE m^{-3} s^{-1}, the relationships being:

$$k_{Fe3+-EDDS}(min^{-1}) = (5.0 \pm 0.2)10^{-4}VRPA_0(\mu\ E\ m^{-3}s^{-1}); \quad r^2 = 0.98 \quad (4)$$

$$k_{H2O2}(min^{-1}) = (1.5 \pm 0.1)10^{-4}VRPA_0(\mu\ E\ m^{-3}s^{-1}); \quad r^2 = 0.97 \quad (5)$$

$$k_{ACTM}(min^{-1}) = (3.7 \pm 0.2)10^{-4}VRPA_0(\mu\ E\ m^{-3}s^{-1}); \quad r^2 = 0.97 \quad (6)$$

It must be considered that the concept of average VRPA is not totally applicable for saturation conditions, but in this study it was calculated only to show that the phenomenon occurs.

These assays were carried out in a stirred tank reactor, with the purpose of determining the photosaturation limit for a correct scaling up of the process in photocatalytic outdoor solar photoreactors such as RPRs. The objective of such photoreactors is to run the process under photolimitation conditions to make the most of the photons reaching the reactor surface. In these reactors the treatment capacity can be changed by altering the liquid depth according to the availability of radiation [22]. Solar UV irradiances higher than 40 W m^{-2} can easily

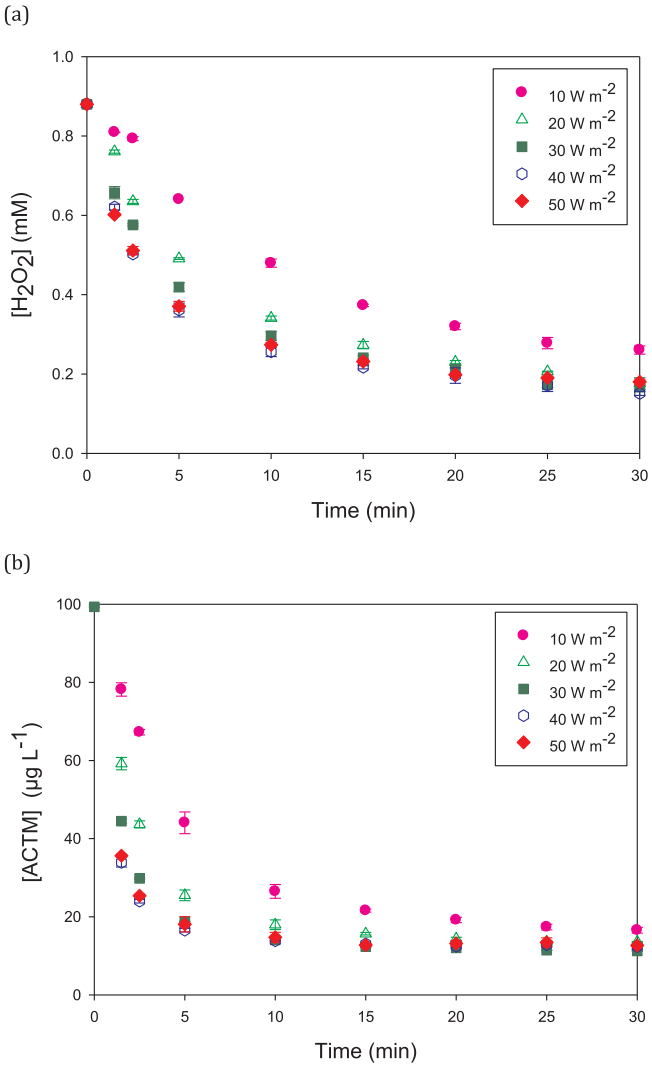

Fig. 5. Effect of the UV irradiance on H_2O_2 consumption (a) and ACTM degradation (b) at 5 cm liquid depth.

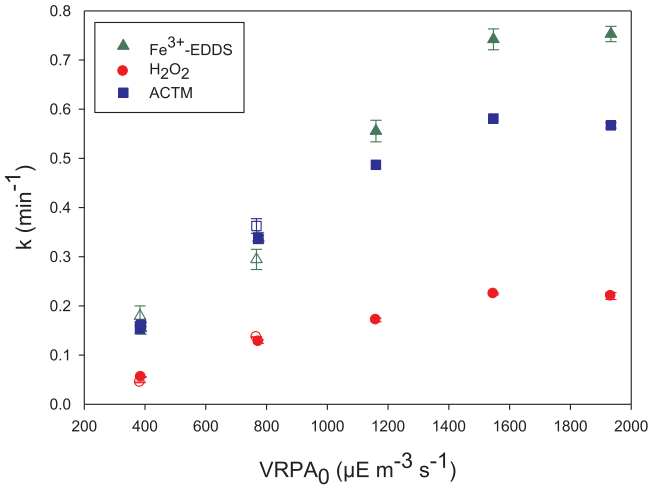

Fig. 6. Effect of the initial VRPA on the rate constant of H_2O_2 consumption, ACTM degradation and Fe^{3+}-EDDS decomposition. Liquid depth: 5 cm closed symbols, 15 cm open symbols.

be reached on sunny days between spring and autumn in many geographical locations all over the world, leading to photosaturation conditions when working at low liquid depth. Accordingly, greater liquid depth would decrease the average VRPA down to the preferred photolimitation conditions. This change in liquid depth is easily set up in photoreactors such as RPRs.

As previously discussed, with Fe^{3+}-EDDS complex 0.1 mM, the photosaturation phenomenon was reached for $VRPA_0$ values above 1547 µE m^{-3} s^{-1}. However, with ferrous iron salt 0.1 mM at acidic pH this phenomenon takes place above 866 µE m^{-3} s^{-1}. This is due to the higher molar absorptivity of iron, when complexed with EDDS, 89.38 mM^{-1} m^{-1} in contrast with 51.11 mM^{-1} m^{-1} at pH 2.8.

It is worth comparing ACTM removal under photosaturating conditions at both pH values. Fig. 7 shows that the main difference took place after 5 min of the reaction, when the Fe^{3+}-EDDS complex had almost completely decomposed, as such halting ACTM removal at 87%, whereas at acidic pH the process continued for a longer time, achieving complete ACTM removal in 9 min.

At pH 2.8, the reaction time can be set according to the availability of radiation since the iron remains in solution throughout the whole reaction. However, at neutral pH the increase in VRPA not only causes an increase in the micropollutant removal rate, but also the decomposition of the complex. Consequently, the photo-Fenton process at neutral pH with Fe^{3+}-EDDS is only efficient at short reaction times, consistent with the application for microcontaminant removal in a few minutes, but not suitable for the degradation of higher concentrations of contaminants in industrial wastewaters, as described by Papoutsakis et al. [39]. As for the operation of the photo-Fenton process in continuous flow with Fe^{3+}-EDDS as recently reported at acidic pH [7], the decomposition of the complex can be balanced with the continuous addition of Fe^{3+}-EDDS allowing the continuous operation at hydraulic residence times as high as 40 min [40].

3.3. Effect of VRPA on the treatment capacity

At 5 cm liquid depth, the optical thickness was 0.45 and it could be increased by increasing iron concentration, albeit with the disadvantage that higher values of iron concentration imply the use of higher EDDS concentrations, and therefore the increase of DOC. Another possibility would be to increase the liquid depth, thereby decreasing VRPA. In fact, as recently reported by de la Obra et al. [21], high micropollutant removal efficiencies were achieved in raceway pond reactors with 15 and 20 cm liquid depth using the Fe^{3+}-EDDS

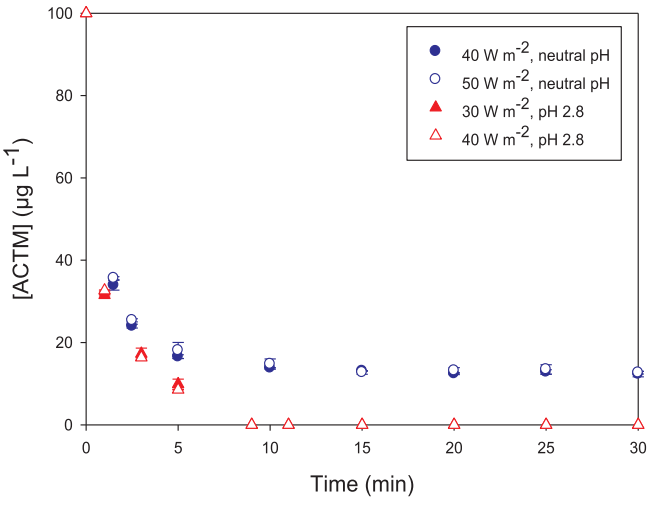

Fig. 7. ACTM removal under photosaturation conditions as a function of pH at initial iron concentration of 0.1 mM. ($VRPA_0$ 867 and 1080 µE m^{-3} s^{-1} at pH 2.8 and 1547 and 1933 µE m^{-3} s^{-1} at neutral pH).

complex.

In line with this rationale, the effect of liquid depth on reactor performance was checked at 20 and 40 W m^{-2} of irradiance and 15 cm liquid depth, corresponding to an optical thickness of 1.34 and $VRPA_0$ values of 383 and 767 μE m^{-3} s^{-1}, respectively. Due to $VRPA_0$ values being in the photolimitation range, the higher the irradiance, the faster the H_2O_2 consumption and ACTM removal, as seen in Fig. 8. As for the rate constants, the calculated values for 15 cm liquid depth were also represented in Fig. 6 pointing out the good concordance with data obtained at 5 cm liquid depth. Indeed, the profiles at 5 cm, 20 W m^{-2} and 15 cm, 40 W m^{-2} overlapped as both experimental conditions gave the same $VRPA_0$.

To seek the best process outcome, the treatment capacity (TC) for 80% ACTM removal was calculated by Eq. (7) [27] and the results are shown in Table 1 as a function of irradiance and liquid depth.

$$TC = \frac{0.8[ACTM]_0 V_R}{S_R t} \quad (7)$$

where t denotes the reaction time to reach 80% ACTM removal.

Operation of RPRs at 5 cm liquid depth has been proposed for winter conditions [21]. In this case, a characteristic irradiance value is 10 W m^{-2}, with the treatment capacity being low,

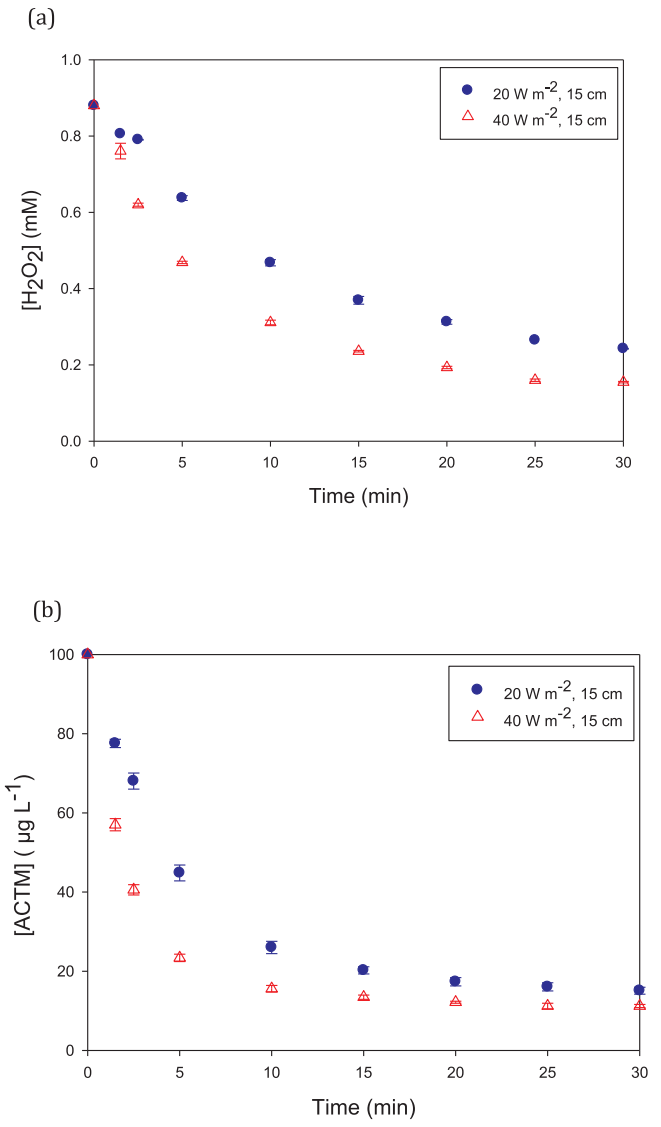

Fig. 8. H_2O_2 consumption (a) and ACTM degradation (b) profiles at 15 cm liquid depth and 20 and 40 W m^{-2} of irradiance.

Table 1
Treatment capacity for 80% ACTM removal.

Liquid depth (cm)	Irradiance (W m^{-2})	$VRPA_0$ (μE m^{-3} s^{-1})	Reaction time (min)	TC (mg m^{-2} h^{-1})
5	10	387	19	13
5	20	773	8	30
5	40	1547	4	60
15	20	383	14	51
15	40	767	8	90

13 mg ACTM m^{-2} h^{-1}. Considering an irradiance close to the annual mean value in Almería (Spain) of 20 W m^{-2}, TC rises to 30 mg ACTM m^{-2} h^{-1} and reaches 60 mg ACTM m^{-2} h^{-1} at irradiance of 40 W m^{-2}, representative of summer conditions. This linear increase is due to the rise of $VRPA_0$ from 387 to 1547 μE m^{-3} s^{-1}, in the photolimitation range, and the consequent decrease in reaction time. Nonetheless, at the annual mean irradiance of 20 W m^{-2}, increasing the liquid depth to 15 cm gives rise to a significant TC improvement, 51 mg ACTM m^{-2} h^{-1}, despite the lower $VRPA_0$ value. As for summer conditions, i.e. 40 W m^{-2}, a 50% increase in the treatment capacity is reached at 15 cm liquid depth when compared to 5 cm. However the reaction time is also higher, but by not three times (ratio 15 cm: 5 cm). Again the linear dependence of the volumetric reaction rate with $VRPA_0$ is shown at ≈770 μE m^{-3} s^{-1} attained at 20 W m^{-2} −5 cm and 40 W m^{-2} −15 cm. In both cases, 8 min is needed for 80% ACTM removal, but TC is three times higher in the latter than in the former. Therefore, VRPA does not directly determine the treatment capacity, but the reaction kinetics and liquid depth become significant variables in photoreactor performance.

The treatment capacity values of 51–90 mg m^{-2} h^{-1} reached with 0.1 mM Fe^{3+}-EDDS at 15 cm liquid depth at neutral pH are in the interval reported at pH 2.8 for ACTM removal, under the same conditions of liquid depth and iron concentration (40–133 mg m^{-2} h^{-1}) [27].

4. Conclusions

The results presented show, for the first time, that reaction kinetics of the photo-Fenton process at neutral pH operated with the Fe^{3+}-EDDS, linearly depend on the initial VRPA, reaching photosaturation at $VRPA_0$ ≈ 1550 μE m^{-3} s^{-1}, a higher value than that reported at acidic pH with free Fe^{3+}, due to the higher absorptivity of the complexed Fe^{3+}. Nonetheless, due to radiation absorption changes with time because of Fe^{3+}-EDDS complex photolysis, the change of the VRPA with reaction time should be taken into account for kinetic modeling. These findings allow new developments for large-scale application due to the relevance of quantifying radiation absorption on process performance as a function of the optical path length. Indeed, although the process is not photosaturated at short optical path lengths, the presented results show that the treatment capacity can be increased by increasing the liquid depth. In spite of the instability of the complex with light, treatment capacities of 90 mg ACTM m^{-2} h^{-1} for 80% ACTM removal can be achieved with low Fe^{3+}-EDDS concentrations and reaction time in the range of tens of minutes. This is consistent with the application for the removal of microcontaminants in secondary effluents. Therefore, EDDS is an alternative to acidic pH (and subsequent neutralization) in photo-Fenton treatment of micropollutants, mainly for applications related with water reuse where remaining non-toxic and biodegradable DOC would not be an issue, for example in irrigation. Moreover, from the set of experiments performed in this study the main reactions affecting the process were revealed.

Acknowledgements

This research was supported by the Ministry for Economy and

Competitiveness (Spanish Government) and the European Regional Development Fund (ERDF), project CTQ2013-46398-R and CTM2015-71054-REDT. Paula Soriano-Molina would like to acknowledge the Ministry of Education, Culture and Sport for her FPU scholarship (AP2014/01030).

Appendix A. Supplementary data

Supplementary data associated with this article can be found, in the online version, at http://dx.doi.org/10.1016/j.cej.2017.08.096.

References

[1] M.C. Campos-Mañas, P. Plaza-Bolaños, J.A. Sáchez Pérez, S. Malato, A. Agüera, Fast determination of pesticides and other contaminants of emerging concern in treated wastewater using direct injection coupled to highly sensitive ultra-high performance liquid chromatography-tandem mass spectrometry, J. Chromatogr. A 1507 (2017) 84–94, http://dx.doi.org/10.1016/j.chroma.2017.05.053.

[2] L. Kong, K. Kadokami, S. Wang, H.T. Duong, H.T.C. Chau, Monitoring of 1300 organic micro-pollutants in surface waters from Tianjin, North China, Chemosphere 122 (2015) 125–130, http://dx.doi.org/10.1016/j. chemosphere.2014.11.025.

[3] S.U. Gerbersdorf, C. Cimatoribus, H. Class, K.H. Engesser, S. Helbich, H. Hollert, C. Lange, M. Kranert, J. Metzger, W. Nowak, T.B. Seiler, K. Steger, H. Steinmetz, S. Wieprecht, Anthropogenic trace compounds (ATCs) in aquatic habitats — research needs on sources, fate, detection and toxicity to ensure timely elimination strategies and risk management, Environ. Int. 79 (2015) 85–105, http://dx.doi.org/10.1016/j.envint.2015.03.011.

[4] M. Stuart, D. Lapworth, E. Crane, A. Hart, Review of risk from potential emerging contaminants in UK groundwater, Sci. Total Environ. 416 (2012) 1–21, http://dx.doi.org/10.1016/j.scitotenv.2011.11.072.

[5] R.I.L. Eggen, J. Hollender, A. Joss, M. Schärer, C. Stamm, Reducing the discharge of micropollutants in the aquatic environment: the benefits of upgrading wastewater treatment plants, Environ. Sci. Technol. 48 (2014) 7683–7689, http://dx.doi.org/10.1021/es500907n.

[6] M.O. Barbosa, N.F.F. Moreira, A.R. Ribeiro, M.F.R. Pereira, A.M.T. Silva, Occurrence and removal of organic micropollutants: an overview of the watch list of EU Decision 2015/495, Water Res. 94 (2016) 257–279, http://dx.doi.org/10.1016/j.watres.2016.02.047.

[7] S. Arzate, J.L. García Sánchez, P. Soriano-Molina, J.L. Casas López, M.C. Campos-Mañas, A. Agüera, J.A. Sánchez Pérez, Effect of residence time on micropollutant removal in WWTP secondary effluents by continuous solar photo-Fenton process in raceway pond reactors, Chem. Eng. J. 316 (2017) 1114–1121, http://dx.doi.org/10.1016/j.cej.2017.01.089.

[8] I. Michael, L. Rizzo, C.S. Mcardell, C.M. Manaia, C. Merlin, T. Schwartz, C. Dagot, D. Fatta-kassinos, Urban wastewater treatment plants as hotspots for the release of antibiotics in the environment: a review, Water Res. 47 (2012) 957–995, http://dx.doi.org/10.1016/j.watres.2012.11.027.

[9] N. De la Cruz, J. Giménez, S. Esplugas, D. Grandjean, L.F. de Alencastro, C. Pulgarín, Degradation of 32 emergent contaminants by UV and neutral photo-fenton in domestic wastewater effluent previously treated by activated sludge, Water Res. 46 (2012) 1947–1957, http://dx.doi.org/10.1016/j.watres.2012.01.014.

[10] L. Prieto-Rodríguez, D. Spasiano, I. Oller, I. Fernández-Calderero, A. Agüera, S. Malato, Solar photo-Fenton optimization for the treatment of MWTP effluents containing emerging contaminants, Catal. Today 209 (2013) 188–194, http://dx.doi.org/10.1016/j.cattod.2013.01.002.

[11] E. Neyens, J. Baeyens, A review of classic Fenton's peroxidation as an advanced oxidation technique, J. Hazard. Mater. 98 (2003) 33–50, http://dx.doi.org/10.1016/S0304-3894(02)00282-0.

[12] I. Carra, J.L. Casas López, L. Santos-Juanes, S. Malato, J.A. Sánchez Pérez, Iron dosage as a strategy to operate the photo-Fenton process at initial neutral pH, Chem. Eng. J. 224 (2013) 67–74, http://dx.doi.org/10.1016/j.cej.2012.09.065.

[13] I. Carra, S. Malato, M. Jiménez, M.I. Maldonado, J.A. Sánchez Pérez, Microcontaminant removal by solar photo-Fenton at natural pH run with sequential and continuous iron additions, Chem. Eng. J. 235 (2014) 132–140, http://dx.doi.org/10.1016/j.cej.2013.09.029.

[14] W. Huang, M. Brigante, F. Wu, K. Hanna, G. Mailhot, Development of a new homogenous photo-Fenton process using Fe(III)-EDDS complexes, J. Photochem. Photobiol. A: Chem. 239 (2012) 17–23, http://dx.doi.org/10.1016/j.jphotochem.2012.04.018.

[15] D.R. Manenti, P.A. Soares, A.N. Módenes, F.R. Espinoza-Quiñones, R.A.R. Boaventura, R. Bergamasco, V.J.P. Vilar, Insights into solar photo-Fenton process using iron(III)–organic ligand complexes applied to real textile wastewater treatment, Chem. Eng. J. 266 (2015) 203–212, http://dx.doi.org/10.1016/j.cej.2014.12.077.

[16] L. Clarizia, D. Russo, I. Di Somma, R. Marotta, R. Andreozzi, Homogeneous photo-Fenton processes at near neutral pH: a review, Appl. Catal. B: Environ. 209 (2017) 358–371, http://dx.doi.org/10.1016/j.apcatb.2017.03.011.

[17] G. Rivas Ibáñez, M. Bittner, Z. Toušová, M.C. Campos-Mañas, A. Agüera, J.L. Casas López, J.A. Sánchez Pérez, K. Hilscherová, Does micropollutant removal by solar photo-Fenton reduce ecotoxicity in municipal wastewater? A comprehensive study at pilot scale open reactors, J. Chem. Technol. Biotechnol. 92 (2017) 2114–2122, http://dx.doi.org/10.1002/jctb.5212.

[18] S. Papoutsakis, S. Miralles-Cuevas, I. Oller, J.L. Garcia Sánchez, C. Pulgarin, S. Malato, Microcontaminant degradation in municipal wastewater treatment plant secondary effluent by EDDS assisted photo-Fenton at near-neutral pH: an experimental design approach, Catal. Today 252 (2015) 61–69, http://dx.doi.org/10.1016/j.cattod.2015.02.005.

[19] N. Klamerth, S. Malato, A. Agüera, A. Fernández-Alba, Photo-Fenton and modified photo-Fenton at neutral pH for the treatment of emerging contaminants in wastewater treatment plant effluents: a comparison, Water Res. 47 (2013) 833–840, http://dx.doi.org/10.1016/j.watres.2012.11.008.

[20] I. Carra, J.L. García Sánchez, J.L. Casas López, S. Malato, J.A. Sánchez Pérez, Phenomenological study and application of the combined influence of iron concentration and irradiance on the photo-Fenton process to remove micropollutants, Sci. Total Environ. 478 (2014) 123–132, http://dx.doi.org/10.1016/j.scitotenv.2014.01.066.

[21] I. De Obra, L. Ponce-Robles, S. Miralles-Cuevas, I. Oller, S. Malato, J.A. Sánchez Pérez, Microcontaminant removal in secondary effluents by solar photo-Fenton at circumneutral pH in raceway pond reactors, Catal. Today 287 (2017) 10–14, http://dx.doi.org/10.1016/j.cattod.2016.12.028.

[22] I. Carra, L. Santos-Juanes, F.G. Acién Fernández, S. Malato, J.A. Sánchez Pérez, New approach to solar photo-Fenton operation. Raceway ponds as tertiary treatment technology, J. Hazard. Mater. 279 (2014) 322–329, http://dx.doi.org/10.1016/j.jhazmat.2014.07.010.

[23] J. Colina-Márquez, F. Machuca-Martínez, G. Li Puma, Radiation absorption and optimization of solar photocatalytic reactors for environmental applications, Environ. Sci. Technol. 44 (2010) 5112–5120, http://dx.doi.org/10.1021/es100130h.

[24] S.L. Orozco, C.A. Arancibia-Bulnes, R. Suárez-Parra, Radiation absorption and degradation of an azo dye in a hybrid photocatalytic reactor, Chem. Eng. Sci. 64 (2009) 2173–2185, http://dx.doi.org/10.1016/j.ces.2009.01.038.

[25] I. Grčić, G. Li Puma, Photocatalytic degradation of water contaminants in multiple photoreactors and evaluation of reaction kinetic constants independent of photon absorption, irradiance, reactor geometry, and hydrodynamics, Environ. Sci. Technol. 47 (2013) 13702–13711, http://dx.doi.org/10.1021/es403472e.

[26] A. Cabrera Reina, L. Santos-Juanes, J.L. García Sánchez, J.L. Casas López, M.I. Maldonado Rubio, G. Li Puma, J.A. Sánchez Pérez, Modelling the photo-Fenton oxidation of the pharmaceutical paracetamol in water including the effect of photon absorption (VRPA), Appl. Catal. B: Environ. 166–167 (2015) 295–301, http://dx.doi.org/10.1016/j.apcatb.2014.11.023.

[27] G. Rivas, I. Carra, J.L. García Sánchez, J.L. Casas López, S. Malato, J.A. Sánchez Pérez, Modelling of the operation of raceway pond reactors for micropollutant removal by solar photo-Fenton as a function of photon absorption, Appl. Catal. B: Environ. 178 (2015) 210–217, http://dx.doi.org/10.1016/j.apcatb.2014.09.015.

[28] J.A. Sánchez Pérez, P. Soriano-Molina, G. Rivas, J.L. García Sánchez, J.L. Casas López, J.L. Fernández Sevilla, Effect of temperature and photon absorption on the kinetics of micropollutant removal by solar photo-Fenton in raceway pond reactors, Chem. Eng. J. 310 (2017) 464–472, http://dx.doi.org/10.1016/j.cej.2016.06.055.

[29] J. Farias, E.D. Albizzati, O.M. Alfano, Kinetic study of the photo-Fenton degradation of formic acid. Combined effects of temperature and iron concentration, Catal. Today 144 (2009) 117–123, http://dx.doi.org/10.1016/j.cattod.2008.12.027.

[30] L.O. Conte, A.V. Schenone, O.M. Alfano, Photo-Fenton degradation of the herbicide 2, 4-D in aqueous medium at pH conditions close to neutrality, J. Environ. Manage. 170 (2016) 60–69, http://dx.doi.org/10.1016/j.jenvman.2016.01.002.

[31] M.I. Polo-López, I. García-Fernández, T. Velegraki, A. Katsoni, I. Oller, D. Mantzavinos, P. Fernández-Ibáñez, Mild solar photo-Fenton: an effective tool for the removal of Fusarium from simulated municipal effluents, Appl. Catal. B: Environ. 111–112 (2012) 545–554, http://dx.doi.org/10.1016/j.apcatb.2011.11.006.

[32] S. Mitroka, S. Zimmeck, D. Troya, J.M. Tanko, How solvent modulates hydroxyl radical reactivity in hydrogen atom abstractions, J. Am. Chem. Soc. 132 (2010) 2907–2913, http://dx.doi.org/10.1021/ja903856t.

[33] Y. Wu, M. Brigante, W. Dong, P. De Sainte-Claire, G. Mailhot, Toward a better understanding of Fe(III)–EDDS photochemistry: theoretical stability calculation and experimental investigation of 4-tert-butylphenol degradation, J. Phys. Chem. A 118 (2014) 396–403, http://dx.doi.org/10.1021/jp409043e.

[34] J. Li, G. Mailhot, F. Wu, N. Deng, Photochemical efficiency of Fe(III)-EDDS complex: ˙OH radical production and 17β-estradiol degradation, J. Photochem. Photobiol. A: Chem. 212 (2010) 1–7, http://dx.doi.org/10.1016/j.jphotochem.2010.03.001.

[35] G.V. Buxton, C.L. Greenstock, W.P. Helman, A.B. Ross, Critical review of rate constants for reactions of hydrated electrons, hydrogen atoms and hydroxyl radicals (˙OH/˙O⁻) in aqueous solution, J. Phys. Chem. Ref. Data 17 (1988) 513–886, http://dx.doi.org/10.1063/1.555805.

[36] Y. Wu, A. Bianco, M. Brigante, W. Dong, P. De Sainte-Claire, K. Hanna, G. Mailhot, Sulfate radical photogeneration using Fe-EDDS: influence of critical parameters and naturally occurring scavengers, Environ. Sci. Technol. 49 (2015) 14343–14349, http://dx.doi.org/10.1021/acs.est.5b03316.

[37] Decree 109/2015 of 17 March 2015, http://www.juntadeandalucia.es/boja/2015/89/3.

[38] Council Directive 91/271/EEC of 21 May 1991 concerning urban waste-water treatment, http://eurlex.europa.eu/LexUriServ/LexUriServ.do?uri=CELEX:31991L0271:EN:HTML.

[39] S. Papoutsakis, F.F. Brites-Nóbrega, C. Pulgarin, S. Malato, Benefits and limitations of using Fe(III)-EDDS for the treatment of highly contaminated water at near-neutral pH, J. Photochem. Photobiol. A: Chem. 303–304 (2015) 1–7, http://dx.doi.org/10.1016/j.jphotochem.2015.01.013.

[40] J.A. Sánchez Pérez, S. Arzate, J.L. García Sánchez, G. Rivas, J.L. Casas López, Solar photo-Fenton process in continuous raceway pond reactors for micropollutant removal in WWTP secondary effluents. Comparison of operating conditions, in: J. Krysa (Ed.), 5th European Conference on Environmental Applications of Advanced Oxidation Processes (EAAOP5). Book of Abstracts, Univeristy of Chemistry and Technology, Prague, 2017, p.94. http://www.eaaop5.com/files/%20Book_of_proceedings_EAAOP5_Prague2.pdf.

Supplementary material for

Effect of Volumetric Rate of Photon Absorption on the kinetics of micropollutant removal by solar photo-Fenton with Fe^{3+}-EDDS at neutral pH

P. Soriano-Molina [a,b], J.L. García Sánchez [a,b], S. Malato [a,c], L. A. Pérez-Estrada[c], J. A. Sánchez Pérez [a,b]

[a] Solar Energy Research Centre (CIESOL), Ctra de Sacramento s/n, ES04120, Almería, Spain.
[b] Chemical Engineering Department, University of Almería, Ctra de Sacramento s/n, ES04120, Almería, Spain.
[c] Plataforma Solar de Almería, CIEMAT, Carretera Senés Km. 4, 04200, Tabernas, Spain.

Supplementary material contains the following:

Fig. S1. Reactor layout inside the solar simulator (a), dimensions (b) and solar box inside view (c).

Fig. S2. UV absorption spectra of Fe^{3+}-EDDS solutions at pH 7.25.

(a)

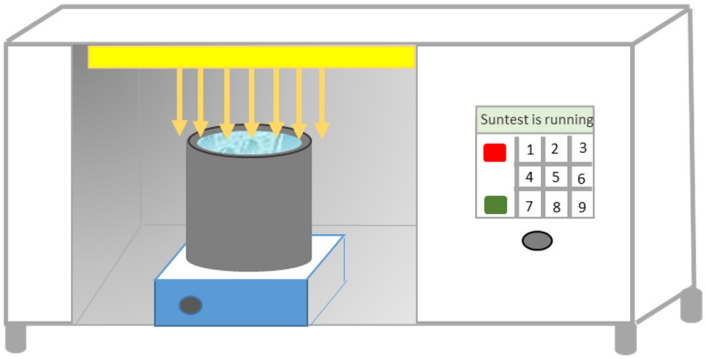

(b)

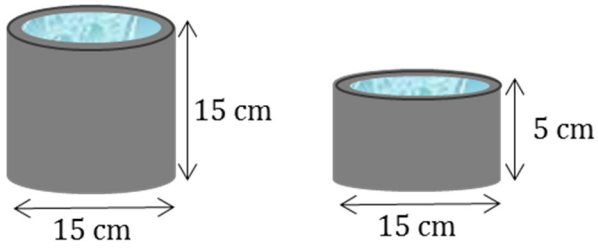

(c)

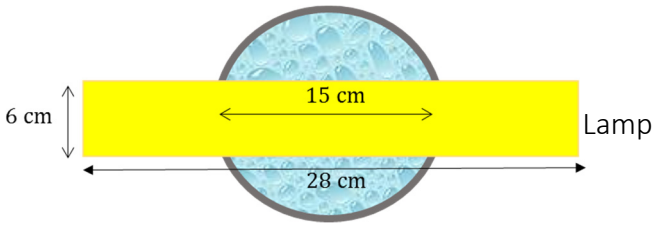

Fig. S1. Reactor layout inside the solar simulator (a), dimensions (b) and solar box inside view (c).

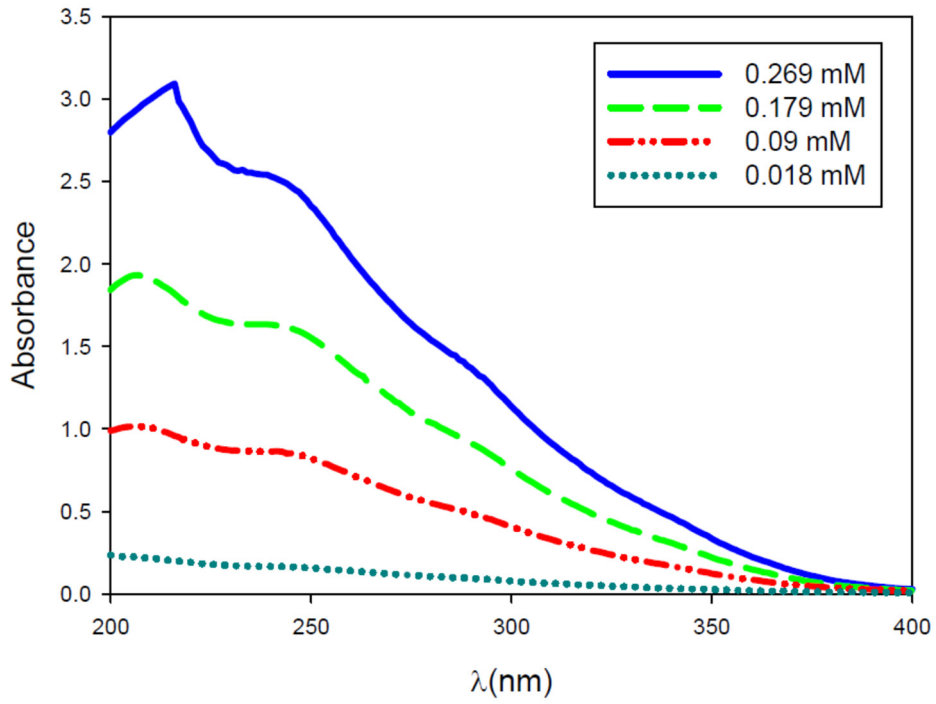

Fig. S2. UV absorption spectra of Fe^{3+}-EDDS solutions at pH 7.25.

4.3- Assessment of solar raceway pond reactors form removal of contaminants of emerging concern by photo-Fenton at circumneutral pH from very different municipal wastewater effluents

Published:

Soriano-Molina, P., Plaza-Bolaños, P., Lorenzo, A., Agüera, A., García Sánchez, J.L., Malato, S. & Sánchez Pérez, J.A. (2019). Assessment of solar raceway pond reactors form removal of contaminants of emerging concern by photo-Fenton at circumneutral pH from very different municipal wastewater effluents. Chemical Engineering Journal, 366, 141 – 149. DOI:10.1016/j.cej.2019.02.074.

Chemical Engineering Journal 366 (2019) 141–149

Contents lists available at ScienceDirect

Chemical Engineering Journal

journal homepage: www.elsevier.com/locate/cej

Assessment of solar raceway pond reactors for removal of contaminants of emerging concern by photo-Fenton at circumneutral pH from very different municipal wastewater effluents

P. Soriano-Molina[a,b], P. Plaza-Bolaños[a], A. Lorenzo[a], A. Agüera[a], J.L. García Sánchez[a,b], S. Malato[a,c], J.A. Sánchez Pérez[a,b,*]

[a] Solar Energy Research Centre (CIESOL), Joint Centre University of Almería-CIEMAT, Carretera de Sacramento s/n, E-04120 Almería, Spain
[b] Chemical Engineering Department, University of Almería, Ctra de Sacramento s/n, E-04120 Almería, Spain
[c] Plataforma Solar de Almería, CIEMAT, Carretera Senés Km. 4, E-04200 Tabernas, Almería, Spain

HIGHLIGHTS

- Photo-Fenton with Fe^{3+}-EDDS removes CECs regardless water composition.
- 80% CEC removal after 15 min in 5 real WWTP effluents.
- Nature and not the load of organic matter has impact on CEC removal.
- Short reaction time to remove CECs encourages continuous flow operation.
- Mechanism developed with synthetic effluent explains reactions in real wastewater.

GRAPHICAL ABSTRACT

ARTICLE INFO

Keywords:
Chloride radicals
Sulfate radicals
EDDS
Micropollutant
Organic matter
Solar photocatalysis

ABSTRACT

This paper presents for the first time the treatment of contaminants of emerging concern (CECs) in a systematic study in different municipal wastewater treatment plants (MWWTPs) of the Mediterranean area, more than 1000 km away. Solar photo-Fenton process at neutral pH with Fe^{3+}-EDDS has been demonstrated to be very efficient under controlled conditions and must be validated in realistic and variable conditions such as real MWWTP effluents of different composition. To this end, CEC removal was studied in effluents from 5 treatment plants in the Mediterranean area of Spain, the inorganic and organic composition varying in the range 161–641 mg L^{-1} (sulfate), 133–538 mg L^{-1} (chloride) and 10–20 mg L^{-1} (dissolved organic carbon). More than 45 CECs were quantified in MWW and results showed that the effect on CEC elimination of the concentration of anions and organic matter was interfered by the nature of the organic matter. However, origin and composition of MWW was not critic for attaining > 80% degradation of CECs after 15 min of reaction. Moreover, conventional anions (sulfate, chloride) had a positive effect on CEC degradation rate. This paper demonstrates the consistency and predictability of the solar photo-Fenton process at circumneutral pH for treating CECs in simple and cheap photoreactors.

* Corresponding author at: Department of Chemical Engineering, University of Almería, 04120 Almería, Spain.
E-mail address: jsanchez@ual.es (J.A. Sánchez Pérez).

https://doi.org/10.1016/j.cej.2019.02.074
Received 15 November 2018; Received in revised form 8 February 2019; Accepted 11 February 2019
Available online 12 February 2019
1385-8947/

1. Introduction

In many regions of the world with water scarcity, the reuse of effluents from wastewater treatment plants (WWTP) becomes an increasingly widespread and desirable alternative. In recent years, the presence of contaminants of emerging concern (CECs) in WWTP effluents has become evident, thanks to the development of advanced analytical techniques capable of detecting contaminants at a very low concentration [1–3]. Within these techniques, the direct injection-based method by ultra-high-performance liquid chromatography quadrupole-linear ion trap analyzer (LC-QqLIT-MS/MS) stands out for being a fast and very sensitive method [4]. Contaminants such as pharmaceuticals, antibiotics, biocides, pesticides and personal care products are detected at low concentrations ($\mu g\,L^{-1}$–$ng\,L^{-1}$), but their accumulation in the ecosystems can cause negative effects on the aquatic organisms, crops (if the water is re-used for irrigation), and consequently, on human health [5,6]. Conventional WWTPs are not designed to eliminate this type of contaminants, and the legislation is becoming stricter with its discharge [7,8]. Therefore, an additional treatment is necessary for the removal of these compounds, which may be the advanced oxidation processes (AOPs), mainly based on the generation of $HO^{\cdot}$ radicals with a high oxidative potential to degrade a wide variety of organic compounds [9,10]. One of the most efficient AOPs is the photo-Fenton process, which consists of the generation of hydroxyl radicals through the reaction between Fe^{2+}/Fe^{3+} and H_2O_2 under UV radiation. This process has been widely studied at its optimum pH, 2.8 [11,12]. However, the need for a previous acidification pretreatment and further neutralization before reusing or discharging as well as pH control to ensure the catalytic activity of iron species increases the effluent salinity as well as the costs of the process [13].

To deal with these drawbacks, the current studies are focused on the operation at neutral pH and the use of low-cost reactors, such as raceway pond reactors (RPRs). These reactors, consisting of two open channels through which water is recirculated, are provided with a paddle wheel connected to an engine to vary the flow conditions. Furthermore, the liquid depth can be changed according to the availability of UV radiation [14]. Previous works show that high CEC removal efficiencies are achieved, both in synthetic municipal and industrial wastewater, in RPRs with different liquid depths (5–15 cm) [15,16]. Indeed, they are more efficient in reference to treatment capacity than the conventional tubular reactors with compound parabolic collectors (CPCs) [15,17]. To carry out the process at neutral pH, the use of EDDS, a biodegradable chelating agent which complex iron and avoid its precipitation, has been widely studied [18–21]. This Fe^{3+}-EDDS complex stands out for its high absorptivity, which allows high removal rates to be achieved at short reaction times [16,22,23]. As for the transformation products (TPs) formed during the oxidation of the CECs, additional irradiation time may be required for complete degradation. Indeed TPs products of some single CECs (spiked at concentration in the range of a few mg/L) after photo-Fenton treatment have been recently reported [24,25]. However, it is not technically possible to quantify TPs generated from dozens of parent compounds found in real secondary effluents at concentration level of ng/L along with tens of mg/L of natural organic matter and other organic compounds, preventing from any reliable study about TPs. As a detailed evaluation of CEC TPs is not possible, studies are focused on environmental impact of TP discharge. Reported studies show the potential phytotoxicity and cytotoxicity of the treated wastewater is attenuated, and the androgenic/glucorticoid activity and estrogenicity are removed after the treatment with Fe^{3+}-EDDS [26].

When working with real MWWTP effluents, the variability of water composition, as well as the lack of analytical techniques to determine all the matter present in the water, hinders the study of the process. Among the ions, HCO_3^-/CO_3^{2-}, chloride and sulfate can have an important effect on the process. Concerning the HCO_3^-/CO_3^{2-} ions, its effect is negative since they act as a scavenger of hydroxyl radicals [27]. As for chloride and sulfate, the corresponding radicals could be formed but with oxidation potentials lower than that of hydroxyl radicals. Otherwise they can contribute to the oxidation of contaminants, since $SO_4^{\cdot -}$ reacts with Cl^- generating $Cl^{\cdot}$, and finally Cl^- reacts with the generated $Cl^{\cdot}$ yielding $Cl_2^{\cdot -}$, which exhibits a higher reactivity with organic pollutants than with other species [28]. Nonetheless, both ions can retard the efficiency of the process by forming complexes with iron and also by scavenging the $HO^{\cdot}$ radicals [29–31].

Previous experiments have shown that it is possible to degrade CECs in a MWWTP effluent with a Fe^{3+}-EDDS molar ratio of 1:2 and H_2O_2 in CPC photoreactors [32]. The drawback of working at a Fe^{3+}-EDDS ratio of 1:2, instead of 1:1, is not only the increase in operating costs, but the concentration of dissolved organic carbon (DOC) added by the EDDS to the water is doubled. When working with 0.1 mM Fe^{3+}-EDDS at a ratio of 1:1, DOC added to the water is $12\,mg\,L^{-1}$ being DOC content of MWWTP around $20\,mg\,L^{-1}$. For instance, taking into account the daily emission limit for DOC to surface waters established by the Andalusian Regional Government, $45.9\,mg\,L^{-1}$ [33], this limit could be exceeded when working at a Fe^{3+}-EDDS ratio of 1:2. Recently, the efficiency of using Fe^{3+}-EDDS at 1:1 M ratio for acetamiprid removal, a neonicotinoid, by photo-Fenton process with synthetic secondary effluents has been demonstrated [16].

In this regard, among the great number of publications on photo-Fenton only a few are related to microcontaminant removal in wastewater, most of them using demineralized water or synthetic wastewater [9,34,35]. Working under these conditions is necessary to understand the phenomenology of the process and the reaction mechanisms. Then, the results must be validated under real conditions. Real wastewater is a very complex and variable water matrix and there is a lack of papers dealing with the removal of CECs in real WWTP effluents, as recently reported not only on photo-Fenton process, but also on advanced oxidation processes [36]. Nonetheless, no studies comparing different real effluents have yet been reported and this assessment is crucial to predict process applicability and robustness because results can largely change from one case to another due to real water variability.

The main objective of this study was to determine if photo-Fenton best operating conditions developed during several years of experimentation with model and real effluents are suitable for treating MWWTP effluents of very different composition. Additionally, identifying the factors with highest impact on results when comparing different water matrices is of paramount interest. Experiments were carried out at neutral pH, with 0.1 mM Fe^{3+}-EDDS at 1:1 M ratio, in secondary effluents from five MWWTPs (see Table 1) located in different areas of Spain more than 1000 km away, with variability in salinity (conductivity 0.9 up to $2.2\,mS\,cm^{-1}$) as well as in organic matter (DOC 10–20 $mg\,L^{-1}$). This paper is aimed at gaining know-how about the effect of effluent composition on CEC removal kinetics and process efficiency.

2. Materials and methods

2.1. Chemicals

Ferric sulfate (75%), hydrogen peroxide (33%), hydrochloric acid (37%) and acetic acid were obtained from Panreac (Barcelona, Spain). Sodium formate was acquired from Merck Millipore (Darmstadt, Germany). Ultrapure water was generated with a Millipore Direct-Q® Ultrapure Water System (Bedford, MA, USA) ($18.2\,M\Omega\,cm^{-1}$ resistance and $2\,mg\,L^{-1}$ total organic carbon). Methanol (MeOH), acetonitrile (AcN) and formic acid (purity, 98%) were HPLC grade and supplied by Honeywell-Riedel-de Haën (Seelze, Germany). Ethylenediamine disuccinic acid (35%), titanium (IV) oxysulfate, tetrabutylammonium bisulfate, sulfuric acid (99%), formic acid (98%), ascorbic acid, o-phenantroline and methanol were purchased from Sigma-Aldrich (Steinheim, Germany). All high purity analytical standards (purity > 97%) were also purchased from Sigma-Aldrich comprising a group of CECs including pharmaceuticals, antibiotics, pesticides and some of their metabolites. ^{13}C-caffeine (Sigma-Aldrich) was used as injection standard.

Table 1
Characterization of MWWTP effluents, mean value ± standard deviation (n.d. = not detected).

	High-level	Medium-level A	Medium-level B	Low-level A	Low-level B
NO_2^- (mg L^{-1})	n.d.	4.2 ± 0.1	n.d.	2.1 ± 0.3	1.6 ± 0.1
Br^- (mg L^{-1})	3.8 ± 1.4	2.8 ± 0.1	3.0 ± 0.2	n.d.	n.d.
NO_3^- (mg L^{-1})	n.d.	17.7 ± 6.6	4.6 ± 3.3	15.3 ± 0.3	4.2 ± 0.1
PO_4^{3-} (mg L^{-1})	5.5 ± 1.6	4.5 ± 3.0	9.3 ± 3.6	n.d.	4.2 ± 0.1
SO_4^{2-} (mg L^{-1})	641 ± 12	238 ± 23	292 ± 33	161 ± 2	231 ± 2
Cl^- (mg L^{-1})	538 ± 3	386 ± 10	481 ± 18	133 ± 1	248 ± 3
DOC (mg L^{-1})	19.7 ± 5.7	16.2 ± 2.3	10.8 ± 0.1	9.8 ± 0.1	16.4 ± 0.4
COD (mg L^{-1})	58.3 ± 9.5	51.6 ± 4.7	32.5 ± 3.1	29.8 ± 1.8	44.9 ± 2.0
IC (mg L^{-1})	125 ± 2	47.0 ± 5.5	44.4 ± 4.5	47.6 ± 1.0	56.7 ± 1.0
IC* (mg L^{-1})	11.9 ± 1.0	11.3 ± 1.2	15.3 ± 4.4	10.4 ± 0.4	15.3 ± 0.4
pH	7.4 ± 0.1	7.9 ± 0.1	7.8 ± 0.1	7.2 ± 0.1	7.6 ± 0.2
Conductivity (mS cm^{-1})	2.2 ± 0.1	1.6 ± 0.1	1.8 ± 0.1	0.9 ± 0.1	1.2 ± 0.1
Turbidity (NTU)	43.8 ± 12.9	9 ± 0.8	4.6 ± 2.8	1.9 ± 0.3	6.9 ± 2.1
Population equivalents	108,000	315,000	52,000	206,250	121,000

* Inorganic carbon (IC) pretreated until IC around 15 mg L^{-1}.

For the determination of CECs by LC–MS/MS analysis, individual stock solutions of each compound were prepared in MeOH or AcN at 1000 mg L^{-1} and stored in amber glass vials at −20 °C. Stock standard solutions containing the compounds were prepared by mixing and diluting the individual stock solutions. A working solution containing all the analytes was prepared daily from the stock solution at 1 μg mL^{-1} in AcN.

2.2. MWWTP effluents

The experiments were carried out in secondary effluents from MWWTPs located in different areas of Spain: El Bobar (Almeria city, southeast of Spain), El Toyo (Almeria province), El Ejido (Almeria province), Alcoy (Alicante province, east of Spain) and Girona (Catalonia, northeast of Spain). The plants have a capacity of 315,000, 520,00, 108,000, 120,679 and 206,250 population equivalents, respectively. El Bobar and Girona WWTPs treat wastewater from the city and nearby villages. Due to its location, El Ejido WWTP treats wastewater from a nearby hospital and it is placed in an area surrounded by an intensive greenhouse agricultural production. In all WWTPs the water line consists of a pretreatment (roughing filtration, desanding and degreasing), a primary treatment (primary decantation), a conventional activated sludge biological treatment (except in El Toyo WWTP provided with extended aeration) followed by a secondary decantation. Furthermore, all the effluents (except El Ejido wastewater) were collected after filtration through sand filters.

In the case of the MWWTP effluents from Alcoy and Girona, once the water was collected from the MWWTP, it was refrigerated and transported to Almeria within the following two days. In this way, all the effluents were used in the experimentation within the same week they were collected. Due to HCO_3^-/CO_3^{2-} ions inhibit CEC degradation, the inorganic carbon (IC) was reduced to around 15 mg L^{-1} by adding H_2SO_4 prior to the experimentation. In this way, the effect related to the scavenger effect of CO_3^{2-}/HCO_3^- was the same in all the effluents, thus avoiding interferences. Table 1 shows the characteristics of the effluents before the treatment. The highest concentration of Chemical oxygen demand (COD) was 58.3 mg L^{-1}. As there was no mineralization, COD was not reduced after the treatment. Indeed, it increased around 20 mg L^{-1}, mainly due to the DOC added by the EDDS to the water. This is not a drawback, since the limit for COD discharge established by the Andalusian Regional Government is 138 mg L^{-1} [33]. Regarding the anionic content, sulfate and chloride were the most abundant anions in all the effluents (sulfate ranged from 161 to 641 mg L^{-1} and chloride from 133 to 538 mg L^{-1}). To study the possible effect of these anions, effluents were classified according to sulfate and chloride concentration level: effluent from El Ejido = high-level, effluent from El Bobar = medium-level A, effluent from El Toyo = medium-level B, effluent from Girona = low-level A and effluent from Alcoy = low-level B.

2.3. Experimental set-up

The experiments were carried out in outdoor conditions at the Solar Energy Research Center (CIESOL) located in Almeria (36°50′17″N, 02°27′35″W). The volume capacity to transport water from the MWWTPs to the research center (specifically from Girona and Alcoy) limited the volume of wastewater collected. Consequently, an RPR with 19-L capacity was used. The reactor consisted of a perfectly mixed RPR with 5-cm liquid depth, 22-cm channel width, and a mixing time of 2 min. Concerning the reactants, the experiments were conducted under mild oxidation conditions with 0.88 mM H_2O_2 (30 mg L^{-1}, the minimum concentration to guarantee the conditions of a Fenton-like process and permitting water disposal at the end of the treatment), and 0.1 mM Fe^{3+} (5.6 mg L^{-1}, the optimal concentration reported for photo-Fenton in RPRs [14]), at a Fe^{3+}-EDDS molar ratio of 1:1. These oxidation conditions were demonstrated to be efficient for CEC removal in synthetic secondary effluents [16]. During the reaction time, the temperature and pH were measured with probes connected to a LabJack USB/Ethernet data acquisition device. The pH ranged between 7 and 8 and the water temperature between 22 and 28 °C. Regarding the incident UV radiation, it was measured with a global UV radiometer (Delta Ohm, LPUVA02AV) in the wavelength range 327–384 nm.

All the experiments were replicated and conducted around noon during sunny days, at a global UV radiation comprised between 28 and 35 W m^{-2}. To compare the results, they were normalized to a constant irradiance of 30 W m^{-2}. The illumination time normalized to this radiation was calculated with Eq. (1), well established for kinetic calculations in solar photoreactors [37]:

$$t_{30W,n} = t_{30W,n-1} + \Delta t_n \cdot \frac{U\bar{V}_G}{30} \cdot \frac{V_i}{V_T} \quad (1)$$

where t_{30W} is the normalized illumination time, t_n is the experimental time for each sample ($n = 1$, $t_{30W} = 0$), $U\bar{V}_G$ is the average global UV irradiance measured during Δt_n ($t_n - t_{n-1}$), V_i and V_T are the illuminated and the total volume of the photoreactor, respectively. Factor $V_i/V_T = 1$ for RPR.

2.4. Chemicals analysis

At each sampling time, two samples were taken from the photoreactor, one for reactant quantification and another for determination of CECs. For the quantification of reagents, the samples were filtered by 0.2-μm nylon filters from Millipore. As for the CECs, 5 mL of sample were taken from the reactor to a 7-mL amber glass bottle (pre-rinsed with ultra-pure water) containing 0.5 mL of AcN. Acetonitrile acts as $HO^{\cdot}$ scavenger, stopping the reaction [38]. Then, an aliquot of this mixture was filtered by 0.22-μm PTFE syringe filters (Aisimo Corporation, London, UK) into a 2-mL injection vial.

Total dissolved iron was spectrophotometrically measured at 510 nm, according to the 1,10-phenanthroline method (ISO 6332). H_2O_2 was determined at 410 nm with titanium (IV) oxysulfate solution (DIN 38 402 H15). For iron, the limit of quantification (LOQ) and the standard deviation (SD) were $4.5{\cdot}10^{-3}$ mM and $6.1{\cdot}10^{-4}$ mM, respectively. As for H_2O_2, LOQ and SD were $2.9{\cdot}10^{-2}$ mM and $4{\cdot}10^{-3}$ mM, respectively.

IC and DOC were measured with a Shimadzu-V CPH TOC analyzer (Shimadzu Corporation, Kyoto, Japan), the LOQ being 1 mg L^{-1}.

The Fe^{3+}-EDDS complex was measured by a 1200 Series system consisting of an ultra-high pressure liquid chromatography with diode array detector (UHPLC-DAD) from Agilent Technologies (Waldbronn, Germany). Isocratic elution was used. The organic phase was MeOH and the aqueous phase consisted of a mixture of sodium formate (15 mM) and tetrabutylammonium hydrogen sulfate (2 mM) in Milli-Q water at pH 4, in a percentage of 95% and 5%, respectively, the flow being of 0.5 mL min^{-1}. The LOQ and the SD were $3.5{\cdot}10^{-3}$ mM and $3.5{\cdot}10^{-4}$ mM, respectively.

The concentration of anions was determined using ion chromatography Metrohm 881 Compact IC pro (Herisau, Switzerland). The system worked with an anionic column, Metrosep A Supp 7, 250–4.0 mm and 5 µm from Metrohm. The eluent was a solution of Na_2CO_3, and the flow was 0.8 mL min^{-1}, and the LOQ was 0.5 mg L^{-1}.

The CECs were monitored using the protocol previously developed and validated by Campos-Mañas et al. [39]. The direct injection technique was applied (no sample pre-treatment) using a sample volume of 10 µL. Sample dilution (1/10) with water was applied when necessary for an adequate quantification. The analyses were carried out by LC coupled to a hybrid quadrupole lineal ion trap MS analyzer (LC-QqLIT-MS/MS). The instrumentation consisted of an Agilent 1200 LC system (Agilent Technologies, Foster City, CA, USA) and a 5500 QTRAP analyzer (AB Sciex Instruments, Wilmington, DE, USA). Table 2 shows the concentration of the CECs detected at the highest concentrations in the five effluents.

2.5. Cost estimation

A cost estimation of the treatment of real secondary effluents by solar photo-Fenton at neutral pH in RPRs operated in continuous flow mode has been carried out. To this end, a design flow rate of 400 m^3 d^{-1} was set to fulfill the European Urban Wastewater Directive 91/271/EEC [40] which establishes the need of wastewater treatment in agglomerations larger than 2000 population equivalents, the wastewater generated per population equivalent being close to 200 L d^{-1}.

Table 2
Initial concentrations (ng L^{-1}) of the most relevant CECs detected in each MWWTP effluent.

CEC	High-level	Medium-level A	Medium-level B	Low-level A	Low-level B
Antipyrine	n.d.	838	141	n.d.	39
Atenolol	391	642	95	287	672
Ciprofloxacin	976	1573	618	n.d.	n.d.
Cotinine	6015	n.d.	n.d.	n.d.	n.d.
DPR-M[a]	28,919	16,911	9073	2014	5741
Gabapentin	7863	1950	1309	943	1711
Lidocaine	244	283	124	n.d.	253
Naproxen	1207	647	56	n.d.	233
O-Desmethyltramadol	740	1916	871	319	590
Ofloxacin	965	792	541	105	311
O-Desmethylvenlafaxine	724	1324	1075	683	774
Ranitidine	881	1597	125	255	n.d.
Sulfametoxazol	798	n.d.	195	128	114
Sulfapyridine	90	201	161	n.d.	35
Theophylline	5041	n.d.	n.d.	n.d.	n.d.
Tramadol	756	n.d.	1170	905	928
Venlafaxine	176	420	177	198	179
Other CECs[b]	4609	3057	1451	336	1018
Total load (µg L^{-1})	58	31	17	6.2	12

[a] Sum of the non-biodegradable metabolites of dipyrone (4-aminoantipyrine, 4-acetylaminoantipyrine, 4-formylaminoantipyrine, 4-methylaminoantipyrine).
[b] Sum of the concentrations of the rest of detected CECs.

Total costs were estimated as the sum of the operating costs (OC) and the amortization costs (AC). Taxes, staff and land costs were not considered, since they are highly dependent on labour regulation as well as the treatment plant location. Operating costs were estimated by Eq. (2), considering maintenance costs as 2% of amortization costs [41].

$$OC = C_R + C_E + 0.02AC \quad (2)$$

where C_R and C_E are the reactant and energy costs, respectively.

Concerning the unitary reactant cost, industrial price was considered: 0.45 € L^{-1} H_2O_2 (33% w/v), 0.71 € kg^{-1} $Fe_2(SO_4)_3{\cdot}H_2O$, 0.1 € L^{-1} H_2SO_4 (98% w/v). In the case of EDDS, 3.5 € L^{-1} EDDS (35% w/v) is the lowest reported cost because no industrial price is available yet. As for energy costs, the price of electricity was considered 0.1 € kW^{-1} h^{-1}. For mixing in the RPR, the unitary power requirement is 4 W m^{-3} [14]. Moreover, the cost of an 18 kW centrifugal pump, for effluent circulation to the reactor, was included, as well as four 50 W pumps for reactant dosing.

Regarding the amortization costs, Eq. (3), the investment cost (I) was referred to the RPR and the pumping systems. The RPR cost was calculated with Eq. (4), the cost per unit area being 10 € m^{-2}. A life cycle (L) of 20 years was assumed.

$$AC = \frac{I}{L} \quad (3)$$

$$C_{RPR} = 10A_{RPR} \quad (4)$$

3. Results and discussion

3.1. Effect of water matrix on reagents consumption and on the removal of contaminants of emerging concern

In a previous work, a reaction mechanism for solar photo-Fenton process at neutral pH was proposed and validated in a synthetic secondary effluent. Briefly, the main steps are the following: firstly, the Fe^{3+}-EDDS is photoreduced by UV radiation. Fe^{2+}-EDDS, as an intermediate state before being decomposed to Fe^{2+} and $EDDS^{\cdot 3-}$, reacts with H_2O_2 giving rise to $HO^{\cdot}$ and Fe^{3+}-EDDS. Finally, Fe^{2+} is oxidized by H_2O_2 (classic Fenton) yielding $HO^{\cdot}$ and Fe^{3+}, which instantaneously precipitates as $Fe(OH)_3$. The hydroxyl radicals oxidize CECs, as well as the Fe^{3+}-EDDS, the organic matter, the inorganic carbon and the H_2O_2 yielding their respective oxidation products. All the reactions and more details about the mechanism were previously reported [42].

$$Fe^{3+} - EDDS + h\upsilon \rightarrow [Fe^{3+}{-}EDDS]^* \quad (R1)$$

$$[Fe^{3+}{-}EDDS]^* \rightarrow Fe^{2+} - EDDS + H^+ \quad (R2)$$

$$Fe^{2+} - EDDS + H_2O_2 \rightarrow Fe^{3+} - EDDS + HO^{\bullet} + HO^- \quad (R3)$$

$$Fe^{2+} - EDDS \rightarrow Fe^{2+} + EDDS^{\bullet 3-} \quad (R4)$$

$$Fe^{2+} + H_2O_2 \rightarrow Fe(OH)_3 + HO^{\bullet} + HO^- \quad (R5)$$

Concerning the Fe^{3+}-EDDS profiles in the real MWWTP effluents, in all cases the complex totally decomposed after 15 min of the reaction, Fig. 1a. Furthermore, the profiles were similar to those obtained in a synthetic effluent at a global average irradiance close to 30 W m^{-2} [16], same as that used for normalizing illumination time according to Eq. (1). This fact shows that complex decomposition depends on the photochemical reactions and its subsequent oxidation with H_2O_2 rather than the water composition, in concordance with the proposed reaction mechanism.

In all cases, some iron remained in solution after complex decomposition. In this case, differences were observed in total dissolved iron profiles between the different MWWTP effluents, Fig. 1b. Whereas the profiles were similar in medium-level A, low-level A and B, the iron precipitated faster in high-level and medium-level B, the fastest

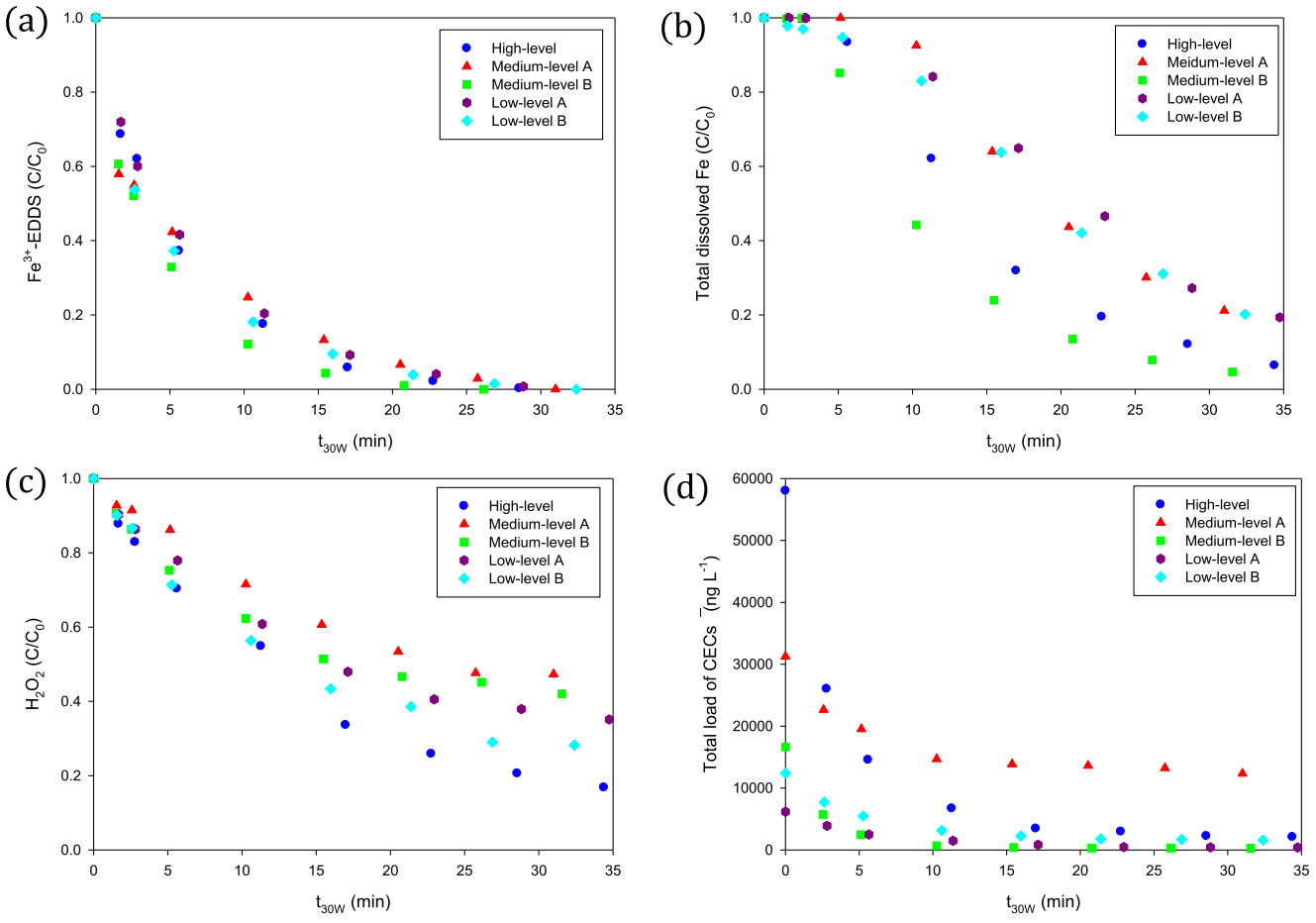

Fig. 1. Fe^{3+}-EDDS complex (a), total dissolved iron (b), H_2O_2 (c) and total load of CECs (d) profiles in the different MWWTP effluents.

precipitation being in medium-level B. It must be mentioned that in medium-level B, the iron profile was similar to that observed in a synthetic secondary effluent [42]. According to the mechanism, total dissolved iron concentration is the sum of the concentrations corresponding to the different species of Fe-EDDS. However, the fact that in the different MWWTP effluents the profiles are different could be related to the formation of other iron complexes, dependent on water composition. Although anions, such as chloride and sulfate can complex iron and therefore keep it in solution, the results show that these differences in iron concentration are not directly related to the concentration of anions, and it could be due to the generation of iron complexes with the organic matter present in the different effluents [43–45]. It should be highlighted that the total dissolved iron profiles are not related to the concentration of DOC, since in high-level (with around 20 mg L^{-1} DOC) the iron precipitated faster than in low-level A and slower than medium-level B (with around 10 mg L^{-1} DOC in both effluents). Therefore it could be concluded that the type of organic matter, which is difficult to determine due to its heterogeneity, structural complexity [46] and variability (between different MWWTP and in the same MWWTP at different hours of the day or seasons) could determine iron in solution.

Concerning H_2O_2 profiles, difference between MWWTP effluents was more significant after Fe^{3+}-EDDS decomposition. During the first minutes of the reaction, in which the complex is present, the H_2O_2 consumption is mainly due to the fast reaction between H_2O_2 and the photoreduced complex. Therefore, H_2O_2 consumption was very similar in the different effluents. However, once the concentration of the complex is low, the reactions of H_2O_2 with the organic matter would compete with those of the photo-Fenton process, substantially lower than during the first minutes as iron in solution was lower. In fact, a slightly higher H_2O_2 consumption can be observed in the high-level effluent, which was the effluent with the highest DOC concentration. It should be noticed that if the iron complexes formed with the organic matter after Fe^{3+}-EDDS decomposition would be photochemically active, it would be reflected in the H_2O_2 consumption profiles: the higher concentration of iron in solution, the higher H_2O_2 consumption. However, Fig. 1 shows that there is no direct relationship between consumption of H_2O_2 and the total dissolved iron profiles. In medium-level A, H_2O_2 consumption was lower than in other effluents, while the iron concentration was higher. This phenomenon could be explained by the formation of iron complexes with the organic matter of the medium that could avoid iron photoreduction and its subsequent reaction with H_2O_2 to generate hydroxyl radicals.

Substantial differences were observed in the CEC degradation during the first minutes of reaction. In concordance with the reaction mechanism, CEC removal rate was substantially lower after 15 min of reaction, once the Fe^{3+}-EDDS was decomposed. The pseudo-first order rate constants, Table 3, show that there is no relationship between CEC removal rate and the concentration of organic matter and anions present in the reaction medium. Therefore, although organic matter and anions act as $HO^{\cdot}$ scavengers, degradation of CECs could be mainly affected by organic matter composition. The rate constants obtained in high level and medium-level B effluents (0.23–0.38 min^{-1}) are in concordance with the results reported for synthetic secondary effluents doped with 100 µg L^{-1} of the pesticide acetamiprid (a highly recalcitrant CEC), being its pseudo-first order rate constant 0.43 min^{-1} at 30 W m^{-2} of UV irradiance [16].

The highest percentage of removal was achieved in medium-level B (98% after t_{30W} = 15 min), despite it being the effluent with the fastest iron precipitation and not the effluent with lower initial concentration. This could be explained by the fact that this effluent came from a

Table 3
Pseudo-first order rate constant of total load of CEC removal calculated over t_{30W}.

MWWTP effluent	k (min^{-1})	r^2
High-level	0.26	0.99
Medium-level A	0.10	0.95
Medium-level B	0.38	0.99
Low-level A	0.16	0.99
Low-level B	0.16	0.99

MWWTP located in a small area with the lowest population equivalents (520,00) in comparison with the other effluents, and its DOC concentration was also low (around 11 mg L^{-1}). As it is known, the lower the DOC, the lower the scavenger effect of hydroxyl radicals. Furthermore, there would be less organic matter to complex the iron, and more iron would be available to contribute to the Fenton reaction once the complex is photoreduced. As for the high-level effluent, it also showed a fast CEC removal (94% of CEC removal after t_{30W} = 17 min) despite it being the effluent with the highest total load of CECs. Furthermore, the lower the CEC concentration, the more hydroxyl radicals react with the organic matter instead of oxidizing the CECs. Even so, 87% and 82% of CEC removal was achieved after t_{30W} = 17 and 16 min in low-level effluents, respectively. In medium-level A only 56% of CEC removal was achieved after t_{30W} = 15 min. This effluent corresponds to the MWWTP with the highest population equivalents, despite it not being the effluent with the highest DOC concentration.

Although chloride and sulfate radicals are less reactive than hydroxyl radicals, previous experiments carried out in demineralized water showed that these ions could have a positive or negative effect on the kinetics of the process, depending on the process conditions [27–31]. Therefore, it is interesting to study the effect of the initial concentration of these ions on CEC removal in real MWWTP effluents. In Fig. 2a, it is observed that the CECs removed increased with the concentration of chlorides present in the effluent until 386 mg L^{-1} (Medium level A). This is consistent with reported results which point out that the addition of 350 mg L^{-1} chloride to the system contributed to accelerate the kinetics of pollutant removal [28]. Nevertheless, from 386 to 481 mg L^{-1} chloride the load of CEC removed was practically the same, whereas the total load removed increased strongly in the effluent with concentration of chlorides of 538 mg L^{-1}. In the case of sulfates, the same effect was observed. From these results, it could be deduced that there is not any detrimental effect of the initial concentration of the main anions on the reaction rate or total load removed, and therefore, on the process efficiency. Within the usual concentration found in natural sweet waters, higher concentration of chloride and sulfate presented higher kinetics.

Concisely, all these results show that the Fe^{3+}-EDDS photo-decomposition does not significantly depend on the secondary effluents composition, but on the photochemical reactions of the process, according to the mechanism already developed with a synthetic effluent and described elsewhere [42]. During the first minutes of the reaction there is not effect of the water composition on the hydrogen peroxide consumption. This is in concordance with the fast reaction between the photoactivated complex and the hydrogen peroxide proposed in the reaction mechanism, giving rise to the fast generation of $HO^{\cdot}$ and most of the CEC removal. Once the Fe^{3+}-EDDS complex is decomposed, an effect of the water composition on the H_2O_2 consumption is observed. Furthermore, there is a remnant of iron in solution as non-photoactive organocomplexes, which do not depend on the organic matter concentration, but on its composition. According to the pseudo-first order kinetics, high degradation rates can be achieved in effluents with a high load of CECs. Although main anions affect the process, there is not any direct relationship between increasing concentration of the anions and a detrimental effect on CEC removal. The composition of the organic matter present in MWWTP effluents is proposed to cause a higher impact on the process than its initial concentration. Overall, CECs were efficiently removed regardless water composition although the kinetics in each type of effluents must be specifically determined case by case.

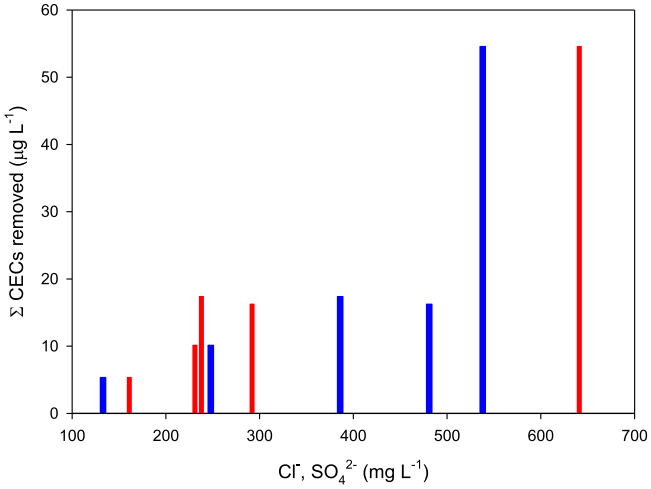

Fig. 2. Effect of chlorides (blue), sulfates (red) concentration on the sum of CECs removed after 15 min of t_{30W}. (For interpretation of the references to colour in this figure legend, the reader is referred to the web version of this article.)

3.2. CEC removal in the MWWTP effluents

In the five effluents studied, a range from 18 to 45 compounds were identified by LC–MS/MS. These compounds were mainly pharmaceuticals, some pesticides, antibiotics and opioids were also found. The degradation profiles of all compounds over time and the removal percentages in each effluent are shown in Tables S1–S5. Fig. 3 shows the degradation profiles of the six most abundant compounds in each effluent (eleven different CECs). In all cases, the sum of the non-biodegradable metabolites of dipyrone [47] (4-aminoantipyrine, 4-acetylaminoantipyrine, 4-formylaminoantipyrine, 4-methylaminoantipyrine), named as DPR-M, represented the highest concentration of CECs (between 33% and 55% of the total load of CECs). Gabapentin, *O*-desmethylvenlafaxine (metabolite of venlafaxine), tramadol and its metabolite *O*-desmethyltramadol were also found with the highest initial concentrations in most wastewaters. DPR-M and tramadol are low-cost analgesics, which can be consumed without medical prescription, and gabapentin and venlafaxine are pharmaceuticals commonly used as anticonvulsant and antidepressant, respectively. Therefore, it is usual to find all these compounds or their metabolites at high concentrations in MWWTP effluents [48,49]. In the case of the high-level effluent, naproxen (anti-inflammatory) was found among the compounds in the highest concentrations. This could be due to the localization of the MWWTP near a hospital. Moreover, theophylline and cotinine, two alkaloids related to the consumption of tea and tobacco, were also often detected.

Despite DPR-M representing the highest load, around 80–100% was removed after a t_{30W} of 15 min in all effluents, except in medium-level A, in which DPR-M was removed 60%. The other five pollutants with the highest initial concentration were removed between 70 and 100% after a t_{30W} of 15 min in all effluents, except in medium-level A, where the percentages were lower again, between 30 and 90%. Therefore, the low percentage of degradation achieved in medium-level A (in comparison with the other effluents) was not due to the degree of recalcitrance of the CECs, since CECs found in the highest concentrations in this effluent were also found and rapidly degraded in other wastewaters. It reinforces the proposed statement that composition of the organic matter present in MWWTP effluents is the key point that governs kinetics under the same treatment conditions.

It is worth mentioning that 88% of the total initial load was removed in the high-level effluent at t_{30W} = 11 min, with a ratio Fe^{3+}-EDDS 1:1 and 0.88 mM H_2O_2 in an RPR. This agrees with the 88% reported at t_{30W} = 8 min for an effluent from the same MWWTP, with a ratio Fe^{3+}-

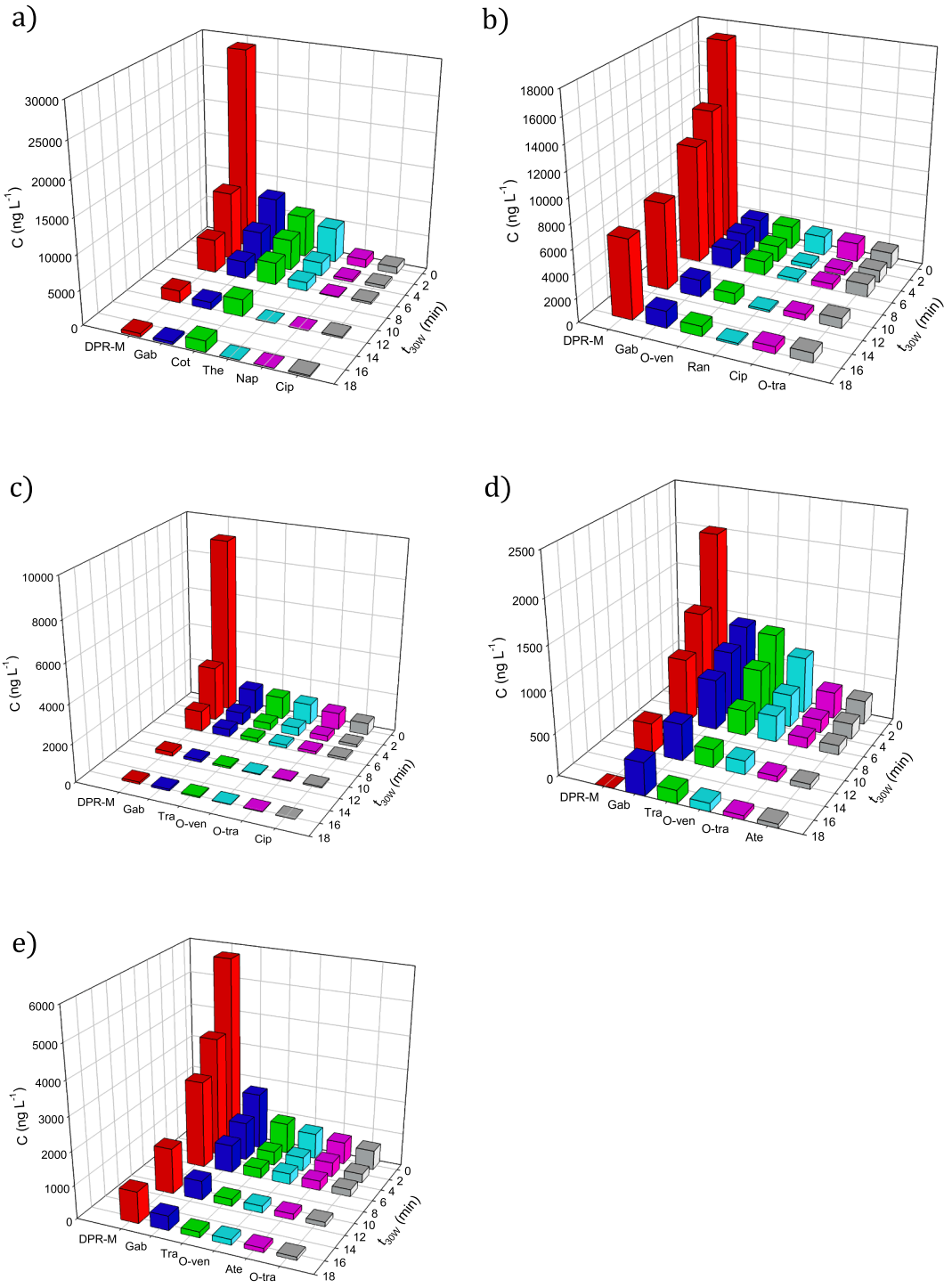

Fig. 3. Degradation of the six CECs with the highest initial concentration in each effluent: high-level (a), medium-level A (b), medium-level B (c), low-level A (d), low-level B (e) effluents (DPR-M = the sum of the non-biodegradable metabolites of dipyrone, Gab = gabapentin, Tra = tramadol, O-ven = *O*-desmethylvenlafaxine, O-tra = *O*-desmethyltramadol, Ate = atenolol, Ran = ranitidine, Cot = cotinine, The = theophylline, Nap = naproxen, Cip = ciprofloxacin).

EDDS 1:2 and 1.47 mM H_2O_2 in a CPC reactor [32]. Thus, the results obtained show the similar removal rate in the low-cost RPRs for the treatment of municipal wastewater in comparison with the CPCs.

The average removal of CECs in the five effluents was 83% at a t_{30W} of 15 min. The new Swiss water protection act entered into force on January 2016 and requires WWTPs upgrade within the next twenty years [50]. According to that, CECs need to be removed by 80% relative to the raw wastewater. The treatment target is defined by the elimination of a selection of CECs from a list of twelve defined compounds [51]. So far, few plants are in full-scale operation in Switzerland, either with ozonation or activated carbon treatment and less than 50% CEC removal is expected from the advanced tertiary treatment. But, to date, results about CEC removal are scarce in full-scale. Therefore, even the lowest percentage of removal attained in this work would fulfill these rules.

3.3. Economic assessment

Once the technical feasibility of the process has been demonstrated, an estimation of the treatment cost gives insight of the potential applicability of the treatment. Nonetheless, to carry out a rigorous

economic assessment data from demonstration plants are needed. Due to the high percentages of CEC removal achieved at short reaction time, the process should be operated in continuous flow mode at large scale [52]. In this work, only the order of magnitude of the cost was estimated considering the operation of an RPR in continuous flow mode at a hydraulic residence time of 15 min, being long enough to achieve more than 80% CEC removal. The treatment capacity would be 1600 $L\,m^{-2}\,d^{-1}$ for the continuous flow operation of a 5-cm deep RPR with 0.1 mM Fe^{3+}-EDDS and 0.88 mM H_2O_2 at 15 min of hydraulic residence time (HRT) for 8 h a day, the annual average sun hours per day in Almería (Spain) [53]. This estimated treatment capacity is 77% higher than the value reported at acidic pH with 20 min HRT [52]. With these data, the estimated area of the RPR was 250 m^2 to treat 400 $m^3\,d^{-1}$, resulting in an amortization cost of 188 € y^{-1}.

Concerning operating costs, the reactant cost, mainly affected by the high cost of EDDS, represented 94% of the total value (67,492 € y^{-1}). Energy cost, mainly affected by wastewater pumping, represented 6%. Maintenance cost was less than 0.1%, thus it could be considered negligible.

Finally, unitary total cost of the treatment was estimated to be 0.46 € m^{-3}. This value is in the reported range for AOPs [54]. Furthermore, it is competitive with the reported costs for the operation of a CPC solar pilot plant at neutral pH with Fe^{3+}-EDDS (in the range 0.71–1.31 € m^{-3} for the treatment of 500 $m^3\,d^{-1}$) [55].

This economic assessment is only a rough estimation, based on the scaling of the results obtained in a 19L-RPR operated in batch mode. In future works, the technical feasibility of the process in continuous flow must be demonstrated. Then, from the results obtained on a larger scale, the economic feasibility could be evaluated. Furthermore, operating cost could be strongly reduced by using chelating agents cheaper than EDDS, such as natural complexing agents, which encourages to continue the study of the process at neutral pH.

4. Conclusions

As far as authors known, the efficiency of the photo-Fenton process for treating MWWTP effluents of very different composition has been demonstrated for the first time. Using a low-cost RPR, more than 80% removal of total load of contaminants of emerging concern was achieved regardless the origin of the secondary effluent in less than 15 min of treatment. No dependence of the photo-Fenton process with the inorganic components of secondary effluents was found, but results show that effluents with high load of chloride or sulfate can contribute to the improvement of the process efficiency. The nature (and not the load, at least until 20 mg L^{-1}) of the organic matter has a great effect on CEC degradation. Composition of the organic matter present in MWWTP effluents is the key point that governs kinetics under given treatment conditions (iron and EDDS concentration, H_2O_2 dose, photoreactor design). It should be highlighted that the results obtained in different real MWWTP effluents can be explained based on reaction mechanisms developed under controlled conditions with synthetic effluents. Finally, the short reaction time to reach substantial removal of CECs and the estimated cost in the range reported for AOPs encourage the study of the process in continuous flow.

Acknowledgements

The authors are grateful to the Ministry for Economy, Industry and Competitiveness (Spanish Government) and the European Regional Development Fund (ERDF), project CTQ2016-78255-R. P. Soriano-Molina would like to acknowledge the Ministry of Education, Culture and Sport for her FPU scholarship (AP2014/01030). P. Plaza-Bolaños is grateful to the University of Almeria for her research contract (Hipatia Program).

Appendix A. Supplementary data

Supplementary data to this article can be found online at https://doi.org/10.1016/j.cej.2019.02.074.

References

[1] J.C.G. Sousa, A.R. Ribeiro, M.O. Barbosa, C. Ribeiro, M.E. Tiritan, M.F.R. Pereira, A.M.T. Silva, Monitoring of the 17 EU Watch List contaminants of emerging concern in the Ave and the Sousa Rivers, Sci. Total Environ. 649 (2019) 1083–1095, https://doi.org/10.1016/j.scitotenv.2018.08.309.

[2] M. Williams, R.S. Kookana, A. Mehta, S.K. Yadav, B.L. Tailor, B. Maheshwari, Emerging contaminants in a river receiving untreated wastewater from an Indian urban centre, Sci. Total Environ. 647 (2019) 1256–1265, https://doi.org/10.1016/j.scitotenv.2018.08.084.

[3] J. Nivala, S. Kahl, J. Boog, M. van Afferden, T. Reemtsma, R.A. Müller, Dynamics of emerging organic contaminant removal by conventional and intensified subsurface flow treatment wetland, Sci. Total Environ. 649 (2019) 1144–1156, https://doi.org/10.1016/j.scitotenv.2018.08.339.

[4] M. Tobiszewski, J. Namieśnik, Direct chromatographic methods in the context of green analytical chemistry, Trends Anal. Chem. 35 (2012) 67–73, https://doi.org/10.1016/j.trac.2012.02.006.

[5] Z. Tousova, P. Oswald, J. Slobodnik, L. Blaha, M. Muz, M. Hu, W. Brack, M. Krauss, C. Di Paolo, Z. Tarcai, T.B. Seiler, H. Hollert, S. Koprivica, M. Ahel, J.E. Schollée, J. Hollender, M.J. Suter, A.O. Hidasi, K. Schirmer, M. Sonavane, S. Ait-Aissa, N. Creusot, F. Brion, J. Froment, A.C. Almeida, K. Thomas, K.E. Tollefsen, S. Tufi, X. Ouyang, P. Leonards, M. Lamoree, V.O. Torrens, A. Kolkman, M. Schriks, P. Spirhanzlova, A. Tindall, T. Schulze, European demonstration program on the effect-based and chemical identification and monitoring of organic pollutants in European surface waters, Sci. Total Environ. 601–602 (2017) 1849–1868, https://doi.org/10.1016/j.scitotenv.2017.06.032.

[6] P. Krzeminski, M.C. Tomei, P. Karaolia, A. Langenhoff, M.R. Almeida, E. Felis, F. Gritten, H.R. Andersen, T. Fernandes, C.M. Manaia, L. Rizzo, D. Fatta-Kassinos, Performance of secondary wastewater treatment methods for the removal of contaminants of emerging concern implicated in crop uptake and antibiotic resistance spread: a review, Sci. Total Environ. 648 (2019) 1052–1081, https://doi.org/10.1016/j.scitotenv.2018.08.130.

[7] Commission Implementing Decision (EU) 2018/840 of 5 June 2018 establishing a watch list of substances for Union-wide monitoring in the field of water policy pursuant to Directive 2008/105/EC of the European Parliament and of the Council and repealing Commission Implementing Decision (EU) 2014/495, Off. J. Eur. Union L 141/9, 7.6.2018. http://data.europa.eu/eli/dec_impl/2018/840/oj.

[8] Emerging Contaminants in River Ecosystems. The Handbook of Environmental Chemistry vol. 46, (2016) 197–216, https://doi.org/10.1007/698_2015_5011.

[9] D. Kanakaraju, B.D. Glass, M. Oelgemöller, Advanced oxidation process-mediated removal of pharmaceuticals from water: a review, J. Environ. Manage. 219 (2018) 189–207, https://doi.org/10.1016/j.jenvman.2018.04.103.

[10] D.B. Miklos, C. Remy, M. Jekel, K.G. Linden, J.E. Drewes, U. Hübner, Evaluation of advanced oxidation processes for water and wastewater treatment – a critical review, Water Res. 139 (2018) 118–131, https://doi.org/10.1016/j.watres.2018.03.042.

[11] I. Velo-Gala, J.A. Pirán-Montaño, J. Rivera-Utrilla, M. Sánchez-Polo, A.J. Mota, Advanced oxidation processes based on the use of UVC and simulated solar radiation to remove the antibiotic tinidazole from water, Chem. Eng. J. 323 (2017) 605–617, https://doi.org/10.1016/j.cej.2017.04.102.

[12] M.C.V.M. Starling, P.H. Rodrigues Dos Santos, F.A. Ribeiro de Souza, M.M.D. Leão, C.C. Amorim, Application of solar photo-Fenton toward toxicity removal and textile wastewater reuse, Environ. Sci. Pollut. Res. 24 (2017) 12515–12528, https://doi.org/10.1007/s11356-016-7395-5.

[13] L. Clarizia, D. Russo, I. Di Somma, R. Marotta, R. Andreozzi, Homogeneous photo-Fenton processes at near neutral pH: a review, Appl. Catal. B: Environ. 209 (2017) 358–371, https://doi.org/10.1016/j.apcatb.2017.03.011.

[14] I. Carra, L. Santos-Juanes, F.G. Acién Fernández, S. Malato, J.A. Sánchez Pérez, New approach to solar photo-Fenton operation. Raceway ponds as tertiary treatment technology, J. Hazard. Mater. 279 (2014) 322–329, https://doi.org/10.1016/j.jhazmat.2014.07.010.

[15] A. Cabrera-Reina, S. Miralles-Cuevas, G. Rivas, J.A. Sánchez, Pérez, Comparison of different detoxification pilot plants for the treatment of industrial wastewater by solar photo-Fenton: are raceway pond reactors a feasible option? Sci. Total Environ. 648 (2019) 601–608, https://doi.org/10.1016/j.scitotenv.2018.08.143.

[16] P. Soriano-Molina, J.L. García Sánchez, S. Malato, L.A. Pérez-Estrada, J.A. Sánchez Pérez, Effect of volumetric rate of photon absorption on the kinetics of micropollutant removal by solar photo-Fenton with Fe^{3+}-EDDS at neutral pH, Chem. Eng. J. 331 (2018) 84–92, https://doi.org/10.1016/j.cej.2017.08.096.

[17] A. Belalcázar-Saldarriaga, D. Prato-García, R. Vasquez-Medrano, Photo-Fenton processes in raceway reactors: technical, economic, and environmental implications during treatment of colored wastewaters, J. Clean. Prod. 182 (2018) 818–829, https://doi.org/10.1016/j.jclepro.2018.02.058.

[18] Y. Zhang, M. Zhou, A critical review of the application of chelating agents to enable Fenton and Fenton-like reactions at high pH values, J. Hazard. Mater. 362 (2019) 436–450, https://doi.org/10.1016/j.jhazmat.2018.09.035.

[19] W. Huang, M. Brigante, F. Wu, C. Mousty, K. Hanna, G. Mailhot, Assessment of the Fe(III) − EDDS complex in Fenton-like processes: from the radical formation to the degradation of bisphenol A, Environ. Sci. Technol. 47 (2013) 1952–1959, https://doi.org/10.1021/es304502y.

[20] S. López-Rayo, I. Sanchis-Pérez, C.M.H. Ferreira, J.J. Lucena, [S, S]-EDDS/Fe: a new chelate for the environmentally sustainable correction of iron chlorosis in calcareous soil, Sci. Total Environ. 647 (2019) 1508–1517, https://doi.org/10.1016/j.scitotenv.2018.08.021.

[21] Y. Zhang, N. Klamerth, S.A. Messele, P. Chelme-Ayala, M. Gamal El-Din, Kinetics

study on the degradation of a model naphthenic acid by ethylenediamine-N,N′-disuccinic acid-modified Fenton process, J. Hazard. Mater. 318 (2016) 371–378, https://doi.org/10.1016/j.jhazmat.2016.06.063.
[22] Y. Wu, M. Brigante, W. Dong, P. de Sainte-Claire, G. Mailhot, Toward a better understanding of Fe(III)–EDDS photochemistry: theoretical stability calculation and experimental investigation of 4-tert-butylphenol degradation, J. Phys. Chem. A 118 (2014) 396–403, https://doi.org/10.1021/jp409043e.
[23] J. Li, G. Mailhot, F. Wu, N. Deng, Photochemical efficiency of Fe(III)-EDDS complex: OH radical production and 17β-estradiol degradation, J. Photochem. Photobiol. A Chem. 212 (2010) 1–7, https://doi.org/10.1016/j.jphotochem.2010.03.001.
[24] S. Giannakis, I. Hendaoui, M. Jovic, D. Grandjean, L.F. De Alencastro, H. Girault, C. Pulgarín, Solar photo-Fenton and UV/H_2O_2 processes against the antidepressant Venlafaxine in urban wastewaters and human urine. Intermediates formation and biodegradability assessment, Chem. Eng. J. 15 (2017) 492–504, https://doi.org/10.1016/j.cej.2016.09.084.
[25] E. Pinheiro da Costa, S.E.C. Bottrel, M.C.V.M. Straling, M.M.D. Leão, C. Costa Amorim, Degradation of carbendazim in water via photo-Fenton in raceway pond reactor: assessment of acute toxicity and transformation products, Environ. Sci. Pollut. Res. (2018), https://doi.org/10.1007/s11356-018-2130-z (in press).
[26] G. Rivas Ibáñez, M. Bittner, Z. Toušová, M.C. Campos-Mañas, A. Agüera, J.L. Casas López, J.A. Sánchez Pérez, K. Hilscherová, Does micropollutant removal by solar photo-Fenton reduce ecotoxicity in municipal wastewater? A comprehensive study at pilot scale open reactors, J. Chem. Technol. Biotechnol. 92 (2017) 2114–2122, https://doi.org/10.1002/jctb.5212.
[27] L.G. Devi, S.G. Kumar, K.M. Reddy, C. Munikrishnappa, Effect of various inorganic anions on the degradation of Congo Red, a di azo dye, bu the photo-assisted Fenton process using zero-valent metallic iron as a catalyst, Desalin. Water Treat. 4 (2009) 294–305, https://doi.org/10.5004/dwt.2009.478.
[28] Y. Wu, A. Bianco, M. Brigante, W. Dong, P. de Sainte-Claire, K. Hanna, G. Mailhot, Sulfate radical photogeneration using Fe-EDDS: influence of critical parameters and naturally Occurring scavengers, Environ. Sci. Technol. 49 (2015) 14343–14349, https://doi.org/10.1021/acs.est.5b03316.
[29] B. Li, Y. Dong, P. Wang, G. Cui, Ferrioxalate-assisted solar photo-fenton degradation of reactive dyes in the presence of inorganic salts, Fiber Polym. 16 (2015) 2325–3233, https://doi.org/10.1007/s12221-015-5077-4.
[30] L.G. Devi, C. Munikrishnappa, B. Nagaraj, K.E. Rajashekhar, Effect of chloride and sulfate ions on the advanced photo Fenton and modified photo Fenton degradation process of Alizarin Red S, J. Mol. Catal. A: Chem. 374–375 (2013) 125–131, https://doi.org/10.1016/j.molcata.2013.03.023.
[31] C. Oliveira, D.L.D. Lima, C.P. Silva, V. Calisto, M. Otero, V.I. Esteves, Photodegradation of sulfamethoxazole in environmental samples: the role of pH, organic matter and salinity, Sci. Total Environ. 648 (2019) 1403–1410, https://doi.org/10.1016/j.scitotenv.2018.08.235.
[32] N. Klamerth, S. Malato, A. Agüera, A. Fernández-Alba, G. Mailhot, Treatment of municipal wastewater treatment plant effluents with modified photo-Fenton as a tertiary treatment for the degradation of micro pollutants and disinfection, Environ. Sci. Technol. 46 (2012) 2885–2892, https://doi.org/10.1021/es204112d.
[33] Decree 109/2015 of 17 March 2015 of the Andalusian Regional Government (Junta de Andalucía), Official Bulletin of the Andalusian Government (Boletín Oficial de la Junta de Andalucía), 89/22, 12.05.2015. http://www.juntadeandalucia.es/boja/2015/89/3.
[34] V.A.B. Paiva, C.E.S. Paniagua, I. Amildon Ricardo, B.R. Gonçalves, S. Pereira Martins, D. Daniel, A.E.H. Machado, A.G. Trovó, Simultaneous degradation of pharmaceuticals by classic and modified photo-Fenton process, J. Environ. Chem. Eng. 6 (2018) 1086–1092, https://doi.org/10.1016/j.jece.2018.01.013.
[35] V. Romero, S. Acevedo, P. Marco, J. Giménez, S. Esplugas, Enhancement of Fenton and photo-Fenton processes at initial circumneutral pH for the degradation of the β-blocker metoprolol, Water Res. 88 (2016) 20–25, https://doi.org/10.1016/j.watres.2015.10.035.
[36] L. Rizzo, S. Malato, D. Antakyali, V.G. Beretsou, M.B. Đolić, W. Gernjak, E. Heath, I. Ivancev-Tumbas, P. Karaolia, A.R. Lado Ribeiro, G. Mascolo, C.S. McArdell, H. Schaar, A.M.T. Silva, D. Fatta-Kassinos, Consolidated vs new advanced treatment methods for the removal of contaminants of emerging concern from urban wastewater, Sci. Total Environ. 655 (2019) 986–1008, https://doi.org/10.1016/j.scitotenv.2018.11.265.
[37] S. Malato, P. Fernández-Ibáñez, M.I. Maldonado, J. Blanco, W. Gernjak, Decontamination and disinfection of water by solar photocatalysis: recent overview and trends, Catal. Today 147 (2009) 1–59, https://doi.org/10.1016/j.cattod.2009.06.018.
[38] S. Mitroka, S. Zimmeck, D. Troya, J.M. Tanko, How solvent modulates hydroxyl radical reactivity in hydrogen atom abstractions, J. Am. Chem. Soc. 132 (2010) 2907–2913, https://doi.org/10.1021/ja903856t.
[39] M.C. Campos-Mañas, P. Plaza-Bolaños, J.A. Sánchez-Pérez, S. Malato, A. Agüera, Fast determination of pesticides and other contaminants of emerging concern in treated wastewater using direct injection coupled to highly sensitive ultra-high performance liquid chromatography-tandem mass spectrometry, J. Chromatogr. A 1507 (2017) 84–94, https://doi.org/10.1016/j.chroma.2017.05.053.
[40] Council Directive, 91/271/EEC of 21 May 1991 Concerning Urban Waste-Water Treatment, 1991.
[41] I. Carra, J.L. Casas López, L. Santos-Juanes, S. Malato, J.A. Sánchez Pérez, Iron dosage as a strategy to operate the photo-Fenton process at initial neutral pH, Chem. Eng. J. 224 (2013) 67–74, https://doi.org/10.1016/j.cej.2012.09.065.
[42] P. Soriano-Molina, J.L. García Sánchez, O.M. Alfano, L.O. Conte, S. Malato, J.A. Sánchez Pérez, Mechanistic modeling of solar photo-Fenton process with Fe^{3+}-EDDS at neutral pH, Appl. Catal. B: Environ. 233 (2018) 234–242, https://doi.org/10.1016/j.apcatb.2018.04.005.
[43] M.J. Apted, G.A. Waychunas, G.E. Brown, Structure and specification of iron complexes in aqueous solutions determined by X-ray absorption spectroscopy, Geochim. Cosmochim. Acta 49 (1985) 2081–2089, https://doi.org/10.1016/0016-7037(85)90065-1.
[44] C. Sukekava, J. Downes, H.A. Slagter, L.J.A. Gerringa, L.M. Laglera, Determination of the contribution of humic substances to iron complexation in seawater by catalytic cathodic stripping voltammetry, Talanta 189 (2018) 359–364, https://doi.org/10.1016/j.talanta.2018.07.021.
[45] E.L. Rue, K.W. Bruland, Complexation of iron (III) by natural organic ligands in the Central North Pacific as determined by a new competitive ligand equilibration/adsorptive cathodic stripping voltammetric method, Mar. Chem. 50 (1995) 117–138, https://doi.org/10.1016/0304-4203(95)00031-L.
[46] J. Mao, X. Cao, D.C. Olk, W. Chu, K. Schmidt-Rohr, Advanced solid-state NMR spectroscopy of natural organic matter, Prog. Nucl. Magn. Reson. Spectrosc. 100 (2017) 17–51, https://doi.org/10.1016/j.pnmrs.2016.11.003.
[47] L.A. Pérez-Estrada, S. Malato, A. Agüera, A.R. Fernández-Alba, Degradation of dipyrone and its main intermediates by solar AOPs: identification of intermediate products and toxicity assessment, Catal. Today 129 (2007) 207–214, https://doi.org/10.1016/j.cattod.2007.08.008.
[48] C. Lindim, J. van Gils, D. Georgieva, O. Mekenyan, I.T. Cousins, Evaluation of human pharmaceutical emissions and concentrations in Swedish river basins, Sci. Total Environ. 572 (2016) 508–519, https://doi.org/10.1016/j.scitotenv.2016.08.074.
[49] A.L. Maulvault, L.H.M.L.M. Santos, J.R. Paula, C. Camacho, V. Pissarra, F. Fogaça, V. Barbosa, R. Alves, P.P. Ferreira, D. Barceló, S. Rodriguez-Mozaz, A. Marques, M. Diniz, R. Rosa, Differential behavioural responses to venlafaxine exposure route, warming and acidification in juvenile fish (Argyrosomus regius), Sci. Total Environ. 634 (2018) 1136–1147, https://doi.org/10.1016/j.scitotenv.2018.04.015.
[50] Waters Protection Ordinance of 28 October 1998 (814.201) (Status of 1 June 2018). https://www.admin.ch/opc/en/classified-compilation/19983281/index.html.
[51] M. Bourgin, B. Beck, M. Boehler, E. Borowska, J. Fleiner, E. Salhi, R. Teichler, U. von Gunten, H. Siegrist, C.S. McArdell, Evaluation of a full-scale wastewater treatment plant upgraded with ozonation and biological post-treatments: abatement of micropollutants, formation of transformation products and oxidation by-products, Water Res. 129 (2018) 486–498, https://doi.org/10.1016/j.watres.2017.10.036.
[52] S. Arzate, J.L. García Sánchez, P. Soriano-Molina, J.L. Casas López, M.C. Campos-Mañas, A. Agüera, J.A. Sánchez Pérez, Effect of residence time on micropollutant removal in WWTP secondary effluents by continuous solar photo-Fenton process in raceway pond reactors, Chem. Eng. J. 316 (2017) 1114–1121, https://doi.org/10.1016/j.cej.2017.01.089.
[53] A. Cabrera-Reina, J.L. Casas López, M.I. Maldonado Rubio, L. Santos-Juanes Jordá, J.L. García Sánchez, J.A. Sánchez Pérez, Effects of environmental variables on the photo-Fenton plant design, Chem. Eng. J. 237 (2014) 469–477, https://doi.org/10.1016/j.cej.2013.10.046.
[54] L. Prieto-Rodríguez, I. Oller, N. Klamerth, A. Agüera, E.M. Rodríguez, S. Malato, Application of solar AOPs and ozonation for elimination of micropollutants in municipal wastewater treatment plant effluents, Water Res. 47 (2013) 1521–1528, https://doi.org/10.1016/j.watres.2012.11.002.
[55] S. Miralles-Cuevas, I. Oller, A. Agüera, J.A. Sánchez Pérez, R. Sánchez-Moreno, S. Malato, Is the combination of nanofiltration membranes and AOPs for removing microcontaminants cost effective in real municipal wastewater effluents? Environ. Sci.: Water Res. Technol. 2 (2016) 511–520, https://doi.org/10.1039/c6ew00001k.

Supplementary data to the paper entitled:

Assessment of solar raceway pond reactors for removal of contaminants of emerging concern by photo-Fenton at circumneutral pH from very different municipal wastewater effluents

P. Soriano-Molina [a,b], P. Plaza-Bolaños [a], A. Lorenzo [a], A. Agüera [a], J.L. García Sánchez [a,b], S. Malato [a,c], J.A. Sánchez Pérez [a,b*]

[a] Solar Energy Research Centre (CIESOL), Joint Centre University of Almería-CIEMAT, Carretera de Sacramento s/n, E-04120, Almería, Spain.

[b] Chemical Engineering Department, University of Almería, Ctra de Sacramento s/n, E-04120, Almería, Spain.

[c] Plataforma Solar de Almería, CIEMAT, Carretera Senés Km. 4, E-04200, Tabernas, Almería, Spain.

This document provides more detailed information to the main paper mentioned above.

The following information is included:

Content

Table S1. CEC removal (ng L^{-1}) over time in high-level effluent.

CEC	t_{30W} (min)								% Removal
	0	2.8	5.6	11	17	23	29	34	
4-Aminoantypirine	6022	n.d.	n.d.	n.d.	n.d.	n.d.	n.d.	n.d.	100
4-Acetylaminoantipyrine	11361	6565	2793	903	n.d.	n.d.	n.d.	n.d.	100
4-Formylaminoantipyrine	5949	3254	2042	824	488	393	307	198	97
4-Methylaminoantipyrine	5587	n.d.	n.d.	n.d.	n.d.	n.d.	n.d.	n.d.	100
Acetamiprid	242	236	184	154	136	149	159	150	38
Atenolol	391	218	110	58	n.d.	n.d.	n.d.	n.d.	100
Azoxystrobin	53	20	n.d.	n.d.	n.d.	n.d.	n.d.	n.d.	100
Carbamazepine	79	29	13	n.d.	n.d.	n.d.	n.d.	n.d.	100
Carbendazim	75	34	18	8	n.d.	n.d.	n.d.	n.d.	100
Ciprofloxacin	976	408	270	191	156	170	119	119	88
Citalopram	122	81	49	23	13	13	12	n.d.	100
Clarithromycin	122	78	40	97	32	33	25	24	80
Cotinine	6015	4483	3213	2412	1594	1381	1123	1164	81
Dimethomorph	40	20	n.d.	n.d.	n.d.	n.d.	n.d.	n.d.	100
Erithromicyn	73	45	32	20	14	14	12	n.d.	100
Fenofibric acid	172	112	51	12	n.d.	n.d.	n.d.	n.d.	100
Gabapentin	7863	4763	2464	1037	357	235	n.d.	n.d.	100
Imidacloprid	306	234	154	102	92	85	87	76	75
Ketoprofen	447	241	139	n.d.	n.d.	n.d.	n.d.	n.d.	100
Lidocaine	244	121	72	34	18	18	20	15	94
Metoclopramide	79	32	21	n.d.	n.d.	n.d.	n.d.	n.d.	100
Naproxen	1207	362	84	n.d.	n.d.	n.d.	n.d.	n.d.	100
O-Desmethyltramadol	740	407	223	103	67	56	56	47	94
Ofloxacin	964	548	322	181	111	88	71	75	92
O-Desmethylvenlafaxine	723	338	247	102	79	69	61	39	95
Propamocarb	191	140	120	89	82	78	79	78	59
Ranitidine	882	53	n.d.	n.d.	n.d.	n.d.	n.d.	n.d.	100
Sulfametoxazol	797	685	371	256	158	131	132	128	84
Sulfapyridine	90	45	n.d.	n.d.	n.d.	n.d.	n.d.	n.d.	100
Theophylline	5042	1968	1230	n.d.	n.d.	n.d.	n.d.	n.d.	100
Tramadol	756	334	236	96	64	64	n.d.	n.d.	100
Trimethopim	243	108	40	20	n.d.	n.d.	n.d.	n.d.	100
Venlafaxine	176	75	32	n.d.	n.d.	n.d.	n.d.	n.d.	100
Total load	58030	26035	14566	6722	3460	2976	2262	2113	96

Table S2. CEC removal (ng L^{-1}) over time in medium-level A effluent.

CEC	t_{30W} (min)								% Removal
	0	2.6	5.2	10	15	20	26	31	
4-Aminoantypirine	3839	65	74	63	68	106	127	137	96
4-Acetylaminoantipyrine	342	300	230	128	113	78	70	38	89
4-Formylaminoantipyrine	12024	11575	9582	7074	6463	6324	6212	5909	51
4-Methylaminoantipyrine	706	n.d.	n.d.	n.d.	n.d.	n.d.	n.d.	n.d.	100
Antipyrine	838	866	760	627	574	607	604	602	28
Atenolol	642	598	497	343	399	389	383	397	38
Carbamazepine	144	133	125	62	57	51	46	43	70
Carbendazim	49	43	36	22	21	17	15	15	70
Ciprofloxacin	1573	404	470	457	579	550	537	514	67
Citalopram	174	262	225	167	162	143	144	135	22
Clarithromycin	29	25	22	19	19	11	12	11	60
Clindamycin	19	19	15	n.d.	n.d.	n.d.	n.d.	n.d.	100
Erithromicyn	81	92	89	85	83	61	74	71	13
Famotidine	53	27	21	19	26	29	27	25	52
Fenofibric acid	224	283	250	173	137	109	96	85	62
Gabapentin	1950	1867	1664	1409	1401	1316	1235	1177	40
Imidacloprid	177	157	147	217	218	210	142	111	37
Ketoprofen	159	139	134	83	55	53	47	18	89
Lidocaine	283	270	220	163	161	146	153	135	52
Lincomycin	79	54	52	36	36	35	33	30	63
Mepivacaine	11	n.d.	n.d.	n.d.	n.d.	n.d.	n.d.	n.d.	100
Methadone	23	30	28	21	19	14	13	11	53
Metoclopramide	82	72	55	43	38	39	26	30	63
Metoprolol	43	41	38	11	16	31	19	n.d.	100
Metronidazol	92	86	71	58	64	68	65	62	32
Naproxen	647	520	389	239	207	184	157	127	80
O-Desmethyltramadol	1916	1336	1200	931	833	800	764	750	61
Ofloxacin	792	657	571	432	415	689	665	595	25
O-Desmethylvenlafaxine	1325	1005	1068	800	788	756	810	644	51
Pentoxifylline	282	294	263	208	202	203	201	177	37
Primidone	132	129	121	99	82	60	59	34	74
Propamocarb	20	22	19	18	18	20	18	19	6
Propanolol	52	71	55	33	24	13	18	12	77
Ranitidine	1597	334	287	150	139	110	99	89	94
Sulfapyridine	202	252	220	155	146	129	122	116	42
Thiabendazole	41	35	32	19	n.d.	n.d.	n.d.	n.d.	100
Trimethopim	186	158	128	93	88	85	74	73	61
Venlafaxine	420	430	367	243	207	189	164	146	65
Total load	31249	22651	19526	14699	13858	13626	13232	12341	61

Table S3. CEC removal (ng L^{-1}) over time in medium-level B effluent.

CEC	t_{30W} (min)								% Removal
	0	2.6	5.1	10	16	21	26	32	
4-Aminoantypirine	1186	28	13	n.d.	n.d.	n.d.	n.d.	n.d.	100
4-Acetylaminoantipyrine	1781	581	136	n.d.	n.d.	n.d.	n.d.	n.d.	100
4-Formylaminoantipyrine	6088	2239	933	213	106	70	80	61	99
4-Methylaminoantipyrine	19	n.d.	n.d.	n.d.	n.d.	n.d.	n.d.	n.d.	100
Acetamiprid	77	67	46	35	28	28	30	27	65
Antipyrine	141	75	47	n.d.	n.d.	n.d.	n.d.	n.d.	100
Atenolol	95	33	n.d.	n.d.	n.d.	n.d.	n.d.	n.d.	100
Azoxystrobin	26	13	n.d.	n.d.	n.d.	n.d.	n.d.	n.d.	100
Carbamazepine	109	31	n.d.	n.d.	n.d.	n.d.	n.d.	n.d.	100
Carbendazim	35	14	n.d.	n.d.	n.d.	n.d.	n.d.	n.d.	100
Chlorpyriphos	16	n.d.	n.d.	n.d.	n.d.	n.d.	n.d.	n.d.	100
Ciprofloxacin	618	135	110	64	n.d.	n.d.	n.d.	n.d.	100
Citalopram	92	49	18	n.d.	n.d.	n.d.	n.d.	n.d.	100
Clindamycin	41	12	n.d.	n.d.	n.d.	n.d.	n.d.	n.d.	100
Diazepam	12	n.d.	n.d.	n.d.	n.d.	n.d.	n.d.	n.d.	100
Diuron	49	34	n.d.	n.d.	n.d.	n.d.	n.d.	n.d.	100
Erithromicyn	12	11	n.d.	n.d.	n.d.	n.d.	n.d.	n.d.	100
Fenhexamid	65	n.d.	n.d.	n.d.	n.d.	n.d.	n.d.	n.d.	100
Gabapentin	1309	649	398	130	89	65	76	74	94
Imidacloprid	29	n.d.	n.d.	n.d.	n.d.	n.d.	n.d.	n.d.	100
Indomethacin	11	n.d.	n.d.	n.d.	n.d.	n.d.	n.d.	n.d.	100
Lidocaine	124	56	26	n.d.	n.d.	n.d.	n.d.	n.d.	100
Mepivacaine	17	n.d.	n.d.	n.d.	n.d.	n.d.	n.d.	n.d.	100
Methadone	28	16	n.d.	n.d.	n.d.	n.d.	n.d.	n.d.	100
Metoclopramide	59	22	n.d.	n.d.	n.d.	n.d.	n.d.	n.d.	100
Metoprolol	23	n.d.	n.d.	n.d.	n.d.	n.d.	n.d.	n.d.	100
Naproxen	56	n.d.	n.d.	n.d.	n.d.	n.d.	n.d.	n.d.	100
O-Desmethyltramadol	872	293	130	36	20	13	13	12	99
Ofloxacin	542	209	86	53	45	43	43	42	92
O-Desmethylvenlafaxine	1075	434	166	37	22	21	20	17	98
Pentoxifylline	11	n.d.	n.d.	n.d.	n.d.	n.d.	n.d.	n.d.	100
Pirimicarb	15	n.d.	n.d.	n.d.	n.d.	n.d.	n.d.	n.d.	100
Ranitidine	125	n.d.	n.d.	n.d.	n.d.	n.d.	n.d.	n.d.	100
Salbutamol	27	14	n.d.	n.d.	n.d.	n.d.	n.d.	n.d.	100
Sotalol	39	22	14	n.d.	n.d.	n.d.	n.d.	n.d.	100
Sulfametoxazol	195	160	71	34	22	18	n.d.	n.d.	100
Sulfapyridine	161	59	20	n.d.	n.d.	n.d.	n.d.	n.d.	100
Tebuconazole	48	25	n.d.	n.d.	n.d.	n.d.	n.d.	n.d.	100
Terbutryn	32	18	12	n.d.	n.d.	n.d.	n.d.	n.d.	100
Thiabendazole	36	14	12	n.d.	n.d.	n.d.	n.d.	n.d.	100
Tramadol	1171	371	210	83	59	50	44	44	96
Venlafaxine	177	66	23	n.d.	n.d.	n.d.	n.d.	n.d.	100
Total load	16643	5753	2470	685	390	308	305	278	98

Table S4. CEC removal (ng L^{-1}) over time in low-level A effluent.

CEC	t_{30W} (min)								% Removal
	0	2.8	5.7	11	17	23	29	35	
4-Acetylaminoantipyrine	771	553	414	111	n.d.	n.d.	n.d.	n.d.	100
4-Formylaminoantipyrine	1243	637	371	254	n.d.	n.d.	n.d.	n.d.	100
Atenolol	287	185	112	59	46	33	n.d.	n.d.	100
Carbamazepine	59	22	n.d.	n.d.	n.d.	n.d.	n.d.	n.d.	100
Citalopram	65	73	48	28	n.d.	n.d.	n.d.	n.d.	100
Clindamycin	25	17	n.d.	n.d.	n.d.	n.d.	n.d.	n.d.	100
Gabapentin	943	781	606	438	389	396	379	364	61
Ketoprofen	67	n.d.	n.d.	n.d.	n.d.	n.d.	n.d.	n.d.	100
Lidocaine	88	66	45	27	n.d.	n.d.	n.d.	n.d.	100
O-Desmethyltramadol	319	161	125	67	48	45	41	34	89
Ofloxacin	105	97	n.d.	n.d.	n.d.	n.d.	n.d.	n.d.	100
O-Desmethylvenlafaxine	684	394	315	164	97	n.d.	n.d.	n.d.	100
Ranitidine	255	29	n.d.	n.d.	n.d.	n.d.	n.d.	n.d.	100
Sulfametoxazol	127	128	94	82	69	n.d.	n.d.	n.d.	100
Thiabendazole	32	n.d.	n.d.	n.d.	n.d.	n.d.	n.d.	n.d.	100
Tramadol	905	628	303	215	157	n.d.	n.d.	n.d.	100
Venlafaxine	198	130	73	38	26	n.d.	n.d.	n.d.	100
Total load	6173	3902	2505	1481	832	474	419	399	94

Table S5. CEC removal (ng L^{-1}) over time in low-level B effluent.

CEC	t_{30W} (min)								% Removal
	0	2.6	5.3	11	16	21	27	32	
4-Aminoantypirine	344	n.d.	n.d.	n.d.	n.d.	n.d.	n.d.	n.d.	100
4-Acetylaminoantipyrine	3303	2242	1584	842	531	407	364	340	90
4-Formylaminoantipyrine	2028	1380	1055	528	415	334	312	283	86
4-Methylaminoantipyrine	66	n.d.	n.d.	n.d.	n.d.	n.d.	n.d.	n.d.	100
Antipyrine	39	33	29	18	16	n.d.	n.d.	n.d.	100
Atenolol	673	437	284	169	124	92	91	84	87
Azithromycin	47	21	n.d.	n.d.	n.d.	n.d.	n.d.	n.d.	100
Carbamazepine	143	85	43	19	13	9	5	n.d.	100
Carbendazim	22	14	9	n.d.	n.d.	n.d.	n.d.	n.d.	100
Citalopram	35	35	21	12	11	n.d.	n.d.	n.d.	100
Clarithromycin	43	28	25	20	15	11	12	15	64
Diazepam	34	n.d.	n.d.	n.d.	n.d.	n.d.	n.d.	n.d.	100
Diuron	24	n.d.	n.d.	n.d.	n.d.	n.d.	n.d.	n.d.	100
Erithromicyn	25	27	24	13	15	11	12	15	41
Fenofibric acid	40	34	19	12	9	n.d.	n.d.	n.d.	100
Gabapentin	1711	1160	844	572	434	363	353	342	80
Imidacloprid	38	n.d.	n.d.	n.d.	n.d.	n.d.	n.d.	n.d.	100
Lidocaine	253	156	107	53	44	37	37	32	87
Mepivacaine	12	n.d.	n.d.	n.d.	n.d.	n.d.	n.d.	n.d.	100
Metoclopramide	18	16	n.d.	n.d.	n.d.	n.d.	n.d.	n.d.	100
Metronidazol	79	68	45	30	23	16	15	11	85
Naproxen	233	119	77	n.d.	n.d.	n.d.	n.d.	n.d.	100
O-Desmethyltramadol	589	265	211	128	94	75	72	73	88
Ofloxacin	311	260	152	102	68	60	55	52	83
O-Desmethylvenlafaxine	774	417	320	208	163	148	110	120	85
Pentoxifilline	145	118	86	50	32	32	31	23	84
Primidone	26	24	14	n.d.	n.d.	n.d.	n.d.	n.d.	100
Propanolol	16	n.d.	n.d.	n.d.	n.d.	n.d.	n.d.	n.d.	100
Sulfametoxazol	114	179	121	103	64	52	61	61	46
Sulfapyridine	35	33	25	10	n.d.	n.d.	n.d.	n.d.	100
Thiabendazole	37	n.d.	n.d.	n.d.	n.d.	n.d.	n.d.	n.d.	100
Tramadol	928	417	303	217	169	118	139	123	87
Trimethopim	47	23	n.d.	n.d.	n.d.	n.d.	n.d.	n.d.	100
Venlafaxine	179	132	89	44	29	23	22	20	89
Total load	12410	7725	5487	3148	2267	1788	1692	1594	87

4.4- Mechanistic modeling of solar photo-Fenton process with Fe^{3+}-EDDS at neutral pH

Published:

Soriano-Molina, P., García Sánchez, J.L., Alfano, O.M., Conte, L.O., Malato, S. & Sánchez Pérez, J.A. (2018). Mechanistic modeling of solar photo-Fenton process with Fe^{3+}-EDDS at neutral pH. Applied Catalysis B: Environmental, 233, 234 – 242. DOI: 10.1016/j.apcatb.2018.04.005.

Applied Catalysis B: Environmental 233 (2018) 234–242

Contents lists available at ScienceDirect

Applied Catalysis B: Environmental

journal homepage: www.elsevier.com/locate/apcatb

Mechanistic modeling of solar photo-Fenton process with Fe^{3+}-EDDS at neutral pH

P. Soriano-Molina[a,b], J.L. García Sánchez[a,b], O.M. Alfano[c], L.O. Conte[c], S. Malato[d], J.A. Sánchez Pérez[a,b,*]

[a] Solar Energy Research Centre (CIESOL), Ctra de Sacramento s/n, ES04120, Almería, Spain
[b] Chemical Engineering Department, University of Almería, Ctra de Sacramento s/n, ES04120, Almería, Spain
[c] Instituto de Desarrollo Tecnológico para la industria Química (INTEC), Consejo Nacional de Investigaciones Científicas y Técnicas (CONICET) and Universidad Nacional del Litoral (UNL), Ruta Nacional N° 168, 3000, Santa Fe, Argentina
[d] Plataforma Solar de Almería, CIEMAT, Carretera Senés Km. 4, 04200, Tabernas, Spain

ARTICLE INFO

Keywords:
Acetamiprid
Kinetic model
Photon absorption
Raceway pond reactor
Solar radiation

ABSTRACT

This paper presents, for first time, a mechanistic model of the solar photo-Fenton process at neutral pH with the Fe^{3+}-EDDS complex for micropollutant removal, taking into account irradiance and reactor geometry. Due to its high photon absorptivity, this biodegradable complex allows high percentages of micropollutant removal to be achieved for short reaction times. Nonetheless, no model of the process with the Fe^{3+}-EDDS has yet been developed, meaning the proposed mechanism relies on photochemical reactions with the complex previously reported, and hypotheses deduced from experimental observation. The data for acetamiprid (ACTM) removal (100 μg L^{-1}) in stirred tank reactors with different liquid depths, under controlled conditions of irradiance and temperature, was used to obtain the model parameters. The model successfully fitted the experimental results obtained outdoors in a raceway pond reactor (RPR), with a change of scale from 0.85 to 19 L. For the calculation of the average volumetric rate of photon absorption (VRPA), the effect of the two components of solar UV radiation (direct and diffuse) as a function of the environmental conditions and the reactor layout was considered. The results showed an important contribution by diffuse radiation, even at noon under spring conditions (≈40% of the total VRPA). In addition, the applicability of the model has been demonstrated in water matrices containing organic matter and HCO_3^-/CO_3^{2-} ions, usually found in secondary wastewater treatment plant (WWTP) effluents. This approach allows for the development of control and optimization tools for the photo-Fenton process at neutral pH in low-cost photoreactors.

1. Introduction

Advanced Oxidation Processes (AOPs) have been proposed as a tertiary wastewater treatment for micropollutant removal [1,2]. These pollutants are organic compounds such as pesticides, pharmaceuticals and hormones which are not completely removed by WWTPs. Although micropollutants are discharged into natural water bodies at very low concentrations (ng L^{-1}-μg L^{-1}), they have a bioaccumulative character and toxic effect on organisms [3,4]. Among AOPs, the photo-Fenton process is one of the most efficient treatments [5]. It involves the oxidation of organic matter with the hydroxyl radicals generated by a redox cycle between hydrogen peroxide and ferrous iron under UV–vis radiation. This process is strongly dependent on parameters such as reactant concentration, irradiance, temperature, reactor layout and pH of water [6]. Although the optimum pH to run the process is 2.8, the treatment at neutral pH has been proposed to reduce operating costs, albeit with the disadvantage of iron precipitation [7]. As a remedy for this, polycarboxilic compounds, such as citrate, oxalate, maleate and ethylennediamine-*N*,N'-disuccinic acid (EDDS) are currently being investigated. They form a complex with iron, being maintained in solution and with fast photochemical reactions taking place under solar UV radiation [8–10]. Among these chelating agents, EDDS is a biodegradable structural isomer of EDTA, efficient in the pH range 3–9 [11]. In recent years, the number of publications on photo-Fenton with Fe^{3+}-EDDS has increased hugely, with degradation rates greater than 80% for short reaction times being reported [12–17]. In addition, a higher photon absorption of iron complexed with EDDS, compared to iron aquo complexes, has been reported [18].

Nowadays, the focus of many industries and researchers is to model and optimize wastewater treatment processes. To facilitate this, the

* Corresponding author at: Department of Chemical Engineering, University of Almería, 04120, Almería, Spain.
E-mail address: jsanchez@ual.es (J.A. Sánchez Pérez).

https://doi.org/10.1016/j.apcatb.2018.04.005
Received 2 February 2018; Received in revised form 24 March 2018; Accepted 2 April 2018
Available online 07 April 2018
0926-3373/

development of instrumentation, control and automation systems of WWTPs plays a fundamental role. It is essential to use computer tools based on mathematical models to optimize their design and development by means of simulation. Regarding the photo-Fenton process, several models to estimate the kinetics of micropollutant removal at acidic pH have been developed [19–22]. At pH close to neutrality, the modeling of the process has been widely studied using the ferrioxalate complex [23–26]. However, despite the large number of publications which highlight the interest of the scientific community in the use of Fe^{3+}-EDDS, a mechanistic model which includes photon absorption has not yet been proposed, to the best of the author's knowledge. Furthermore, most models have been developed in demineralized water matrices. Due to the effect of organic matter and HCO_3^-/CO_3^{2-} ions ($HO^{\bullet}$ scavengers) on the process, the inclusion of these species in the modeling could be of interest for a wider application.

The main goal of this work is to develop a mechanistic model of the solar photo-Fenton process with the Fe^{3+}-EDDS complex at neutral pH as a function of irradiance and reactor geometry for micropollutant removal. ACTM is frequently used as a model microcontaminant because it is a highly recalcitrant pesticide [27] included in a first watch list of priority hazardous substances [28]. To obtain the model parameters, experimental ACTM degradation data from a synthetic secondary effluent was used. These assays were conducted at lab scale under controlled conditions of irradiance (10–50 W m^{-2}) and temperature (25 °C). The kinetic model was validated outdoors in winter and spring conditions, with a change of scale from 0.85 L to 19 L in a RPR. These low-cost reactors have the advantage of being able to vary the liquid depth to achieve optimum use of photons, according to the availability of UV radiation and iron concentration. Moreover, they are more efficient regarding micropollutant removal (mass of micropollutant per surface of photoreactor) than the conventional tubular photoreactors with compound parabolic collectors (CPCs) [17]. The effect of photon absorption corresponding to diffuse UV light is included in the activated steps of the reaction mechanism. This component of solar radiation, not usually considered for photon absorption calculations, could account for a high percentage of total radiation in flat photoreactors, especially in winter or under cloudy conditions [29,30].

2. Experimental

2.1. Chemicals

Sodium hydroxide and sulphuric acid (98%) were purchased from J.T Baker®. Hydrogen peroxide (33%), ammonium nitrate, ferric sulphate (75%), hydrochloric acid (37%), acetic acid and $CaSO_4 \cdot H_2O$ were obtained from Panreac. Acetamiprid ($C_{10}H_{11}ClN_4$, 20% w/w) was purchased from EPIK®. Sodium formate was acquired from Merck Millipore and HPLC grade Acetonitrile from BDH Prolabo Chemicals. Peptone and beef extract were obtained from BD Bacto and Biolife, respectively. Ethylenediamine disuccinic acid (35%), titanium (IV) oxysulfate, ortho-phenantroline, peptone, sodium lauryle sulfonate, $MgSO_4$, acacia gum powder, sodium lignin sulfonate, ascorbic acid, arabic acid, formic acid (98%), $(NH_4)_2SO_4$, KCl, tetrabutylammonium bisulfate, methanol and humic salt were purchased from Sigma-Aldrich.

2.2. Experimental set-up

A synthetic secondary effluent with a Dissolved Organic Carbon (DOC) concentration of around 12 mg L^{-1} and 14 mg L^{-1}. Total Inorganic Carbon (IC) was used as a water matrix, according to [31,32]. Initial and final pH in the 7.0–7.5 range were recorded for each assay. In all the experiments, the ACTM, H_2O_2 and Fe^{3+} concentrations were 100 μgL^{-1} (representing the total concentration of micropollutant in secondary effluents) 0.88 mM (30 mg L^{-1}) and 0.1 mM, respectively. The Fe^{3+}-EDDS complex was prepared with 1:1 stoichiometry [11], as described in previous work [18].

The data obtained in cylindrical PVC stirred tank reactors, under controlled conditions to study the effect of VRPA on the kinetics of micropollutant removal, [18] was used to obtain the model parameters. The reactors (0.85 L volume, 15 cm diameter) were placed inside a SunTest CPS + solar box from Atlas, with an emission range from 250 to 765 W m^{-2}. The UVA irradiance range in the reactor surface was set from 10 to 50 W m^{-2} and the liquid depth was increased from 5 to 15 cm, keeping temperature constant at 25 °C with a cooling coil connected to a thermostatic bath. This temperature was set accordingly for experimentation because it is the average annual temperature recorded at the WWTP in Almeria, located in southeastern Spain. To avoid any incoming radiation through the reactor walls, they were made opaque (in PVC). Irradiance was measured on the reactor surface with a spectroradiometer (Avantes AvaSpec Dual-Cannel Fiber Optic Spectrometer), the wavelength range being 327 to 384 nm. This wavelength range was set because it is the wavelength range of the measurements given by the radiometer used in outdoor experiments.

For the model validation, experiments were conducted outdoors at the Solar Energy Research Centre (CIESOL) in Almería, Spain, in a 19-L PVC-RPR with 5 cm liquid depth and 22 cm channel width. The mixing time was low (2 min) compared to the reaction time (tens of minutes); hence the hypothesis of perfect mixing could be assumed. Temperature and pH were monitored online with probes connected to a LabJack USB/Ethernet data acquisition device. Incident UV radiation (direct and diffuse), averaged over the wavelength range 327–384 nm, was measured with a global UV radiometer (Delta Ohm, LPUVA02AV).

2.3. Chemical analysis

The samples collected from the reactor were filtered through 0.20-μm Millipore filters. After that, the filter was washed with acetonitrile (10:1, sample: acetonitrile), which stops the reaction and draws out any trace of contaminant retained [33].

Total dissolved iron was determined by the 1,10-phenanthroline method (ISO 6332), the limit of quantification (LOQ) being 4.5 10^{-3} mM. Hydrogen peroxide was quantified according to the spectrophotometric method DIN 38 402 H15, the LOQ being 2.9 10^{-2} mM.

Fe^{3+}-EDDS and ACTM concentrations were determined by liquid chromatography (HPLC Agilent 1100 Series and HPLC Agilent 1200 Series, respectively). For Fe^{3+}-EDDS, the mobile phases were methanol and an aqueous solution of sodium formiate (15 mM) and tetrabutylamonium hydrogen sulfate (2 mM) at pH 4. The LOQ was 1.8 10^{-3} mM. For ACTM, the phases were acetonitrile and dilute formic acid (0.1%, v/v). The LOQ was 5 μg L^{-1}. Methods and equipment characteristics were previously reported [18,22].

TIC and DOC concentrations were determined in a Shimadzu-V CPH TOC analyser, the LOQ being 2 mg L^{-1}.

2.4. Determination of the average volumetric rate of photon absorption (VRPA)

2.4.1. Experiments in a solar box

In a photoreactor, in which radiation emission is in parallel planes (the variation of the radiation can be considered as a function of a single spatial coordinate), and the scattering effect of the radiation can be considered negligible, the local volumetric rate of photon absorption (LVRPA) of an absorbent species can be determined by Eq. (1) [24,34]:

$$LVRPA\ (t, x) = q_{w,\lambda} \cdot k_\lambda(t) \cdot \exp(-k_{T,\lambda}(t) \cdot x) \quad (1)$$

where $q_{w,\lambda}$ is the spectral distribution of incident radiation (lamp power) at a specific wavelength (W m^{-2} nm^{-1}), k_λ is the volumetric absorption coefficient of the photon absorbing species (m^{-1}), $k_{T,\lambda}$ is the total volumetric absorption coefficient of the medium (m^{-1}) and x is the spatial coordinate (m). $q_{w,\lambda}$ was measured in the wavelength range

327–384 nm with a spectroradiometer (Avantes AvaSpec Dual-Cannel Fiber Optic Spectrometer), and Planck's equation was used to convert data from W m^{-2} to μE m^{-2} s^{-1}.

In perfect mixing systems, in which the concentration of species can be considered the same for any position in the reactor, the LVRPA can be averaged across the reactor volume [24,31,35–38]. Therefore, the average VRPA in the reactor for each of the absorbing species (Fe^{3+}-EDDS and Fe^{3+}-$EDDS_{ox}$, defined in 2.5) was calculated by integrating Eq. (1) over the liquid depth, D (m), Eqs. (2) and (3), since the reactor surface was constant. Due to the reactor layout inside the solar box, the light rays could be considered as being parallel in the direction perpendicular to the reactor surface. The change in Fe^{3+}-EDDS concentration over time was also taken into account.

$$VRPA_1(t) = \frac{1}{D}\sum_{\lambda}\frac{q_{w,\lambda}\cdot k_{Fe^{3+}-EDDS,\lambda}(t).\,[1-\exp(-k_{T,\lambda}(t)\bullet D)]}{k_{T,\lambda}(t)} \quad (2)$$

$$VRPA_2(t) = \frac{1}{D}\sum_{\lambda}\frac{q_{w,\lambda}\cdot k_{Fe^{3+}-EDDSox,\lambda}(t).\,[1-\exp(-k_{T,\lambda}(t)\bullet D)]}{k_{T,\lambda}(t)} \quad ((3))$$

The molar absorptivity of Fe^{3+}-EDDS (mM^{-1} m^{-1}), $\alpha_{Fe^{3+}-EDDS,\lambda}$ was determined from the UV absorption spectra obtained in synthetic secondary effluent, as previously reported [18]. As for Fe^{3+}-$EDDS_{ox}$, $\alpha_{Fe^{3+}-EDDSox,\lambda}$ was estimated from a photo-Fenton assay, assuming that once the experiment is started, the optical thickness of the solution at a given time is the sum of the optical thickness of all absorbent species, Eq. (4). Therefore, $\alpha_{Fe^{3+}-EDDSox,\lambda}$ could be isolated from Eq. (4). Finally, $k_{T,\lambda}$ could be calculated according to Eq. (5), [24].

$$\alpha_{\text{total dissolved Fe},\lambda}\cdot C_{\text{total dissolved Fe}} = \alpha_{Fe^{3+}-EDDS,\lambda}\cdot C_{Fe^{3+}-EDDS} + \alpha_{Fe^{3+}-EDDSox,\lambda}\cdot C_{Fe^{3+}-EDDSox} \quad (4)$$

where $\alpha_{\text{total dissolved Fe},\lambda}$ is the molar absorptivity of the medium, calculated from the UV absorption spectrum of dilutions of a sample taken after 5 min of the reaction, and measured instantaneously.

$$k_{T,\lambda}(t) = k_{Fe^{3+}-EDDS,\lambda} + k_{Fe^{3+}-EDDSox,\lambda} = \alpha_{Fe^{3+}-EDDS,\lambda}\cdot C_{Fe^{3+}-EDDS}(t) + \alpha_{Fe^{3+}-EDDSox,\lambda}\cdot C_{Fe^{3+}-EDDSox}(t) \quad ((5))$$

2.4.2. Outdoor experiments in an RPR

For experiments carried out in the RPR, the solar radiation that reaches the reactor surface is made up of direct radiation, which reaches the surface without being absorbed or scattered in the atmosphere, and diffuse radiation, that is, scattered radiation. Regarding direct radiation, its optical light path length depends on the solar zenith angle, θ_s, Fig. 1. The refracted angle inside the reactor, θ_{direct}, was estimated using Snell's law, assuming the refraction index of water matrix to be 1.33 [31]. Accordingly, for outdoor experiments, the expressions to calculate the average VRPA, Eqs. (2) and (3), were replaced by Eqs. (6) and (7):

Here, the value of $q_{wdirect,\lambda}$ is the product of the direct radiation and $\cos\theta_{direct}$.

$$VRPA_{direct1}(t) = \frac{1}{D}\sum_{\lambda}\frac{q_{wdirect,\lambda}\cdot k_{Fe^{3+}-EDDS,\lambda}(t)\cdot\left[1-\exp(-k_{T,\lambda}(t)\bullet\frac{D}{\cos\theta_{direct}})\right]}{k_{T,\lambda}(t)} \quad (6)$$

$$VRPA_{direct2}(t) = \frac{1}{D}\sum_{\lambda}\frac{q_{wdirect,\lambda}\cdot k_{Fe^{3+}-EDDSox,\lambda}(t)\cdot\left[1-\exp(-k_{T,\lambda}(t)\bullet\frac{D}{\cos\theta_{direct}})\right]}{k_{T,\lambda}(t)} \quad (7)$$

For the experiments in the solar box all the radiation could be considered direct and perpendicular to the reactor surface. However, due to the influence of the solar zenith angle on the UV radiation, the diffuse component was taken into account for outdoor experiments.

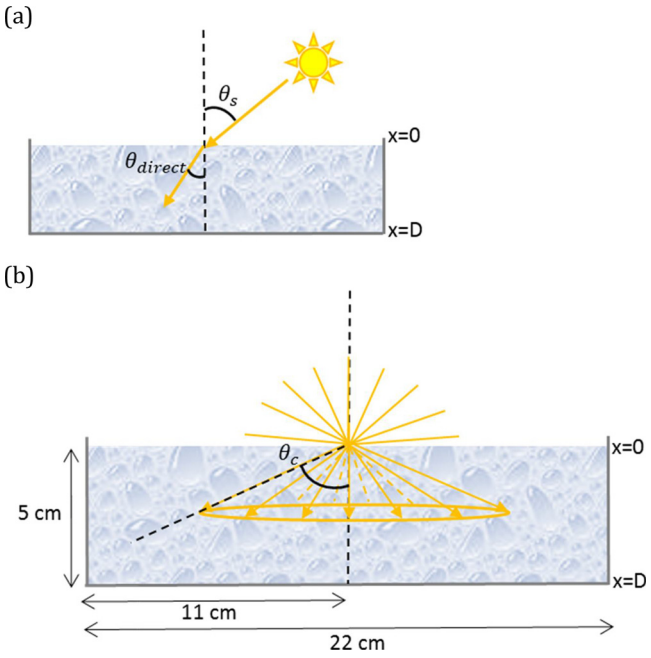

Fig. 1. Scheme for direct (a) and diffuse (b) light paths in a channel of the RPR (θ_c = 48.75°).

According to the Radiative Transfer Equation (RTE) [39], the LVRPA corresponding to the diffuse radiation can be determined by Eqs. (8) and (9), taking into account only photons moving towards the bottom of the reactor and azimuthal symmetry (propagation of rays as a function of the liquid depth, x, and an angular coordinate, $\theta_{diffuse}$),and the critical angle, θ_c, of the angular coordinate as a consequence of the refraction of light in the reactor [40].

$$LVRPA_{diffuse1}(x,\,t) = \sum_{\lambda} 2\cdot q_{wdiffuse,\lambda}\cdot k_{Fe^{3+}-EDDS,\lambda}(t)\cdot\int_0^{\theta_c} e^{-\frac{k_{T,\lambda}(t).x}{\cos\theta_{diffuse}}}\cdot \sin\theta_{diffuse}\,(d\theta_{diffuse}) \quad (8)$$

$$LVRPA_{diffuse2}(x,\,t) = \sum_{\lambda} 2\cdot q_{wdiffuse,\lambda}\cdot k_{Fe^{3+}-EDDSox,\lambda}(t)\cdot\int_0^{\theta_c} e^{-\frac{k_{T,\lambda}(t).x}{\cos\theta_{diffuse}}}\cdot \sin\theta_{diffuse}\,(d\theta_{diffuse}) \quad (9)$$

Finally, the reactor volume average LVRPA can be calculated by Eqs. (10) and (11):

$$VRPA_{diffuse1}(t) = \frac{1}{D}\cdot\int_0^D \sum_{\lambda} 2\cdot q_{w,\lambda}\cdot k_{Fe^{3+}-EDDS,\lambda}(t)\cdot\left(\int_0^{\theta_c} e^{-\frac{k_{T,\lambda}(t).x}{\cos\theta_{diffuse}}}\cdot\sin\theta_{diffuse}\,(d\theta_{diffuse})dx\right) \quad (10)$$

$$VRPA_{diffuse2}(t) = \frac{1}{D}\cdot\int_0^D \sum_{\lambda} 2\cdot q_{w,\lambda}\cdot k_{Fe^{3+}-EDDSox,\lambda}(t)\cdot\left(\int_0^{\theta_c} e^{-\frac{k_{T,\lambda}(t).x}{\cos\theta_{diffuse}}}\cdot\sin\theta_{diffuse}\,(d\theta_{diffuse})dx\right) \quad (11)$$

$q_{wdirect,\lambda}$ and $q_{wdiffuse,\lambda}$ were obtained with the solar software SMARTS2. This simple model estimates the atmospheric radiative transfer of sunshine from spectral transmittance functions for the main extinction processes in the atmosphere, such as Rayleigh scattering, ozone and aerosol extinction [41]. The SMARTS2 code prediction of the spectral distribution of UV radiation was determined at the latitude for the city of Almería, Spain (36°50´17´´N, 2°27´35´´W, at sea level). The main atmospheric conditions were characterized by the following input variables: the Angstrom's Beta and Schuepp's B coefficients for atmospheric turbidity (0.087 and 0.088, respectively), and the wavelength

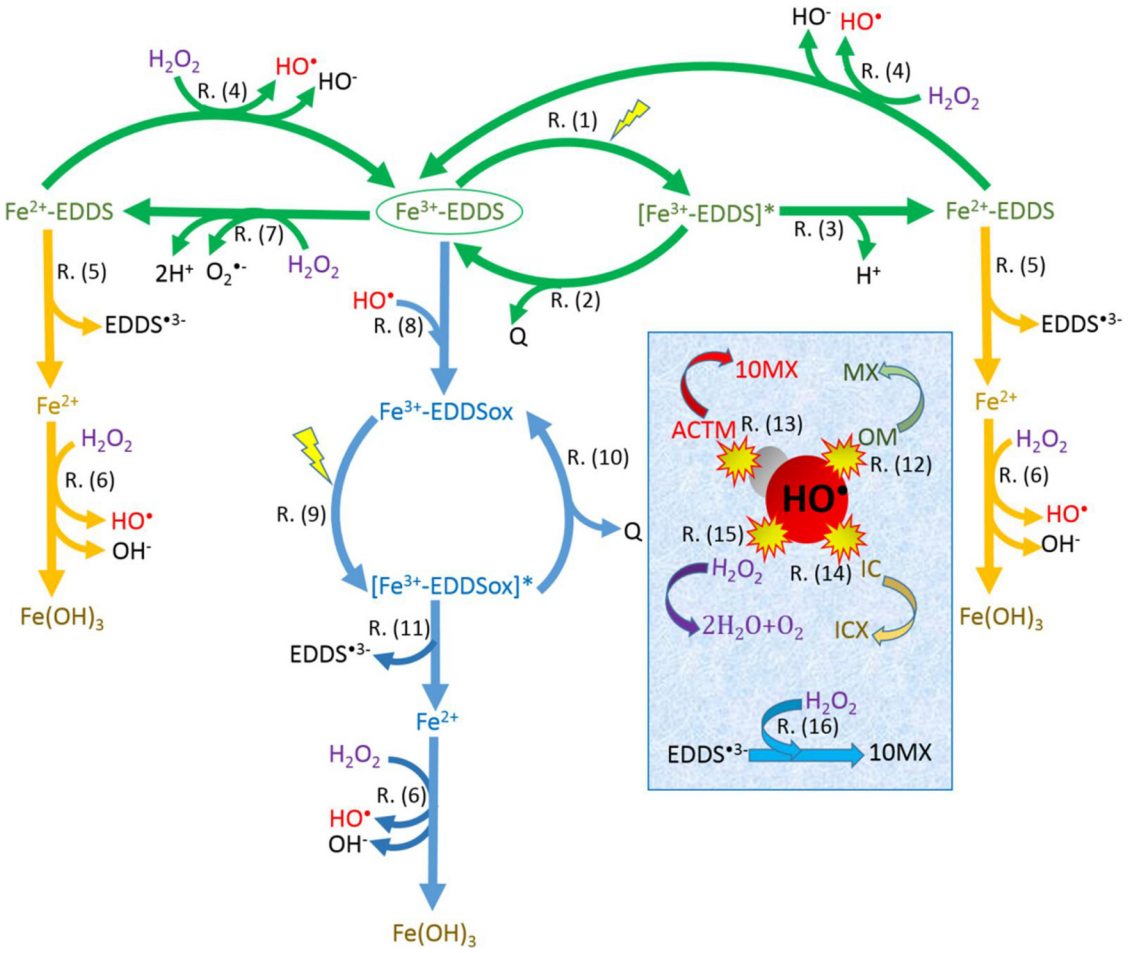

Fig. 2. Model reactions. Green, orange and blue arrows correspond to Fe^{3+}-EDDS, Fe^{2+}-EDDS and Fe^{3+}-$EDDS_{ox}$ paths, respectively (For interpretation of the references to colour in this figure legend, the reader is referred to the web version of this article).

exponents α_1 and α_2 (close to 0.9 and 1.2, respectively), obtained from the Shettle and Fenn urban aerosol model as a function of wavelength and humidity. The average values of direct and diffuse irradiance obtained from this model were corroborated by the measurement given by the global UV radiometer (Delta Ohm, LPUVA02AV).

2.5. Kinetic model

The iron precipitation and the presence of species, such as HCO_3^-/CO_3^{2-}ions, increase the complexity of the reaction system and, consequently, the process modeling at the natural pH of water. In line with previous work focused on the photochemical study of the Fe^{3+}-EDDS complex [11–13,18], a kinetic model has been proposed. It justifies the presence of iron in solution after complex decomposition, in addition to modeling the kinetics of the micropollutant degradation. The scheme for the reaction mechanism and rate equations are shown in Fig. 2 and Table 1, respectively. Once Fe^{3+}-EDDS is photoactivated by UV radiation, R. (1), a fraction of the absorbed radiation is used in iron reduction, R. (2), while another fraction is converted into heat (Q), with the complex returning to its initial state as Fe^{3+}-EDDS, R. (3), [18,22]. The formation of the Fe^{2+}-EDDS complex has been reported for the Fenton process, as well as for the activated persulfate process [42,43], and some authors have pointed out that once the complex is reduced, it is decomposed to Fe^{2+} and $EDDS^{\bullet 3-}$ [12,14]. Along the same lines, this study proposes that the photoreduced iron could remain as Fe^{2+}-EDDS, as an intermediate state, before being decomposed to Fe^{2+} and $EDDS^{\bullet 3-}$, R. (5). Consequently, Fe^{2+}-EDDS could be oxidized by H_2O_2 (Fenton) returning to its initial state as Fe^{3+}-EDDS [42,44]. It is known that Fe^{2+}-polycarboxylate complexes, such as ferrous-oxalate, react much faster with H_2O_2 than Fe^{2+} aquo complexes [23,45]. Therefore, the presence of Fe^{2+}-EDDS after the irradiation of Fe^{3+}-EDDS could explain the high H_2O_2 consumption for the first few minutes of reaction. Fe^{2+} reacts with H_2O_2 (classic Fenton, R. (6)) giving rise to $HO^{\bullet}$ and Fe^{3+}, which precipitates as $Fe(OH)_3$ at neutral pH instantaneously. Fe^{3+}-EDDS is also reduced by H_2O_2, R. (7) [42], through a much slower reaction than R. (2).

Table 1
Rate law equations.

Rate equation	Reaction number
$r_1 = VRPA_1$	R. (1)
$r_2 = k_2\,[[Fe^{3+}\text{–}EDDS]^{-*}]$	R. (2)
$r_3 = k_3\,[[Fe^{3+}\text{–}EDDS]^{-*}]$	R. (3)
$r_4 = k_4\,[Fe^{2+}\text{–}EDDS]\,[H_2O_2]$	R. (4)
$r_5 = k_5\,[Fe^{2+}\text{–}EDDS]$	R. (5)
$r_6 = k_6\,[Fe^{2+}]\,[H_2O_2]$	R. (6)
$r_7 = k_7\,[[Fe^{3+}\text{–}EDDS]^{-}]\,[H_2O_2]$	R. (7)
$r_8 = k_8\,[[Fe^{3+}\text{–}EDDS]^{-}]\,[HO^{\bullet}]$	R. (8)
$r_9 = VRPA_2$	R. (9)
$r_{10} = k_{10}\,[[Fe^{3+}\text{–}EDDS_{ox}]^{*}]$	R. (10)
$r_{11} = k_{11}\,[[Fe^{3+}\text{–}EDDS_{ox}]^{*}]$	R. (11)
$r_{12} = k_{12}\,[MO]\,[HO^{\bullet}]$	R. (12)
$r_{13} = k_{13}\,[ACTM]\,[HO^{\bullet}]$	R. (13)
$r_{14} = k_{14}\,[IC]\,[HO^{\bullet}]$	R. (14)
$r_{15} = k_{15}\,[H_2O_2]\,[HO^{\bullet}]$	R. (15)
$r_{16} = k_{16}\,[H_2O_2]\,[EDDS^{\bullet 3-}]$	R. (16)

Since these paths are not cyclic, iron would rapidly precipitate after being oxidized by H_2O_2. Nonetheless, experimental data showed a longer lifespan of iron in solution after complex decomposition, which could be explained by the presence of oxidized species of the complex (Fe^{3+}-$EDDS_{ox}$) derived from the oxidation of Fe^{3+}-EDDS with $HO^{\bullet}$ radicals, R. (8) [18,42]. Moreover, the absorption of the oxidized complex was checked experimentally and calculated as described in Section 2.4.1. Thus, Fe^{3+}-$EDDS_{ox}$ could absorb radiation giving rise to Fe^{2+} and $EDDS^{\bullet 3-}$. The generated hydroxyl radicals also react with the organic matter (OM), R. (12), the model pollutant ACTM, R. (13), the inorganic carbon (IC), R. (14), and the H_2O_2, R.(15), giving rise to their respective oxidation products. Finally, $EDDS^{\bullet 3-}$ radicals are able to react with H_2O_2 giving rise to oxidized matter, R. (16).

3. Results and discussion

3.1. Model parameters estimation

Assuming the hypothesis of perfect mixing and operation in batch mode, the dynamic model was obtained by imposing mass balances on each of species of the system, Table 2. Since the mass balance to the oxidized organic matter was expressed in carbon moles, the reactions corresponding to the oxidation of the ACTM and $EDDS^{\bullet 3-}$, R. (13) and R. (16), were multiplied by 10 (the number of carbon atoms in both ACTM and EDDS) in Eq. (24). The set of differential equations was solved using the MATLAB function ode23s, and the model parameters were obtained by the built-in optimization routine: fmincon. The objective function was defined by Eq. (12), where the errors of each species are normalized and a weight is assigned to them, w_A, w_H, w_F and w_C. In order to achieve a good fit to reagent consumption and micropollutant removal, the highest weight was imposed for H_2O_2 consumption and ACTM degradation errors, while the lowest weight was assigned to that of the total dissolved iron: $w_A = 1$, $w_H = 1$, $W_F = 0.25$ and $w_C = 0.75$.

$$J = \sum_{j=1}^{m}\left[\sum_{i=1}^{n} w_A\cdot\left(\frac{A_{x(i,j)}-A_{m(i,j)}}{A_{x(1,j)}}\right)^2 + w_H\cdot\left(\frac{H_{x(i,j)}-H_{m(i,j)}}{H_{x(1,j)}}\right)^2 + w_F\cdot\left(\frac{F_{x(i,j)}-F_{m(i,j)}}{F_{x(1,j)}}\right)^2 + w_C\cdot\left(\frac{C_{x(i,j)}-C_{m(i,j)}}{C_{x(1,j)}}\right)^2\right] \quad (12)$$

Table 2
Dynamic model equations.

Mass balance model	Equation number
$\frac{d[[Fe^{3+}-EDDS]^-]}{dt} = -r_1 + r_2 + r_4 - r_7 - r_8$	Eq. (14)
$\frac{d\left[[Fe^{3+}-EDDS]^{-*}\right]}{dt} = r_1 - r_2 - r_3$	Eq. (15)
$\frac{d[Fe^{2+}]}{dt} = r_5 - r_6 + r_{11}$	Eq. (16)
$\frac{d[Fe^{2+}-EDDS]}{dt} = r_3 - r_4 - r_5 + r_7$	Eq. (17)
$\frac{d[Fe^{3+}-EDDSox]}{dt} = r_8 - r_9 + r_{10}$	Eq. (18)
$\frac{d[[Fe^{3+}-EDDSox]^*]}{dt} = r_9 - r_{10} - r_{11}$	Eq. (19)
$\frac{d[H_2O_2]}{dt} = -r_4 - r_6 - r_7 - r_{15} - r_{16}$	Eq. (20)
$\frac{d[HO^{\bullet}]}{dt} = r_4 + r_6 - r_8 - r_{12} - r_{13} - r_{14} - r_{15}$	Eq. (21)
$\frac{d[ACTM]}{dt} = -r_{13}$	Eq. (22)
$\frac{d[OM]}{dt} = -r_{12}$	Eq. (23)
$\frac{d[MX]}{dt} = r_{12} + 10\,r_{13} + 10\,r_{16}$	Eq. (24)
$\frac{d[IC]}{dt} = -r_{14}$	Eq. (25)
$\frac{d[ICX]}{dt} = r_{14}$	Eq. (26)
$\frac{d[EDDS^{\bullet 3-}]}{dt} = r_5 + r_{11} - r_{16}$	Eq. (27)

In Eq. (12), n is the number of data points in each experiment (n = 9), m is the number of assays used in the search for parameters from the total of 14 experimental conditions (m = 7) and finally, A, H, F and C are ACTM, H_2O_2, total dissolved iron and Fe^{3+}-EDDS concentration, respectively. Subscript x refers to experimental data and m to model data.

The root mean square error (RMSE) equation was used to calculate the error percentage between experimental data and model estimations for each species:

$$RMSE = \sqrt{\frac{1}{m\cdot n}\cdot\sum_{j=1}^{m}\sum_{i=1}^{n}\left(\frac{C_{i,x(i,j)}-C_{i,m(i,j)}}{C_{i,x(1,j)}}\right)^2}\cdot 100 \quad (13)$$

where $C_{i,x}$ and $C_{i,m}$ are the experimental and model estimated concentrations of total dissolved iron, H_2O_2, Fe^{3+}-EDDS and ACTM, respectively.

From the total of 14 kinetic constants, 3 were taken from literature: $k_6 = 4.56\ mM^{-1}\ min^{-1}$ (classic Fenton), $k_{14} = 5.1{\cdot}10^5\ mM^{-1}\ min^{-1}$ (HCO_3- oxidation by $HO^{\bullet}$) [46], and $k_{15} = 1.6{\cdot}10^6\ mM^{-1}\ min^{-1}$ (H_2O_2 oxidation by $HO^{\bullet}$) [47]. The estimated kinetic constants are shown in Table 3. Standard deviation for each constant was estimated by resampling the residuals of the best fit and implementing a bootstrap estimate to be used with the search algorithm of fmincon. The obtained standard deviations were assumable taking into account that the procedure was repeated for 500 times to get an estimation of the parameter distribution, statistical analysis being conducted over these distributions.

According to the determined parameters, most of the energy absorbed by the Fe^{3+}-EDDS is employed in its reduction, $k_3 > > k_2$, while that absorbed by its oxidized form, Fe^{3+}-$EDDS_{ox}$, is released into the medium as heat, $k_{10} > k_{11}$. This would appear to be logical, since the quantum efficiency of the Fe^{3+}-EDDS may well decrease after being oxidized. Concerning Fe^{2+}-EDDS oxidation by H_2O_2, R. (4), k_4 is three orders of magnitude higher than k_6 (classic Fenton). Although as far as the authors know the kinetic constant for Fe^{2+}-EDDS oxidation has not been reported, values as high as $1.86{\cdot}10^3 mM^{-1}min^{-1}$ (coincident with that determined for Fe^{2+}-EDDS in this work, $k_4 = 1.9{\cdot}10^3 mM^{-1}min^{-1}$) have been published for Fe^{2+}-oxalate oxidation [23] and mentioned in previous work with Fe^{3+}-EDDS [12]. Such a fast reaction rate between H_2O_2 and Fe^{2+}-EDDS points out the relevance of Fe^{2+}-EDDS being proposed as an intermediate state for the photo-Fenton process in this work. R. (7) is much lower than R. (3), in concordance with the slower Fenton reduction when compared to photo-Fenton [42] and the observation in previous Fenton assays, in which the concentration of the species hardly changed [18]. The resulting kinetic constant corresponding to the Fe^{3+}-EDDS oxidation by $HO^{\bullet}$ radicals, k_8, is of the order of magnitude of that corresponding to Fe^{3+}-EDTA oxidation, $3.1{\cdot}10^7\ mM^{-1}min^{-1}$, a value which has been directly imposed on k_8 in certain studies [42]. Regarding the oxidation of organic compounds with the generated $HO^{\bullet}$, k_{13} is higher than k_{12}, which is consistent with the observation that the parent compound degrades much faster than the organic matter mineralizes [22].

Table 3
Model parameters obtained from minimizing the objective function.

Kinetic constant	Value	Standard deviation	Unit
k_2	0.25	0.095	min^{-1}
k_3	17.14	4.81	min^{-1}
k_4	$1.9{\cdot}10^3$	$0.23{\cdot}10^3$	$mM^{-1}\,min^{-1}$
k_5	35.69	4.09	min^{-1}
k_7	0.40	0.18	$mM^{-1}\,min^{-1}$
k_8	$5.6{\cdot}10^7$	$0.53{\cdot}10^7$	$mM^{-1}\,min^{-1}$
k_{10}	10.50	1.92	min^{-1}
k_{11}	3.31	0.55	min^{-1}
k_{12}	$6.2{\cdot}10^6$	$0.81{\cdot}10^6$	$mM^{-1}\,min^{-1}$
k_{13}	$6.4{\cdot}10^7$	$0.43{\cdot}10^7$	$mM^{-1}\,min^{-1}$
k_{16}	$1.2{\cdot}10^6$	$0.24{\cdot}10^6$	$mM^{-1}\,min^{-1}$

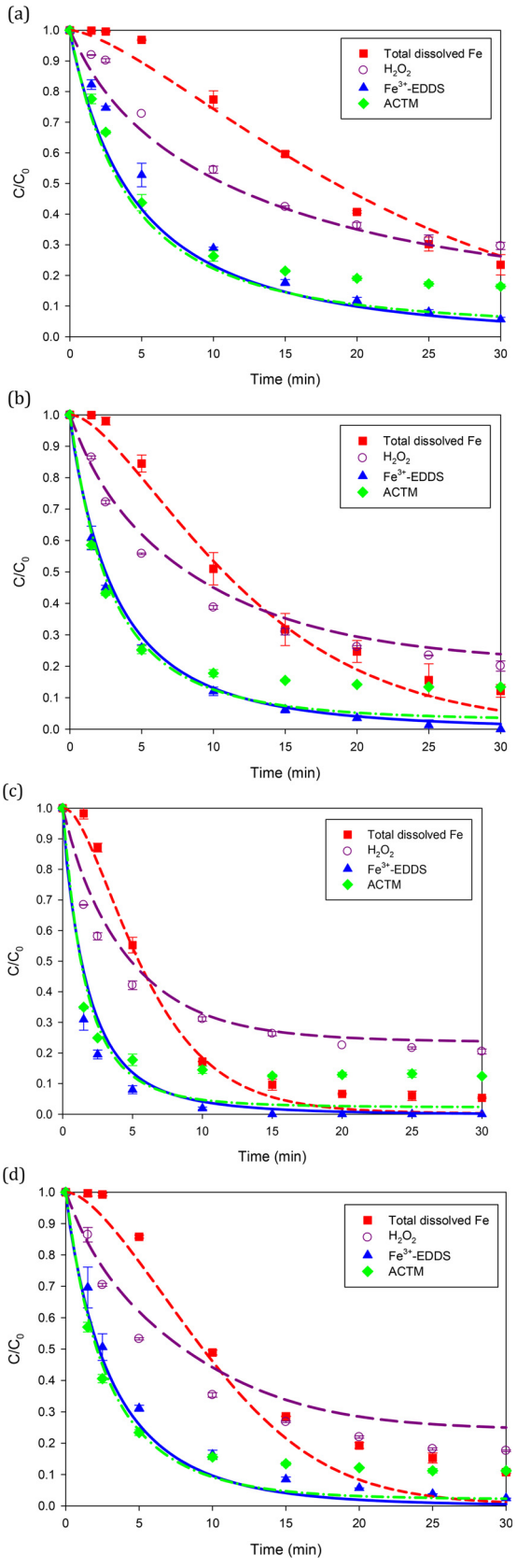

Fig. 3. Total dissolved iron, H_2O_2, Fe^{3+}-EDDS and ACTM profiles as a function of irradiance and liquid depth: 10 W m^{-2} and 5 cm (a), 20 W m^{-2} and 5 cm (b) 50 W m^{-2} and 5 cm (c), 40 W m^{-2} and 15 cm (d). Lines represent model estimations (short dashes for total dissolved iron, long dashes for H_2O_2, solid for Fe^{3+}-EDDS, and dash-dot for ACTM).

Despite the complexity of the reaction medium (a synthetic secondary WWTP effluent at neutral pH), the proposed model acceptably fits the experimental data for all the experimental conditions, both at 5 and 15 cm liquid depth. The RMSE was 5.6%, 6.8%, 5.4% and 7.2% for total dissolved iron, H_2O_2, Fe^{3+}-EDDS and ACTM, respectively. Fig. 3 shows the comparison between kinetic data predicted by the model and experimental results obtained in the solar box for 4 selected conditions, corresponding to the different seasons of the year. As can be seen, the model adequately reproduces the presence of iron in solution after complex decomposition, with an acceptable fit. As for H_2O_2 consumption, the simulation results show a good fit to the experimental data over 30 min of reaction. Due to the process is photosaturated at 40 W m^{-2} and 5 cm [18], Fig. 3(d) shows the model predictions when the liquid depth is increased. In this case, the model also fits the data, with a slightly slower reaction rate predicted for H_2O_2, pointing out that the model could be useful for predicting the treatment capacity by optimizing the liquid depth to take advantage of the photons that reach the reactor surface, at these mild oxidation conditions. In all the cases, the model reproduces almost exactly experimental data for ACTM removal in the first 5 min of the reaction and with good prediction until 10 min. After that, according to the experimental results, the ACTM degradation is stopped and the model predicts a slight drop in its concentration, the error in micropollutant removal being around 10% at 30 min. This deviation could be due to that once the complex concentration is low (due to its degradation), the generation rate of HO• radicals is lower and ACTM removal is stopped due to competence with organic matter (in the range of tens of mg L^{-1}) that could easier react with HO• radicals and other radicals formed during the process. Legislation in Switzerland demands 80% micropollutant removal in WWTPs, from the entrance to the exit of the WWTP [48]. Taking into account that this error between the experimental and simulated data occurs when ≥ 80% micropollutant removal has been directly achieved in the photo-Fenton process (tertiary treatment), this overestimation would not be very significant when using the model in practical applications.

3.2. Outdoor model performance

The kinetics parameters, obtained from experiments in the solar box under controlled conditions of irradiance and temperature, were used to validate the model with experimental data obtained outdoors in an RPR with 5 cm liquid depth. The assays were conducted at noon during winter and spring days and the temperature was in the range 20–30 °C. Within this range, the change in molar absorptivity can be considered negligible [22], thus it was assumed to be the same as that calculated for indoor experiments. Due to the fact that the direct beams only reach the illuminated zones of the reactor, whereas diffuse beams reach all the zones, the reactions R. (1) and R. (9) were modified accordingly:

$$r_1 = \frac{V_i}{V}VRPA_{direct1} + VRPA_{diffuse1} \qquad \text{R. ((17))}$$

$$r_9 = \frac{V_i}{V}VRPA_{direct2} + VRPA_{diffuse2} \qquad \text{R. ((18))}$$

where V_i and V denote irradiated and reaction volume, respectively. Vi was calculated taking into account the dark areas generated by the reactor walls as a function of the solar zenith angle. In all the experiments V was 19 L.

As can be observed in Fig. 4, outdoor experimental data reproduces the phenomenon observed in the experiments carried out in the solar simulator. As a result, both for winter and spring conditions, values close to 70% and 80% of H_2O_2 consumption and ACTM degradation, respectively, were achieved. The model resulted in a successful fit to the experimental data of H_2O_2 consumption, total dissolved iron profile, Fe^{3+}-EDDS decomposition and ACTM degradation for winter conditions. The RMSE values were 1.1%, 5.9%, 1.9% and 4.3%, respectively. As for spring conditions, Fig. 4(b), the model reproduces H_2O_2 consumption and the

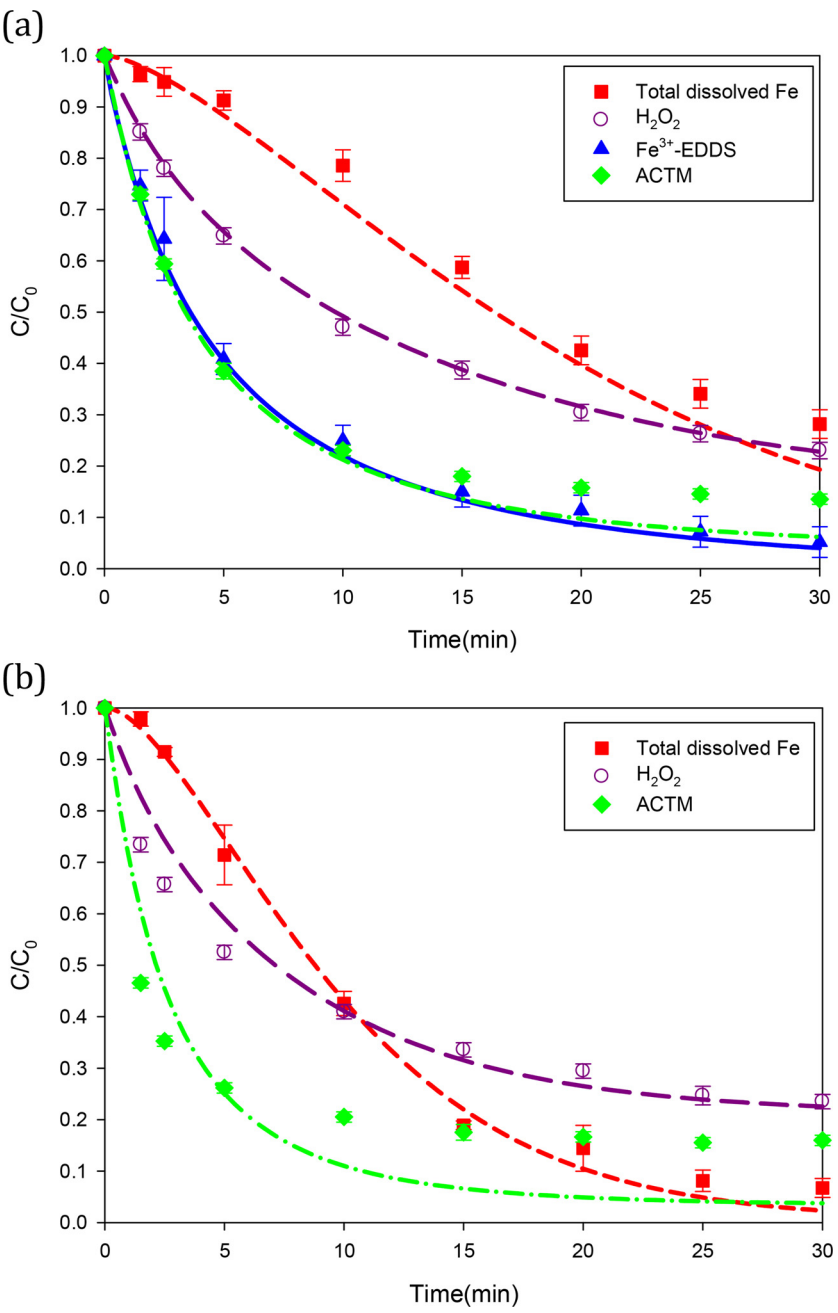

Fig. 4. Model validation in an RPR with 5 cm liquid depth in winter (a) and spring (b) conditions (Winter: average water temperature: 21.1 °C, θ_s = 58.24°, direct irradiance = 5.86 W m^{-2}, diffuse irradiance = 10.09 W m^{-2}, V_i = 16.1 L. Spring: average water temperature: 28.3 °C, θ_s = 27.13°, direct irradiance = 18.69 W m^{-2}, diffuse irradiance = 13.38 W m^{-2}, V_i = 17.3 L). Lines represent model estimations (short dashes for total dissolved iron, long dashes for H_2O_2, solid for Fe^{3+}-EDDS, and dash-dot for ACTM).

total dissolved iron profile, with a RMSE value of 5.0% and 2.8%, respectively. The experimental data of ACTM is reproduced for the first 5 min of the reaction. Subsequently, after 80% ACTM degradation, an overestimation in its removal rate is observed, as in the experiment at lab scale, the total RMSE being 9.9%. These results show that the kinetics model, obtained from lab scale data in cylindrical stirred reactors, could be applied on a larger scale to perfectly mixed reactors of different geometry, such as RPRs. The model could therefore be useful for optimizing the treatment capacity in WWTPs as a function of the availability of UV radiation.

It is worth mentioning the contribution of diffuse irradiance towards the kinetics of the process, whose value represents more than 50% of the total irradiance at noon in winter (63% in the experimental condition shown in Fig. 4(a)). Fig. 5 shows the time-courses of VRPA values predicted by the model for Fe^{3+}-EDDS and Fe^{3+}-$EDDS_{ox}$ for the best radiation condition (spring). At the beginning of the reaction, the VRPA values corresponding to direct and diffuse radiation for Fe^{3+}-EDDS were 643 μE m^{-3} s^{-1} and 462 μE m^{-3} s^{-1}, respectively, pointing out the effect of diffuse radiation on the kinetics of the process, even under clear day conditions in spring. Furthermore, as mentioned above, the decrease in the Fe^{3+}-EDDS concentration, observed in all experimental conditions, has an important effect on photon absorption. In this case, the VRPA is reduced by more than three times after 5 min of the reaction. Nonetheless, the VRPA due to the Fe^{3+}-EDDSox complex increases in the first few minutes, being equal to the VRPA due to the parent complex (Fe^{3+}-EDDS) at 3.5 min of reaction. Despite this increase in the VRPA of the oxidized species, most of the radiation absorbed by them is released as heat, as mentioned above. These results agree with the low reaction rates observed after 5 min of the reaction, highlighting the relevance of the VRPA corresponding to the Fe^{3+}-EDDS, R. (1), on the kinetics of the process.

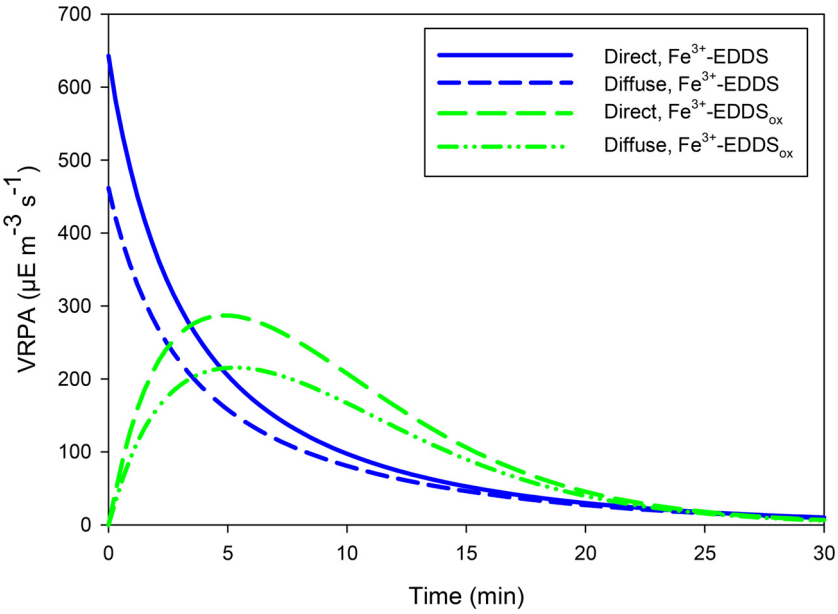

Fig. 5. Effect of decomposition and oxidation of Fe^{3+}-EDDS on direct and diffuse VRPA at noon in spring.

4. Conclusions

A mechanistic model of the photo-Fenton process in an effluent from a WWTP at neutral pH with the Fe^{3+}-EDDS complex is proposed for the first time. This model was developed based on previous kinetic studies and hypotheses deduced from experimental data. It was able to reproduce the kinetics of Fe^{3+}-EDDS decomposition, iron precipitation, H_2O_2 consumption and microcontaminant removal at short reaction times in complex water matrices. The importance of diffuse radiation on the kinetics of the process carried out in flat photoreactors was demonstrated, the diffuse VRPA representing values as high as 40% of the total VRPA at noon in spring. The model was successfully validated outdoors in an RPR, thus being, of great application for the control and optimization of the process in scalable and low-cost photocatalytic reactors.

Acknowledgements

This research was supported by the European Regional Development Fund (ERDF) and the Ministry for Economy and Competitiveness (Spanish Government), project CTM2015-71054-REDT and CTQ2016-78255-R. O.M. Alfano and L.O. Conte would like to acknowledge Universidad Nacional del Litoral (UNL), Consejo Nacional de Investigaciones Científicas y Técnicas (CONICET), and Agencia Nacional de Promoción Científica y Tecnológica (ANPCyT) for their financial support. P. Soriano-Molina is grateful to the Ministry of Education, Culture and Sport for her FPU scholarship (AP2014/01030) and the funding for her placement at Instituto de Desarrollo Tecnológico para la Industria Química (INTEC), Santa Fe (Argentina) (EST16/00602). Finally, the authors sincerely acknowledge G. Mailhot and M. Brigante, from Institut de Chimie de Clermont-Ferrand (France), for their verbal collaboration in the kinetic model formulation.

References

[1] N. Serpone, Y.M. Artemev, V.K. Ryabchuk, A.V. Emeline, S. Horikoshi, Light-driven advanced oxidation processes in the disposal of emerging pharmaceutical contaminants in aqueous media: a brief review, Curr. Opin. Green Sustain. Chem. 6 (2017) 18–33, http://dx.doi.org/10.1016/j.cogsc.2017.05.003.

[2] O.M. Rodriguez-Narvaez, J.M. Peralta-Hernandez, A. Goonetilleke, E.R. Bandala, Treatment technologies for emerging contaminants in water: A review, Chem. Eng. J. 323 (2017) 361–380, http://dx.doi.org/10.1016/j.cej.2017.04.106.

[3] R. Münze, C. Hannemann, P. Orlinskiy, R. Gunold, A. Paschke, K. Foit, J. Becker, O. Kaske, E. Paulsson, M. Peterson, H. Jernstedt, J. Kreuger, G. Schüürmann, M. Liess, Pesticides from wastewater treatment plant effluents affect invertebrate communities, Sci. Total Environ. 599–600 (2017) 387–399, http://dx.doi.org/10.1016/j.scitotenv.2017.03.008.

[4] D. Destrieux, F. Laurent, H. Budzinski, J. Pedelucq, P. Vervier, M. Gerino, Drug residues in urban water: A database for ecotoxicological risk management, Sci. Total Environ. 609 (2017) 927–941, http://dx.doi.org/10.1016/j.scitotenv.2017.07.043.

[5] I. Velo-Gala, J.A. Pirán-Montaño, J. Rivera-Utrilla, M. Sánchez-Polo, A.J. Mota, Advanced Oxidation Processes based on the use of UVC and simulated solar radiation to remove the antibiotic tinidazole from water, Chem. Eng. J. 323 (2017) 605–617, http://dx.doi.org/10.1016/j.cej.2017.04.102.

[6] A. Delavaran Shiraz, A. Takdastan, S. Mehdi Borghei, Photo-Fenton like degradation of catechol using persulfate activated by UV and ferrous ions: Influencing operational parameters and feasibility studies, J. Mol. Liq. 249 (2018) 463–469, http://dx.doi.org/10.1016/j.molliq.2017.11.045.

[7] L. Clarizia, D. Russo, I. Di Somma, R. Marotta, R. Andreozzi, Homogeneous photo-Fenton processes at near neutral pH: A review, Appl. Catal. B: Environ. 209 (2017) 358–371, http://dx.doi.org/10.1016/j.apcatb.2017.03.011.

[8] A.A. Nogueira, B.M. Souza, M.W.C. Dezotti, R.A.R. Boaventura, V.J.P. Vilar, Ferrioxalate complexes as strategy to drive a photo-FENTON reaction at mild pH conditions: A case study on levofloxacin oxidation, J. Photochem. Photobiol. A: Chem. 345 (2017) 109–123, http://dx.doi.org/10.1016/j.jphotochem.2017.05.020.

[9] J.A. Lima, A.L. Tonetti, C. Vidal, C.C. Montagner, R.F. Pupo Nogueira, Simultaneous degradation of ciprofloxacin, amoxicillin, sulfathiazole and sulfamethazine, and disinfection of hospital effluent after biological treatment via photo-Fenton process under ultraviolet germicidal irradiation, Appl. Catal. B: Environ. 224 (2018) 761–771, http://dx.doi.org/10.1016/j.apcatb.2017.11.021.

[10] D. Seibert, T. Diel, J.B. Welter, A.L. de Souza, A.N. Módenes, F.R. Espinoza-Quiñones, F.H. Borba, Performance of photo-Fenton process mediated by Fe(III)-carboxylate complexes applied to degradation of landfill leachate, J. Environ. Chem. Eng. 5 (2017) 4462–4470, http://dx.doi.org/10.1016/j.jece.2017.08.043.

[11] W. Huang, M. Brigante, F. Wu, K. Hanna, G. Mailhot, Development of a new homogenous photo-Fenton process using Fe(III)-EDDS complexes, J. Photochem. Photobiol. A: Chem. 239 (2012) 17–23, http://dx.doi.org/10.1016/j.jphotochem.2012.04.018.

[12] J. Li, G. Mailhot, F. Wu, N. Deng, Photochemical efficiency of Fe(III)-EDDS complex : •OH radical production and 17β-estradiol degradation, J. Photochem. Photobiol. A: Chem. 212 (2010) 1–7, http://dx.doi.org/10.1016/j.jphotochem.2010.03.001.

[13] Y. Wu, M. Passananti, M. Brigante, W. Dong, G. Mailhot, Fe(III)–EDDS complex in Fenton and photo-Fenton processes: from the radical formation to the degradation of a target compound, Environ. Sci. Pollut. Res. 21 (2014) 12154–12162, http://dx.doi.org/10.1007/s11356-014-2945-1.

[14] N. Klamerth, S. Malato, A. Agüera, A. Fernández-Alba, Photo-Fenton and modified photo-Fenton at neutral pH for the treatment of emerging contaminants in wastewater treatment plant effluents: a comparison, Water Res. 47 (2013) 833–840, http://dx.doi.org/10.1016/j.watres.2012.11.008.

[15] S. Papoutsakis, S. Miralles-Cuevas, I. Oller, J.L. García Sánchez, C. Pulgarín, S. Malato, Microcontaminant degradation in municipal wastewater treatment plant secondary effluent by EDDS assisted photo-Fenton at near-neutral pH: An experimental design approach, Catal. Today. 252 (2015) 61–69, http://dx.doi.org/10.1016/j.cattod.2015.02.005.

[16] G. Rivas Ibáñez, M. Bittner, Z. Toušová, M.C. Campos-Mañas, A. Agüera, J.L. Casas,

J.A. Sánchez Pérez, K. Hilscherová, Does micropollutant removal by solar photo-Fenton reduce ecotoxicity in municipal wastewater? A comprehensive study at pilot scale open reactors, J. Chem. Technol. Biotechnol. 92 (2017) 2114–2122, http://dx.doi.org/10.1002/jctb.5212.

[17] I. De la Obra, L. Ponce-Robles, S. Miralles-Cuevas, I. Oller, S. Malato, J.A. Sánchez Pérez, Microcontaminant removal in secondary effluents by solar photo-Fenton at circumneutral pH in raceway pond reactors, Catal. Today 287 (2016) 10–14, http://dx.doi.org/10.1016/j.cattod.2016.12.028.

[18] P. Soriano-Molina, J.L. García Sánchez, S. Malato, L.A. Pérez-Estrada, J.A. Sánchez Pérez, Effect of volumetric rate of photon absorption on the kinetics of micropollutant removal by solar photo-Fenton with Fe^{3+}-EDDS at neutral pH, Chem. Eng. J. 331 (2018) 84–92, http://dx.doi.org/10.1016/j.cej.2017.08.096.

[19] O.M. Alfano, E.D. Albizzati, L.O. Conte, Modelling of Photo-Fenton Solar Reactors for Environmental Applications, in: D. Bahnemann, P. Robertson (Eds.), Environmental Photochemistry Part III. The Handbook of Environmental Chemistry, vol. 35, Springer, Berlin, Heidelberg, 2013, , http://dx.doi.org/10.1007/698_2013_246.

[20] F. Speck, S. Raja, V. Ramesh, V. Thivaharan, Modelling and Optimization of Homogenous Photo-Fenton Degradation of Rhodamine B by Response Surface Methodology and Artificial Neural Network, Int. J. Environ. Res. 10 (2016) 543–554, http://dx.doi.org/10.22059/ijer.2016.59683.

[21] S. Giannakis, I. Hendaoui, S. Rtimi, J.M. Fürbringer, C. Pulgarín, Modeling and treatment optimization of pharmaceutically active compounds by the photo-Fenton process: The case of the antidepressant Venlafaxine, J. Environ. Chem. Eng. 5 (2017) 818–828, http://dx.doi.org/10.1016/j.jece.2016.12.050.

[22] J.A. Sánchez Pérez, P. Soriano-Molina, G. Rivas, J.L. García Sánchez, J.L. Casas López, J.M. Fernández Sevilla, Effect of temperature and photon absorption on the kinetics of micropollutant removal by solar photo-Fenton in raceway pond reactors, Chem. Eng. J. 310 (2017) 464–472, http://dx.doi.org/10.1016/j.cej.2016.06.055.

[23] M. Simunovic, H. Kusic, N. Koprivanac, A.L. Bozic, Treatment of simulated industrial wastewater by photo-Fenton process: Part II. The development of mechanistic model, Chem. Eng. J. 173 (2011) 280–289, http://dx.doi.org/10.1016/j.cej.2010.09.030.

[24] L.O. Conte, A.V. Schenone, O.M. Alfano, Photo-Fenton degradation of the herbicide 2,4-D in aqueous medium at pH conditions close to neutrality, J. Environ. Manage. 170 (2016) 60–69, http://dx.doi.org/10.1016/j.jenvman.2016.01.002.

[25] L.O. Conte, A.V. Schenone, O.M. Alfano, Ferrioxalate-assisted solar photo-Fenton degradation of a herbicide at pH conditions close to neutrality, Environ. Sci. Pollut. Res. 24 (2017) 6205–6212, http://dx.doi.org/10.1007/s11356-016-6400-3.

[26] A.V. Schenone, L.O. Conte, M.A. Botta, O.M. Alfano, Modeling and optimization of photo-Fenton degradation of 2,4-D using ferrioxalate complex and response surface methodology (RSM), J. Environ. Manage. 155 (2015) 177–183, http://dx.doi.org/10.1016/j.jenvman.2015.03.028.

[27] S. Arzate, J.L. García Sánchez, P. Soriano-Molina, J.L. Casas López, M.C. Campos-Mañas, A. Agüera, J.A. Sánchez Pérez, Effect of residence time on micropollutant removal in WWTP secondary effluents by continuous solar photo-Fenton process in raceway pond reactors, Chem. Eng. J. 316 (2017) 1114–1121, http://dx.doi.org/10.1016/j.cej.2017.01.089.

[28] M.O. Barbosa, N.F.F. Moreira, A.R. Ribeiro, M.F.R. Pereira, A.M.T. Silva, Occurrence and removal of organic micropollutants: An overview of the watch list of EU Decision 2015/495, Water Res. 94 (2016) 257–279, http://dx.doi.org/10.1016/j.watres.2016.02.047.

[29] A.C.S.C. Teixeira, R. Guardani, C.A.O. Nascimento, Solar Photochemical Degradation of Aminosilicones Contained in Liquid EffluentsProcess Studies and Neural Network, Modeling, Ind. Eng. Chem. 42 (2003) 5751–5761, http://dx.doi.org/10.1021/ie0303350.

[30] A.J. Gutiérrez-Trashorras, E. Villicaña-Ortiz, E. Álvarez-Álvarez, J.M. González-Caballín, J. Xiberta-Bernat, M.J. Suarez-López, Attenuation processes of solar radiation. Application to the quantification of direct and diffuse solar irradiances on horizontal surfaces in Mexico by means of an overall atmospheric transmittance, Renew. Sustain. Energy Rev. 81 (2018) 93–106, http://dx.doi.org/10.1016/j.rser.2017.07.042.

[31] G. Rivas, I. Carra, J.L. García Sánchez, J.L. Casas López, S. Malato, J.A. Sánchez Pérez, Modelling of the operation of raceway pond reactors for micropollutant removal by solar photo-Fenton as a function of photon absorption, Appl. Catal. B: Environ. 178 (2015) 210–217, http://dx.doi.org/10.1016/j.apcatb.2014.09.015.

[32] M.I. Polo-López, I. García-Fernández, T. Velegraki, A. Katsoni, I. Oller, D. Mantzavinos, P. Fernández-Ibáñez, Mild solar photo-Fenton: An effective tool for the removal of *fusarium* from simulated municipal effluents, Appl. Catal. B: Environ. 111–112 (2012) 545–554, http://dx.doi.org/10.1016/j.apcatb.2011.11.006.

[33] S. Mitroka, S. Zimmeck, D. Troya, J.M. Tanko, How Solvent Modulates Hydroxyl Radical Reactivity in Hydrogen Atom Abstractions, J. Am. Chem. Soc. 132 (2010) 2907–2913, http://dx.doi.org/10.1021/ja903856t.

[34] O.M. Alfano, R.L. Romero, A.E. Cassano, A cylindrical photoreactor irrradiated from the bottom-I. Radiation flux density generated by a tubular source and a parabolic reflector, Chem. Eng. Sci. 40 (1985) 2119–2127, http://dx.doi.org/10.1016/0009-2509(85)87030-5.

[35] J. Colina-Márquez, F. Machuca-Martínez, G. Li Puma, Radiation absorption and optimization of solar photocatalytic reactors for environmental applications, Environ. Sci. Technol. 44 (2010) 5112–5120, http://dx.doi.org/10.1021/es100130h.

[36] I. Grčić, G. Li Puma, Photocatalytic Degradation of Water Contaminants in Multiple Photoreactors and Evaluation of Reaction Kinetic Constants Independent of Photon Absorption, Irradiance, Reactor Geometry, and Hydrodynamics, Environ. Sci. Technol. 47 (2013) 13702–13711, http://dx.doi.org/10.1021/es403472e.

[37] A. Cabrera Reina, L. Santos-Juanes, J.L. García Sánchez, J.L. Casas López, M.I. Maldonado Rubio, G. Li Puma, J.A. Sánchez Pérez, Modelling the photo-Fenton oxidation of the pharmaceutical paracetamol in water including the effect of photon absorption (VRPA), Appl. Catal. B: Environ. 166–167 (2015) 295–301, http://dx.doi.org/10.1016/j.apcatb.2014.11.023.

[38] A. Cabrera Reina, J.L. Casas López, M.I. Maldonado Rubio, L. Santos-Juanes Jordá, J.L. García Sánchez, J.A. Sanchez Pérez, Effects of environmental variables on the photo-Fenton plant design, Chem. Eng. J. 237 (2014) 469–477, http://dx.doi.org/10.1016/j.cej.2013.10.046.

[39] R.J. Brandi, M.A. Citroni, O.M. Alfano, A.E. Cassano, Absolute quantum yields in photocatalytic slurry reactors, Chem. Eng. Sci. 58 (2003) 979–985, http://dx.doi.org/10.1016/S0009-2509(02)00638-3.

[40] M.L. Satuf, R.J. Brandi, A.E. Cassano, O.M. Alfano, Photocatalytic degradation of 4-chlorophenol: A kinetic study, Appl. Catal. B: Environ. 82 (2008) 37–49, http://dx.doi.org/10.1016/j.apcatb.2008.01.003.

[41] C. Gueymard, SMARTS2, a Simple Model of the Atmospheric Radiative Transfer of Sunshine: Algorithms and Performance Assessment. Rep. FSEC-PF-270-95, Florida Solar Energy Center, Cocoa, USA, 1995.

[42] W. Huang, M. Brigante, F. Wu, C. Mousty, K. Hanna, G. Mailhot, Assessment of the Fe(III) − EDDS complex in Fenton-Like Processes: from the radical formation to the degradation of bisphenol A, Environ. Sci. Technol. 47 (2013) 1952–1959, http://dx.doi.org/10.1021/es304502y.

[43] D. Han, J. Wan, Y. Ma, Y. Wang, M. Huang, Enhanced decolorization of Orange g in a Fe(II)-EDDS activated persulfate process by accelerating the regeneration of ferrous iron with hydroxylamine, Chem. Eng. J. 256 (2014) 316–323, http://dx.doi.org/10.1016/j.cej.2014.06.006.

[44] Y. Zhang, N. Klamerth, S.A. Messele, P. Chelme-Ayala, M.G. El-Din, Kinetics study on the degradation of a model naphthenic acid by ethylenediamine- N, N'-disuccinic acid-modified Fenton process, J. Hazard. Mater. 318 (2016) 371–378, http://dx.doi.org/10.1016/j.jhazmat.2016.06.063.

[45] P. Cieśla, P. Kocot, P. Mytych, Z. Stasicka, Homogeneous photocatalysis by transition metal complexes in the environment, J. Mol. Catal. A: Chem. 224 (2004) 17–33, http://dx.doi.org/10.1016/j.molcata.2004.08.043.

[46] G.V. Buxton, C.L. Greenstock, W.P. Helman, A.B. Ross, Critical review of rate constants for reactions of hydrated electrons, hydrogen atoms and hydroxyl radicals ($^{\bullet}OH/^{\bullet}O^{-}$) in aqueous solution, J. Phys. Chem. Ref. Data 17 (1998) 513–886, http://dx.doi.org/10.1063/1.555805.

[47] R. Chen, J.J. Pignatello, Role of Quinone Intermediates as Electron Shuttles in Fenton and Photoassisted Fenton Oxidations of Aromatic Compounds, Environ. Sci. Technol. 31 (1997) 2399–2406, http://dx.doi.org/10.1021/es9610646.

[48] R.I.L. Eggen, J. Hollender, A. Joss, M. Schärer, C. Stamm, Reducing the discharge of micropollutants in the aquatic environment: the benefits of upgrading wastewater treatment plants, Environ. Sci. Technol. 48 (2014) 7683–7689, http://dx.doi.org/10.1021/es500907n.

4.5- On the design and operation of solar photo-Fenton open reactors for the removal of contaminants of emerging concern from WWTP effluents at neutral pH

Soriano-Molina, P., García Sánchez, J.L., Malato, S., Plaza-Bolaños, P., Agüera, A. & Sánchez Pérez, J.A.

Submitted

On the design and operation of solar photo-Fenton open reactors for the removal of contaminants of emerging concern from WWTP effluents at neutral pH

P. Soriano-Molina[a,b], J.L. García Sánchez[a,b], S. Malato[a,c], P. Plaza-Bolaños[a], A. Agüera[a], J.A. Sánchez Pérez[a,b*]

[a] Solar Energy Research Centre (CIESOL), Joint Centre University of Almería-CIEMAT, Carretera de Sacramento s/n, E-04120, Almería, Spain.
[b] Chemical Engineering Department, University of Almería, Ctra de Sacramento s/n, E-04120, Almería, Spain.
[c] Plataforma Solar de Almería, CIEMAT, Carretera Senés Km. 4, E-04200, Tabernas, Almería, Spain.
*Corresponding author:
J. A. Sánchez Pérez, Department of Chemical Engineering, University of Almería, 04120, Almería, Spain; Tel.: +34 950015314.
E-mail address: jsanchez@ual.es

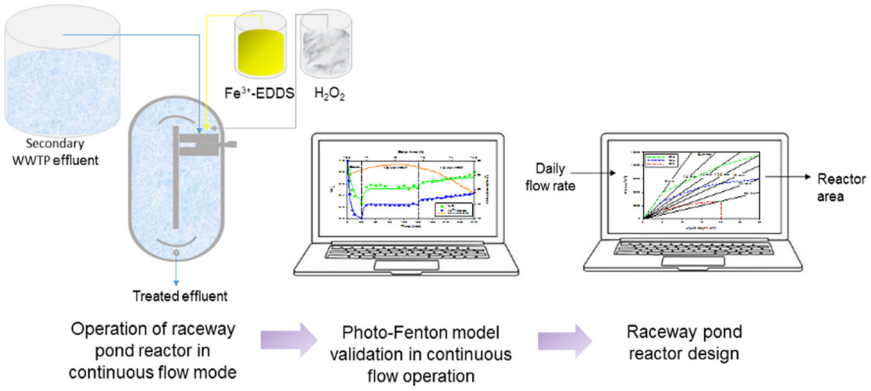

Abstract

This work presents for the first time a tool for the design of continuous raceway pond reactors (RPRs) to remove contaminants of emerging concern (CECs) from WWTP secondary effluents by solar photo-Fenton process at neutral pH. The effects of the hydraulic residence time (HRT) and the liquid depth on the treatment capacity were studied, the availability of solar UV radiation being the main environmental variable affecting the process (external variable). Treatment capacities, in terms of volume of treated water per reactor surface area and day, as high as 1800 and 9000 L m^{-2} d^{-1} were estimated for 70% CEC removal in winter and summer solstices, respectively. To this aim, the performance of a kinetic model of the photo-Fenton process developed with Fe^{3+}-EDDS as a function of water composition, availability of UV radiation as well as reactor geometry was studied. The capability of the model to predict both the removal of the most abundant compounds detected in the wastewater treatment plants (WWTPs) (*O*-desmethyltramadol and *O*-desmethylvenlafaxine and gabapentin) and the reactant consumption was successfully validated in a 5-cm (19 L) and 15-cm (78 L) deep-RPRs operated in continuous flow mode with short hydraulic residence time in the range 10 – 30 min. In order to reach a goal of percentage of elimination of CEC, the treatment capacity can be maximized as a function of the HRT and the liquid depth, and consequently the surface area of the reactor is calculated to treat a given flow rate.

Keywords:

Advanced oxidation process; EDDS; Microcontaminant; Raceway pond reactor; Wastewater

1. Introduction

The development of anthropogenic activities, such as agriculture or chemical and pharmaceutical industry, has brought along the production of different chemical compounds including personal care products, pharmaceuticals, hormones or pesticides. Currently, they are known as contaminants of emerging concern (CECs), since they are considered as a potential threat to the environment and biota [1,2]. One of the main sources of CECs are effluents from conventional wastewater treatment plants (WWTPs), which are not designed to remove these compounds, and consequently a high proportion of them are discharged to the aquatic environment. Although the discharge of CECs has not been regulated yet, rules in Switzerland demand 80% removal efficiency of total load of CECs with respect to raw wastewater [3]. Furthermore, the Commission Decision 2015/495/EU provides a list of 17 CECs to be monitored in the European Union (EU) [4]. Consequently, there is a global interest in the development of tertiary treatments for the removal of these compounds in municipal WWTPs (MWWTPs)[5]. Among these treatments, solar photo-Fenton has been demonstrated to be an environmentally friendly and highly efficient advanced oxidation process (AOP) [6,7].

Nowadays, the research is focused on the operation of the process at neutral pH to deal with the drawbacks of the conventional photo-Fenton process at acidic pH, reducing operating cost and avoiding the increase in the salinity of the effluents. To maintain iron in solution, the use of chelating agents such us ethylenediamine-N,N'-disuccinic acid (EDDS) has been proposed [8]. The removal of CECs by photo-Fenton with Fe^{3+}-EDDS has been widely demonstrated in synthetic and real effluents [9–11]. A recent work shows that high removal efficiencies of around 80% can be achieved in real effluents of very different composition by the process operated at neutral pH with Fe^{3+}-EDDS [12].

Once the process efficiency is demonstrated, it is important to study the reaction mechanisms for further development of models to control and optimize the treatment. Wastewater composition, irradiance, reactant concentration as well as reactor geometry are the variables that most affect the kinetics of the process [13]. Therefore, they must be considered for the design of treatment plants. Regarding the photo-Fenton process, there are few models reported for CEC removal. Schenone et al. [14] proposed a model for the degradation of the herbicide 2,4-dichlorophenoxyacetic (2,4-D) at circumneutral pH using ferrioxalate complex. Giannakis et al. [15] developed a strategy to optimize the operating range concerning the reagents and pH by using the Response Surface methodology. In a recent work, a mechanistic modeling of the process with Fe^{3+}-EDDS has been obtained and successfully validated outdoors in a low-cost RPRs with simulated secondary effluent [16].

These models have been developed under controlled conditions, in demineralized water or synthetic wastewater. The experimental results may differ greatly from the predicted results when applying the models in real conditions, since the reaction mechanisms are affected by variations in WWTP effluent composition. Inorganic ions such as chlorides, sulfates and bicarbonates can substantially affect CEC removal [17,18]. Moreover, author's recent work carried out in secondary effluents from different MWWTPs shows that the nature of organic matter has a great effect on the kinetics of the process [12].

Therefore, extending the application of mechanistic models of solar photo-Fenton to cover CEC removal in real MWWTP effluents of very different composition would be desirable. In order to maximize the treatment capacity of a treatment plant, it is very important to evaluate the performance of models and its degree of adaptability to different perturbations under different operating conditions. To this aim, this paper presents for the first time a design tool for the real treatment of MWWTP effluents by solar photo-Fenton. The hydraulic residence time (HRT) and the liquid depth in RPRs were the operating variables, whereas the solar UV radiation was the external uncontrollable variable. Meanwhile, maximizing the treatment capacity in terms of volume of water treated per unit of reactor surface area and time (L m^{-2} d^{-1}) was the design target. The three most abundant CECs detected in secondary effluents from five MWWTPs were selected as target compounds (*O*-desmethyltramadol (O-DSMT*)* and *O*-desmethylvenlafaxine (O-DSMV) and gabapentin (GBP)). These compounds are drugs or their metabolites (tramadol and venlafaxine) commonly used and highly persistent to conventional treatments, and consequently, they are being detected at high concentrations in MWWTPs located in different countries [19–22].

2. Experimental

2.1. Chemicals

Hydrogen peroxide (33%, w/v), ferric sulfate hydrate (75%, w/w), acetic acid (99.7%, w/v), 1,10-phenantroline (99%, w/w) and hydrochloric acid (37%, w/v) were supplied by Panreac (Barcelona, Spain). Methanol (MeOH) and acetonitrile were high pressure liquid chromatography (HPLC) grade and acquired from Sigma-Aldrich (Steinheim, Germany). Sodium formate (99% w/w) was obtained from Merck Millipore (Darmstadt, Germany). Ultrapure water was produced with a Millipore Direct-Q® Ultrapure Water System

(Bedford, MA, USA). Formic acid (95%, w/v), sulfuric acid (95%, w/v), tetrabutylammonium bisulfate (97%, w/w), titanium (IV) oxysulfate (1.9%, w/v), ascorbic acid (99%, w/w), EDDS (35%, w/v) and high purity analytical standards were supplied by Sigma-Aldrich.

2.2. Chemical analysis

The concentration of H_2O_2 and total dissolved iron were determined by standard colorimetric procedures, according to DIN 38 402 H15 method and1,10-phenanthroline (ISO 6332) methods, respectively. The limits of quantification (LOQs) were 6.1 10^{-4} mM and 4.5 10^{-3} mM, respectively.

The concentration of Fe^{3+}-EDDS was determined by ultrahigh-pressure liquid chromatography with diode array detection (UHPLC-DAD) in an Agilent Technologies 1200 Series instrument (Waldbronn, Germany). Isocratic elution was applied, using a mobile phase composed of 5% of MeOH and 95% of 2 mM tetrabutylamonium hydrogen sulfate and 15 mM sodium formiate in water. The flow was 0.5 mL min^{-1}. The LOQ was 3.5 10^{-3} mM.

The direct injection technique was used to determine the concentration of CECs by high-performance liquid chromatography quadrupole-linear ion trap analyzer (LC-QqLIT-MS/MS); further details can be found elsewhere [23].

Dissolved organic carbon (DOC) and inorganic carbon (IC) were quantified with a Shimadzu-V CPH TOC analyzer (Shimadzu Corporation, Kyoto, Japan). The LOQ was 1 mg L^{-1}.

The concentration of anions was measured using ion chromatography Metrohm 881 Compact IC pro (Herisau, Switzerland). The eluent consisted of a solution of 3.6 mM Na_2CO_3 with flow rate of 0.8 mL min^{-1}.

2.3. Experimental set-up

The experiments were carried outdoors at the Solar Energy Research Center (CIESOL) located at the University of Almeria (Andalusia, Spain) in RPRs. This type of photoreactor consists of a pond divided in two channels with a paddlewheel to maintain an uniformly mixed flow [24]. The RPRs were made of PVC with 5 and 15 cm liquid depth, respectively (19-L and 78-L capacity). The concentration of H_20_2 and Fe^{3+} (at a Fe^{3+}-EDDS molar ratio of 1:1) were set at 0.88 mM (30 mg L^{-1}) and 0.1 mM (5.6 mg L^{-1}), respectively. These are the optimal conditions reported for the photo-Fenton process in this type of reactor [25]. The software SMARTS2 (version 2.9.5, Florida, USA) [26] was used to estimate discretized UV irradiance, both direct and diffuse, in Almeria city (36°50´17´´N, 2°27´35´´W). The data were corroborated with the measurements obtained with a solar global UV radiometer (LPUVA02AV, Delta Ohm, Padua, Italy), the spectral response being in the range 327-384 nm. pH (in the range 7 - 8) and water temperature (in the range 22 - 26 ˚C) were measured online with sensors connected to a LabJack USB/Ethernet data logging device.

In this paper, a recently published mechanistic model for solar photo-Fenton process with Fe^{3+}-EDDS [16] has been applied to the experimental data of CEC removal in effluents from different MWWTPs using a 5-cm RPR [12]. The effluents were classified as follows: high-level (effluent from El Ejido, Almeria, Spain), medium-level A (effluent from El Bobar, Almeria, Spain), medium-level B (effluent from El Toyo, Almeria, Spain), low-level A (effluent from Girona, Spain), low-level B (effluent from Alcoy, Alicante, Spain), based on salinity and CEC load, which was in the range 6 - 58 µg L^{-1}. Details about the MWWTPs and the characterization of effluents were previously reported [12].

To evaluate the capability of the model to predict CEC removal when operating RPRs in continuous flow mode, experiments were carried out with medium-level B effluent (see Table S1). The 5-cm RPR was operated with 10 and 15-min HRT, which correspond to 1.90 L min^{-1} and 1.27 L min^{-1} total flow rate, respectively. The experiment was performed as follows: firstly, the RPR was operated in batch mode for 30 min, until Fe^{3+}-EDDS photo-decomposition. Then, both the reactant and the wastewater supply pumps were turned on and the RPR was operated in continuous flow mode with a 15-min HRT for 120 min. After 120 min of the reaction with a 15-min HRT, the flow rate was increased, and the process was performed with a 10-min HRT for 120 min.

As for the experiment in 15-cm RPR, 20 and 30-min HRT were assayed, the total flow rate being 3.90 and 2.60 L min^{-1}, respectively. As in the 5-cm RPR, the reactor was operated in batch mode for 30 min. Then, the RPR was operated in continuous flow mode with a 30-min HRT for 180 min. After 180 min of the reaction with a 30-min HRT, the flow rate was increased, and the reaction was carried out with a 20-min HRT for 120 min.

3. Parameter estimation of the Fe^{3+}-EDDS photo-Fenton kinetic model for real secondary effluents

The target CECs to fit the model were the metabolite of the opioid tramadol, O-DSMT (319 – 1976 ng L^{-1}), the metabolite of the pharmaceutical venlafaxine, O-DSMV (684 – 1325 ng L^{-1}) and the pharmaceutical GBP (943 – 7863 ng L^{-1}). The range shown in parenthesis corresponds to the five effluents assayed. The reaction mechanism above referred is shown in Table 1.

Table 1. Model reactions and rate law equations.

Reaction	Rate equation	Reaction number
$Fe^{3+} - EDDS + h\upsilon \rightarrow [Fe^{3+} - EDDS]^{*}$	$r_1 = VRPA_1^h$	R. (1)
$[Fe^{3+} - EDDS]^{*} \rightarrow Fe^{3+} - EDDS + Q$	$r_2 = k_2\,[[Fe^{3+} - EDDS]^{-*}]$	R. (2)
$[Fe^{3+} - EDDS]^{*} \rightarrow Fe^{2+} - EDDS + H^{+}$	$r_3 = k_3\,[[Fe^{3+} - EDDS]^{-*}]$	R. (3)
$Fe^{2+} - EDDS + H_2O_2 \rightarrow Fe^{3+} - EDDS + HO^{\bullet} + HO^{-}$	$r_4 = k_4\,[Fe^{2+} - EDDS]\,[H_2O_2]$	R. (4)
$Fe^{2+} - EDDS \rightarrow Fe^{2+} + EDDS^{\bullet 3-}$	$r_5 = k_5\,[Fe^{2+} - EDDS]$	R. (5)
$Fe^{2+} + H_2O_2 \rightarrow Fe(OH)_3 + HO^{\bullet} + HO^{-}$	$r_6 = k_6\,[Fe^{2+}]\,[H_2O_2]$	R. (6)
$Fe^{3+} - EDDS + H_2O_2 \rightarrow Fe^{2+} - EDDS + O_2^{\bullet -} + 2H^{+}$	$r_7 = k_7\,[[Fe^{3+} - EDDS]^{-}]\,[H_2O_2]$	R. (7)
$Fe^{3+} - EDDS + HO^{\bullet} \rightarrow Fe^{3+} - EDDS_{ox}$	$r_8 = k_8\,[[Fe^{3+} - EDDS]^{-}]\,[HO^{\bullet}]$	R. (8)
$Fe^{3+} - EDDS_{ox} + h\upsilon \rightarrow [Fe^{3+} - EDDS_{ox}]^{*}$	$r_9 = VRPA_2^i$	R. (9)
$[Fe^{3+} - EDDS_{ox}]^{*} \rightarrow Fe^{3+} - EDDS_{ox} + heat$	$r_{10} = k_{10}\,[[Fe^{3+} - EDDS_{ox}]^{*}]$	R. (10)
$[Fe^{3+} - EDDS_{ox}]^{*} \rightarrow Fe^{2+} + EDDS^{\bullet 3-}$	$r_{11} = k_{11}\,[[Fe^{3+} - EDDS_{ox}]^{*}]$	R. (11)
$OM^{a} + HO^{\bullet} \rightarrow MX^{b}$	$r_{12} = k_{12}\,[MO]\,[HO^{\bullet}]$	R. (12)
$IC^{c} + HO^{\bullet} \rightarrow ICX^{d}$	$r_{13} = k_{13}\,[IC]\,[HO^{\bullet}]$	R. (13)
$H_2O_2 + HO^{\bullet} \rightarrow 2H_2O + O_2$	$r_{14} = k_{14}\,[H_2O_2]\,[HO^{\bullet}]$	R. (14)
$EDDS^{\bullet 3-} + H_2O_2 \rightarrow 10MX$	$r_{15} = k_{15}\,[H_2O_2]\,[EDDS^{\bullet 3-}]$	R. (15)
$O - DSMT^{e} + HO^{\bullet} \rightarrow 15MX$	$r_{16} = k_{16}\,[O - DSMT]\,[HO^{\bullet}]$	R. (16)
$O - DSMV^{f} + HO^{\bullet} \rightarrow 16MX$	$r_{17} = k_{17}\,[O - DSMV]\,[HO^{\bullet}]$	R. (17)
$GBP^{g} + HO^{\bullet} \rightarrow 9MX$	$r_{18} = k_{18}\,[GBP]\,[HO^{\bullet}]$	R. (18)

[a]Organic matter; [b]Oxidized organic matter; [c]Inorganic carbon; [d]Oxidized inorganic carbon; [e]*O*-Desmethyltramadol; [f]*O*-Desmethylvenlafaxine; [g]Gabapentin; [h]Volumetric rate of photon absorption of Fe^{3+}-EDDS; [i]Volumetric rate of photon absorption of Fe^{3+}-$EDDS_{ox}$.

The kinetic parameters were determined using the built-in functions of the MATLAB optimization toolbox, the objective function being the minimization of the squared errors between experimental data and model estimation for the set of measured variables, Equation 1. In this expression, p refers to the number of experimental conditions used (p=2), n is the number of data point in each assay, (n=8). G, T, V, H and F denote GBP, O-DSMT, O-DSMV, H_2O_2 and Fe^{3+}-EDDS concentration, respectively. Subscript m stands for model data and x experimental data.

$$J = \sum_{j=1}^{p}\left[\sum_{i=1}^{n}\left(\frac{G_{x(i,j)} - G_{m(i,j)}}{G_{x(1,j)}}\right)^2 + \left(\frac{T_{x(i,j)} - T_{m(i,j)}}{T_{x(1,j)}}\right)^2 + \left(\frac{V_{x(i,j)} - V_{m(i,j)}}{V_{x(1,j)}}\right)^2 + \left(\frac{H_{x(i,j)} - H_{m(i,j)}}{H_{x(1,j)}}\right)^2 + \left(\frac{F_{x(i,j)} - F_{m(i,j)}}{F_{x(1,j)}}\right)^2\right] \quad \text{Eq. (1)}$$

Due to the variability in the experimental results obtained in each MWWTP effluent, the search for parameters was carried out separately for each type of effluent. Table 2 shows the kinetic constants obtained for each type of effluent.

Table 2. Model parameters estimated in each MWWTP effluent.

Kinetic constant	High-Level	Medium-Level A	Medium-Level B	Low-Level A	Low-Level B
k_2 (min^{-1})	0.65	0.65	0.69	0.57	0.45
k_3 (min^{-1})	15.79	7.40	17.52	20.66	17.35
k_4 ($mM^{-1}\,min^{-1}$)	$1.2\cdot10^3$	$1.0\cdot10^3$	$1.7\cdot10^3$	$1.2\cdot10^3$	$1.3\cdot10^3$
k_5 (min^{-1})	37.66	48.27	59.28	39.82	45.23
k_7 ($mM^{-1}\,min^{-1}$)	0.13	0.10	0.14	0.19	0.23
k_8 ($mM^{-1}\,min^{-1}$)	$3.6\cdot10^7$	$5.1\cdot10^7$	$3.9\cdot10^7$	$5.0\cdot10^7$	$4.9\cdot10^7$

Kinetic constant	High-Level	Medium-Level A	Medium-Level B	Low-Level A	Low-Level B
k_{10} (min^{-1})	11.30	49.60	15.94	15.72	20.86
k_{11} (min^{-1})	3.25	1.02	2.95	1.70	1.36
k_{12} (mM^{-1} min^{-1})	$5.6 \cdot 10^6$	$2.9 \cdot 10^6$	$3.9 \cdot 10^6$	$7.0 \cdot 10^6$	$3.8 \cdot 10^6$
k_{15} (mM^{-1} min^{-1})	$2.2 \cdot 10^6$	$1.3 \cdot 10^6$	$2.2 \cdot 10^6$	$3.4 \cdot 10^6$	$3.7 \cdot 10^6$
k_{16} (mM^{-1} min^{-1})	$7.5 \cdot 10^7$	$2.3 \cdot 10^7$	$8.8 \cdot 10^7$	$5.6 \cdot 10^7$	$5.0 \cdot 10^7$
k_{17} (mM^{-1} min^{-1})	$7.7 \cdot 10^7$	$1.7 \cdot 10^7$	$7.9 \cdot 10^7$	$5.8 \cdot 10^7$	$4.4 \cdot 10^7$
k_{18} (mM^{-1} min^{-1})	$6.8 \cdot 10^7$	$1.1 \cdot 10^7$	$5.1 \cdot 10^7$	$2.2 \cdot 10^7$	$3.6 \cdot 10^7$

The kinetic constants corresponding to the Fenton reaction, R. (6), as well as the oxidation of IC and H_2O_2 with $HO^{\bullet}$, R. (13) and R. (14), were taken from the literature (k_6=4.56 mM^{-1} min^{-1} [27], $k_{13}=5.1 \cdot 10^5$ mM^{-1} min^{-1}, $k_{14}=1.6 \cdot 10^6$ mM^{-1} min^{-1} [28]). As it can be observed, they are of the same order of magnitude in the five effluents. Briefly, k_3 is much higher than k_2 in all the effluents, which points out that most of the energy absorbed by Fe^{3+}-EDDS is used in its reduction, whereas a small fraction of energy is released as heat. k_{10} ($[Fe^{3+}-EDDS]^*$ deactivation) is higher than k_2 ($[Fe^{3+}-EDDS_{ox}]^*$ deactivation) which is explained by the lower quantum efficiency of the complex after being oxidized. The kinetic constant corresponding to Fe^{2+}-EDDS oxidation with $HO^{\bullet}$, k_4, is three orders of magnitude higher than the kinetic constant for the classic Fenton, k_6. All these observations are in concordance with the kinetic model reported for synthetic effluent [16]. In medium-level A, the values corresponding to the oxidation of the three CECs are lower than in the rest of effluents. This agrees with the values of the pseudo-first order rate constants reported for the removal of total load of CECs in these effluents [12].

The model successfully fits experimental data of all the measured species, both the consumption of reagents and the kinetics of the CEC removal. The quality of the fit computed through the RMSE is shown in Table 3. The highest RMSE values were 5.6%, 8.2%, 4.4%, 6.3% and 4.3% for Fe^{3+}-EDDS, H_2O_2, O-DSMT and O-DSMV and GBP, respectively. As an example, Fig. 1 shows the reactant consumption as well as the CEC profiles in high-level and low-level A effluents.

Table 3. Root mean squared errors between experimental data and model predictions.

Compound	High-level	Medium-level A	Medium-level B	Low-level A	Low-level B
Fe^{3+}-EDDS	3.9	5.6	2.9	2.1	3.9
H_2O_2	6.3	5.0	8.2	2.8	5.2
O-DSMT[a]	2.9	3.9	4.1	4.4	3.7
O-DSMV[b]	4.0	6.3	4.8	5.5	3.3
GBP[c]	3.7	4.2	4.0	4.3	2.2

[a]*O*-Desmethyltramadol; [b]*O*-Desmethylvenlafaxine; [c] Gabapentin.

(a)

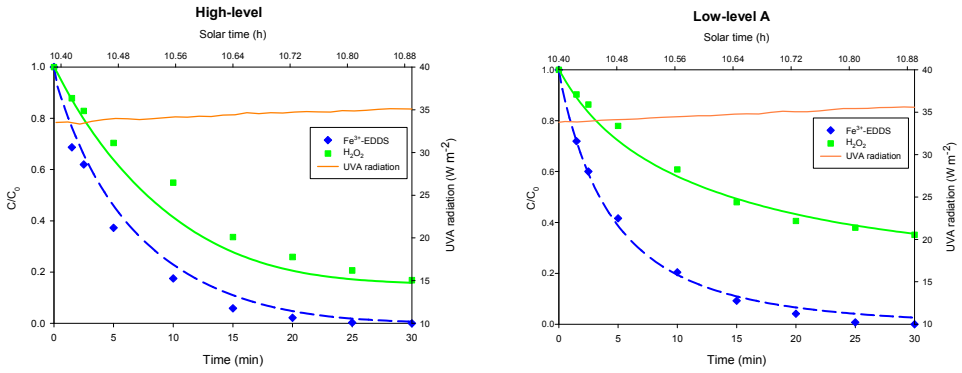

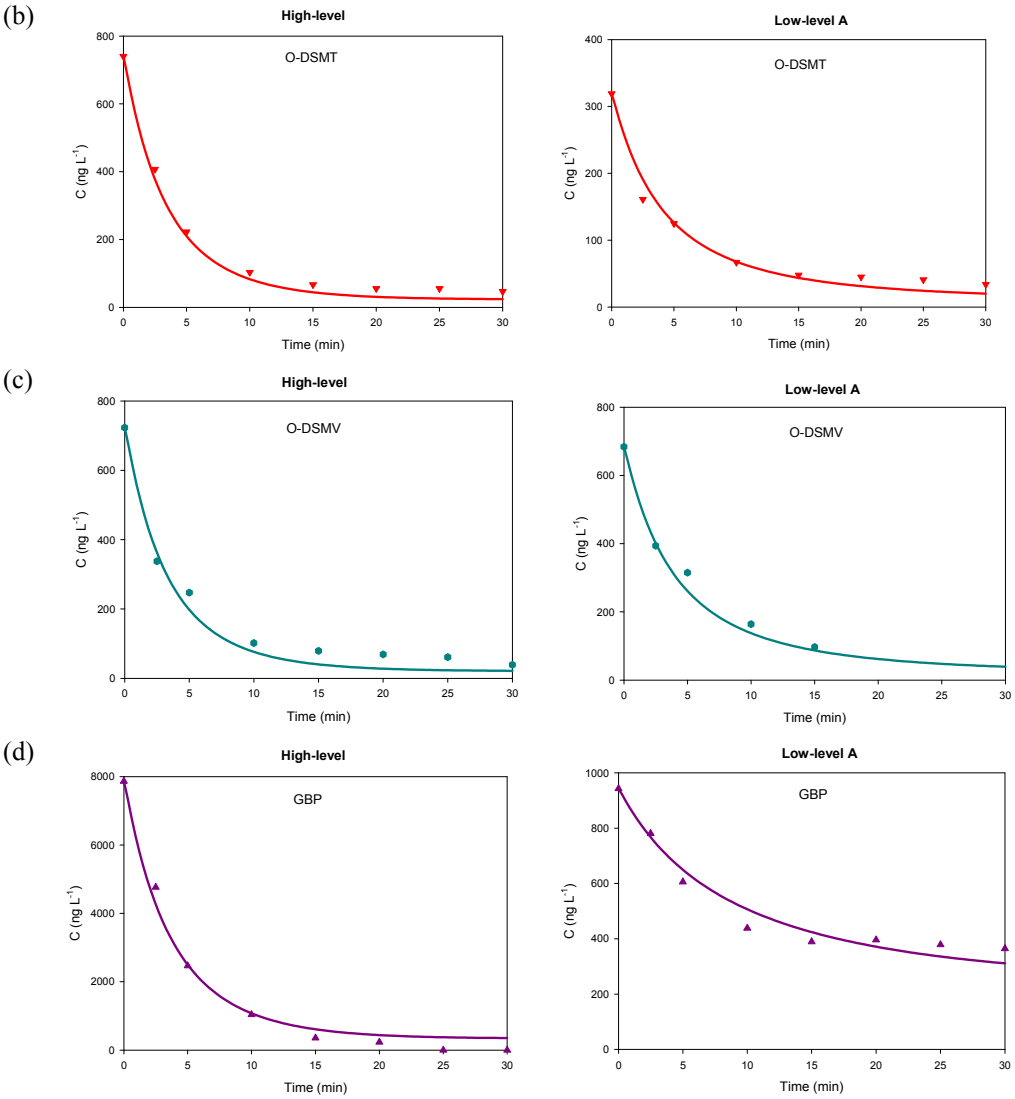

Fig. 1. Fe^{3+}-EDDS, H_2O_2 (a), *O*–DSMT (b), *O*–DSMV (c) and GBP (d) profiles in high-level and low-level A effluents. Lines represent model estimations.

The obtained results show that the model for the photo-Fenton process previously proposed (which was developed under controlled conditions and synthetic wastewater) can be tuned to predict the kinetic of CEC removal in real municipal WWTP effluents, these compounds being in concentrations in the range from few μg L^{-1} to hundreds of ng L^{-1}. Therefore, the model could be a useful tool for the control and optimization of the process in MWWTPs.

4. Results and discussion

4.1. Kinetic model validation in continuous flow operation

After 30 min of reaction time, the complex is completely decomposed [11,12]. At such a short reaction time, the reactor should be operated in continuous flow on a larger scale. In this way, the treatment capacity is increased, and the costs associated with charge and discharge operations are avoided. To simulate the operation of the process, the kinetic parameters of medium level B effluent were selected. The mass balance in continuous flow for the species shown in Table 1, are shown in Table 4. Q_F, Q_H and Q_W (m^3 min^{-1}) stand for the incoming flow rate of Fe^{3+}-EDDS, H_2O_2 and wastewater, respectively; Q_S (m^3 min^{-1}) is the outgoing flow rate; V (m^3) is the reaction volume; and e denotes inlet stream. Constant volume in continuous operation is set by overflow and so the outgoing flow rate is defined by Eq. (2):

$$Q_S = Q_H + Q_W + Q_F \qquad \text{Eq. (2)}$$

Table 4. Dynamic model equations for continuous flow operation.

Mass balance model states	Equation number
$\frac{\mathrm{d}[[Fe^{3+}-EDDS]^{-}]}{\mathrm{dt}} = \frac{Q_F}{V}[Fe^{3+}-EDDS]^{-}{}_e - \frac{Q_S}{V}[Fe^{3+}-EDDS]^{-} - r_1 + r_2 + r_4 - r_7 - r_8$	Eq. (3)
$\frac{\mathrm{d}[[Fe^{3+}-EDDS]^{-*}]}{\mathrm{dt}} = -\frac{Q_S}{V}[Fe^{3+}-EDDS]^{-*} + r_1 - r_2 - r_3$	Eq. (4)
$\frac{\mathrm{d}[Fe^{2+}]}{\mathrm{dt}} = -\frac{Q_S}{V}[Fe^{2+}] + r_5 - r_6 + r_{11}$	Eq. (5)
$\frac{\mathrm{d}[Fe^{2+}-EDDS]}{\mathrm{dt}} = -\frac{Q_S}{V}[Fe^{2+}-EDDS] + r_3 - r_4 - r_5 + r_7$	Eq. (6)
$\frac{\mathrm{d}[Fe^{3+}-EDDSox]}{\mathrm{dt}} = -\frac{Q_S}{V}[Fe^{3+}-EDDSox] + r_8 - r_9 + r_{10}$	Eq. (7)
$\frac{\mathrm{d}[[Fe^{3+}-EDDSox]^{*}]}{\mathrm{dt}} = -\frac{Q_S}{V}[Fe^{3+}-EDDSox]^{*} + r_9 - r_{10} - r_{11}$	Eq. (8)
$\frac{\mathrm{d}[H_2O_2]}{\mathrm{dt}} = \frac{Q_H}{V}[H_2O_2]_e - \frac{Q_S}{V}[H_2O_2] - r_4 - r_6 - r_7 - r_{14} - r_{15}$	Eq. (9)
$\frac{\mathrm{d}[HO^{\bullet}]}{\mathrm{dt}} = -\frac{Q_S}{V}[HO^{\bullet}] + r_4 + r_6 - r_8 - r_{12} - r_{13} - r_{14} - r_{16} - r_{17} - r_{18}$	Eq. (10)
$\frac{\mathrm{d}[OM^{a}]}{\mathrm{dt}} = \frac{Q_w}{V}[OM^{a}]_e - \frac{Q_S}{V}[OM^{a}] - r_{12}$	Eq. (11)
$\frac{\mathrm{d}[MX^{b}]}{\mathrm{dt}} = -\frac{Q_S}{V}[MX^{b}] + r_{12} + 10\,r_{15} + 15\,r_{16} + 16\,r_{17} + 9\,r_{18}$	Eq. (12)
$\frac{\mathrm{d}[IC^{c}]}{\mathrm{dt}} = \frac{Q_w}{V}[IC^{c}]_e - \frac{Q_S}{V}[IC^{c}] - r_{13}$	Eq. (13)
$\frac{\mathrm{d}[ICX^{d}]}{\mathrm{dt}} = -\frac{Q_S}{V}[ICX^{d}] + r_{13}$	Eq. (14)
$\frac{\mathrm{d}[EDDS^{\bullet 3-}]}{\mathrm{dt}} = -\frac{Q_S}{V}[EDDS^{\bullet 3-}] + r_5 + r_{11} - r_{15}$	Eq. (15)
$\frac{\mathrm{d}[O-DSMT^{e}]}{\mathrm{dt}} = \frac{Q_w}{V}[O-DSMT^{e}]_e - \frac{Q_S}{V}[O-DSMT^{e}] - r_{16}$	Eq. (16)
$\frac{\mathrm{d}[O-DSMV^{f}]}{\mathrm{dt}} = \frac{Q_w}{V}[O-DSMV^{f}]_e - \frac{Q_S}{V}[O-DSMV^{f}] - r_{17}$	Eq. (17)
$\frac{\mathrm{d}[GBP^{g}]}{\mathrm{dt}} = \frac{Q_w}{V}[GBP^{g}]_e - \frac{Q_S}{V}[GBP^{g}] - r_{18}$	Eq. (18)

[a]Organic matter; [b]Oxidized organic matter; [c]Inorganic carbon; [d]Oxidized inorganic carbon; [e]*O*-Desmethyltramadol; [f]*O*-Desmethylvenlafaxine; [g] Gabapentin.

Fig. 2 shows model validation in 5-cm and 15-cm RPRs, respectively. Once the operation in continuous flow mode was started, the concentration of reactant and CECs increased up to the steady state, it being reached after 20 min. The concentration of Fe^{3+}-EDDS and H_2O_2 increased when the HRT was decreased. This effect was less significant in CEC profiles, the average removal percentages (with respect to the sum of the three CECs) being 78% and 76% in 5-cm RPR with 15 and 10-min HRT. In the 15-cm RPR, the removal percentages were 87% and 82% with 30 min and 20-min HRT, respectively.

Concerning the experiment in the 5-cm RPR, the model successfully predicts experimental data for both the reactant consumption and the CECs. When operating the process at solar noon (assay at 15-min HRT), the concentration remained constant at the value corresponding to the steady state. However, the plateau corresponding to the steady state is not observed at 10-min HRT, the concentration being increased over the course of the process. This is due to the experiment was conducted after solar noon, and consequently UV radiation decreased. This effect is clearly observed in Fe^{3+}-EDDS concentration, since the photodecomposition of the complex depends strongly on the availability of UV radiation and would be implemented through a proper control system. It is important to remark the agreement between the model and the experimental results when the irradiation changed, indicating the consistency of the model.

In the 15-cm RPR, the Fe^{3+}-EDDS conversion is slightly overestimated. This could be due to the geometrical proportions of the 15-cm RPR are different from those of the 5-cm RPR (5.1 vs 2.4

length of the straight section of the reactor: channel width), and the kinetics parameters were previously determined from the data obtained in the 5-cm RPR.

Even so, the model successfully predicts the H_2O_2 consumption and CEC removal.

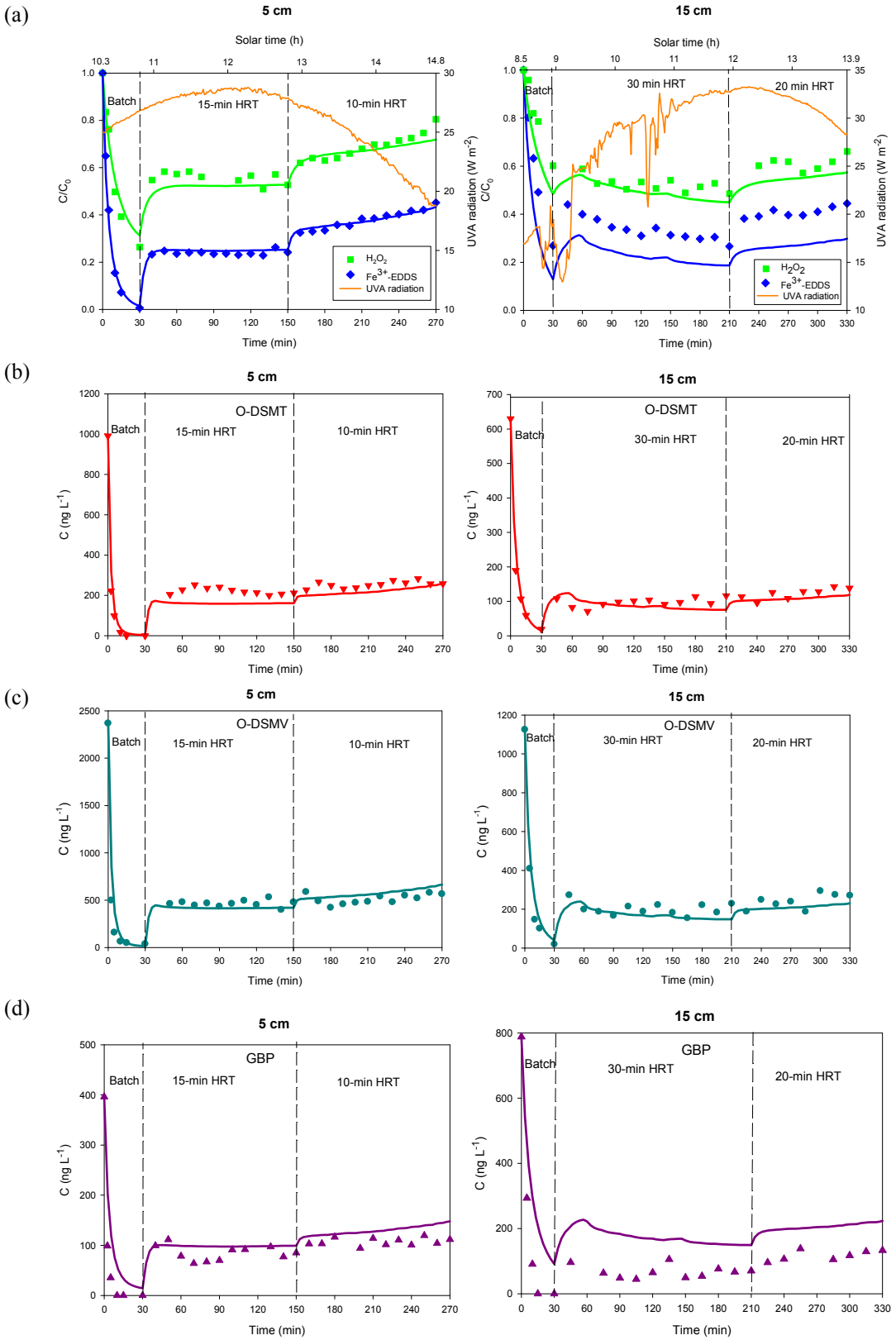

Fig. 2. Model validation in 5-cm and 15-cm RPRs operated in continuous flow mode: (a) Fe^{3+}-EDDS and H_2O_2, (b) O-DSMT, (c) O-DSMV, (d) GBP. Solid lines represent model predictions.

4.2. Effect of HRT and liquid depth on the treatment capacity

In RPRs, liquid depth can be varied, and consequently, the treatment capacity, according to the availability of UV radiation. Therefore, liquid depth could be tuned according to solar irradiance, if needed.

Simulation of the continuous flow operation of the RPR was carried out as a function of HRT and liquid depth both in winter and summer clear day solstices, which correspond to the days with the lowest and highest hours of sunlight, respectively. To simplify the presentation of results and better understand the application of the developed model to the continuous operation, the hours in the day at which the global UV radiation is ≥ 10 W m^{-2} were set as total hours of operation [13], 4.5 h in winter solstice (December 21st) and 10 h in summer solstice (June 21st).

Table 5 shows the effect of HRT as a function of liquid depth in winter and summer solstices on the removal of the selected CECs (with respect to the sum of the three CECs). The contribution of the dark Fenton reactions is also shown, reaching CEC removal as high as 57% at 30-min HRT. Nonetheless, the treatment target should be significantly higher, around 80% [3]. Furthermore, the Fe^{3+}-EDDS is the limiting reactant and the most expensive. Therefore, for economic purposes, high Fe^{3+}-EDDS conversions are desirable. These goals can only be attained by the Fenton process but at so long and not realistic HRT for any application.

In winter solstice, the 81% CEC removal is estimated at 30-min HRT in 5-cm deep RPRs. Accordingly, the treatment capacity would be 450 L m^{-2} d^{-1}. Under these conditions, the conversion of the Fe^{3+}-EDDS complex is 77%. As for summer solstice, several combinations of HRT and liquid depth give rise to CEC removal > 80%. The shortest HRT is 15 min with 5 cm of liquid depth, giving 2000 L m^{-2} d^{-1} of treatment capacity, and it could be doubled (4000 L m^{-2} d^{-1}) by increasing at the same time both the HRT and the liquid depth to 30 min and 20 cm, respectively. In all cases, the Fe^{3+}-EDDS conversion is above 76%.

Table 5. Effect of hydraulic residence time (HRT) on CEC removal as a function of liquid depth in winter and summer solstices. Green, blue and red areas correspond to 60, 70 and 80% CEC removal, respectively.

HRT (min)	CEC removal (%)										
	Fenton	Winter					Summer				
		Liquid depth (cm)									
		5	10	15	20	30	5	10	15	20	30
5	28	51	44	41	38	36	62	55	50	47	42
7.5	34	59	53	49	46	43	70	64	59	56	51
10	39	65	59	55	52	49	74	69	65	62	57
12.5	43	68	63	59	57	53	77	73	70	66	61
15	46	71	66	63	60	57	80	76	73	70	65
20	51	76	71	68	65	62	83	80	77	75	70
25	55	78	75	72	69	66	85	83	80	78	74
30	57	81	77	74	72	69	86	85	83	81	77

On the other hand, the range of operation depends on the targeted removal of CECs as shown by the colored areas in Table 5 and Fig. 3, which show the treatment capacity to achieve a target percentage of CEC removal as a function of the liquid depth and the HRT. As it can be observed, a higher target of removal would imply a less flexible operating range in terms of liquid depth and HRT. Furthermore, at a specific HRT, the treatment capacity achieved in winter solstice is much lower than in summer solstice, in concordance with the greater availability of solar radiation. In winter solstice, 15-min HRT would be enough to achieve 70% degradation at short liquid depths of 5 cm, the treatment capacity being 900 L m^{-2} d^{-1}, point A in Fig. 3a. In summer, the HRT could be hafted using 5 cm, giving rise to 4000 L m^{-2} d^{-1} treatment capacity, point B in Fig. 3b, or extended to 20 min with 30-cm liquid depth, the treatment capacity being increased to 9000 L m^{-2} d^{-1}, point C in Fig. 3b.

Of course, simulations were done using two extreme situations (winter and summer solstices) and therefore the treatment capacity would change along the year between 900 and 9000 L m^{-2} d^{-1} permitting a smooth operation by a proper and simple control of HRT and liquid depths. The objective would be to maximize the treatment capacity in a day by day basis.

(a)

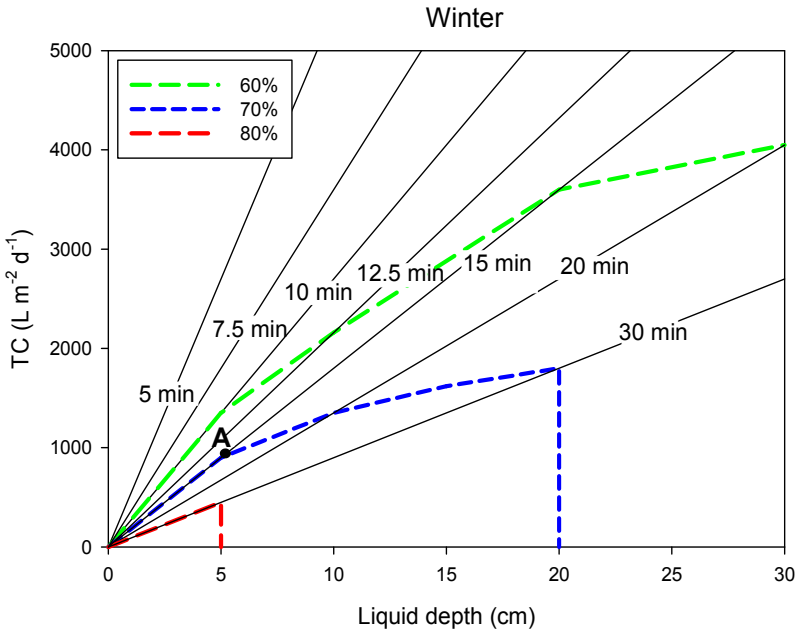

(b)

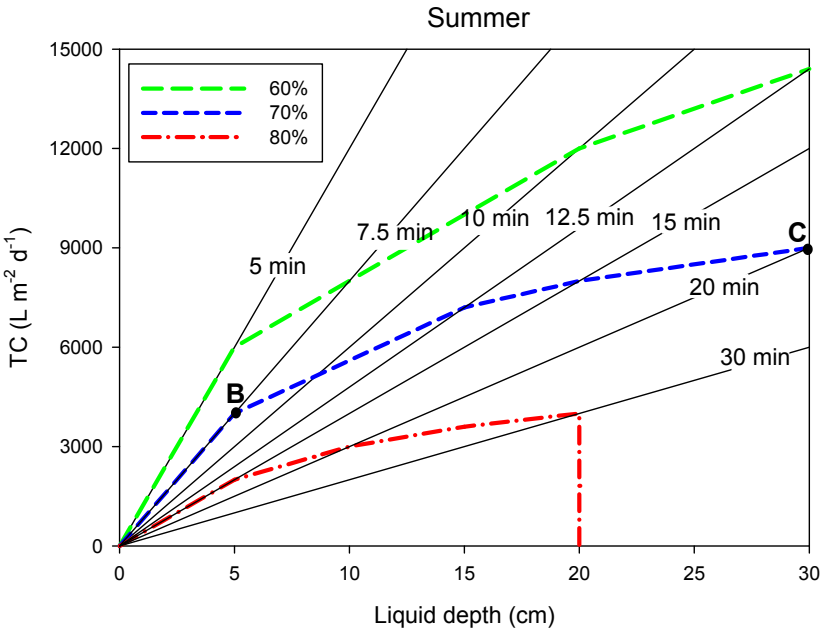

Fig. 3. Model estimation of treatment capacity in winter solstice (a) and summer solstice (b) as a function of liquid depth with the HRT as a parameter (lines). The area inside the dashed lines represents operating range to achieve a target percentage of CEC removal.

These simulation results are useful for RPR design on a larger scale, since the reactor area, which is the main parameter for photoreactor design and investment costs, could be estimated given the daily flow rate and the target removal percentage (Fig. 3). As an example, to treat 400 m^3 d^{-1} [29] and remove 80% CECs in winter solstice, 5-cm liquid depth and 30-min HRT would be required to achieve the highest treatment capacity (450 L m^{-2} d^{-1}), an RPR area of 888 m^2 being estimated. In summer solstice, 20 cm liquid depth and 30 min HRT would be required to achieve the highest treatment capacity (4000 L m^{-2} d^{-1}) an RPR area of 100 m^2 being estimated. Furthermore, the final reactor design strongly depends on fluid-dynamics and mixing. When conducting the process with Fe^{3+}-EDDS, the reactor should be operated in turbulent flow to reduce mixing time. In this regard, energy consumption necessary for strong mixing in RPRs is fundamental.

5. Conclusions

A designing tool for wastewater treatment in RPRs is proposed. The kinetic parameters of photo-Fenton model developed with synthetic effluent were slightly tuned to predict CEC removal in real MWWTP effluents. The model is able to predict both the reactant consumption and CEC removal when operating RPRs with different liquid depths in continuous flow mode. In these conditions, it is possible to achieve a high conversion (>80%) at short reaction times (in the range 10 – 30 min) when performing the process at neutral pH with Fe^{3+}-EDDS (not stable at long reaction times). Simulations showed that 80% CEC removal can be achieved at 30-min HRT in 5-cm deep RPRs in winter solstice, the treatment capacity (supposing 4.5 hours of operation per day) being 450 L m^{-2} d^{-1}, and it could be increased up to 4000 L m^{-2} d^{-1} in summer solstice (supposing 10 hours of operation per day), increasing the liquid depth by four times. In both conditions, high Fe^{3+}-EDDS conversions of around 80% were estimated. The results presented are of relevance for RPR design, since for a given target CEC removal, the reactor area could be estimated as a function of the hydraulic HRT and liquid depth. This maximizes the treatment capacity as a function of solar irradiation conditions.

Acknowledgements

The authors would like to acknowledge the Ministry for Economy, Industry and Competitiveness (Spanish Government) and the European Regional Development Fund (ERDF), project CTQ2016-78255-R. P. Soriano-Molina is grateful to the Ministry of Education, Culture and Sport for her FPU scholarship (AP2014/01030). P. Plaza-Bolaños would like to acknowledge the University of Almeria for her research contract (Hypatia Program).

References

[1] M. Salimi, A. Esrafili, M. Gholami, A. Jonidi Jafari, R. Rezaei Kalantary, M. Farzadkia, M. Kermani, H.R. Sobhi, Contaminants of emerging concern: a review of new approach in AOP technologies, Environ. Monit. Assess. 189 (2017) 414, doi:10.1007/s10661-017-6097-x.

[2] E.A. Serna-Galvis, A.M. Botero-coy, D. Martínez-Pachón, A. Moncayo-Lasso, M. Ibáñez, R.A. Torres-Palma, Degradation of seventeen contaminants of emerging concern in municipal wastewater effluents by sonochemical advanced oxidation processes, Water Res. 154 (2019) 349 – 360, doi:10.1016/j.watres.2019.01.045.

[3] Waters Protection Ordinance of 28 October 1998 (814.201) (Status of 1 June 2018),https://www.admin.ch/opc/en/classifiedcompilation/19983281/index.html.

[4] J.C.G. Sousa, A.R. Ribeiro, M.O. Barbosa, C. Ribeiro, M.E. Tiritan, M.F.R. Pereira, A.M.T. Silva, Monitoring of the 17 EU Watch List contaminants of emerging concern in the Ave and the Sousa Rivers, Sci. Total Environ. 649 (2019) 1083–1095, doi:10.1016/j.scitotenv.2018.08.309.

[5] L. Rizzo, S. Malato, D. Antakyali, V.G. Beretsou, M.B. Đolić, W. Gernjak, E. Heath, I. Ivancev-Tumbas, P. Karaolia, A.R. Lado Ribeiro, G. Mascolo, C.S. McArdell, H. Schaar, A.M.T. Silva, D. Fatta-Kassinos, Consolidated vs new advanced treatment methods for the removal of contaminants of emerging concern from urban wastewater, Sci. Total Environ. 655 (2019) 986–1008, doi.org/10.1016/j.scitotenv.2018.11.265.

[6] R. Ameta, A.K. Chohadia, A. Jain, P.B. Punjabi, Advanced Oxidation Processes for Wastewater Treatment: Emerging Green Chemical Technology, S.C. Ameta, R. Ameta, Academic Press, 2018, 49–87, doi:10.1016/B978-0-12-810499-6.00003-6.

[7] N. Diaz-Elsayed, N. Rezaei, T. Guo, S. Mohebbi, Q. Zhang, Wastewater-based resource recovery technologies across sclae: A review, Resour Conserv. Recy 145 (2019) 94 – 112, doi:10.1016/j.resconrec.2018.12.035.

[8] L. Clarizia, D. Russo, I. Di Somma, R. Marotta, R. Andreozzi, Homogeneous photo-Fenton processes at near neutral pH: a review, Appl. Catal. B: Environ. 209 (2017)358 – 371, doi:10.1016/j.apcatb.2017.03.011

[9] S. Papoutsakis, S. Miralles-Cuevas, I. Oller, J.L. Garcia Sanchez, C. Pulgarin, S. Malato, Microcontaminant degradation in municipal wastewater treatment plant secondary effluent by EDDS assisted photo-Fenton at near-neutral pH: An experimental design approach, Catal. Today 252 (2015) 61–69, doi:10.1016/j.cattod.2015.02.005.

[10] E. Cuervo Lumbaque, D. Salmoria Araújo, T. Moreira Klein, E.R. Lopes Tiburtius, J. Argüello, C. Sirtori, Solar photo-Fenton-like process at neutral pH: Fe(III)-EDDS complex formation and optimization of experimental conditions for degradation of pharmaceuticals, Catal. Today 328 (2019) 259 – 266, doi:10.1016/j.cattod.2019.01.006.

[11] P. Soriano-Molina, J.L. García Sánchez, S. Malato, L.A. Pérez-Estrada, J.A. Sánchez Pérez, Effect of volumetric rate of photon absorption on the kinetics of micropollutant removal by solar photo-Fenton with Fe^{3+}-EDDS at neutral pH, Chem. Eng. J. 331 (2018) 84 – 92, doi:10.1016/j.cej.2017.08.096.

[12] P. Soriano-Molina, P. Plaza-Bolaños, A. Lorenzo, A. Agüera, J.L. García Sánchez, S. Malato, J.A. Sánchez Pérez, Assessment of solar raceway pond reactors for removal of contaminants of emerging concern by photo-Fenton at circumneutral pH from very different municipal wastewater effluents, Chem. Eng. J. 366 (2019) 141–149, doi:10.1016/j.cej.2019.02.074.

[13] A. Cabrera Reina, J.L. Casas Liópez, M.I. Maldonado Rubio., L. Santos-Juanes Jordá, J.L. Garcia Sanchez´, J.A. Sánchez Pérez, Effects of environmental variables on the photo-Fenton plant design, Chem. Eng. J. 237 (2014) 469–477, doi:10.1016/j.cej.2013.10.046.

[14] A.V. Schenone, L.O. Conte, M.A. Botta, O.M. Alfano, Modeling and optimization of photo-Fenton degradation of 2,4-D using ferrioxalate complex and response surface methodology (RSM), J. Environ.

Manage. 155 (2015) 177–183, doi:10.1016/j.jenvman.2015.03.028.

[15] S. Giannakis, I. Hendaoui, S. Rtimi, J. Fürbringer, C. Pulgaría, Modeling and treatment optimization of pharmaceutically active compounds by the photo-Fenton process: The case of the antidepressant Venlafaxine, J. Environ. Chem. Eng. 5 (2017) 818 – 828, doi:10.1016/j.jece.2016.12.050.

[16] P. Soriano-Molina, J.L. García Sánchez, O.M. Alfano, L.O. Conte, S. Malato, J.A. Sánchez Pérez, Mechanistic modeling of solar photo-Fenton process with Fe^{3+}-EDDS at neutral pH, Appl. Catal. B: Environ. 233 (2018) 234 – 242, doi:10.1016/j.apcatb.2018.04.005.

[17] E.M. Siedlecka, P. Stepnowski, Decomposition rates of methyl tert-butyl ether and its by-products by the Fenton system in saline wastewaters, Sep. Purif Technol. 52 (2006) 317–324, doi:10.1016/j.seppur.2006.05.014.

[18] A.R. Lado Ribeiro, N.F.F. Moreira, G. Li Puma, A.M.T. Silva, Impact of water matrix on the removal of micropollutants by advanced oxidation technologies, Chem. Eng. J. 363 (2019) 155–173, doi:10.1016/j.cej.2019.01.080.

[19] M. Herrmann, J. Menz, O. Olsson, K. Kümmerer, Identification of phototransformation products of the antiepileptic drug gabapentin: Biodegradability and initial assessment of toxicity, Water Res. 85 (2015) 11–21, doi:10.1016/j.watres.2015.08.004.

[20] P.C. Rúa-Gómez, W. Püttmann, Degradation of lidocaine , tramadol , venlafaxine and the metabolites O-desmethyltramadol and O-desmethylvenlafaxine in surface waters, Chemosphere 90 (2013) 1952–1959, doi:10.1016/j.chemosphere.2012.10.039.

[21] N.F.F. Moreira, M.J. Sampaio, A.R. Ribeiro, C.G. Silva, J.L. Faria, A.M.T. Silva, Metal-free g-C_3N_4 photocatalysis of organic micropollutants in urban wastewater under visible light, Appl. Catal. B: Environ. 248 (2019) 184–192, doi:10.1016/j.apcatb.2019.02.001.

[22] M.C. Campos-Mañas, I. Ferrer, E.M. Thurman, A. Agüera, Opioid occurrence in environmental water samples—A review, Trends Environ. Anal. 20 (2018) e00059, doi:10.1016/j.teac.2018.e00059.

[23] M.C. Campos-Mañas, P. Plaza-Bolaños, J.A. Sánchez-Pérez, S. Malato, A. Agüera, Fast determination of pesticides and other contaminants of emerging concern in treated wastewater using direct injection coupled to highly sensitive ultra-high performance liquid chromatography-tandem mass spectrometry, J. Chromatogr. A. 1507 (2017) 84 – 94, doi:10.1016/j.chroma.2017.05.053.

[24] A. Belalcázar-Saldarriaga, D. Prato-García, R. Vasquez-Medrano, Photo-Fenton processes in raceway reactors: Technical, economic, and environmental implications during treatment of colored wastewaters, J. Clean. Prod. 182 (2018) 818 – 829, doi:10.1016/j.jclepro.2018.02.058.

[25] I. Carra, L. Santos-Juanes, F.G. Acién Fernández, S. Malato, J.A. Sánchez Pérez, New approach to solar photo-Fenton operation. Raceway ponds as tertiary treatment technology, J. Hazard. Mater. 279 (2014) 322–329, doi:10.1016/j.jhazmat.2014.07.010.

[26] C. Gueymard, SMARTS2, a Simple Model of the Atmospheric Radiative Transfer of Sunshine: Algorithms and Performance Assessment. Rep. FSEC-PF-270-95, Florida Solar Energy Center, Cocoa, USA, 1995.

[27] G.V. Buxton, C.L. Greenstock, W.P. Helman, A.B. Ross, Critical Review of Rate Constants for Reactions of Hydrated Electrons, Hydrogen Atoms and Hydroxyl Radicals ($^{\bullet}OH/O^{-}$) in Aqueous Solution, J. Phys. Chem. Ref. Data 17 (1988) 513–886, doi:10.1063/1.555805.

[28] R. Chen, J.J. Pignatello, Role of Quinone Intermediates as Electron Shuttles in Fenton and Photoassisted Fenton Oxidations of Aromatic Compounds, Environ. Photochem. 31 (1997) 2399–2406, doi:10.1021/es9610646.

[29] Council Directive of 21 May 1991 concerning urban waste water treatment (91/271/EEC). Off. J. L 135, 30.5.1991, p. 40 – 52, https://eur-lex.europa.eu/eli/dir/1991/271/oj.

Supplementary material to the paper entitled:

On the design and operation of solar photo-Fenton open reactors for the removal of contaminants of emerging concern from WWTP effluents at neutral pH

P. Soriano-Molina[a,b], J.L. García Sánchez[a,b], S. Malato[a,c], P. Plaza-Bolaños[a], A. Agüera[a], J.A. Sánchez Pérez[a,b*]

[a] Solar Energy Research Centre (CIESOL), Joint Centre University of Almería-CIEMAT, Carretera de Sacramento s/n, E-04120, Almería, Spain.

[b] Chemical Engineering Department, University of Almería, Ctra de Sacramento s/n, E-04120, Almería, Spain.

[c] Plataforma Solar de Almería, CIEMAT, Carretera Senés Km. 4, E-04200, Tabernas, Almería, Spain.

This document provides more detailed information to the main paper mentioned above.

The following information is included:

Content

Table S1. Characterization of MWWTP effluents used for model validation in continuous flow operation.

Parameter	Mean value ± standard deviation
Br^- (mg L^{-1})	2.7 ± 0.2
NO_3^- (mg L^{-1})	2.7 ± 0.6
PO_4^{3-} (mg L^{-1})	11.5 ± 1.2
SO_4^{2-} (mg L^{-1})	257 ± 41
Cl^- (mg L^{-1})	402 ± 84
DOC (mg L^{-1})	10.9 ± 0.6
COD (mg L^{-1})	28.5 ± 5.1
IC (mg L^{-1})	40.3 ± 9.5
IC* (mg L^{-1})	16.2 ± 3.5
pH	7.1 ± 0.1
Conductivity (mS cm^{-1})	1.6 ± 0.5
Turbidity (NTU)	10.1 ± 3.5

*inorganic carbon (IC) pretreated until IC around 15 mg L^{-1}.

CONCLUSIONS
CONCLUSIONES

5. CONCLUSIONS

The main contribution of this Ph.D. thesis is the development of mechanistic models involving the solar photo-Fenton process as a tool for the design of scalable and low-cost RPRs to remove micropollutants from MWWTP secondary effluents.

In response to the objectives set out in this Ph.D. thesis, the following specific conclusions are presented:

Conclusions drawn from the results presented in Section 4.1:

1. In the range 10 to 40 °C, the photo-Fenton process is enhanced by temperature due to the increase in Fenton reaction rate (thermal Fenton) and the increase in the light absorption coefficient of iron, with the VRPA also being increased.

2. The iron activation state allows the photosaturation phenomenon at VRPA values above 866 μE m^{-3} s^{-1} to be explained. In RPRs, this value is achieved with 5 cm liquid depth, 30 W m^{-2} UVA irradiance and 0.1 mM Fe^{3+}.

3. The mechanistic model proposed for the process at acidic pH is able to predict micropollutant removal as a function of temperature, solar irradiance, light path length and reactant concentration in RPRs.

Conclusions drawn from the results presented in Section 4.2:

4. When conducting the process at neutral pH with Fe^{3+}-EDDS, the VRPA decreases as the process proceeds, since the complex photo-decomposes. This change in the VRPA should be taken into account for the development of kinetic models.

5. Due to the higher photon absorption of Fe^{3+}-EDDS when compared with Fe^{3+}, photosaturation occurs at VRPA above 1547 μE m^{-3} s^{-1}. In RPRs, this value is achieved with 5 cm liquid depth, 40 W m^{-2} UVA irradiance and 0.1 mM Fe^{3+}.

6. Even under photolimitation conditions, the treatment capacity can be increased by increasing the liquid depth. This is an advantage for large scale application of RPRs.

Conclusions drawn from the results presented in Section 4.3:

7. In real MWWTP effluents of very different composition solar photo-Fenton in RPRs with 0.1 mM Fe^{3+}, at Fe^{3+}:EDDS molar ratio of 1:1, and 0.88 mM H_2O_2 can remove more than 80% total load of micropollutants in less than 15 min.

8. The nature of the organic matter present in the effluent has a significant effect, greater than the concentration, on the kinetics of the process. Although previous studies pointed out a negative effect of salinity when different ions were added to model wastewater, this effect was not found during the treatment of real effluents.

Conclusions drawn from the results presented in Section 4.4:

9. The mechanistic model proposed for the photo-Fenton process at neutral pH with Fe^{3+}-EDDS is able to predict micropollutant removal, H_2O_2 consumption and Fe^{3+}-EDDS photo-decomposition at short reaction times as a function of the VRPA.

10. This model takes into account the hydroxyl radical-scavenging effect of organic matter and HCO_3^-/CO_3^{2-}. Furthermore, it combines the effect of both components of solar radiation (direct and diffuse), this being very useful for the design of RPRs.

Conclusions drawn from the results presented in Section 4.5:

11. The kinetic model proposed in Section 4.4 is capable of predicting micropollutant removal in real MWWTP effluents when operating RPRs in continuous flow mode for short hydraulic residence times.

12. The photoreactor area can be estimated as a function of liquid depth and hydraulic residence time which maximizes the treatment capacity for a given target micropollutant removal. This is relevant for the scaling up of the photo-Fenton process.

5. CONCLUSIONES

La principal contribución de este trabajo de tesis doctoral es el desarrollo de modelos del proceso foto-Fenton solar como herramienta para el diseño de reactores tipo ``raceway´´, escalables y de bajo coste, para la eliminación de microcontaminantes en efluentes secundarios de EDAR urbanas.

Como respuesta a los objetivos planteados en esta Memoria de Tesis Doctoral, se presentan las siguientes conclusiones específicas:

Conclusiones extraídas de los resultados expuestos en el Apartado 4.1:

1. En el intervalo de 10 a 40 ºC, la temperatura contribuye al proceso foto-Fenton debido al aumento de la velocidad de la reacción Fenton (Fenton térmico) y al aumento del coeficiente de absorción de fotones del hierro, que da lugar al aumento de la velocidad volumétrica de absorción de fotones.

2. La formación de un estado activado del hierro permite explicar el fenómeno de fotosaturación alcanzado a valores de velocidad volumétrica de absorción de fotones superiores a 866 μE m^{-3} s^{-1}. En los reactores tipo raceway, este valor se alcanza con 5 cm de profundidad de líquido, 30 W m^{-2} de irradiancia UVA y 0.1 mM Fe^{2+}.

3. El modelo mecanístico propuesto para el proceso foto-Fenton a pH ácido es capaz de predecir la eliminación de microcontaminantes ante cambios en la temperatura, la irradiancia solar, la longitud de paso óptico y la concentración de reactivos en los reactores tipo ``raceway´´.

Conclusiones extraídas de los resultados expuestos en el Apartado 4.2:

4. Cuando el proceso se lleva a cabo a pH neutro con Fe^{3+}-EDDS, la velocidad de absorción de fotones disminuye a medida que avanza el proceso debido a la foto-descomposición del complejo. Esta variación en la absorción de fotones debería tenerse en cuenta en el diseño de reactores solares.

5. Debido a la mayor absortividad del Fe^{3+}-EDDS en comparación con el Fe^{3+}, la fotosaturación tiene lugar a valores de velocidad volumétrica de absorción de fotones superiores a 1547 μE m^{-3} s^{-1}. En los reactores tipo ``raceway´´, este valor se alcanza con 5 cm de profundidad de líquido, 40 W m^{-2} de irradiancia UVA y 0.1 mM Fe^{3+}.

6. Incluso en condiciones de fotolimitación, la capacidad de tratamiento aumenta al aumentar la longitud de paso óptico. Esto supone una ventaja para la aplicación de los reactores tipo ``raceway´´ a gran escala.

Conclusiones extraídas de los resultados expuestos en el Apartado 4.3:

7. En los efluentes reales de EDAR de muy diferente composición, el proceso foto-Fenton solar en reactores tipo ``raceway´´, con 0.1 mM Fe^{3+}, a relación molar Fe^{3+}:EDDS 1:1, y 0.88 mM H_2O_2, elimina más del 80% de la carga total de microcontaminantes en menos de 15 min.

8. La naturaleza de la materia orgánica presente en el efluente tiene un efecto significativo, mayor que la concentración, en la cinética del proceso. Aunque los estudios previos en efluentes sintéticos dopados con diversos iones indicaban un efecto negativo de la salinidad en el proceso, este efecto no se observó durante el tratamiento de efluentes reales.

Conclusiones extraídas de los resultados expuestos en el Apartado 4.4:

9. El modelo mecanístico propuesto para el proceso foto-Fenton a pH neutro con Fe^{3+}-EDDS es capaz de predecir la eliminación de microcontaminantes, el consumo de H_2O_2 y la fotodescomposión del Fe^{3+}-EDDS a tiempos cortos de reacción en función de la velocidad volumétrica de absorción de fotones.

10. Este modelo tiene en cuenta el efecto ``scavenger´´ de la materia orgánica y los iones $HCO_3^-/CO_3^{2-}$. Además, integra el efecto de ambas componentes de la radiación solar (directa y difusa), resultando de gran utilidad para el diseño de reactores tipo ``raceway´´.

Conclusiones extraídas de los resultados expuestos en el Apartado 4.5:

11. El modelo cinético propuesto in el Apartado 4.4 es capaz de predecir la eliminación de microcontaminantes presentes en efluentes reales de EDAR cuando los reactores tipo ``raceway´´ se operan en modo flujo continuo con tiempos residencia hidráulicos cortos.

12. El área del fotorreactor se puede estimar en función de la profundidad de líquido y el tiempo de residencia hidráulico que maximizan la capacidad de tratamiento para un determinado porcentaje de eliminación de microcontaminantes. Esto es relevante para el escalado del proceso foto-Fenton.

LIST OF ABBREVIATIONS

ACTM	Acetamiprid
AOP	Advanced Oxidation Process
CEC	Contaminant of emerging concern
COD	Chemical oxygen demand
CPC	Compound parabolic collector
DOC	Dissolved organic carbon
EDDS	Ethylenediamine-N,N'-disuccinic acid
EDTA	Ethylenediaminetetraacetic acid
IC	Inorganic carbon
LC-QqLiT-MS/MS	Liquid chromatography-triple quadrupole-linear ion trap-mass spectrometry
LMCT	Ligand-metal charge transfer
LOQ	Limit of quantification
LVRPA	Local volumetric rate of photon absorption
MWWTP	Municipal wastewater treatment plant
NTA	Nitrilotriacetic acid
PTC	Parabolic-trough collector
RPR	Raceway pond reactor
RTE	Radiative Transfer Equation
TOC	Total organic carbon
TP	Transformation product
UHPLC-DAD	Ultra-high pressure liquid chromatography with diode array detector
UV	Ultraviolet
UVA	Ultraviolet A
UV-Vis	Ultraviolet-visible
VRPA	Volumetric rate of photon absorption
WFD	Water Framework Directive
WWTP	Wastewater treatment plant

OTHER SCIENTIFIC PRODUCTIONS

From the results showed in this Ph.D. thesis, the following Conference contributions have been presented:

- Sánchez Pérez, J.A., Soriano-Molina, P., García Sánchez, J.L., Malato, S. Solar photo-Fenton as a tertiary wastewater treatment. From mechanisms to reactor design. Plenary Session. 19th European Meeting on Environmental Chemistry (EMEC19). 3rd – 6th December 2018, Clermont-Ferrand (France).

- Soriano-Molina, P., Lorenzo, A., Plaza-Bolaños, P., Agüera, A., García Sánchez, J.L., Malato, S. & Sánchez Pérez, J.A. Microcontaminant removal in secondary effluents of variable composition from different municipal wastewater treatment plants by solar photo-Fenton in raceway ponds reactors. Poster Communication. VII Symposium of Research in Experimental Science. 14th – 15th November 2018, Almería (Spain).

- Soriano-Molina, P., García Sánchez, J.L., Alfano, O.M., Conte, L.O., Malato, S. & Sánchez Pérez, J.A. Modelo mecanístico del proceso foto-Fenton a pH neutro con Fe^{3+}-EDDS. Poster Communication. XIII Congreso Español de Tratamiento de Aguas (META 2018). 18th – 20th June 2018, León (Spain).

- Soriano-Molina, P., García Sánchez, J.L., Alfano, O.M., Conte, L.O., Malato, S. & Sánchez Pérez, J.A. Modeling of solar photo-Fenton process with Fe^{3+}-EDDS at neutral pH. Poster Communication. 10th European meeting of Solar Chemistry and Photocatalysis: Environmental Applications (SPEA10). 4th – 8th June 2018, Almería (Spain).

- Soriano-Molina, P., García Sánchez, J.L., Malato, S. & Sánchez Pérez, J.A. Effect of volumetric rate of photon absorption on the kinetics of micropollutant removal by solar photo-Fenton with Fe^{3+}-EDDS at neutral pH. Poster Communication. VI Mini-Symposium of Research in Experimental Science. 14th – 15th November 2017, Almería (Spain).

- Soriano-Molina, P., Rivas, G., Fernández Sevilla, J.M. & Sánchez Pérez. Poster Communication. Efecto de la temperatura y la absorción de fotones en la degradación

de microcontaminantes mediante foto-Fenton solar en reactores tipo "raceway". V Mini-Symposium of Research in Experimental Science. 15th November 2016, Almería (Spain).

- Sánchez Pérez, J.A., Soriano-Molina, P., Rivas, G., García Sánchez, J. L. Casas López, J.L. & Fernández Sevilla, J.M. Effect of temperature and photon absorption on the kinetics of micropollutant removal by solar photo-Fenton in raceway the pond reactors. Oral Communication. 251st American Chemical Society NATIONAL Meeting & Exposition. 13th – 17th March 2016, San Diego (California, United States).

Award communications:

- Soriano-Molina, P., Lorenzo, A., Plaza-Bolaños, P., García Sánchez, J.L., Malato, S. & Sánchez Pérez, J.A. Assessment of solar photo-Fenton in raceway pond reactors at neutral pH with Fe(III)-EDDS for micropollutant removal in municipal wastewater treatment plant effluents of different composition. Poster Communication. 19th European Meeting on Environmental Chemistry (EMEC19). 3rd – 6th December 2018, Clermont-Ferrand (France).

- Soriano-Molina, P., De la Obra, I., Malato, S. & Sánchez Pérez, J.A. Kinetics of micropollutant removal by solar photo-Fenton with Fe(III)-EDDS at neutral pH. Student Paper Communication. 5th European Conference on Enviromental Applications of Advanced Oxidation Processes (EAAOP5). 25th – 29th June 2017, Prague (Czech Republic).

Furthermore, Paula Soriano Molina is co-author of the following publications:

- Mejri, A., Soriano-Molina, P., Miralles-Cuevas, S., Trabelsi, I. & Sánchez Pérez, J.A. Effect of liquid depth on microcontaminant removal by solar photo-Fenton with Fe(III):EDDS at neutral pH in high salinity wastewater. Environmental Science and Pollution Research. Under review.

- Arzate, S., García Sánchez, J.L., Soriano-Molina, P., Casas López, J.L., Campos-Mañas, M.C., Agüera, A. & Sánchez Pérez, J.A. (2017). Effect of residence time on

micropollutant removal in WWTP secondary effluents by continuous solar photo-Fenton process in raceway pond reactors. Chemical Engineering Journal, 316, 1114 – 1121. DOI: 10.1016/j.cej.2017.01.089.

JCR IMPACT FACTOR

The impact factor and quartile of the publications presented in this Ph.D. thesis are shown below:

4.1. Effect of temperature and photon absorption on the kinetics of micropollutant removal by solar photo-Fenton in raceway pond reactors

Published in Chemical Engineering Journal (2017).

JCR Impact factor (2017): 6.735, **Quartile: Q1**, Rank: 3/50 (Engineering, Environmental), 7/137 (Engineering, Chemical).

4.2. Effect of volumetric rate of photon absorption on the kinetics of micropollutant removal by solar photo-Fenton with Fe^{3+}-EDDS at neutral pH

Published in Chemical Engineering Journal (2018).

JCR Impact factor (2017): 6.735, **Quartile: Q1**, Rank: 3/50 (Engineering, Environmental), 7/137 (Engineering, Chemical).

4.3. Assessment of solar raceway pond reactors form removal of contaminants of emerging concern by photo-Fenton at circumneutral pH from very different municipal wastewater effluents

Published in Chemical Engineering Journal (2019).

JCR Impact factor (2017): 6.735, **Quartile: Q1**, Rank: 3/50 (Engineering, Environmental), 7/137 (Engineering, Chemical).

4.4. Mechanistic modeling of solar photo-Fenton process with Fe^{3+}-EDDS at neutral pH

Published in Applied Catalysis B: Environmental (2018).

JCR Impact factor (2017): 11.698, **Quartile: Q1**, Rank: 1/50 (Engineering, Environmental), 3/137 (Engineering, Chemical).

REFERENCES

Ajona, J.A. & Vidal A. (2000). The use of CPC collectors for detoxification of contaminated water: design, construction and preliminary results. Solar Energy, 681, 109-120. DOI: 10.1016/S0038-092X(99)00047-X.

Alfano, O.M., Bahnemann D., Cassano A.E., Dillert, R. & Goslich R. (2000). Photocatalysis in water environments using artificial and solar light. Catalysis Today, 58, 299 – 230. DOI: 10.1016/S0920-5861(00)00252-2.

Alfano, O.M., Albizzati, E.D., Conte, L.O. (2015). Modelling of photo-Fenton solar reactors for environmental applications. In: Bahnemann, D.W., Robertson, P.K.J. (Eds.), Environmental Photochemistry Part III. The Handbook of Environmental Chemistry, vol. 35. Springer, pp. 1 – 22.

Alvarez-Gallegos, A.A. & Silva-Martínez S. (2018). Modeling of electro-Fenton process. In: Zhou M., Otura, M.A., Sirés, I. (Eds.), Electro-Fenton Process: New Trends and Scale-Up. The Handbook of Environmental Chemistry, vol. 61. Springer, pp. 287 – 312. DOI:10.1007/698_2017_73.

Anderson, J.V., Link H., Bohn, M. & Gupta, B. (1991). Development of U.S. Solar Detoxification Technology - An Introduction. Solar Energy Materials, 24, 538 – 549. DOI: 10.1016/0165-1633(91)90089-4.

Andreozzi, R., Caprio, V., Insola, A. & Marotta, R. (1999). Advanced oxidation processes (AOP) for water purification and recovery. Catalysis Today, 53, 51 – 59. DOI:10.1016/S0920-5861(99)00102-9.

Andreozzi, R., D'Apuzzo, A. & Marotta, R. (2000). A kinetic model for the degradation of benzothiazole by Fe3+-photo-assisted Fenton process in a completely mixed batch reactor. Journal of Hazardous Materials, 80, 241 – 257. DOI:10.1016/S0304-3894(00)00308-3.

Andreozzi, R., Marotta, R. & Paxéus, N. (2003). Pharmaceuticals in STP effluents and their solar photodegradation in aquatic environment. Chemosphere, 50, 1319 – 1330. DOI:10.1016/S0045-6535(02)00769-5.

Arzate, S., García Sánchez, J.L., Soriano-Molina, P., Casas López, J.L., Campos-Mañas, J.L., Agüera A. & Sánchez Pérez, J.A. (2017). Effect of residence time on micropollutant removal in WWTP secondary effluents by continuous solar photo-Fenton process in raceway pond reactors. Chemical Engineering Journal, 316, 1114 – 1121. DOI: 10.1016/j.cej.2017.01.089.

Bacardit, J., Stötzner, J., Chamarro, E. & Esplugas, S. (2007). Effect of Salinity on the Photo-Fenton Process. Industrial & Engineering Chemistry Research, 46, 7615 – 7619. DOI: 10.1021/ie070154o.

Ballesteros Martín, M.M., Casas López, J.L., Oller, I., Malato, S., Sánchez Pérez, J.A. (2010). A comparative study of different tests for biodegradability enhancement determination during AOP treatment of recalcitrant toxic aqueous solutions. Ecotoxicology and Environmental Safety, 73, 1189-1195. DOI:

10.1016/j.ecoenv.2010.07.021.

Barbosa, M.O., Moreira, N.F.F., Ribeiro, A.R., Pereira, M.F.R., Silva, A.M.T. (2016). Occurrence and removal of organic micropollutants: An overview of the watch list of EU Decision 2015/495. Water Research, 94, 257 – 279. DOI: 10.1016/j.watres.2016.02.047.

Belalcázar-Saldarriaga, A., Prato-Garcia, D. & Vasquez-Medrano, R. (2018). Photo-Fenton processes in raceway reactors: Technical, economic, and environmental implications during treatment of colored wastewaters. Journal of cleaner production, 182, 818 – 819. DOI:10.1016/j.jclepro.2018.02.058.

Blanco, J., Malato, S., Fernández, P., Vidal, A., Morales, A., Trincado, P., de Oliveira, J.C., Minero, C., Musci, M., Casalle, C., Brunotte, M., Tratzky, S., Dischinger, N., Funken, K.-H., Sattler, C., Vincent, M., Collares-Pereira, M., Mendes, J.F. & Rangel, C.M. (1999). Compound parabolic concentrator technology development to commercial solar detoxification applications. Solar Energy, 67, 317 – 330. DOI: 10.1016/S0038-092X(00)00078-5.

Bockelmann, D., Weichgrebe, D., Goslich, R. & Bahnemann, D. (1995). Concentrating versus Non-Concentrating Reactors for Solar Water Detoxification. Solar Energy Materials and Solar Cells, 381, 441 – 451. DOI: 10.1016/0927-0248(95)00005-4.

Bourgin, M., Beck, B., Boehler, M., Borowska, E., Fleiner, J., Salhi, E., Teichler R., von Gunten, U., Siegrist, H. & McArdell, C.S. (2018). Evaluation of a full-scale wastewater treatment plant upgraded with ozonation and biological post-treatments: Abatement of micropollutants, formation of transformation products and oxidation by-products. Water Research, 129, 486 – 498. DOI:10.1016/j.watres.2017.10.036.

Brandi, R.J., Citroni, M.A., Alfano, O.M. & Cassano, A.E. (2003). Absolute quantum yields in photocatalytic slurry reactors. Chemical Engineering Science, 58, 979 – 985. DOI:10.1016/S0009-2509(02)00638-3.

Burek, P., Satoh, Y., Fischer, G., Kahil, M., Scherzer, A., Tramberend, S., Nava, L., Wada, Y., Eisner, S. & Flörke, M., Hanasaki, N., Magnuszewski, P, Cosgrove, B., Wiberg, D. (2016). Water Futures and Solution: Fast Track Initiative (Final Report). IIASA Working Paper. Laxenburg, Austria, International Institute for Applied Systems Analysis (IIASA).

Buxton, G.V., Greenstock, C.L., Helman, W.P. & Ross, A.B. (1988). Critical review of rate constants for reactions of hydrated electrons, hydrogen atoms and hydroxyl radicals (•OH/•O−) in aqueous solution. Journal of Physical and Chemical Reference Data, 17, 513 – 886. DOI:10.1063/1.555805.

Cabrera Reina, A., Santos-Juanes Jordá, L., Casas López, J.L., Maldonado Rubio, M.I., García Sánchez, J.L. & Sánchez Pérez, J.A. (2015a). Biological oxygen demand as a tool to predict membrane bioreactor best operating conditions for a photo-Fenton pretreated toxic wastewater. Journal of Chemical Technology and Biotechnology, 90, 110 – 119. DOI: 10.1002/jctb.4295.

Cabrera Reina, A., Santos-Juanes, L., García Sánchez, J.L., Casas López, J.L., Maldonado Rubio, M.I., Li Puma, G. & Sánchez Pérez, J.A. (2015b). Modelling the photo-Fenton oxidation of the pharmaceutical paracetamol in water including the effect

of photon absorption (VRPA). Applied Catalysis B: Environmental, 166–167, 295–301. DOI:10.1016/j.apcatb.2014.11.023.

Cabrera-Reina, A., Miralles-Cuevas, S., Rivas, G., Sánchez Pérez, J.A. (2019). Comparison of different detoxification pilot plants for the treatment of industrial wastewater by solar photo-Fenton: Are raceway pond reactors a feasible option? Science of The Total Environment, 648, 601 – 608. DOI: 10.1016/j.scitotenv.2018.08.143.

Campos-Mañas, M.C., Plaza-Bolaños, P., Sánchez-Pérez, J.A., Malato, S. & Agüera, A. (2017). Fast determination of pesticides and other contaminants of emerging concern in treated wastewater using direct injection coupled to highly sensitive ultra-highperformance liquid chromatography-tandem mass spectrometry. Journal of Cromatography A, 1507, 84 – 94. DOI: 10.1016/j.chroma.2017.05.053.

Carra, I., García Sánchez J.L., Casas López, J.L., Malato, S., Sánchez Pérez, J.A. (2014a). Phenomenological study and application of the combined influence of iron concentration and irradiance on the photo-Fenton process to remove micropollutants. Science of the Total Environment, 478, 123 – 132. DOI:10.1016/j.scitotenv.2014.01.066.

Carra, I., Santos-Juanes, L., Acién Fernández, F.G., Malato, S. & Sánchez Pérez, J.A. (2014b). New approach to solar photo-Fenton operation. Raceway ponds as tertiary treatment technology. Journal of Hazardous Materials, 279, 322–329. DOI:10.1016/j.jhazmat.2014.07.010.

Cassano, A.E., Martin, C.A., Brandi, R.J. & Alfano, O.M. (1995). Photoreactor Analysis and Design: Fundamentals and Applications. Industrial and Engineering Chemistry Research, 34, 2155 – 2201. DOI: 10.1021/ie00046a001.

Clarizia, L., Russo, D., Di Somma, I., Marotta, R. & Andreozzi, R. (2017) Homogeneous photo-Fenton processes at near neutral pH: A review. Applied Catalysis B: Environmental, 209, 358–371. DOI:10.1016/j.apcatb.2017.03.011.

Collares-Pereira, M., Gordon, J.M., Rabl, A. & Winston, R. (1991). High concentration two-stage optics for parabolic trough Solar Collectors with tubular absorber and large rim angle. Solar Energy, 47, 457-466. DOI: 10.1016/0038-092X(91)90114-C.

Conte, L.O., Farias, J., Albizzati, E.D. & Alfano, O.M. (2012). Photo-Fenton degradation of the herbicide 2,4-dichlorophenoxyacetic acid in laboratory and solar pilot-plant reactors. Industrial & Engineering Chemistry Research, 51, 4181 – 4191. DOI: 10.1021/ie2023228.

Conte, L.O., Schenone, A.V. & Alfano, O.M. (2016). Photo-Fenton degradation of the herbicide 2,4-D in aqueous medium at pH conditions close to neutrality. Journal of Environmental Management, 170, 60 – 69. DOI: 10.1016/j.jenvman.2016.01.002.

Cuervo Lumbaque, E., Salmoria Araújo, D., Moreira Klein, T., Lopes Tiburtius, E.R., Argüello, J. & Sirtori, C. (2019). Solar photo-Fenton-like process at neutral pH: Fe(III)-EDDS complex formation and optimization of experimental conditions for degradation of pharmaceuticals. Catalysis Today, 328, 259 – 266.

De la Cruz, N., Giménez, J., Esplugas, S., Grandjean, D., de Alencastro, L.F. & Pulgarín, C. (2012). Degradation of 32 emergent contaminants by UV and neutral photo-fenton in

domestic wastewater effluent previously treated by activated sludge. Water Research, 46, 1947 – 1957. DOI:10.1016/j.watres.2012.01.014.

De la Obra, I., Ponce-Robles, L., Miralles-Cuevas, S., Oller, I., Malato, S. & Sánchez Pérez, J.A. (2017). Microcontaminant removal in secondary effluents by solar photo-Fenton at circumneutral pH in raceway pond reactors, Catalysis Today, 287, 10 – 14, DOI:10.1016/j.cattod.2016.12.028.

De Luca, A., Dantas, R.F. & Esplugas, S. (2014). Assessment of iron chelates efficiency for photo-Fenton at neutral pH. Water Research, 61, 232 – 242. DOI:10.1016/j.watres.2014.05.033.

De Luca, A., Dantas, R.F. & Esplugas, S. (2015). Study of Fe(III)-NTA chelates stability for applicability in photo-Fenton at neutral pH. Applied Catalysis B: Environmental, 179, 372 – 379. DOI: 10.1016/j.apcatb.2015.05.025.

Decree 109/2015 of 17 March 2015 of the Andalusian Regional Government (Junta de Andalucía), Official Bulletin of the Andalusian Government (Boletín Oficial de la Junta de Andalucía), 89/22, 12.05.2015. http://www.juntadeandalucia.es/boja/2015/89/3.

Directive 2000/60/EC of the European Parliament and of the Council of 23 October 2000 establishing a framework for Community action in the field of water policy. (2000). Oficial Journal of the European Parliament, L327, 1 – 82.

Eggen, R.I.L., Hollender, J., Joss, A., Schärer, M. & Stamm, C. (2014). Reducing the Discharge of Micropollutants in the Aquatic Environment: The Benefits of Upgrading Wastewater Treatment Plants. Environmental Science and Technology, 48, 7683 – 7689. DOI: 10.1021/es500907n.

European Commission (2015). Commission implementing decision (EU) 2015/495 of 20 March 2015 establishing a watch list of substances for Union-wide monitoring in the field of water policy pursuant to Directive 2008/105/EC of the European Parliament and of the Council. Official Journal of the European Union L78, 40 – 42. https://publications.europa.eu/en/publication-detail/-/publication/a90868de-d1f9-11e4-9de8-01aa75ed71a1/language-en.

European Commission (2018). Commission Implementing Decision (EU) 2018/840 of 5 June 2018 establishing a watch list of substances for Union-wide monitoring in the field of water policy pursuant to Directive 2008/105/EC of the European Parliament and of the Council and repealing Commission Implementing Decision (EU) 2014/495. Official Journal of the European Union, L141/9, 7.6.2018. http://data.europa.eu/eli/dec_impl/2018/840/oj.

European Parliament (2019). http://www.europarl.europa.eu/sides/getDoc.do?pubRef=-//EP//TEXT+TA+P8-TA-2019-0071+0+DOC+XML+V0//EN&language=EN.

Farias, J., Albizzati, E.D. & Alfano, O.M. (2009). Kinetic study of the photo-Fenton degradation of formic acid. Combined effects of temperature and iron concentration. Catalysis Today, 144, 117 – 123. DOI: 10.1016/j.cattod.2008.12.027.

Fenton, H.J.H. (1894). Oxidation of tartaric acid in presence of iron. Journal of the Chemical Society, 65, 899–910. DOI: 10.1039/CT8946500899.

Gallego-Schmid, A., Zepon Tarpani, R.R., Miralles-Cuevas, S., Cabrera-Reina, A., Malato, S. & Azapagic, A. (2019). Environmental assessment of solar photo-Fenton processes in combination with nanofiltration for the removal of micro-contaminants from real wastewaters. Science of the Total Environment, 650, 2210 – 2220. DOI:10.1016/j.scitotenv.2018.09.361.

Giannakis, S., Hendaoui, I., Rtimi, S., Fürbringer, J.M. & Pulgarin, C. (2017). Modeling and treatment optimization of pharmaceutically active compounds by the photo-Fenton process: The case of the antidepressant Venlafaxine. Journal of Environmental Chemical Engineering, 5, 818 – 828. DOI:10.1016/j.jece.2016.12.050.

Gueymard, C. (1995). SMARTS2, a Simple Model of the Atmospheric Radiative Transfer of Sunshine: Algorithms and Performance Assessment. Rep. FSEC-PF-270-95, Florida Solar Energy Center, Cocoa, USA.

Huang, W., Brigante, M., Wu, F., Hanna, K. & Mailhot, G. (2012). Development of a new homogenous photo-Fenton process using Fe(III)-EDDS complexes. Journal of Photochemistry and Photobiology A: Chemistry, 239, 17 – 23, DOI:10.1016/j.jphotochem. 2012.04.018.

Huang, W., Brigante, M., Wu, F., Mousty, C., Hanna, K., Mailhot, G. (2013). Assessment of the Fe(III)−EDDS complex in Fenton-Like Processes: from the radical formation to the degradation of bisphenol A. Environmental Science and Technology, 47, 1952 – 1959. DOI:10.1021/es304502y.

Jain, B., Singh, A.K., Kim, H., Lichtfouse, E., Sharma, V.K. (2018). Treatment of organic pollutants by homogeneous and heterogeneous Fenton reaction processes. Environmental Chemistry Letters, 16, 947 – 967. DOI: 10.1007/s10311-018-0738-3.

Kelly, B.D. & De Laquil, P. (1992). Conceptual Design of a Photocatalytic Wastewater Treatment Plant. Solar Energy, 1, 65 – 69.

Kiwi, J., Lopez, A. & Nadtochenko, V. (2000). Mechanism and Kinetics of the OH-Radical Intervention during Fenton Oxidation in the Presence of a Significant Amount of Radical Scavenger (Cl^-). Environmental Science & Technology, 34, 2162–2168. DOI: 10.1021/es991406i.

Klamerth, N., Miranda, N., Malato, S., Agüera, A., Fernández-Alba, A.R., Maldonado, M.I. & Coronado, J.M. (2009). Degradation of emerging contaminants at low concentrations in MWTPs effluents with mild solar photo-Fenton and TiO2. Catalysis Today, 144, 124 – 130. DOI: 10.1016/j.cattod.2009.01.024.

Klamerth, N., Malato, S., Agüera, A., Fernández-Alba, A. & Mailhot, G. (2012). Treatment of municipal wastewater treatment plant effluents with modified photo- Fenton as a tertiary treatment for the degradation of micro pollutants and disinfection. Environmental Science and Technology, 46, 2885 – 2892. DOI:10.1021/es204112d.

Klamerth N., Malato S., Agüera A. & Fernández-Alba A. (2013). Photo-Fenton and modified photo-Fenton at neutral pH for the treatment of emerging contaminants in wastewater treatment plant effluents: a comparison. Water Research, 478, 833 – 840. DOI:10.1016/j.watres.2012.11.008.

Krishnan, S., Rawindran, H., Sinnathambi, C.M., Lim, J.W. (2017). Comparison of various advanced oxidation processes used in remediation of industrial wastewater laden with recalcitrant pollutants. IOP Conference Series: Materials Science and Engineering. 206, 012089. DOI: 10.1088/1757-899X/206/1/012089.

Krzeminski, P., Tomei, M.C., Karaolia, P.C., Langenhoff, A., Almeida, C.M.R., Felis, E., Gritten, F., Andersen, H.R., Fernandes, T., Manaia, C.M., Rizzo, L. & Fatta-Kassinos, D. (2019). Performance of secondary wastewater treatment methods for the removal of contaminants of emerging concern implicated in crop uptake and antibiotic resistance spread: A review. Science of the Total Environment, 648, 1052 – 1081. DOI: 10.1016/j.scitotenv.2018.08.130.

Lado Ribeiro, A.R., Moreira, N.F.F., Li Puma, G. & Silva, A.M.T. (2019) Impact of water matrix on the removal of micropollutants by advanced oxidation technologies. Chemical Engineering Journal, 363, 155 – 173. DOI: 10.1016/j.cej.2019.01.080.

Li, J., Mailhot, G., Wu, F. & Deng, N.S. (2010). Photochemical efficiency of Fe(III)-EDDS complex: OH radical production and 17β-estradiol degradation, Journal of Photochemistry and Photobiology A: Chemistry, 212, 1 – 7. DOI:10.1016/j.jphotochem.2010.03.001.

Lipczynska-Kochany, E. & Kochany, J. (2008). Effect of humic substances on the Fenton treatment ofwastewater at acidic and neutral pH, Chemosphere, 73, 745 - 750. DOI: 10.1016/j.chemosphere.2008.06.028.

Machulek Jr., A., Moraes, J.E.F., Okano, L.T., Silvério, C.A. & Quina, F.H. (2009). Photolysis of Ferric Ion in the Presence of Sulfate or Chloride Ions: Implications for the Photo-Fenton Process. Photochemical & Photobiological Sciences, 8, 985 – 991. DOI: 10.1039/b900553f.

Mahamallik P. & Pal A. (2017). Degradation of textile wastewater by modified photo-Fenton process: Application of Co(II) adsorbed surfactant-modified alumina as heterogeneous catalyst. Journal of Environmental Chemical Engineering, 5, 2886 – 2893. DOI: 10.1016/j.jece.2017.05.044.

Malato, S., Gimenez, J., Richter, C., Curcó, D. & Blanco, J. (1997). Low concentrating CPC collectors for photocatalytic water detoxification. Comparison with a medium concentrating solar collector. Water Science and Technology, 35, 157 – 164. DOI: 10.1016/S0273-1223(97)00021-8.

Malato, S., Blanco, J., Vidal, A. & Richter, C. (2002). Photocatalysis with solar energy at a pilot-plant scale: an overview. Applied Catalysis B: Enviromental, 37, 1 – 15. DOI: 10.1016/S0926-3373(01)00315-0.

Malato Rodríguez, S., Blanco Gálvez, J., Maldonado Rubio, M.I., Fernández Ibánez, P., Alarcón Padilla, D., Collares Pereira, M., Farinha Mendes, J., & Correia de Oliveira, J. (2004). Engineering of solar photocatalytic collectors. Solar Energy, 77, 513 – 524. DOI: 10.1016/j.solener.2004.03.020.

Malato, S., Fernández-Ibáñez, P., Maldonado, M. I., Blanco, J. & Gernjak, W. (2009). Decontamination and disinfection of water by solar photocatalysis: Recent overview and trends. Catalysis Today, 147, 1 – 59. DOI: 10.1016/j.cattod.2009.06.018.

Miklos, D.B., Remy, C., Jekel, M., Linden, K.G., Drewes, J.E. & Hübner, U. (2018). Evaluation of advanced oxidation processes for water and wastewater treatment - A critical review. Water Research, 139, 118 – 131. Doi:10.1016/j.watres.2018.03.042.

Minero, C., Pelizzetti, E., Malato, S. & Blanco, J., (1993). Large Solar Plant Photocatalytic Water Decontamination: Degradation of Pentachlorophenol. Chemosphere, 26, 2103 – 2119. DOI: 10.1016/0045-6535(93)90337-5.

Miralles-Cuevas, S., Oller, I., Sánchez Pérez, J.A. & Malato, S. (2014). Removal of pharmaceuticals from MWTP effluent by nanofiltration and solar photo-Fenton using two different iron complexes at neutral pH. Water Research, 64, 23 – 31. DOI:10.1016/j.watres.2014.06.032.

Papoutsakis, S., Miralles-Cuevas, S., Oller, I., Pulgarín, C. & Malato, S. (2015). Microcontaminant degradation in municipal wastewater treatment plant secondary effluent by EDDS assisted photo-Fenton at near-neutral pH: An experimental design approach. 252, 61 – 69. DOI:10.1016/j.cattod.2015.02.005.

Pignatello, J.J. (1992). Dark and photoassisted Fe3+-catalyzed degradation of chlorophenoxy herbicides by hydrogen peroxide. Environmental Science and Technology, 26, 944 – 951. DOI: 10.1021/es00029a012.

Pignatello, J.J., Oliveros, E. & MacKay, A. (2006). Advanced Oxidation Processes for Organic Contaminant Destruction Based on the Fenton Reaction and Related Chemistry. Critical Reviews in Environmental Science and Technology, 36, 1 – 84. DOI: 10.1080/10643380500326564.

Pinheiro da Costa, E., Bottrel, S.E.C., Starling, M.C.V.M., Leão, M.M.D. & Amorim, C.C. (2019). Degradation of carbendazim in water via photo-Fenton in Raceway Pond Reactor: assessment of acute toxicity and transformation products. Environmental Science and Pollution Research, 26, 4324 – 4336. DOI:10.1007/s11356-018-2130-z.

Rabl, A., Goodman, N.B. & Winston R. (1979). Practical Design Considerations for CPC solar Collectors. Solar Energy, 22, 373 – 381. DOI:10.1016/0038092X(79)90192-0.

Redouane-Salah, Z., Malouki, M.A., Khennaoui, B., Santaballa, J.A. & Canle, M. (2018). Simulated sunlight photodegradation of 2-mercaptobenzothiazole by heterogeneous photo-Fenton using a natural clay powder. Journal of Environmental Chemical Engineering, 6, 1783 – 1793. DOI:10.1016/j.jece.2018.02.011.

Ribeiro, A.R., Nunes, O.C., Pereira M.F.R. & Silva, A.M.T. (2015). An overview on the advanced oxidation processes applied for the treatment of water pollutants defined in the recently launched Directive 2013/39/EU. Environmental International, 75, 33 – 51. DOI:10.1016/j.envint.2014.10.027.

Rivas, G., Carra, I., García Sánchez, J.L., Casas López, J.L., Malato, S. & Sánchez Pérez, J.A. (2015). Modelling of the operation of raceway pond reactors for micropollutant removal by solar photo-Fenton as a function of photon absorption. Applied Catalysis B: Environmental, 178, 210 – 217, doi:10.1016/j.apcatb.2014.09.015.

Rivas Ibáñez, G., Bittner, M., Toušová, Z., Campos-Mañas, M.C., Agüera, A., Casas López, J.L., Sánchez Pérez, J.A. & Hilscherová, K. (2017). Does micropollutant removal

by solar photo-Fenton reduce ecotoxicity in municipal wastewater? A comprehensive study at pilot scale open reactors. Journal of Chemical Technology and Biotechnology, 92, 2114 – 2122. DOI:10.1002/jctb.5212.

Rizzo, L., Krätke, R., Linders, J., Scott, M., Vighi, M. & de Voogt, P. (2018). Proposed EU minimum quality requirements for water reuse in agricultural irrigation and aquifer recharge: SCHEER scientific advice. Current Opinion in Environmental Science & Health, 2, 7 – 11.

Rizzo, L., Malato, S., Antakyali, D., Beretsou V.G., Đolić, M.B., Gernjak, W., Heath, E., Ivancev-Tumbas, I., Karaolia, P., Lado Ribeiro, A.R., Mascolo, G., McArdell, C.S., Schaar, H., Silva, A.M.T. & Fatta-Kassinos D (2019). Consolidated vs new advanced treatment methods for the removal of contaminants of emerging concern from urban wastewater. Science of the Total Environment, 655, 986 - 1008. DOI:10.1016/j.scitotenv.2018.11.265.

Salimi, M., Esrafili, A., Gholami M., Jonidi Jafari, A., Rezaei Kalantary, R., Farzadkia, M., Kermani, M. & Sobhi, H.R. (2017). Contaminants of emerging concern: a review of new approach in AOP technologies. Environmenral Monitoring and Assessment, 189, 414. DOI:10.1007/s10661-017-6097-x.

Santos-Juanes, L., Amat, A.M. & Arques, A. (2017). Strategies to drive photo-Fenton process at mild conditions for the removal of xenobiotics from aqueous systems. Current Organic Chemistry, 21, 1074 – 1083. DOI: 10.2174/1385272821666170102150337.

Sato, T., Qadir, M., Yamamoto, S., Endo., T. & Zahoor, M. (2013). Global, regional, and country level need for data on wastewater generation, treatment, and use. Agricultural Water Management, 130, 1 – 13. DOI:10.1016/j.agwat.2013.08.007.

Scaratti, G., Rauen, T.G., Baldissarelli, V.Z., José, H.J. & Moreira R.D.F.P.M. (2018). Residue-based iron oxide catalyst for the degradation of simulated petrochemical wastewater via heterogeneous photo-Fenton process. Environmental Technology (United Kingdom), 39, 2559 – 256. DOI: 10.1080/09593330.2017.1361474.

Schenone, A.V., Conte, L.O., Botta, M.A. & Alfano, O.M. (2015). Modeling and optimization of photo-Fenton degradation of 2,4-D using ferrioxalate complex and response surface methodology (RSM). Journal of Environmental Management, 155, 177 – 183. DOI:10.1016/j.jenvman.2015.03.028.

Shokry, A., Audino, F., Vicente, P., Escudero, G., Perez Moya, M., Graells, M. & Espuña, A. (2015). Modeling and Simulation of Complex Nonlinear Dynamic Processes Using Data Based Models: Application to Photo-Fenton Process. Computer Aided Chemical Engineering, 37, 191 – 196. Doi:10.1016/B978-0-444-63578-5.50027-X.

Spasiano, D., Marotta, R., Malato, S., Fernandez-Ibáñez, P. & Di Somma, I. (2015). Solar photocatalysis: Materials, reactors, some commercial, and pre-industrialized applications. A comprehensive approach. Applied Catalysis. B: Environmental, 170, 90 – 123. DOI:10.1016/j.apcatb.2014.12.050.

Tousova, Z., Oswald, P., Slobodnik, J., Blaha, L., Muz, M., Hu, M., Brack, W., Krauss, M., Di Paolo, C., Tarcai, Z., Seiler, T.B., Hollert, H., Koprivica, S., Ahel, M., Schollée, J.E., Hollender, J., Suter, M.J., Hidasi, A.O., Schirmer, K., Sonavane, M., Ait-Aissa, S.,

Creusot, N., Brion, F., Froment, J., Almeida, A.C., Thomas, K., Tollefsen, K.E., Tufi, S., Ouyang, X., Leonards, P., Lamoree, M., Torrens, V.O., Kolkman, A., Schriks, M., Spirhanzlova, P., Tindall, A. & Schulze, T. (2017). European demonstration program on the effect-based and chemical identification and monitoring of organic pollutants in European surface waters, Science of the Total Environment, 601 – 602, 1849 – 1868, DOI:10.1016/j.scitotenv.2017.06.032.

United Nations Water (2018). World Water Development Report 2018. Nature-based Solutions for Water. http://www.unwater.org/publications/world-water-development-report-2018/.

Wyness, P., Klausner, J.F., Goswami, D.Y. & Schanze, K.S. (1994). Performance of nonconcentrating solar photocatalytic oxidation reactors. Part I: Flat-plate configuration. Journal of Solar Energy Engineering, 116, 2 – 7. DOI: 10.1115/1.2930062.

Wu, Y., Brigante, M., Dong, M., De Sainte-Claire, P. & Mailhot, G. (2014) Toward a better understanding of Fe(III)–EDDS photochemistry: theoretical stability calculation and experimental investigation of 4-tert-butylphenol degradation. Journal of Physical Chemistry A, 118, 396 – 403. DOI:10.1021/jp409043e.

Zhang, C. (2009). Photodegradation of organic pollutants induced by iron-carboxylate complexes in aqueous solutions. Organic chemistry. Universite Blaise Pascal - Clermont-Ferrand II; Universite de Wuhan (Chine). English. <NNT: 2009CLF21925>. <tel-00725597>.

Zhang, X., Gu, X., Lu, S., Miao, Z., Xu, M., Fu, X., Qiu, Z. & Qian, S. (2016). Application of calcium peroxide activated with Fe(II)-EDDS complex in trichloroethylene degradation. Chemosphere, 160, 1 – 6. DOI: 10.1016/j.chemosphere.2016.06.067.

Zhang Y. & Zhou M. (2019). A critical review of the application of chelating agent in Fenton process at high pH values. Journal of Hazardous Materials 362, 436 – 450. doi:10.1016/j.jhazmat.2018.09.035.